HOW DOES THE COMPOSITION OF ATMOSPHERIC AEROSOL PARTICLES AFFECT $PM_{2.5}$ TOXICITY?

by

Steven Thomson

A thesis submitted to the University of Birmingham for the degree of

DOCTOR OF PHILOSOPHY

School of Geography, Earth and Environmental Sciences

College of Life and Environmental Sciences

University of Birmingham

September 2021

ABSTRACT

Epidemiological studies have shown that exposure to $PM_{2.5}$ increases the chance of mortality or morbidity due to respiratory and cardiovascular diseases. The causes for this are not completely understood yet, however, one widely proposed biochemical pathway is $PM_{2.5}$-induced oxidative stress.

This study aims to determine the impact of $PM_{2.5}$ concentration on the oxidative potential (OP) of the air mass, and the effect of PM chemical composition on the intrinsic OP of $PM_{2.5}$ particles. These factors were investigated through several intensive periods of $PM_{2.5}$ measurement across different seasons in Beijing and Delhi, with a shorter campaign in Birmingham, followed by detailed laboratory chemical analysis, and application of an OP assay to the collected PM samples.

The dithiothreitol (DTT) assay was chosen as the method for OP determination and a laboratory protocol was developed, meeting the requirements and limitations of the project and available laboratories. This protocol was validated using $PM_{2.5}$ samples collected during a short sampling campaign in Birmingham.

$PM_{2.5}$ concentration was found to be strongly correlated with air mass OP (DTTv, nmol DTT min^{-1} m^{-3}) at lower $PM_{2.5}$ concentrations ($r = 0.85$ at < 110.6 μg m^{-3}, being the median concentration), however, at higher concentrations a non-linear relationship formed ($r = 0.41$ at > 110.6 μg m^{-3}). This was due to an inverse relationship between $PM_{2.5}$ concentration and intrinsic toxicity (DTTm, pmol DTT min^{-1} μg^{-1} $PM_{2.5}$) at higher $PM_{2.5}$ concentrations ($r = -0.47$). During some extreme $PM_{2.5}$ pollution events DTTv values were lower than those seen

during much lower $PM_{2.5}$ concentration days, demonstrating the importance of intrinsic PM OP to human exposure (DTTv) and consequent health effects.

The relative impact of different PM chemical components on DTTm was determined through various correlation, multiple linear regression, and t-test analyses performed on composition measurements within PM, and meteorological and gas-phase data for the Beijing and Delhi campaigns. The impact of these species and meteorological conditions on DTTm was determined by the gradient of their correlation with DTTm, the gradient for each species was denoted by $DTTm^{specie}$ (i.e. $DTTm^{Fe}$ representing pmol DTT min^{-1} ng^{-1} Fe).

Data from all campaigns showed significant correlations between vehicle related emissions and DTTm. Crustal material, re-suspended road dust, and non-exhaust vehicle emissions were also significantly correlated with DTTm during the Beijing winter and all Delhi campaigns. Species most commonly associated with these sources consistently showed the highest gradients such as Ce, Cr, Ni, and Sr.

During the Delhi autumn campaign biomass burning is the dominant source of $PM_{2.5}$. Biomass associated species such as OC and K showed a weaker effect on OP assessed as DTTm values, compared with non-exhaust vehicle emissions and crustal materials i.e. 0.153 ± 0.023 $DTTm^{OC}$ compared to 358 ± 34 $DTTm^{Ce}$. Multiple linear regression analysis showed that 78 % of DTTm variance was accounted for by non-exhaust vehicle emissions in this campaign. This study shows that $PM_{2.5}$ concentration is key in determining the overall oxidative potential of the air, however, it is not sufficient to solely predict this oxidative potential. The sources and composition of the particulate matter must also be considered to better predict the health effects of particulate matter oxidative potential.

ACKNOWLEDGEMENTS

There are a number of people I wish to thank and without whom I would not have been able to complete this project. First and foremost I'd like to thank my supervisors: Professor William Bloss and Professor Zongbo Shi for their continued support, expertise, and advice over the last five years. I would also like to thank the National Centre for Atmospheric Science and National Environmental Research Council for their financial support during this project.

I wish to also thank Dr James Brean, Dr Leigh Crilley, Dr Louisa Kramer, Dr Tuan Vu, and everyone else on the APHH field campaigns who provided with so much guidance through sampling and the many challenges during this project. Thanks is also due to those at the Chinese Research Academy of Environmental Science for so readily sacrificing their time to help with my project and then to help me through one of my lowest points during the last five years.

Thank you also to Dr Nicholas Davidson, Dr Eimear Orgill, and Gretchel Coldicott for helping me out so much, I wish I could repay you all for all the time and advice you have given me.

I'd also like to thank Room 425, especially the Seven Dwarfs, for their friendship, laughs, advice, and much needed coffee breaks. I would also like to thank my family for their support and patience over the years.

Finally, I'd like to say a huge thank you to Angharad Thomas. Thank you for pretending to be interested in my research and always believing in me, even when I didn't believe in myself. Your love and support has never gone unnoticed and the porcelain pebble has gotten me through to the end.

CONTENTS

LIST OF FIGURES

LIST OF TABLES

LIST OF ABBREVIATIONS AND ACRONYMS

AA	Ascorbic Acid
APHH	Atmospheric Pollution & Human Health in a megacity programme
AQI	Air Quality Index
ATD	Arizona Test Dust
CFC	Chlorofluorocarbon
CNY	Chinese Yuan
COPD	Chronic Obstructive Pulmonary Disease
CV	Coefficient of Variation
DALY	Disability-Adjusted Life Years
DCFH	2-7-dichlorofluoroscin/hydrogen peroxidase
DTNB	5,5'-dithiobis(2-nitrobenzoic acid)
DTT	Dithiothreitol
DTTm	Dithiothreitol activity μg^{-1} of PM2.5
DTTv	Dithiothreitol activity m^{-3} of sampled air
EC	Elemental Carbon
ELF	Epithelial Lining Fluid
EPA	Environmental Protection Agency
EPR	Electron Parametric Resonance
GBD	Global Burden of Disease
GC-MS	Gas Chromatography Mass Spectrometry
GDP	Gross Domestic Product

GSH	Reduced Glutathione
HPLC	High Performance Liquid Chromatography
HRP	Horseradish Peroxidase
IC	Ion Chromatography
ICP-MS	Inductively Coupled Plasma Mass Spectrometry
IGP	Indo-Gangetic Plain
IHD	Ischemic Heart Disease
IIT Delhi	Indian Institute of Technology Delhi
k-buffer	Potassium phosphate buffer
LC	Lung Cancer
LPG	Liquid Petroleum Gas
LRI	Lower Respiratory Infection
MLR	Multiple Linear Regression
NAAQS	National Ambient Air Quality Standards
NADH	Nicotinamide Adenine Dinucleotide
NCP	North China Plain
NCT	North Capital Territory
OC	Organic Carbon
OP	Oxidative Potential
PAH	Polycyclic Aromatic Hydrocarbon
PM	Particulate Matter
PM_1	Particulate Matter: diameter < 1 µm
PM_{10}	Particulate Matter: diameter < 10 µm

$PM_{2.5}$	Particulate Matter: diameter < 2.5 µm
ppb	Parts Per Billion
PQN	9,10-phenanthroquinone
RH	Relative Humidity
ROS	Reactive Oxygen Species
RTLF	Respiratory Tract Lining Fluid
SOA	Secondary Organic Aerosols
SVOC	Semi-Volatile Organic Compounds
TCA	Trichloroacetic Acid
TEOM	Tapered Element Oscillating Microbalance
TNB	2-nitro-5-thiobenzoic acid
UA	Urate
UK	United Kingdom
US	United States
VOC	Volatile Organic Compounds
WHO	World Health Organisation
XRF	X-Ray Fluorescence
YLL	Years of Life Lost

1 INTRODUCTION

1.1 Background

Urbanisation has been rapidly increasing over the last few decades around the globe and especially in developing countries. In 1990 there were 20 megacities (cities with populations of 10 million or more) and 43 % of people lived in an urban area worldwide, in 2018 that number had increased to 55 %. While most of this growth was not in megacities; in 2018, 7% of the global population lived in 33 megacities, of which the majority were in India and China. It is projected that by 2050, 68 % of the global population will live in urban areas (Mage et al., 1996; United Nations, Department of Economic and Social Affairs, 2018).

This increase in urbanisation across many developing countries has led to worsening air quality in cities and increased air pollution exposure to their rapidly rising populations. Urban living in developed countries is often associated with lower levels of residential carbon emissions compared with rural populations. This is due to many reasons such as increased use of public transport, decreased housing sizes, and the prevalence of natural gas heating in urban areas. This trend is not often observed in developing countries where increasing urbanisation has increased national energy consumption. The major pathways for increased energy consumption from urban areas are:

- Increased urban sprawl which requires a higher energy consumption for the new buildings and accompanying public transport sector.
- Growing vehicle fleets in urban areas.

- Rising quality of energy intensive lifestyles such as lighting, heating / cooling, and electronics.

Rural populations in developing countries, in comparison, are less likely to have access to these resources and therefore use less energy than their urban counterparts. Zhao & Zhang, 2018 found that in China during the period of 1980 – 2010 for every 1 % increase in urban population, relative to total population, the national energy consumption rose by 1.4 %, while industrialisation was not significantly associated with the increased energy consumption during the same period (Timmons et al., 2016; Zhao & Zhang, 2018).

Due to this urbanisation and industrialisation, in most developing countries human exposure and air pollution emissions are increasing. The emissions of particulate matter and trace gases such as nitrogen oxides (NO_x) and ozone (O_3, formed in the atmosphere) have increased in these countries due to increasing intensive infrastructure development, energy demands and industrial, transport, and agricultural activities (Guttikunda & Gurjar, 2012; Zheng et al., 2017a).

China has undergone rapid urbanisation over the past three decades with the urban population increasing from 17.9% in 1978 to 54.8% of the total population in 2015. One of the regions to experience this large increase in urban population and subsequently have severe air pollution problems is the North China Plain (NCP), a region containing the capital city, Beijing. Air pollution in the NCP often puts it among the worst regions in China for air quality (along with regions such as the Pearl River Delta and Yangtze River Delta). There are several reasons for this such as the cities in the NCP relying on carbon-intensive industries (mostly constrained to the cities of Tianjin and Tangshan), transportation of air pollution

from neighbouring regions, heavy vehicle emissions, and stagnant weather with weak winds (W. J. Liu et al., 2018a; Z. Liu et al., 2018; Shaojian Wang et al., 2017; Y. Yang et al., 2020).

In recent decades, haze pollution has become a national concern in China. Haze is an atmospheric phenomenon where dust, smoke, moisture, and vapour are suspended in the air, impairing visibility. The main component of haze is fine particulate matter ($PM_{2.5}$, particles with an aerodynamic diameter <2.5 μm). $PM_{2.5}$ is a complex heterogeneous mixture with its size distribution and composition changing significantly depending on the type of emission source, meteorological conditions and atmospheric chemistry. The main sources of $PM_{2.5}$ are industrial emissions, biomass burning, vehicle exhaust emissions, and secondary aerosols that form through photochemical reactions (W. J. Liu et al., 2018a; X. G. Liu et al., 2013; Z. Liu et al., 2018; Sun et al., 2014; Watson, 2002; Zheng et al., 2017a).

Several epidemiological studies have shown that exposure to $PM_{2.5}$ increases the chance of mortality or morbidity due to respiratory and cardiovascular diseases (Simonetti et al., 2018). Long-term exposure to high concentrations of $PM_{2.5}$ has been linked to serious medical conditions such as lung cancer, stroke, chronic obstructive pulmonary disease (COPD), and heart failure (Brook et al., 2010; Ting Fang, Verma, T Bates, et al., 2016a; Hoek et al., 2013; Simonetti et al., 2018; Song et al., 2017). The underlying causes for these diseases are not completely understood yet, however, one widely proposed biochemical pathway is $PM_{2.5}$-induced oxidative stress (Rui et al., 2016; Valavanidis et al., 2013; Wang et al., 2019).

Due to the complex nature in which $PM_{2.5}$ is formed the emissions, atmospheric particles, and formation conditions that are involved in $PM_{2.5}$ production are covered in the next section before discussing the health implications in more detail. As such this introduction

chapter will start by going over the sources and formation mechanisms for $PM_{2.5}$ and atmospheric species that coagulate into $PM_{2.5}$. Then the health implications of air pollution and the legislative response shall be covered before giving an overview of the larger Atmospheric Pollution & Human Health (APHH) in a megacity programme that this project is a part of.

1.2 General air pollution

Air pollution can be defined as the presence of toxic chemicals or compounds (anthropogenic or biogenic) in the air, at concentrations that pose a health risk. In a broader sense air pollution refers to the presence of chemicals or compounds in the air which are not usually present and have a negative impact on the quality of air or quality of life. This impact is wide ranging, from the negative health effects of exposure to ground level air pollution to long-term climate change due to the presence of greenhouse gases in the atmosphere, although in this study we will not be focussing on greenhouse gases. Air pollutants can be emitted directly into the atmosphere such as from biomass burning, these pollutants are called primary air pollutants. Others are formed through secondary chemical and physical processes in the atmosphere, these being chemical or photochemical reactions and/or gas to particle deposition and are collectively called secondary air pollutants (Environmental Pollution Centers, 2020; Seigneur, 2019).

1.2.1 Sources of air pollution

The sources of pollution in the air are often split into biogenic (pollutants from plants and animals) and anthropogenic (pollution released from human activities) emissions. By the definition of air pollution in the previous section, being the presence of toxic chemicals at concentrations that pose a health risk, there are also natural sources of air pollution such as

sulphur dioxide released from volcanic eruptions. The three most important gaseous pollutants based on concentration and overall effects on animals, humans, and plants are sulphur dioxide (SO_2), NO_x and O_3. NO_x is the total concentration of nitric oxide (NO) and nitrogen dioxide (NO_2), as these two nitrogen oxides are rapidly interconverted from one to the other by reactions with O_3 and through photolysis. SO_2 and NO are both primary air pollutants, O_3 is entirely formed in the atmosphere through secondary processes. NO_2 can be considered both primary and secondary as it is emitted through combustion but also forms through photochemical reactions in the atmosphere (Colls & Tiwary, 2009; Mollenhauer & Tschoeke, 2010a).

SO_2 is produced through the combustion of sulphur-containing fossil fuels such as coal and oil as well as through smelting of sulphur containing mineral ores. The main source of SO_2 is the burning of fossil fuels for domestic heating, vehicles, and power generation. Historically vehicle emissions contributed significantly to the total SO_2 burden, however, with the reduction of sulphur content in fossil fuels (both oil and coal) and the widespread adoption of oxidation catalytic converters in vehicle exhausts impact of motor vehicles on SO_2 concentrations has decreased massively since the 1970s. The largest natural source of SO_2 is from volcanic eruptions but owing to the unpredictability of eruptions this changes a lot from year to year. Seigneur, 2019 concluded that almost half of anthropogenic global SO_2 is produced through electrical and heat generation. SO_2 is an important precursor for other sulphur species such as sulphate formed through the oxidation of SO_2, sulphate is a key component of PM (Gschwandtner et al., 1986; Gurjar et al., 2010; Mollenhauer & Tschoeke, 2010a; Seigneur, 2019).

1.2.1.1 Daytime NO_x and O_3 formation

At high temperatures such as those found inside internal combustion engines oxygen (O_2) and nitrogen (N_2) dissociate into their respective atoms, these atoms then go on to form nitrogen oxides, mostly NO (>90 %) with a smaller fraction of NO_2 (<10 %). This process is called the Zeldovich chain reaction, O_2 can dissociate into atomic oxygen at temperatures above 2200 K (this process occurs at local peak temperatures and does not require the entire combustion chamber to reach this temperature). When N_2 is exposed to the resulting oxygen atom, NO and atomic nitrogen (N) is formed. This N then goes on to react with O_2 to produce more NO and recreate the oxygen radical, thereby completing the cycle. NO is also emitted from soils and lighting, however these sources are harder to quantify and produce significantly less NO than vehicle emissions (Ball, 2014; Colls & Tiwary, 2009; Dutta, 1932; Mollenhauer & Tschoeke, 2010a; Seigneur, 2019).

Before moving onto the atmospheric processing of secondary NO_2 it is important to first introduce hydroxyl radical formation as these radicals play a key role in the chemistry of NO_x and as such are also important to the formation of tropospheric ozone. Hydroxyl radicals (OH) are very important in atmospheric chemistry, as OH removes many trace gases from the atmosphere and these reactions are often the rate determining step for trace gas removal. This means that only the few gases that do not react with OH can survive long enough in the troposphere to be transported to the stratosphere (e.g. chlorofluorocarbons). The production of OH in the atmosphere is a two-step reaction where in the first step near-ultraviolet light photolyses O_3 producing an O atom in its first excited state; singlet oxygen ($O(^1D)$) where all electron spins align:

$$O_3 + \text{light}\ (\lambda < 340\text{nm}) \rightarrow O(^1D) + O_2$$

The $O(^1D)$ atom has enough excitation energy to overcome the activation barrier and react with water vapour to produce OH (reaction [R1]). Hydroperoxyl radicals (HO_2) are usually produced when OH reacts with trace gases in the atmosphere. HO_2 then goes on to react with NO, which is oxidised to NO_2 and the OH radical is reformed (reaction [R2]) (Ball, 2014; Flynn, 2003; Pitts et al., 1969):

$$O(^1D) + H_2O \rightarrow 2\ OH \quad [R1]$$

$$HO_2 + NO \rightarrow OH + NO_2 \quad [R2]$$

Reaction R2 is also the pathway for NO_2 formation within engines. NO_2 can then undergo photolysis to reproduce NO (reaction [R3]), this also produces a ground-state oxygen atom ($O(^3P)$) that recombines with molecular oxygen to produce ozone (reaction [R4]). In reaction R4 M is any non-reactive species that can take up the energy released in the reaction to stabilise O_3 and prevent it from splitting apart immediately due to the excess of collisional energy initially present. Due to the abundance of N_2 and O_2 in the atmosphere, M is essentially either N_2 or O_2. Reactions R3 and R4 are the major pathway for O_3 formation in the troposphere, however there is only net production of O_3 if NO_2 is formed through reaction R2 (as it does not consume O_3). At ambient temperatures during daylight, another pathway for NO_2 formation is the reaction of NO with tropospheric O_3. O_3 is consumed

rapidly near sources of NO by this fast titration of O_3 (reaction [R5]) (Ball, 2014; Flynn, 2003; Mollenhauer & Tschoeke, 2010a; Pison & Menut, 2004):

$$NO_2 + \text{light}\ (\lambda < 420\text{nm}) \rightarrow NO + O(^3P) \quad [R3]$$

$$O(^3P) + O_2 + M \rightarrow O_3 + M \quad [R4]$$

$$NO + O_3 \rightarrow NO_2 + O_2 \quad [R5]$$

Reaction R5 is effectively reversible during daylight hours as NO_2 absorbs UV radiation and decomposes back to NO and O_3. This produces a photochemical equilibrium between these four gases, in urban areas where O_3 is depleted the equilibrium shifts in favour of NO (Colls & Tiwary, 2009). This equilibrium is also impacted heavily by the presence of volatile organic compounds (VOCs) in the atmosphere as OH reactions initiate the degradation of these compounds forming HO_2, shifting the equilibrium toward NO_2 and O_3. Another source of tropospheric O_3 is the diffusion of naturally occurring O_3 from the stratosphere. This exchange is estimated to account for 30-40 % of the total tropospheric O_3 burden. However, it is uncertain how much of this permeates to the surface and therefore the impact of this O_3 is likely less than previously discussed O_3 produced through the photochemical NO_x and VOCs pathways (Colls & Tiwary, 2009; Seigneur, 2019).

1.2.1.2 Night-time NO_x and O_3 chemistry

In light deprived conditions the main pathways producing O_3 and OH radicals are almost entirely stopped. Another oxidant takes over the role of OH in these conditions, the nitrate radical (NO_3). NO_3, like OH is an important oxidant for trace gases in the atmosphere. However, NO_3 is less reactive than OH and mostly reacts with carbon-carbon double bonds. As concentrations of NO_3 are typically found to be two orders of magnitude greater than OH comparable amounts of unsaturated VOCs can be oxidised. NO_3 is produced through the reaction of O_3 with NO_2, NO_3 then further reacts with NO_2 to produce dinitrogen pentoxide (N_2O_5) in the presence of N_2 and O_2 (M) (Ball, 2014; Mentel et al., 1996; Wallington et al., 1987):

$$\mathrm{NO_2 + O_3 \rightarrow NO_3 + O_2}$$

$$\mathrm{NO_3 + NO_2 + M \rightleftharpoons N_2O_5 + M}$$

During daytime, the reaction producing NO_3 undergoes rapid photolysis and therefore both NO_3 and the subsequent N_2O_5 are supressed during daylight hours. The products of NO_3 oxidation of trace gases are organic nitrates containing alcohol, peroxide, or carbonyl groups that have low vapour pressures and they therefore deposit onto atmospheric particles generating secondary organic aerosols (SOA). More SOA is produced through the NO_3 and VOC reactions than through the daytime OH / VOC reactions (Ball, 2014).

The primary sink for NO_x is oxidation to nitric acid (HNO_3), this can happen during both the day and night and results in NO_x having a lifetime of about a day. In the daytime:

$$NO_2 + OH + M \rightarrow HNO_3 + M$$

At night, HNO_3 is formed through N_2O_5 reacting heterogeneously with water vapour:

$$N_2O_5 + H_2O \rightarrow 2\,HNO_3$$

Due to NO_2 being consumed to produce N_2O_5 and the subsequent loss of N_2O_5 to HNO_3 this process limits the amount of NO_2 available for O_3 production during the next day. The daytime and night-time nitric acid sinks remove about the same amount of NO_2 from the atmosphere. HNO_3 is highly soluble and so can be removed easily from the atmosphere by precipitation (Ball, 2014; Colls & Tiwary, 2009; Mentel et al., 1996; Seigneur, 2019).

To summarise the previous sections, the main gaseous oxidants are OH and O_3 during the day and NO_3 and O_3 during the night (Ball, 2014).

1.2.1.3 Particulate matter

Particulate matter is a complex mixture of suspended solid and liquid particles in the air. These particles have large variation in terms of size, composition, and impact on environmental and human health. The chemical species found in PM include both primary and secondary pollutants, inorganic and organic species. These species may be

anthropogenic or biogenic. PM has slow sedimentation speeds and may remain in the air for days or may be washed out by precipitation shortly after forming. This wide ranging variability in particle size and composition as well as the negative impacts of the particles on human health, loss of visual range through smog, damage to vegetation, and its role in the climate system makes the study of PM very important (Colls & Tiwary, 2009; Gurjar et al., 2010; Seigneur, 2019).

There are two main definitions of particle size, which differ by how they measure particle density. The Stokes diameter is the diameter of a spherical particle that has the same density and sedimentation velocity as the particle of interest. The aerodynamic diameter is the diameter of a spherical particle with a fixed density of 1 g cm^{-3} that has the same sedimentation velocity as the particle of interest. For this project particle size refers to the aerodynamic diameter (Seigneur, 2019).

Particle diameters can range from a few nanometres (nm) to a few micrometres (µm). For the purposes of research and mitigation PM is grouped into three size categories, being PM_{10} (diameter of less than 10 µm) which contains larger primary particles such as brake dust or sea salt particles (particles that are larger than this tend to settle from the atmosphere relatively quickly). The next size fraction is $PM_{2.5}$ or the fine fraction (diameter of less than 2.5 µm), this fraction is small enough to reach the deepest parts of human lungs. The last size fraction is PM_1 or the ultrafine fraction (diameter of less than 0.1 µm), these particles are often new particles formed by the nucleation of atmospheric trace gases and are small enough to enter the bloodstream through the lungs (Colls & Tiwary, 2009; Gurjar et al., 2010; Seigneur, 2019).

Figure 1-1 shows a hypothetical distribution of particles of different size with the contributions to total particle number, surface area, and volume / mass. Typically there are three modes in the particle size distribution. The nucleation mode occurs when new particle are formed from gaseous molecules, these particles grow via condensation of other gaseous molecules and coagulation with other nucleated particles. The nucleation mode results in a large number of low mass particles with an aerodynamic diameter less than 0.1 µm. Primary emissions of fine particles and dynamic processes such as condensation and coagulation results in the accumulation mode, which mostly occurs in the size range of 0.1 – 1.0 µm. This mode leads to particle growth and an increase in particle surface area, particle dynamics favour these fine particles due to their greater numbers and larger available surface area. The last mode is the coarse mode which results from direct emissions of larger particles and is characterised by larger particle mass with lower particle numbers. Condensation and coagulation have little effect on the coarse mode due to the lower number and surface area of larger particles compared with fine particles (McClellan & Miller, 1997; National Research Council (US) Committee on Research Priorities for Airborne Particulate Matter, 1998; Seigneur, 2019).

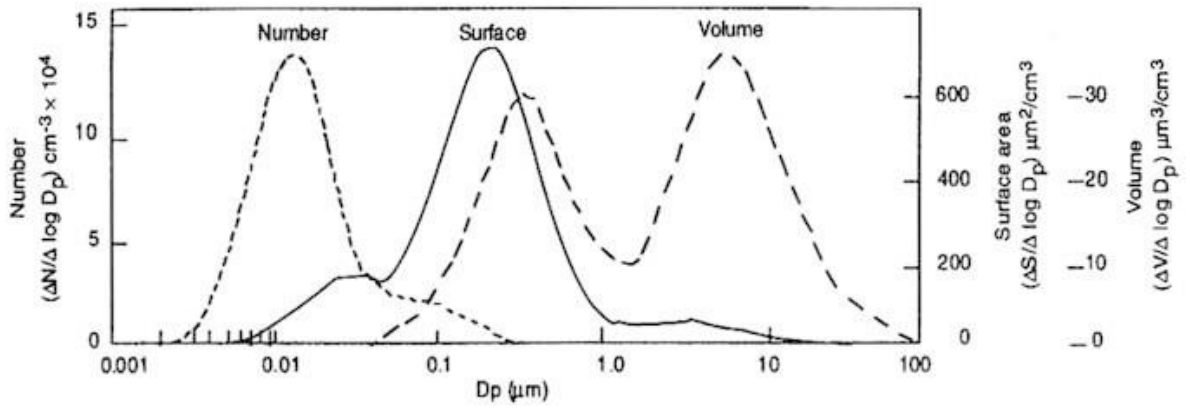

Figure 1-1: A hypothetical distribution of airborne particle diameters as described by particle number, particle surface area, and particle volume (or mass). D_p refers to the aerodynamic diameter of the particle. Particles with a diameter < 0.1 µm are in the nucleation mode, those between 0.1 – 1.0 µm are in the accumulation mode. (McClellan & Miller, 1997; National Research Council (US) Committee on Research Priorities for Airborne Particulate Matter, 1998).

By total mass, the largest emission of PM globally is sea salt from the Earth's oceans. Other large-scale natural sources of PM are soil and sand dust, particularly through wind action in arid regions. These sources are the largest fraction of PM mass globally primarily due to their particle size as can be seen in Figure 1-1, however the number of these particles is much lower than those in the fine and ultrafine fraction. Particle number concentration is given in number of particles per cm^3 of air. This can range from tens of particles per cm^3 in remote regions to millions of particles per cm^3 in more polluted urban areas. Although PM_{10} is a large mass fraction it has less of an impact on mortality from PM exposure than the smaller fractions for multiple reasons such as:

- Having a lower particle number concentration.
- Smaller surface area.
- Decreased presence of secondary PM.
- The inability of these larger particles to travel into deeper areas of the lungs.

(Griffin, 2013; National Research Council (US) Committee on Research Priorities for Airborne Particulate Matter, 1998; World Health Organisation Regional Office For Europe, 2013).

There are many primary anthropogenic sources of PM including:

- Petrol and diesel internal combustion engines.
- Solid fuel combustion for power generation, industry, and household heating / cooking. Such as coal, biomass, or heavy oil.
- Other industrial activities, these are wide ranging but include activities such as mining, building, smelting of ores, waste management, and zinc coating industries.
- Agricultural sources, primarily stubble burning of crop residues after harvest and wind transport of pesticides and fertilisers.

- Road dust which is a combination of road surface erosion through road traffic and the abrasion of brake pads and tyres.

Anthropogenic sources account for some of the most toxic components of PM such as polycyclic aromatic hydrocarbons (PAHs), black carbon, and metals (including cadmium, copper, nickel, and zinc). Some of the gaseous species discussed previously are precursors to the secondary fraction of PM, these are: NO_x, SO_2, VOC, and SVOC (semi-volatile organic compounds). This secondary fraction is generally the dominant mass fraction of fine particles. Chloride, nitrate, and ammonium (source for ammonium is agriculture) make up most of the secondary inorganic compounds found in PM. Atmospheric PM contains many secondary organic compounds, this fraction of PM is called secondary organic aerosol (SOA). The semi-volatile fraction of organic emissions from combustion processes such as biomass burning, and vehicle engines may be an important source of SOA. SOA can also be formed from the photooxidation of biogenic precursors such as isoprene, α-pinene, and β-caryophyllene. These species can condense onto a soot core and may also be oxidised into SVOCs which due to their higher molar mass are more likely to condense (Z. Fang et al., 2017; Gurjar et al., 2010; Pietrogrande et al., 2018; Seigneur, 2019; Tuet et al., 2017; World Health Organisation Regional Office For Europe, 2013).

The condensed species make up the secondary fraction of photochemical PM. These physical and chemical processes favour the accumulation of particles in the range of 0.1 – 1 µm, resulting in photochemical PM being fine particles. These fine particles can cause more significant adverse health effects than larger particles due to the ability of the particles to reach deeper parts of the lungs. Particulate matter is also associated with poor visibility, this is due to the fine particles scattering and absorbing light passing over them. Some of the

particles also contain a core of soot (primary PM emitted from combustion, a combination of EC and associated organic compounds) which is strongly light absorbing, further degrading visibility (Seigneur, 2019).

1.2.2 Health and economic impacts of air pollution

Air pollution is a major cause of premature mortality and disease globally. These deaths occur mainly in the form of heart disease, chronic obstructive pulmonary disease, stroke, lung cancer, and acute respiratory infections in children. PM, O_3, NO_2, and SO_2 are species with the largest body of evidence for public health impact. Air pollution also damages livestock, plants and some historical buildings, a large pathway for this damage was found to be the formation of acid rain from atmospheric SO_2 and NO_x. This damage to plant life was first brought to attention by the destruction of forests in Europe and North America during the 1970s due to deposition of sulphuric (H_2SO_4) and nitric acid (HNO_3), which mobilised the nutrients in the soil allowing them to be washed away whilst providing the roots access to some toxic metals (Gurjar et al., 2010; Seigneur, 2019; World Health Organisation, 2020a).

1.2.2.1 Health effects of NO_x exposure

NO_x can travel to all parts of the respiratory system due to its low solubility in water and therefore it cannot be effectively removed in the upper respiratory tract. NO_x disrupts the structure and functions of alveoli in the lungs by diffusing through the alveolar cells and adjacent capillary vessels. The US EPA has reported a causal link between short-term NO_2 exposure and respiratory effects, specifically the ability of NO_2 to independently trigger asthma attacks. This is due to reactive species that form from the reaction of NO_2 and antioxidants in the lungs. These reactive species can enhance airway responsiveness and allergic inflammation, decreasing lung function. There is also evidence of a causal or likely

causal relationship between NO_x exposure (frequently measured as NO_2) and impaired host defence systems, respiratory morbidity, and increased hospital visits. The main uncertainty in these relationships is whether these effects of NO_x exposure are independent of other traffic related pollutants (Boningari & Smirniotis, 2016; Peel et al., 2013; U.S. EPA, 2016).

1.2.2.2 Health effects of ozone exposure

The health effects of ozone exposure have been especially important in the last couple of decades due to the increase in ozone exposure around the world mostly in developing counties, such as a 11.9 % increase in ozone concentration (37.23 ppb increasing to 41.67 ppb) found by Dang & Liao, 2019 in eastern China for the period 2012-2017. Y. Wang et al., 2020 reported a 14 % increase in the 8-hr average ozone exposure (37.5 ppb to 42.9 ppb) for the period of 2013-2017 at a national level. This increase was occurring even as clean air actions reduced the concentration of $PM_{2.5}$ by 21.0 % during the same period. Weschler, 2006 reported that even short-term exposure to ozone can result in an increase in mortality rate with a 0.39-0.41 % increase in mortality per 10 ppb increase in 1-hr daily maximum ozone. Aside from deaths due to air pollution another health metric reported is DALYs (disability-adjusted life years), which can be thought of as the number of healthy years lost to disease. An example of an air pollution DALY would be the number of years spent suffering from lung cancer caused by air pollution exposure. The 2016 Global Burden of Disease (GBD) study reported that 4.1 million DALYs were attributable to ozone exposure in 2015, rising to 6.2 million in 2019. The breakdown of the 2019 ozone related DALYs are shown in Figure 1-2, by age group and sex. Figure 1-2 shows that ozone exposure predominantly affects the older population and impacts males more than females in terms of years of life lost (YLLs, number of deaths multiplied by the standard life expectancy at

time of death) (Dang & Liao, 2019; Forouzanfar et al., 2015; Global Health Metrics, 2020; Nuvolone et al., 2018; Weschler, 2006; World Health Organisation, 2020b).

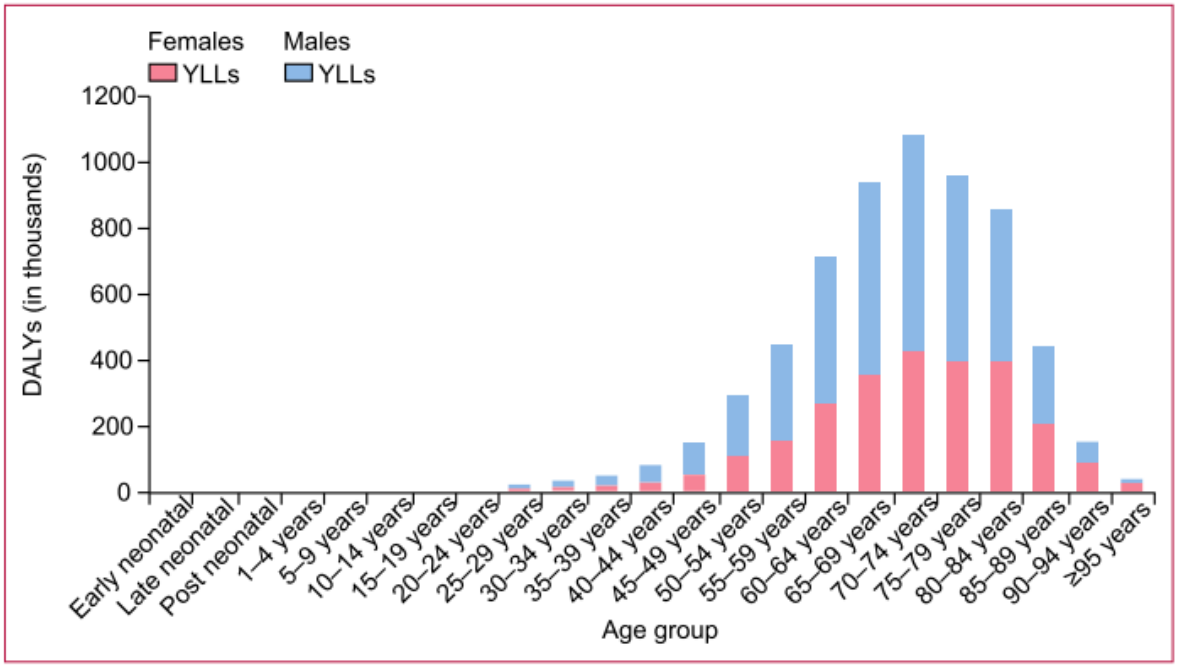

Figure 1-2: Composition of attributable global DALYs by YLLs and YLDs (years lost to disease), age group, and sex, 2019 (Global Health Metrics, 2020)

The only confirmed pathway of ozone absorption into the human body is through inhalation, where it is mostly absorbed by the upper respiratory tract. Ozone, like NO_x has a low solubility in water, this means that it cannot be effectively removed from the upper respiratory tract. Therefore the majority of inhaled ozone reaches the lower respiratory tract and dissolves in the epithelial lining fluid (ELF), a thin layer of fluid covering the epithelial surface which contains antioxidants such as glutathione, uric acid, and ascorbic acid. The ELF is likely the first defence against inhaled toxic pollutants such as ozone, NO_x, and PM. Kelly et al., 1996 found that when the ELF is exposed to environmentally relevant concentrations of ozone and NO_2 these antioxidants are consumed. The amount of ozone able to reach the tissue surface is influenced by the thickness of the ELF. Ozone that makes

it past the ELF is able to react with the tissue and penetrate into the respiratory tract (F J Kelly et al., 1996; Nuvolone et al., 2018).

The reaction of ozone with the components of the ELF form various secondary oxidation products with differing reactivity, reducing the amount of ozone able to reach the tissue surface. The formation of these secondary oxidation products is strongly dependent on the concentration of antioxidants and other substances in the ELF. These secondary oxidation products induce oxidative stress in the respiratory tract and may cause cellular injury, altered cell signalling, and an inflammatory cascade that occurs following exposure to ozone. People with pre-existing pulmonary disease, such as asthma or chronic bronchitis, are at a higher risk of ozone related health effects due to the difference in the quantity of absorbed ozone (Nuvolone et al., 2018). Bell et al., 2014 found that the most robust susceptibility factor for ozone exposure is age, with the elderly having major health risks with ozone exposure.

1.2.2.3 Health effects of particulate matter exposure

The State of Global Air, 2019 reported that 2.9 million deaths globally were attributed to ambient $PM_{2.5}$ exposure in 2017. Household air pollution from the burning of solid fuels such as wood, crop waste, and dried animal dung resulted in an additional 1.6 million deaths. This makes air pollution exposure the 5^{th} ranked risk factor globally by total number of deaths in 2017 (Health Effects Institute, 2019).

Household air pollution can consist of high concentrations of PM, carbon monoxide, NO_2, as well as volatile and semi-volatile organic species. Exposure to high concentrations of indoor PM significantly increases the rate of acute respiratory infections, particularly in women and children who are often exposed for longer periods of time in developing countries. A

significant proportion of the deaths attributed to indoor air pollution are due to chronic obstructive pulmonary disease (COPD) and lung cancer in women. Kulkarni et al., 2005 performed a study comparing the alveolar macrophages carbon loading of women and children exposed to biomass PM in Gonar, Ethiopia to women and children exposed to fossil fuel PM in Leicester, UK. The study consisted of 10 women and 10 children from Ethiopia and 10 women and 10 children from the UK. It was found that the women in Ethiopia had almost 13 times greater carbon surface area in their lower respiratory tract than the women in the UK, for the children it was 7.5 times higher in Ethiopian children compared to UK children (Forouzanfar et al., 2015; Kulkarni et al., 2005; Mudway et al., 2005; Viegi et al., 2004).

Epidemiological studies have also demonstrated that long term exposure to PM can promote and increase the vulnerability of atherosclerotic plaques (the build-up of plaque on the inside of arteries). This is a potential mechanism by which PM exposure could trigger cardiovascular morbidity and mortality (Kelly et al., 2012; Künzli et al., 2005).

The capacity of inhaled PM to induce localised and systematic inflammation through oxidative stress processes in the nose, lungs, and cardiovascular system has emerged as a unifying hypothesis to explain the acute and chronic health effects seen in populations exposed to high PM concentrations. There are several pathways for inhaled particles to generate reactive oxygen species (ROS) in the lungs:

- Through the direct inhalation of oxidising species such as redox active transition metals. These species are capable of catalysing oxidation reactions in the lungs producing ROS, through the reduction of oxygen by biological reducing agents found inside the cells such as nicotinamide adenine dinucleotide (NADH).

- PAHs absorbed onto the PM surface can undergo biotransformation in vivo to generate ROS.
- Volatile organic compounds may be metabolically activated to ROS in vivo.
- Redox cycling of particle bound quinones which produces the reactive oxygen species: superoxide anions ($O_2^- \cdot$) and hydrogen peroxide (this redox cycling is shown in Figure 1-10 in section: 1.3 Oxidative potential).

It is believed that high levels of oxidative damage occurs when the body's antioxidant defence is overwhelmed. This damage can lead to damage to the epithelial cells and lead to cell death. The ultrafine portion of PM is also able to cross the lung-blood barrier into the blood stream due to its size, charge, and chemical composition (Du et al., 2016; Guilbert et al., 2019; Kelly & Fussell, 2012; Mudway et al., 2005; Simonetti et al., 2018; Valavanidis et al., 2013).

1.2.2.4 Socioeconomic effects on air pollution exposure

There is a strong inverse relation between a population's exposure to $PM_{2.5}$ and the social and economic development of the country, as shown in Figure 1-3, resulting in less-developed countries suffering $PM_{2.5}$ concentrations that can be 4-5 times those found in more-developed countries. However, ozone exposure is similar across the sociodemographic index with the highest population-weighted exposure being in high income countries, this is likely due to higher NO_x emissions in these countries (Health Effects Institute, 2019).

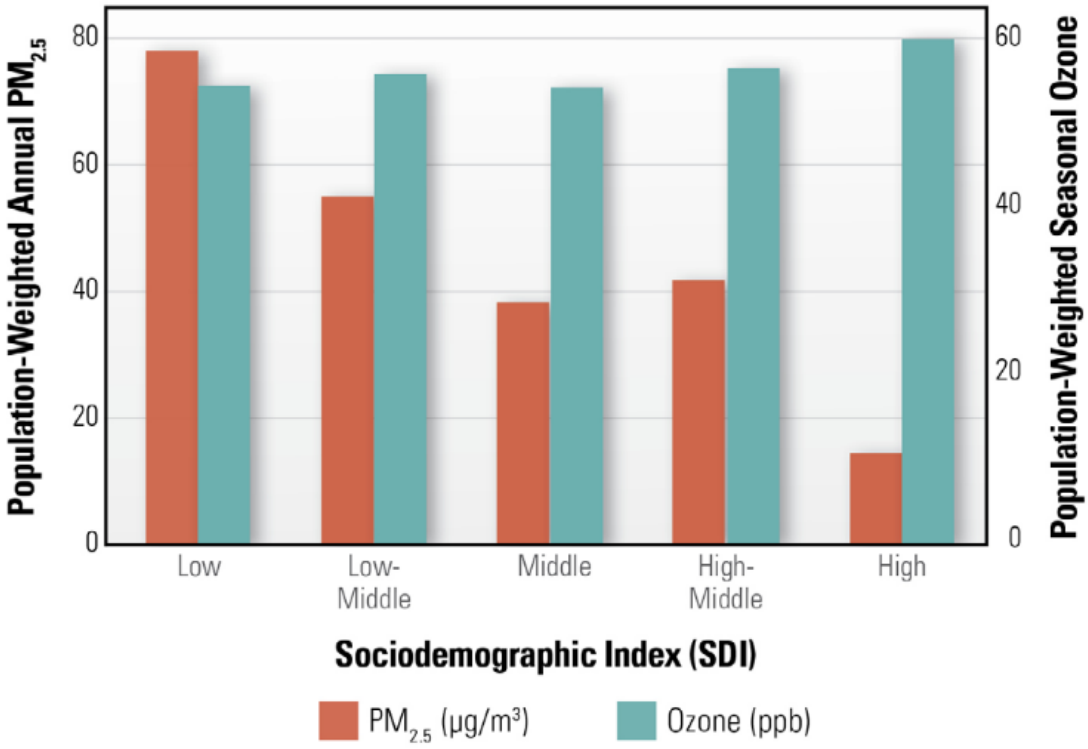

Figure 1-3: Trends in pollution concentrations by sociodemographic index for population-weighted annual average PM2.5 and population-weighted seasonal average ozone (Health Effects Institute, 2019).

Socioeconomic status within countries also contribute to different susceptibilities to air pollution exposure due to various factors such as the higher prevalence of pre-existing diseases, limited access to fresh foods and vitamins, and reduced or differential access to medical care. Epidemiological studies have reported increased risk of mortality from short-term $PM_{2.5}$ exposure in low socioeconomic status groups (using median household income in the United States). Air pollution exposure may also differ between different racial-ethnic groups due to socioeconomic status and proximity to major roads. In the US in 2009 17.5 % of the total year-round occupied housing units were within 300 feet (92 meters) of a 4+ lane highway, airport, or railroad. The percentages were higher for households below the poverty line (22 %), Hispanic households (22 %), and African-American households (25 %) (Peel et al., 2013; Sacks et al., 2011).

1.2.3 Air pollution impact and legislative response in China, India, and the United Kingdom

The following section covers the impact and legislative response to air pollution in the countries sampled as part of this project: China, India, and the United Kingdom. The concentration of most air pollutants rose rapidly in most industrialised countries in the first half of the 20th century due to the increased use of fossil fuels and rapidly growing demand for energy and mobility. The first major legislation in the UK to focus on mitigating the negative health effects of air pollution was the 1956 Clean Air Act. The catalyst for passing this legislation was the London smog episode of 1952, where thick smog settled over London during December 1952. This resulted in between 4,500 – 13,500 deaths attributed to the event in the months after. The concentration of most pollutants have decreased in the majority of high income countries due to air pollution control policies, and improved fuel and pollution abatement technology such as three-way catalytic converters. In recent decades a major pollutant of concern for the UK was the rise in NO_x concentration due to the increase in road transport and expansion in diesel usage. With increasingly stringent emissions standards and catalytic converters the mean concentration of NO_x in the UK has been decreasing since 1990. This decrease in NO_x has likely led to the rise seen in mean surface ozone concentration. However, there is a negative trend in maximum annual ozone indicating fewer extreme ozone events over time. Finch & Palmer, 2020 suggest that the notably sharper rise in ozone since 2016 may be due to recent hemispheric changes in tropospheric ozone, as the rise is seen in sites across the UK. Air pollution killed 25,000 people in the UK in 2017 (Health Effects Institute estimate) with 485,000 DALYs, this accounts for 4.7 % of all UK deaths in 2017. The Committee on the Medical Effects of Air Pollution (COMEAP), which advises the government on all matters concerning the health

effects of air pollutants, estimated premature deaths attributable to air pollution in 2013 ranged from 28,000 to 36,000 (M. Bell et al., 2004; Carnell et al., 2019; COMEAP, 2018; Finch & Palmer, 2020; Health Effects Institute, 2019).

China and India had the highest mortality burden attributable to air pollution in 2017, with 1.2 million deaths each, far surpassing the country in third place: Pakistan with 128,000 deaths and accounting for 50.6 % of all global air pollution deaths. India experienced higher DALYs of 38.7 million compared with 28 million for China, accounting for 26.3 and 19 % of global DAILYs respectively (Health Effects Institute, 2019).

1.2.3.1 Air pollution impact in China

Of the deaths attributable to ambient $PM_{2.5}$ exposure in China the five most important causes are in order of deaths caused: stroke, ischemic heart disease (IHD), lung cancer (LC), COPD, and lower respiratory infection (LRI). Deaths caused by ambient $PM_{2.5}$ increased continuously from 1990 to 2013 rising to a high of 916,000. The first Action Plan for Air Pollution Prevention and Control, issued by the state council in 2013 set air quality targets through reducing reliance on coal, controlling the number of vehicles in some cities, cutting industrial emissions, and increasing the number of lower emission energy sources. Through these actions the deaths attributable to ambient $PM_{2.5}$ decreased to 852,000 in 2017 (Health Effects Institute, 2019). Further work is required to improve air quality in China as the population weighted annual mean $PM_{2.5}$ concentration is still higher than the global average and the WHO's least stringent target (IT-1, 35 μg m^{-3} $PM_{2.5}$). There has also been limited reach of the actions taken in China as ozone exposures have remained largely untouched, as can be seen in Figure 1-4 the annual deaths attributable to ozone exposure

have been increasing since 2013 (GBD MAPS Working Group, 2016; Health Effects Institute, 2019).

Poor air quality in China also leads to an economic impact on the nation due to the increased cost of health expenditure, life loss, and lost productivity. In the years 2015, 2016, and 2017 the economic value of health loss due to air quality represented 4.34 %, 4.07 %, and 3.85 % of gross domestic product (GDP) in China (Guan et al., 2019). Xie et al., 2019 estimates that without adequate control policies the economic cost due to $PM_{2.5}$ pollution in 2030 could be 12,900 billion Chinese Yuan (CNY, ~ 1.5 billion GBP) (Guan et al., 2019; Xie et al., 2019).

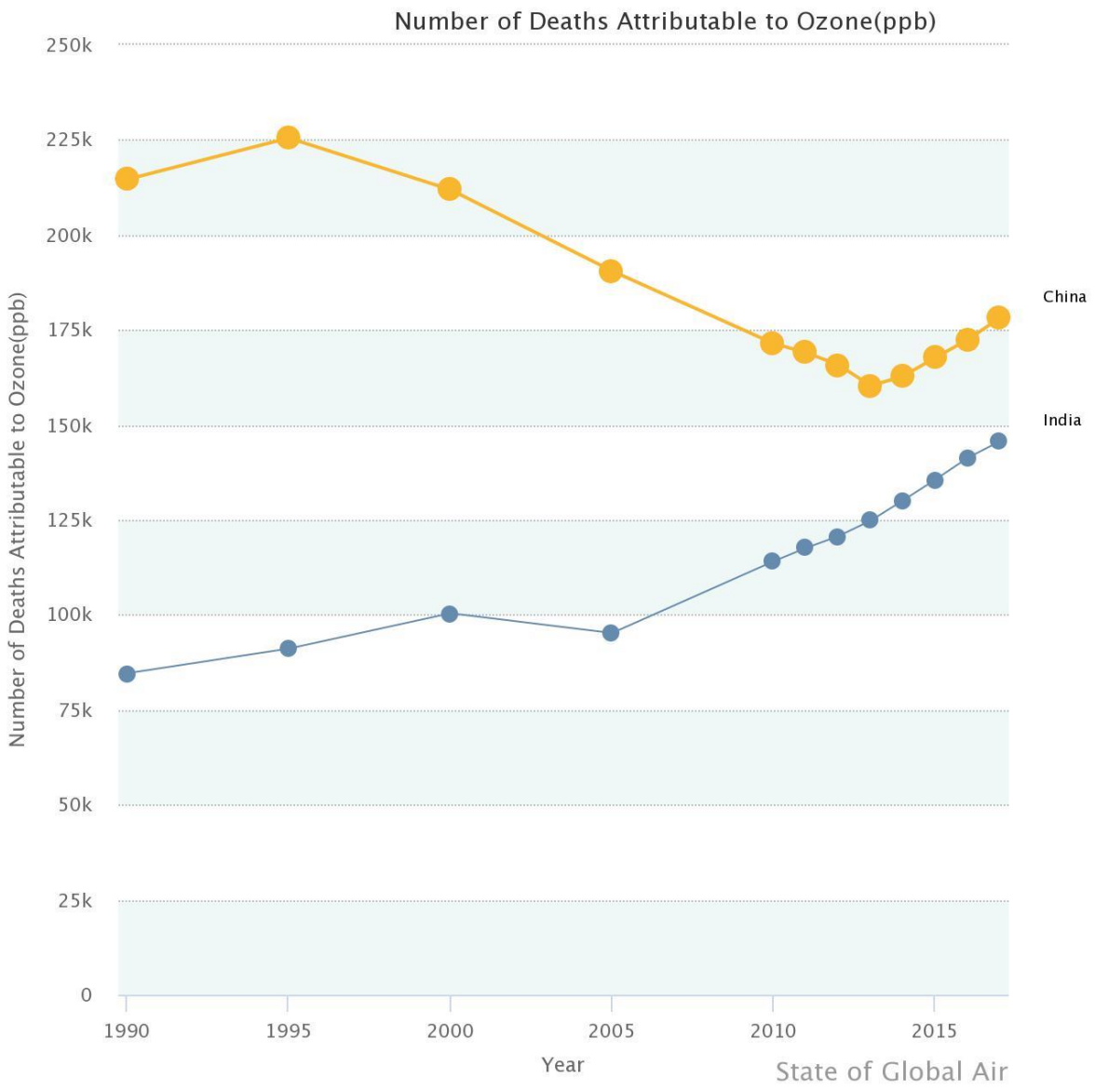

Figure 1-4: Comparison of deaths attributable to ozone exposure in China and India over 25 years (Health Effects Institute. 2019. State of Global Air 2019. Data source: Global Burden of Disease Study 2017. IHME, 2018).

1.2.3.2 Air pollution impact in India

In 2017, the population-weighted annual average $PM_{2.5}$ concentration in India was 91 µg m^{-3} almost three times higher than the WHO's least stringent interim target (IT-1 < 35 µg m^{-3}). With 84.8 % of the population exposed to $PM_{2.5}$ levels above IT-1, 93.7 % exposed to levels exceeding IT-2 (< 25 µg m^{-3}), and 99.9 % exposed to levels exceeding IT-3 (< 15 µg m^{-3}). The five most important causes of deaths for which exposure to $PM_{2.5}$ is a risk factor are, in order of deaths caused: IHD, COPD, stroke, LRI, and LC. In 2017 these five causes accounted

for 38.5 % of all deaths in India (both sexes and all age groups) (GBD MAPS Working Group, 2018; Institute for Health Metrics and Evaluation, 2020; The World Bank Group, 2020).

The Health Effects Institute categorises deaths attributable to air pollution into three categories: ambient PM exposure, household air pollution from solid fuels, and ambient ozone pollution. In India in 2017 these accounted for 51.8 %, 37 %, and 11.2 % of the total 1.241 million deaths attributed to air pollution respectively. Deaths attributable to indoor air pollution in India are the highest in the world (481,700) and the proportion of deaths attributable to indoor air pollution are higher in India than China where 20.8 % deaths are caused by indoor air pollution. However, indoor air pollution deaths in India have been decreasing over the past few decades with a 30.4 % decrease since 1990. The main pollutant of concern in India is ambient $PM_{2.5}$, as can be seen in Figure 1-5 the deaths attributable to ambient $PM_{2.5}$ exposure in India has been increasing rapidly over the past decade whereas in China mitigation policies have slowed this growth (Health Effects Institute, 2019).

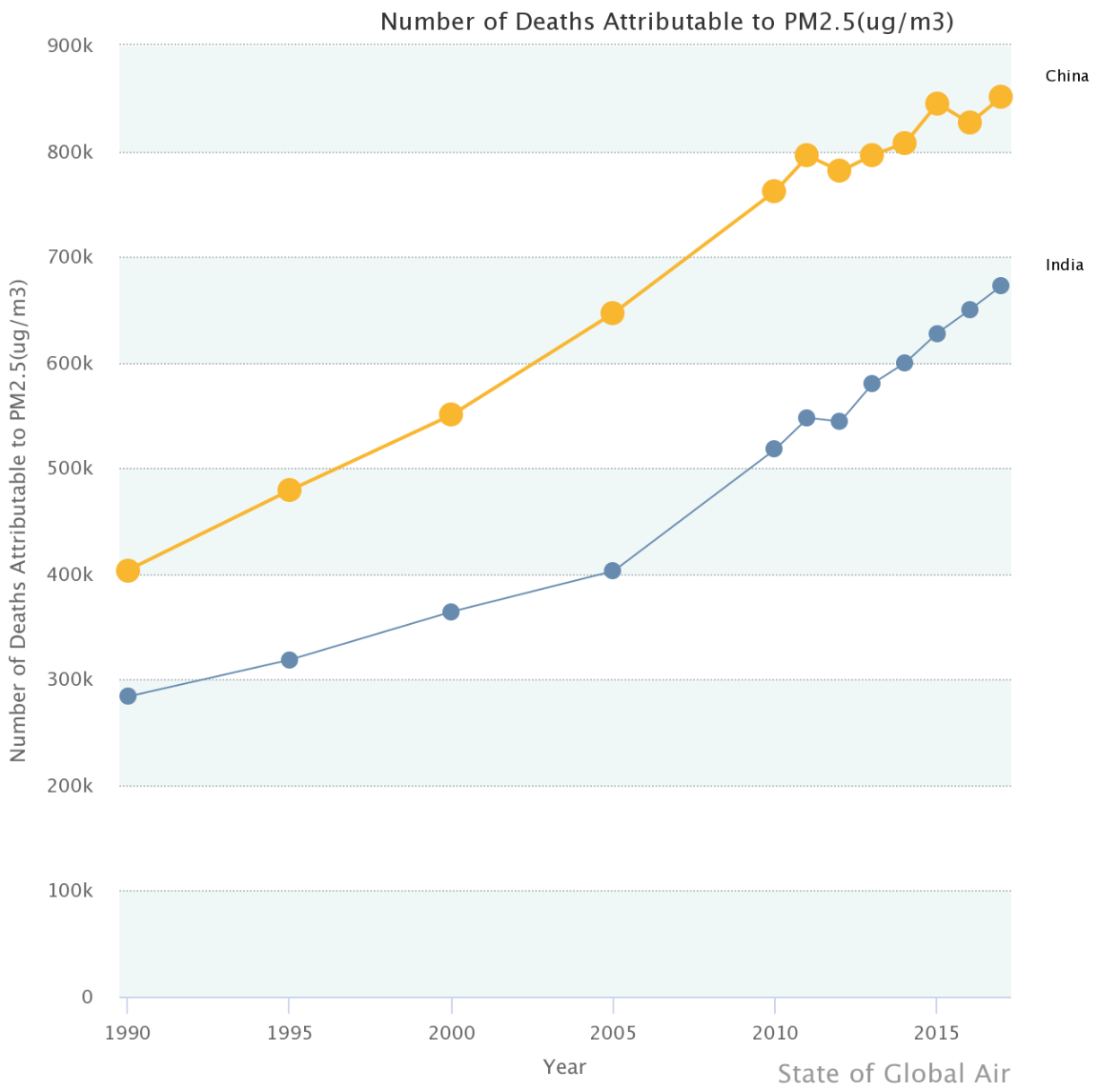

Figure 1-5: Comparison of deaths attributable to ambient $PM_{2.5}$ exposure in China and India over 25 years (Health Effects Institute. 2019. State of Global Air 2019. Data source: Global Burden of Disease Study 2017. IHME, 2018).

Although the contribution of ozone to air-pollution related deaths in India has been much smaller than that of $PM_{2.5}$ recent research has suggested that exposures to ozone in India are likely to continue to increase into the future. As can be seen in Figure 1-4 deaths attributed to ozone exposure in India have been increasing at a steady pace for the last decade (GBD MAPS Working Group, 2018).

The increasing numbers of deaths attributed to air pollution in India is also influenced by the growing and aging population, with an increase in the number of people with disorders that are affected by air pollution exposure, such as cardiovascular disease. According to analysis carried out by the World Bank and the Institute for Health Metrics and Evaluation (2016), the estimated economic loss due to air pollution in India was US$550 billion in 2013 due to lost labour and welfare losses (GBD MAPS Working Group, 2018).

Centralised air pollution mitigation in India is under the Air (Prevention and Control of Pollution) Act, 1981. This act assigned powers to Central and State Pollution Control Boards to monitor air pollutants and issue regulatory standards. Under this act, the central board adopted the National Ambient Air Quality Standards (NAAQS) in 1982, the first ambient air quality standards in India. This set standards for major pollutants such as NO_2, SO_2, CO, and O_3, with stricter standards introduced in 2009 to bring the NAAQS closer to WHO guidelines. A major problem for the NAAQS has been the lack of strict enforcement of the standards (GBD MAPS Working Group, 2018; Guttikunda et al., 2014).

There have been many programmes in India to reduce air pollution from specific sources. One of these programmes was a liquefied petroleum gas (LPG) subsidy for poorer households below the poverty line (income of less than $1.90 / day) to mitigate household air pollution introduced by the Ministry of Petroleum and Natural Gas in 2014. This programme increased the coverage of LPG from 56 % of households in 2014-15 to 73 % in 2015-16. Another example is the levying of fines for agricultural field burning introduced in the states of Punjab, Haryana, and Uttar Pradesh (GBD MAPS Working Group, 2018).

1.2.4 Meteorological factors that contribute to air pollution

Air pollution can have a significant spatial spread, depending on the lifetime of the species this can be regional or even global. More reactive pollutants will have a more limited spread due to their relatively short atmospheric lifetime, such as volatile vehicle emissions which have a residence time of a couple hours to 10 days. However, certain pollutants such as carbon monoxide (CO) have lifespans in the months allowing for more regional transport of these pollutants away from the emission source. Figure 1-6 shows a breakdown of various atmospheric pollutants by their residence times and spatial distribution. These range from species like OH which is consumed within ~ 1 second after forming to compounds like CFCs (chlorofluorocarbons) whose low reactivity allows them to be transported, over time into the stratosphere (Gurjar et al., 2010; National Research Council, 1998; Seigneur, 2019).

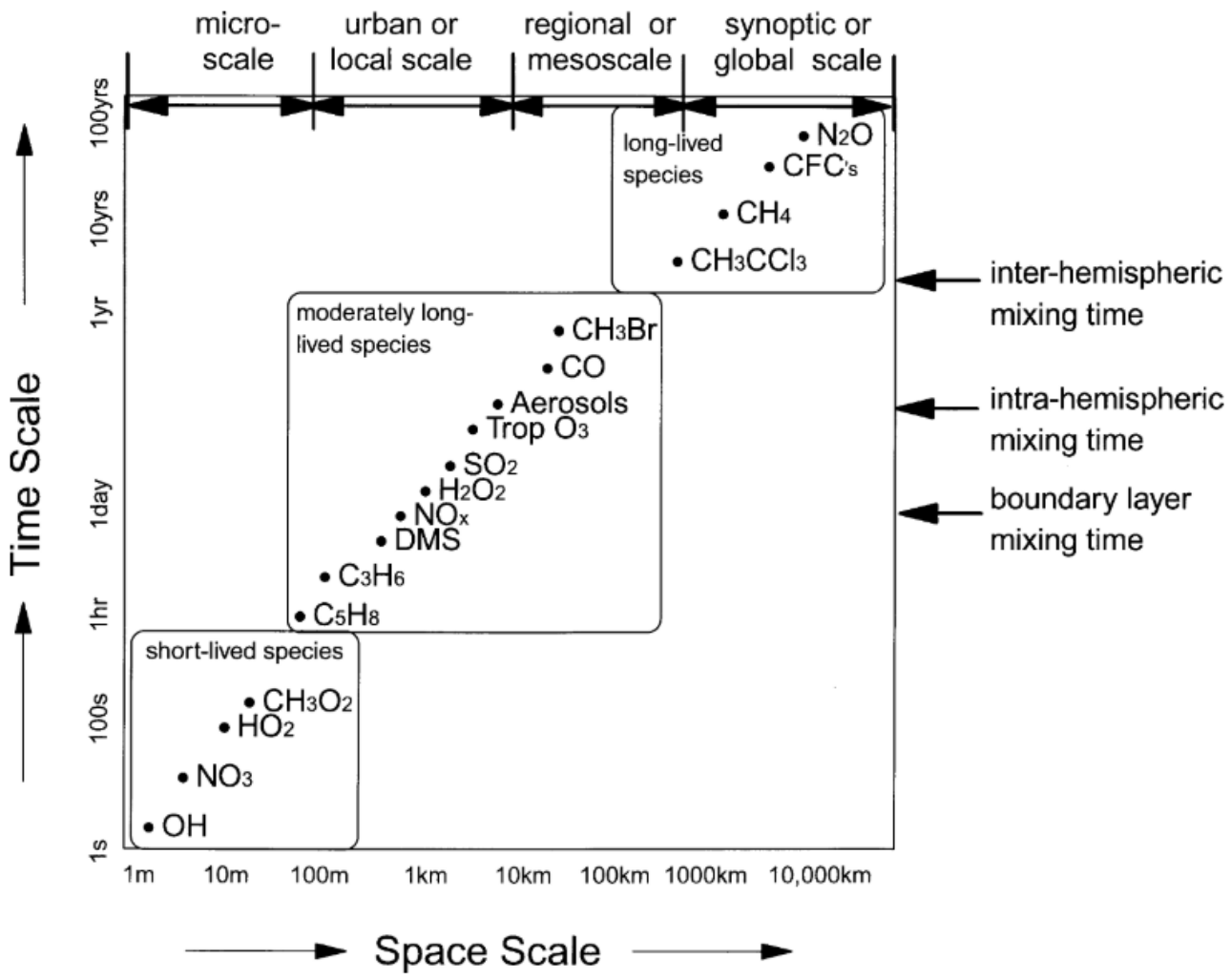

Figure 1-6: Spatial and temporal scales of variability of a number of key constituents in the atmosphere. Note: C_3H_6 = isoprene; C_5H_8 = isoprene; CH_3Br = methyl bromide; CH_3CCl_3 = methyl chloroform; CH_3O_2 = methyl peroxy radical; DMS = dimethyl sulphide; H_2O_2 = hydrogen peroxide (National Research Council, 1998).

The lifetime of atmospheric pollutants shown in Figure 1-6 are the general lifespan of these species, however most species exhibit a range of residence times depending on the physical and chemical properties of the locality. For example: tropospheric ozone, which typically has a lifetime ranging from several hours to a few days, however in the presence of NO (such as at roadsides) the ozone is converted to NO_2 and therefore the lifetime of ozone is reduced to a couple of minutes (Seigneur, 2019).

Particulate matter lifetime can vary significantly based on the particle size and meteorological conditions. As mentioned in the previous particulate matter section,

nucleation mode particles which are the highest number concentration particles are mostly lost to agglomeration as gases condense onto particle surfaces and particles coagulate together. The lifetime of the accumulation mode particles generated from this agglomeration is largely determined by precipitation. Finally the larger coarse mode particles are primarily lost to gravitational settling (Bloss, 2014; Seigneur, 2019).

1.2.4.1 Atmospheric boundary layer and surface temperature inversions

The atmospheric boundary layer is the lowest section of the atmosphere extending from the surface to a height of ~ 1-2 km, this is shown in Figure 1-7. This layer of the atmosphere is characterised by a near constant turbulent mixing generated by buoyant convection and / or wind shear. In contrast, the free troposphere above this layer is largely statically stable with limited small-scale turbulent mixing occurring, aside from the breaking of gravity waves caused by weather fronts and airflow over mountains (Feng et al., 2020; Fritts & Alexander, 2003; Mason & Thomson, 2015).

Vertical mixing is especially important in the boundary layer. A feature of the boundary layer is a frequently distinct interface at the altitude where the mixing of the boundary layer reaches the base of the stable free troposphere above. The atmospheric boundary layer is also affected by multiple processes such as:

- Coriolis forces produced by planetary rotation.
- Radiative heat transfer.
- Cloud formation.

Radiative heat transfer in the boundary layer is a daily cycle of sensible and latent heat fluxes between the land and air due to the radiative heating and cooling of Earth's surface. Under normal conditions the Earth's surface is heated by solar radiation, this heat is

transferred to the air at the surface causing this air to rise due to convection. As the air rises through the troposphere it loses heat to its surroundings at a rate of 9.8 K km^{-1}. At night, the Earth's surface loses its radiative heat quickly and cools the air at surface level. This causes temperature to increase with increasing height with the warmer air acting as a cap on the cooler air below, this is called a temperature inversion (Jacobson, 2005; Stull, 2017).

As the boundary layer is often turbulent and because turbulence causes mixing, warmer air from the top of the boundary layer is mixed with cooler air from near the bottom. This results in the boundary layer often having a uniform temperature over its entire altitude. In Figure 1-7 the free atmosphere refers to the section of tropospheric air above the mixed layer where the standard atmosphere temperature profile is retained. There is a sharp increase in temperature at the boundary of the mixed boundary layer and the free atmosphere above, this transition zone is very stable and is often a temperature inversion. The middle of this inversion is considered the top of the turbulent boundary layer and is given the symbol z_i (Mason & Thomson, 2015; Stull, 2017)

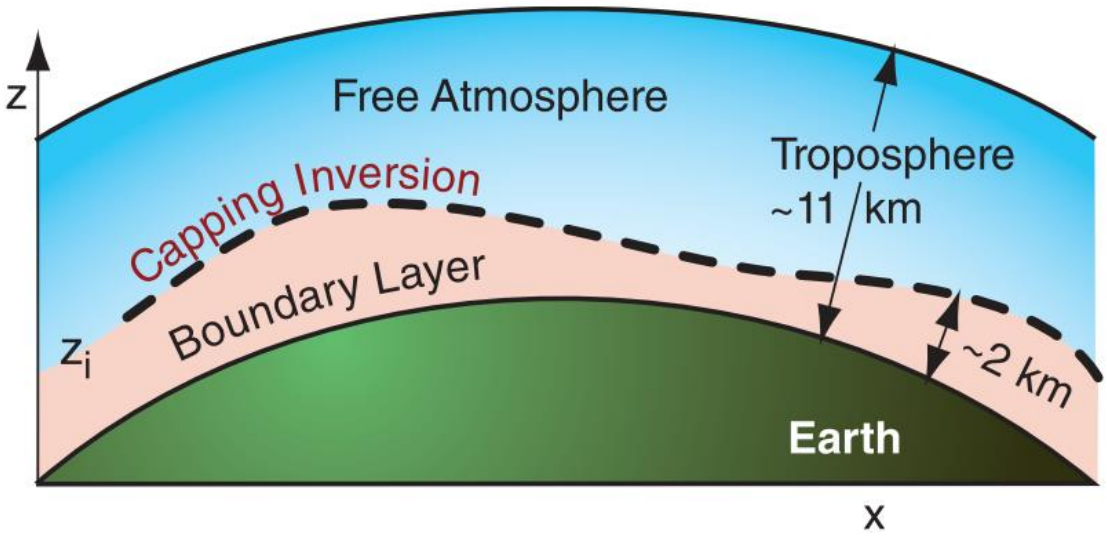

Figure 1-7: Location of the boundary layer, with the top at z_i (Stull, 2017).

The temperature difference between the boundary layer and the free atmosphere above can range from a few degrees to 25 ^{o}C in the strongest surface temperature inversions found in Antarctica. If an air parcel in the boundary layer were to be pushed out the top of the mixed layer by turbulence the pocket would be so much colder than the surrounding air that a strong buoyant force would push the pocket back down. Due to this lack of mixing during a temperature inversion, pollutants released into the atmosphere are concentrated in the boundary layer (Connolley, 1996; Stull, 2017).

The type of inversion mentioned above is a surface temperature inversion. These inversions are not very long lived as the inversion tends to be destroyed as the sun heats up the surface, correcting the temperature imbalance. They are however quite common, factors that are favourable for temperature inversion formation are:

- A clear and cloudless sky results in more rapid loss of heat from the surface.
- Dry air at ground level decreases the absorption of heat from the Earth's surface.
- Low wind speed limits the mixing of air in the boundary layer preventing a homogeneous temperature.
- A snow-covered surface results in the reflection of solar radiation, preventing the surface from heating up during the day.
- During long winter nights the loss of heat by terrestrial radiation can exceed the amount of solar radiation absorbed during the day.
- During the winter the angle of the sun in the sky is also lower, limiting the amount of solar radiation the surface receives.

Due to the multiple factors contributing to the atmospheric boundary layer the height of the boundary layer can vary from 200 m to 4 km above the ground. These inversions are

normally destroyed a few hours after sunrise as the surface is heated and the temperature profile normalises. This process takes longer if snow is covering the surface, reflecting solar radiation. Snow is also a bad conductor of heat and as such reduces the flow of heat from the ground to surface level air (Drishti, 2020; Feng et al., 2020; Jacobson, 2005; Stull, 2017).

Many valleys observe persistent inversions during the winter depending on their topography. In these locations the air pollution is exclusively of local origin. These persistent inversions can lead to severe haze events in cities that are located in valleys and basins as vertical mixing is blocked (Feng et al., 2020).

1.2.4.2 Impact of seasons and weather on air pollution

The weather and seasons play a vitally important role in the impact of air pollution on human health. From rain and wind removing pollutants through deposition and dispersion to the seasonal differences in energy consumption, changing the sources of air pollution. Many cities experience prolonged periods of cold weather during the winter months, depending on the city this can result in an increased use of personal vehicles, increased energy consumption for heating, and more persistent temperature inversions (Drishti, 2020; S. Wang et al., 2017).

In the North China Plain the cities Beijing and Tianjin often have $PM_{2.5}$ concentrations that are two times higher in the winter compared with those in the summer. This has mainly been put down to the increased combustion of coal for domestic heating in this region. However domestic heating is not the only cause for seasonal variation in $PM_{2.5}$ concentrations, as in southern Chinese cities such Shenzhen and Chengdu where domestic coal combustion is not widely observed significant seasonal variation in $PM_{2.5}$ concentration is still seen. These seasonal differences were likely caused by weaker winds, less

precipitation, and lower temperatures and boundary layer heights. In some tropical regions of China such as Lijiang where precipitation, temperature, and wind speed have less seasonal difference there is negligible difference between winter and summer $PM_{2.5}$ concentrations (Atony Chen et al., 2001; R. Li et al., 2019; M. Yu et al, 2014).

These examples show that there are varying impacts of seasonal variation in China, largely due to the size of the country and the different climates experienced across the country. Most developed countries in the world lie in the middle latitudes in the northern and southern hemispheres and as such, experience four distinct seasons: summer, autumn, winter, and spring. However, in the tropics region around the equator where temperature does not vary as much year round, many countries have two seasons; wet and dry. Such as India where the summer monsoon season accounts for 75-90 % of annual rainfall across the country and normally occurs from the 1st June to 30th September (Moon et al., 2017; Parthasarathy et al., 1987; Xavier et al., 2007).

In New Delhi seasons are often caterogised as winter (December – February), pre-monsoon (March – May), monsoon (June – August), and post-monsoon (September – November). Strong seasonal trends in air pollution are seen in India with the worst haze events usually seen in the winter with all pollutants decreasing during the monsoon season. This is due to the wet scavenging of air pollutants due to increased precipitation. Sahu and Kota, 2017 found that during 2011 – 2014 in New Delhi the winter season had very poor and severe (AQI measure based on $PM_{2.5}$, SO_2, O_3, NO_2, and CO concentrations) pollution days 72 % of the time compared with 32 % for the monsoon season (Bhaskar & Mehta, 2010; Sahu & Kota, 2017).

The effects of solar energy on the formation of pollutants such as ozone and the formation of secondary aerosols in PM have been discussed in the 1.2.1 Sources of air pollution section, showing the importance of sunny weather on air pollution. Higher temperatures have been shown to promote fugitive dust suspension through the drying of soils. Wind speed is also very important in modulating air pollution levels, through dispersion of pollutants at higher speeds and the accumulation of pollutants during stagnant times. Higher relative humidity (RH) has been shown to generally increase the number of haze events due to the gas phase to particle phase conversion of NO_x and SO_2 at high RH. RH also contributes to particle growth due to water uptake at high RH. Li *et al.*, 2019 reported that temperature and wind speed were major factors affecting the accumulation of PM and gaseous pollutants nationally in China during 2015 – 2016 (Cheng et al., 2016; R. Li et al., 2019a; Quan et al., 2014).

1.2.4.3 Regional transportation of air pollution

One of the major problems facing local authorities when trying to tackle air pollution is the varying impact of regionally transported pollution from sources outside of the city. Beijing is one example of a city which faces a significant air pollution burden from surrounding cities and as such the entire North China Plain (Beijing-Tianjin-Hebei region) is often looked at as a single air basin (Chang et al., 2019; P. Li et al., 2015).

Multiple studies looking at the impact of regional sources on the air quality in Beijing were carried out after its selection to be the host city for the 2008 Olympic Games. An *et al.*, 2007 reported that during a heavy air pollution episode during 3-7 April 2005, an average of 39 % of $PM_{2.5}$ was contributed by non-Beijing sources. To curtail air pollution during the games the Chinese government implemented strict control measures in Beijing such as:

- Banning ~ 300,000 heavily polluting vehicles from driving in the Beijing Municipality.
- Implementing an alternative day-driving scheme, where half of the city's 3.5 million vehicles were banned from the roads. Alternating days based on whether the last number of their licence plate was odd or even.
- The halting of all construction work within the city.
- Shutting down or reducing output from factories and coal-fired power plants in Beijing and Tianjin.

Air quality improved significantly during the games, especially for vehicle related compounds such as NO_x and VOCs. However, $PM_{2.5}$ and O_3 concentrations did not significantly decrease, with Wang *et al.*, 2010 reporting that during eight ozone pollution days regional sources from the south contributed 34-88 % of the peak ozone concentrations in Beijing (An et al., 2007; X. H. Liu et al., 2010; T. Wang et al., 2010).

Regional transport of air pollution into Beijing plays a more important role in the summer than the winter and may not be a significant source during the more polluted haze events. As these typically occur during stagnant conditions, with weak winds from variable sources. Chang *et al.*, 2019 concluded that during 2014 local contributions to $PM_{2.5}$ concentration in Beijing were dominant in January and March (62 % and 69 %) but during July and October local contributions only account for 33 % and 38 % respectively, with most of the $PM_{2.5}$ originated from a range of regions to the south (Chang et al., 2019; R. Zhang et al., 2015).

Sahu and Kota, 2017 also suggests that long range transport of air pollution affects New Delhi with air parcels mostly originating in Punjab and Haryana during the winters of 2011-2014. Possibly leading to the negligible weekday-weekend differences seen in the percentage of good – severe AQI days as shown in (Sahu & Kota, 2017).

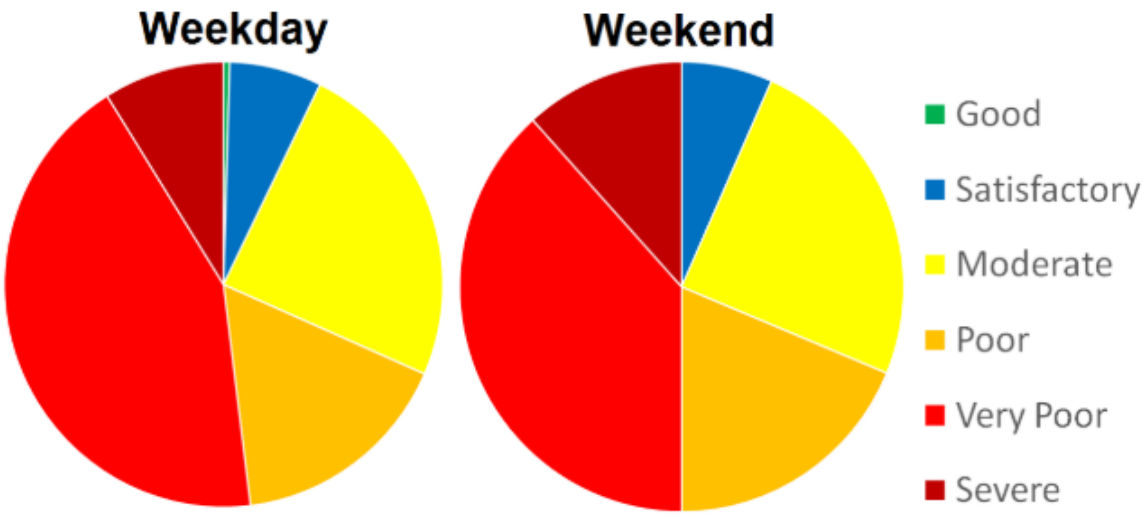

Figure 1-8: Days (%) in each IND-AQI category on weekdays and weekends. IND-AQI here consists of measurements of SO_2, NO_2, $PM_{2.5}$, CO, and O_3. Collected hourly at a busy traffic intersection continuously between 2011 – 2014 (Sahu & Kota, 2017).

1.3 Oxidative potential

As mentioned in previous sections there is a growing body of epidemiological studies linking increases in PM concentration with adverse health effects such as cardiovascular diseases and respiratory disorders. The mechanisms that drive these associations are not entirely clear but one biologically plausible mechanism that has been gaining epidemiological evidence is that of reactive oxygen species (ROS) driven oxidative stress in the human respiratory system (Bates et al., 2015; T Fang et al., 2015).

Oxidative stress occurs when the level of ROS produced in the human respiratory system by several types of aerosol overwhelms the natural antioxidant defences of the biological system (Patel & Rastogi, 2018a; Simonetti et al., 2018). ROS are chemical species with unpaired electrons (free radicals) and reactive molecules such as hydrogen peroxide, these species are derived from molecular oxygen and their formation is shown in Figure 1-9. These unstable species can readily react with other molecules in cells leading to DNA damage and possible cell death (Borlaza et al., 2018a).

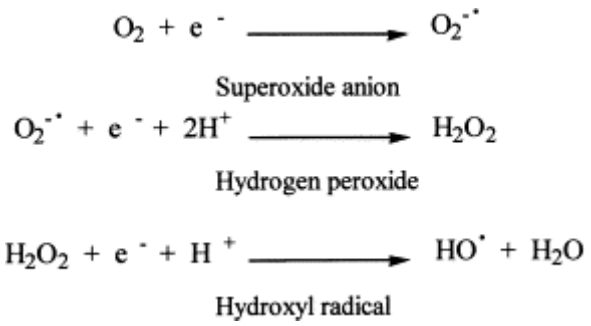

Figure 1-9: Formation of ROS from molecular oxygen (Magnani et al., 2000).

ROS can enter the respiratory system bound to particulate matter surfaces; however, a large part of ROS exposure is through ROS formation *in vivo* through the redox cycling of compounds such as quinones by the redox active compounds in PM (shown in Figure 1-10). $PM_{2.5}$ can generate large quantities of radicals *in vivo* depending on the particulate properties such as particle size, surface area, and composition. (Campbell et al., 2020; Chuang et al., 2011).

Toxicological studies have shown that inhaled PM has the ability to induce pro-inflammatory effects in the lungs and cardiovascular system by interfering in the oxidative stress processes (Li et al., 2003; Simonetti et al., 2018).

$PM_{2.5}$ exposure may stimulate excessive ROS production in cells and disturb the redox homeostasis; causing inflammation, DNA damage, and cell death (Wang et al., 2019; Xu et al., 2018). ROS formation in cells occurs through the reduction of oxygen to superoxide anion by biological reducing agents such as nicotinamide adenine dinucleotide and nicotinamide adenine dinucleotide phosphate (NADPH), these processes are facilitated by electron transfer enzymes and redox active chemical species, such as PM (Li et al., 2003; Simonetti et al., 2018).

1.3.1 Methods for measuring aerosol oxidative potential

There are several methods used to measure aerosol oxidative potential (OP), the objective of these assays is to provide a proxy of the oxidative capacity of PM samples. Since 2005, a wide range of acellular chemical methods has been developed to determine the total OP of PM and that of particle bound ROS. These acellular methods have the benefit of being faster and less labour intensive compared to *in vivo* and cell culture methods for determining OP such as using rat lung exposure (Campbell et al., 2020; Cho et al., 2005a).

In the following section several of the available OP chemical assays are briefly described before a more detailed discussion about the dithiothreitol (DTT) method applied in this project. This was due to the relative ease of this method, availability of instruments, and this assay having a particularly large body of results from previous studies for comparison (Bates et al., 2015; Borlaza et al., 2018; Charrier & Anastasio, 2012; Cho et al., 2005; T. Fang et al., 2015; Gao et al., 2017; H. Jiang et al., 2016; Q. Liu et al., 2014; J. Wang et al., 2018; W. Xu et al., 2015).

1.3.1.1 2-7-dichlorofluoroscin/hydrogen peroxidase (DCFH) assay

The 2-7-dichlorofluoroscin/hydrogen peroxidase (DCFH) assay was originally developed to determine *in vitro* ROS in biological cells, however in recent years it has been adapted into an acellular method. In the DCFH assay, the non-fluorescent DCFH is oxidised into its fluorescent form: dichlorofluorescein (DCF) by ROS in the presence of horseradish peroxidase (HRP) enzyme. DCF is then measured using fluorescence spectroscopy. Unlike DTT, DCFH does not give a rate of antioxidant depletion but rather a measure of the amount of ROS present (Campbell et al., 2020; Chuang et al., 2011; Simonetti et al., 2018).

1.3.1.2 Ascorbic acid (AA) assay

Ascorbic acid (AA) is one of the physiological antioxidants in the lung lining fluid; it prevents the oxidation of lipids and proteins. The AA assay involves the incubation of AA with filter extracts of $PM_{2.5}$ suspension under biologically relevant conditions (37 ^{o}C, pH = 7.4). The rate of AA depletion is then measured using ultraviolet-visible spectroscopy (UV-Vis). This rate of depletion is used as a measurement of the ability of PM redox-active species to catalytically transfers electrons from AA to oxygen. AA is more sensitive to redox-active transition metals and organic carbon than most of other species (Campbell et al., 2020; Ting Fang, Verma, Bates, et al., 2016; Simonetti et al., 2018).

1.3.1.3 Respiratory tract lining fluid (RTLF) assay

The respiratory tract lining fluid (RTLF) assay measures the rate at which PM oxidises three antioxidants that are commonly found in the RTLF at the surface of the lung: ascorbate (AA), urate (UA), and reduced glutathione (GSH) under biological relevant conditions (37 ^{o}C, pH = 7.4). The benefit of using multiple antioxidants is that the RTLF is more sensitive to multiple compounds found PM, whereas other assays can be more sensitive to certain compounds. The disadvantage of the RTLF assay comes from it being more labour intensive and requiring an expensive high performance liquid chromatography with an electrochemical detector (Campbell et al., 2020; Moreno et al., 2016; Mudway et al., 2005).

1.3.1.4 Dithiothreitol (DTT) assay

The DTT assay is an acellular assay where DTT acts as a chemical surrogate for cellular reducing agents (such as NADH or NADPH) (Simonetti et al., 2018). Figure 1-10 shows how DTT mimics the cellular reducing agent NADH using the production of ROS via redox cycling of quinones in vivo as an example.

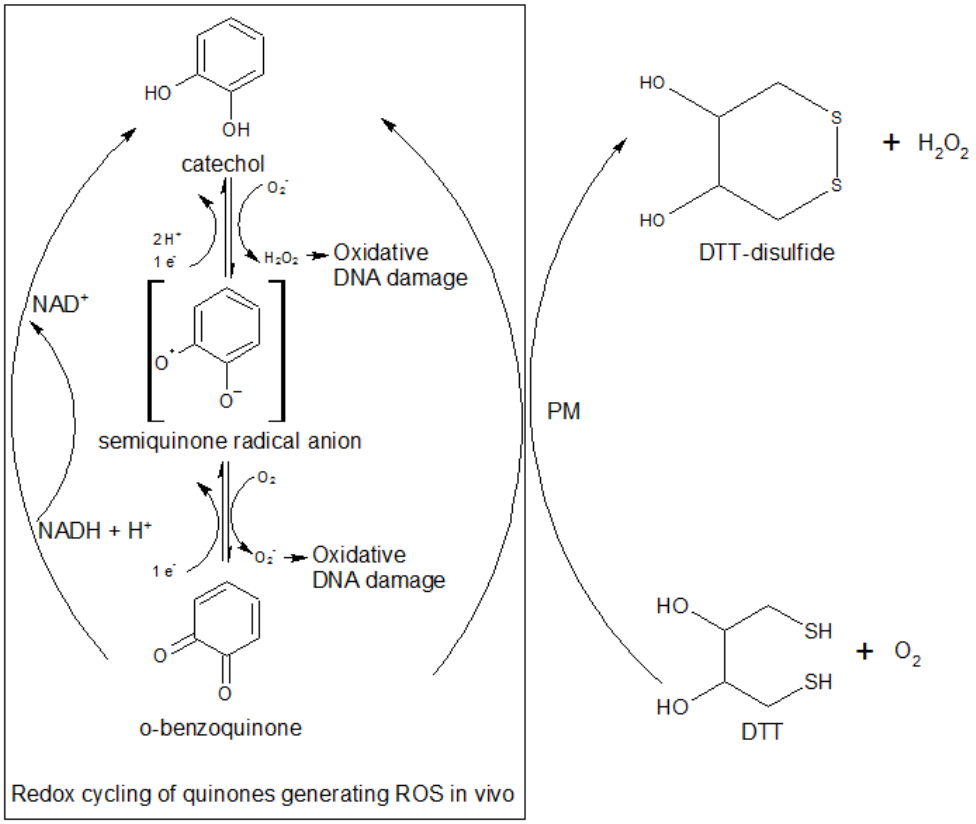

Figure 1-10: Redox cycling of quinones generating ROS in vivo and the similar reaction in the DTT assay (modified from Li et al., 2009).

The DTT assay is widely used by oxidative potential studies, it is an acellular assay where redox-active compounds in PM oxidise added DTT to its disulfide form by transferring electrons from DTT to oxygen thereby producing ROS (Borlaza et al., 2018a; Charrier & Anastasio, 2012; Cho et al., 2005a; Verma et al., 2012). The experiment is carried out under biologically relevant conditions (37 ^{o}C, pH = 7.4) and is in principle relatively simple to carry out, however, it is a labour-intensive and time-consuming protocol requiring precise attention to reagent preparation, purity, and conditions (Fang et al., 2015; Wang et al., 2018). The assay estimates the oxidative capacity of PM through the linear rate of DTT loss to its disulfide, through a two step reaction (Charrier & Anastasio, 2012).

The first step simulates in vivo ROS production using the catalytic ability of redox active compounds within PM such a quinones to transfer electrons from DTT to oxygen, the

reduction of oxygen to superoxide anion then facilitates the formation of hydrogen peroxide as shown in Figure 1-11-A, in the presence of metals the superoxide anion may also form hydroxyl radicals. During this step DTT is oxidised to its disulfide form (DTT-disulfide) (Charrier & Anastasio, 2012; Fang et al., 2015; Li et al., 2009). In the second step the remaining DTT is reacted with 5,5'-dithiobis(2-nitrobenzoic acid) (DTNB) to form DTT-disulfide and 2-nitro-5-thiobenzoic acid (TNB) as shown in Figure 1-11-B, this is a fast reaction. TNB is the coloured product that has a high molar extinction coefficient (14150 M^{-1} cm^{-1}) at 412 nm and is measured using UV-visible spectrophotometry (Li et al., 2009).

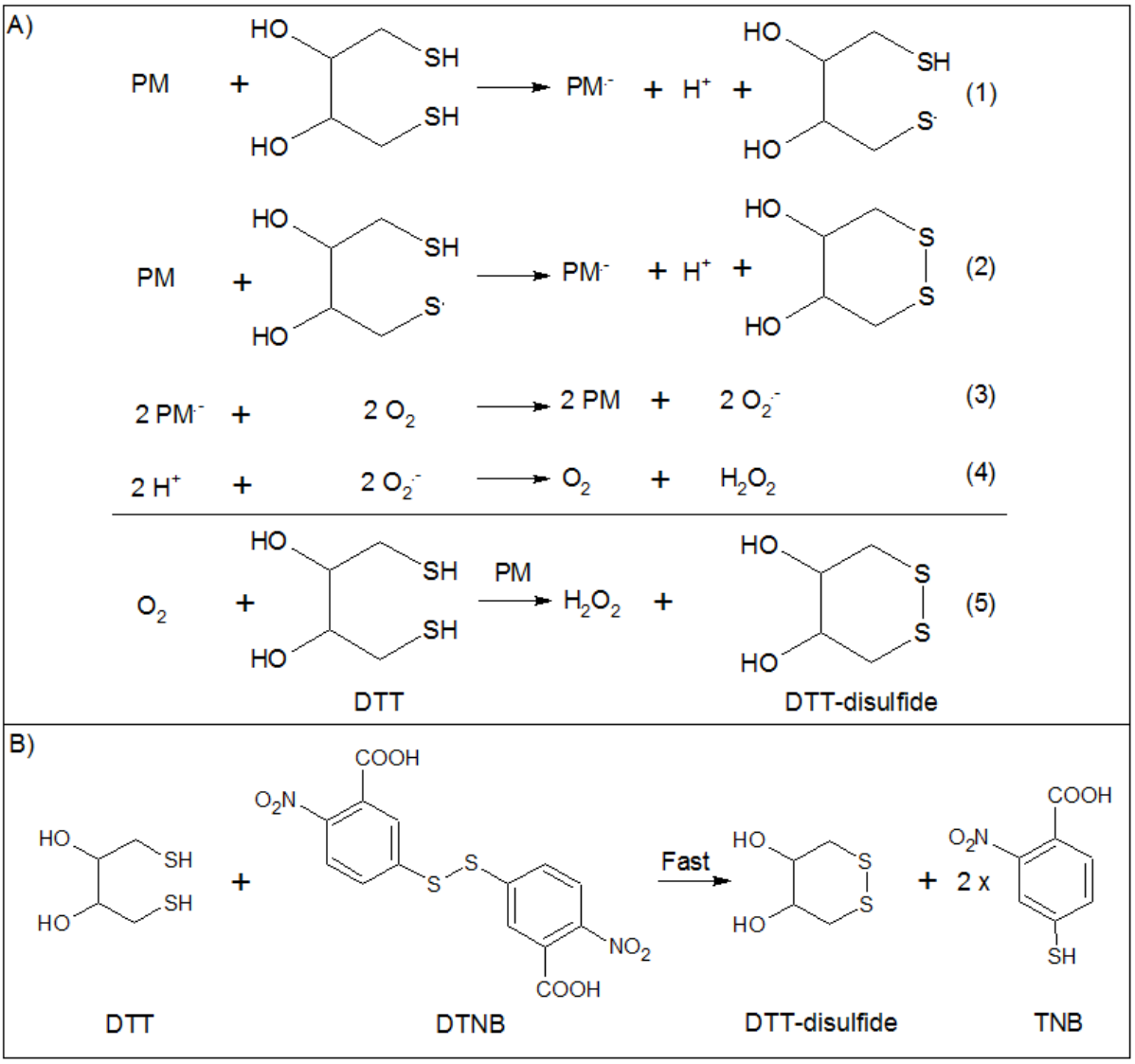

Figure 1-11: A) Reduction of O_2 by dithiothreitol (DTT) forming ROS with PM as the catalyst. B) DTT reaction with 5,5'-dithiobis(2-nitrobenzoic acid) (DTNB) this is a fast reaction forming the coloured product 2-nitro-5-thiobenzoic acid (TNB) (modified from Ayres et al., 2008; Rattanavaraha et al., 2011; Visentin., 2016)

The DTT assay uses these two reaction pathways to provide a quantitative measure of the oxidative capacity of the PM being analysed. By adding DTT in excess and stopping the reaction at several time points by the addition of DTNB the rate of DTT consumption can be determined by the slope of the linear regression of DTT degradation over time (nmol min^{-1}) (Charrier & Anastasio, 2012; Rattanavaraha et al., 2011; S. Y. Yu et al., 2018). For comparison of results across studies, two units are used for presenting DTT results. The first being volume-normalised DTT (DTT_v) which is the rate of DTT consumption per minute per

volume of sampled air (nmol DTT min^{-1} m^{-3}), this value is considered more relevant to human exposure. The second unit is mass-normalised (DTT_m) where the rate of DTT consumption is divided by the mass of PM present in the reaction (nmol DTT min^{-1} μg^{-1}) and is a measure of the intrinsic OP of PM (Bates et al., 2015; W. J. Liu et al., 2018b; S. Y. Yu et al., 2018).

1.4 Atmospheric Pollution & Human Health (APHH) in a Developing Megacity programme and sampling campaigns

The Atmospheric Pollution & Human Health (APHH) in a Developing Megacity was a Natural Environment Research Council (NERC) and Medical Research Council (MRC) programme which encompassed clusters of research projects grouped into project themes (listed in section 1.4.1). These projects concerned researching the causes of urban air pollution and its impact on health in two megacities through research partnerships with UK and Chinese / Indian researchers. The first programme conducted was the Atmospheric Pollution and Human Health in a Chinese Megacity (APHH-Beijing) programme in partnership with the National Natural Science Foundation of China (NSFC) which focussed on the megacity Beijing. The second programme conducted was the Atmospheric Pollution and Human Health in an Indian Megacity (APHH-Delhi) programme in partnership with the Ministry of Earth Sciences (MoES) and Department for Biotechnology (DBT) focussed on the megacity Delhi (NERC, 2014a).

1.4.1 APHH-Beijing programme details

The programme was split into four project themes (NERC, 2014b):

- Sources and emissions of urban atmospheric pollution.

- Processes affecting urban atmospheric pollution.
- Exposure science and impacts on health.
- Interventions and solutions.

Two intensive field campaigns made up the core activity of the APHH-Beijing programme. Providing observations of the atmospheric chemistry and physics at a central Beijing site: The Institute of Atmospheric Physics and a rural Beijing site: Pinggu, a town to the East-Northeast of Beijing that is within the Beijing municipality. These field campaigns occurred during 10th November – 10th December 2016 (winter campaign) and 21st May – 22nd June 2017 (summer campaign) (NERC, 2015; Z. Shi et al., 2019).

1.4.2 APHH-Delhi programme details

Three field campaigns during 2018 made up the core activity of APHH-Delhi. The two sites that hosted these campaigns were the Indian Institute of Technology Delhi (IIT Delhi) an urban background site in the new city and the Indira Gandhi Delhi Technical University for Women (IGDTUW) in the old city. These campaigns occurred during 16th January – 12th February 2018 (winter campaign), 30th April – 5th June 2018 (summer campaign), and 12th October – 12th November 2018 (autumn campaign) (NERC, 2016).

1.4.3 Geography and general air quality in Beijing

Beijing, the capital of the People's Republic of China, is in the northern part of the North China Plain. Located about 180 km northwest of the Bohai Sea and major port city of Tianjin. Beijing is governed as a municipality, meaning the political status of the region is equivalent to that of a province. The Beijing municipality has area of 16,800 km^2, encompassing the city core, surrounding mountains, and some villages. At the centre of the municipality is the Beijing metropolitan area (when Beijing is used in this thesis it refers to the metropolitan

area), which is surrounded by mountains on the west, north, and northeast. The city itself is located on a flat plain that extends to the south and southeast. Beijing has long, cold, dry winters with little snow; short springs; hot and humid summer; and short, sunny autumns. Most rainfall occurs in the months of July and August (Cheng et al., 2016; *Geography: Beijing*, 2020; National Bureau of Statistics of China, 2004).

Beijing has frequent haze events during the winter. These events are typically characterised by stagnant meteorological conditions, high relative humidity, low boundary layer height, as well as large emissions of primary air pollutants. Nucleation of gaseous pollutants consistently proceed haze events in Beijing, leading to a high number concentration of ultrafine particles during the clean conditions before events. The haze event starts during the accumulation and particle growth of these nucleation-mode particles over multiple days, generating enough larger particles to cause the distinctive reduced visibility of haze events (Cheng et al., 2016; Guo et al., 2014).

AQI values (SO_2, NO_2, CO, O_3, $PM_{2.5}$, and PM_{10}) for Beijing tend to be lowest during the summer and autumn, specifically from April to October with the lowest values observed during the height of summer. Jiang and Bai, 2018 suggests that the biggest explanation for this pattern is heating during the colder months. This was particularly attributed to the widespread availability of central heating services during the coldest months between November and March. The reliance on coal-fired power plants to provide the energy for this heating is a major source of air pollution during the winter months. Although the overall AQI values are relatively low in the summer in Beijing some pollutants such as ozone has been increasing during the summer months for several years. Lu *et al.*, 2020 reported that ozone concentration in the North China Plain (NCP) has been increasing at a rate of 3.3 ppb / year

(warm-season daily maximum 8-h average) during the warmer months of April – September over the years 2013 – 2019. Emission control measures have decreased NO_x emissions by 21 % during 2013 – 2017 nationwide. As ozone production in the NCP is likely VOC-limited, the increase in VOC emissions could contribute to this increase. Another cause could be the decrease in $PM_{2.5}$ concentration in the NCP with a ~40 % decrease during 2013 – 2017, slowing down the aerosol sink of hydroperoxy radicals (HO_2) leading to increased ozone production (L. Jiang & Bai, 2018; H. Li et al., 2017; K. Li et al., 2019; Lu et al., 2020).

1.4.4 Geography and general air quality in Delhi

Delhi, officially known as the National Capital Territory (NCT) is the capital of India. The urban area of Delhi is now considered to have expanded to include the nearby satellite cities of Faridabad, Gurgaon, Ghaziabad, and Noida making the larger National Capital Region (NCR). The NCR is in the Indo-Gangetic Plain (IGP) an area home to most of the Indian population along with highly populated regions of Bangladesh and Pakistan. The NCT is the second largest metropolitan area in India and has a population projected to be 19.3 million in 2020 based on the latest census in 2011. The city has experienced rapid population growth over recent decades with the population rising by 38.8 % since the 2001 census (Bikkina et al., 2019; Census Organization of India, 2020; UNCCD COP 14, 2020).

Air quality in Delhi is often the worst amongst all megacities, particularly in the autumn and winter where low wind speeds and lower boundary layer depth exacerbate the impact of local sources and that of crop burnings taking place in Haryana, Punjab, and Uttar Pradesh whose emissions are transported into Delhi. These regional sources of air pollution are especially important to Delhi as air quality regulatory measures are mostly assigned to municipal authorities who cannot impose control measures on neighbouring regions.

Bikkina *et al.*, 2019 reported that air masses in Delhi originated from the northwest most of the time during the winter (90 – 100 %), autumn (~ 80 %), and spring (~ 70 – 80 %) seasons. Black carbon (from incomplete combustion) loading in $PM_{2.5}$ from Delhi is almost twice that of Beijing aerosols (Bikkina et al., 2019; Puthussery et al., 2020).

Local air pollution sources in Delhi have changed over the latter half of the 20th century from being driven primarily by industrial emissions in 1970 to being overwhelmingly dominated by vehicle emissions in the early 2000s. Bikkina *et al.*, 2019 used OC / EC ratios to determine the relative contributions from regional biomass burning and local fossil fuel combustion sources. It was reported that biomass burning had more of an impact in the winter and autumn but during the spring and summer fossil fuel combustion sources dominated. BC concentrations peak in the autumn and winter being largely driven by liquid fossil fuel combustion and biomass burning, concentrations then fall in the spring and summer, coinciding with the summer monsoon season. Local coal and liquid fossil fuel combustion overwhelmingly dominates BC contributions during the summer season (Bikkina et al., 2019; Foster & Kumar, 2011b).

Delhi also experiences sporadic extreme pollution events during some special events, most notably the Diwali festival – the festival of light. Diwali celebrations take place for about a week each year between mid-October to mid-November, the festival is celebrated by widespread use of firecrackers and fireworks as well as the lighting of candles and oil lamps in most houses on Diwali day. Due to this widespread use of fireworks the Diwali celebrations account for the worst air pollution days in Delhi, with $PM_{2.5}$ concentrations sometimes reaching 1200 µg m^{-3} whereas average winter concentrations in Delhi are normally between 100 to 500 µg m^{-3}. The global burden of disease 2018 report has outlined

the growing body of literature showing acute health effects as a result of episodic extreme air pollution events in India, specifically during Diwali and crop burnings (GBD MAPS Working Group, 2018; Singh & Sharma, 2012; Zheng et al., 2017b).

1.5 Aims and hypotheses of the project

This study aims to determine the impact of $PM_{2.5}$ concentration on the oxidative potential (OP) of the air mass, and the effect of PM chemical composition on the intrinsic OP of $PM_{2.5}$ particles. With the hypotheses that:

- Redox active species within PM would increase the OP of the PM sampled and less reactive species would have little effect on the OP or a negative effect (such as SO_2 through consuming reactive sites on the PM).
- Higher $PM_{2.5}$ concentrations reduce the intrinsic OP of the PM, through a combination of reducing the photochemical reactions within the air mass (during extreme PM smog events) and the increased contribution of less reactive species within the PM.
- The OP of PM is higher during the colder seasons than warmer seasons, due to the increased emissions of redox active species, especially through increased fossil fuel combustion via residential heating.
- That the OP of PM at night is lower than during the day, due to the lack of photochemical reactions taking place during the night. Products of these reactions have been shown in previous studies to contribute to the OP of PM.

2 METHOD DEVELOPMENT

This chapter discusses the literature, strengths, and limitations of various oxidative potential assays and the rationale for the selected assay is presented. The process of developing this method for use on $PM_{2.5}$ samples collected during field campaigns is discussed, along with the quality assurance measures applied to the final protocol. This protocol was used to analyse $PM_{2.5}$ oxidative potential, the results of which are discussed in chapters 4 to 6.

2.1 Background: oxidative potential assays and specifically the dithiothreitol assay

The concept of Oxidative Potential (OP) was introduced in the previous chapter, alongside a brief overview of several different chemical assays used to measure it, with a more detailed look at the chemistry of the dithiothreitol (DTT) assay. Here, the background and literature to each OP assay is discussed in depth, including the strengths and weaknesses of each.

OP assays are often split into cellular and acellular (inside and outside a cell, respectively) assays, with the first largely revolving around assays on cells from rat lungs to test oxidative impacts on DNA damage and cellular inflammation, although they can also use other cell types without looking at cellular oxidation or inflammation. The acellular assays involve both antioxidant and fluorescent probe assays, with the aim to capture a broad range of PM characteristics such as composition, size, and surface area into a single measure of toxicity (used throughout this thesis as a shorthand to reflect that PM OP is linked to toxicity in cells). Although the assays discussed here measure a wide range of factors they all employ volume and mass standardisation in the reporting of their results i.e. all results are

published as per meter cubed of air sampled or per mass of PM used in reaction. During the following section acellular methods for measuring OP are discussed in depth (Mudway et al., 2009; Mudway et al., 2004; Willis & Kratzing, 1974).

2.1.1 Ascorbic acid (AA) assay

Ascorbic acid (AA) is an antioxidant found in the respiratory tract lining fluid of the lungs. The AA assay indirectly measures the rate of AA loss when exposed to PM extracts by quantifying the oxidation product of AA: dehydroascorbic acid (DHA). DHA reacts with *o*-phenylenediamine (OPDA) in a 1:1 reaction stoichiometry, forming the highly fluorescent product 3-(1,2-dihydroxyethyl)fluoro[3,4-b]quinoxaline-1-one (DFQ). DFQ is then measured using fluorescence spectroscopy at an excitation wavelength of 365 nm. Due to the stoichiometry between DHA and OPDA, the rate of DFQ formation can be used to determine the loss of DHA, in turn measuring the loss of AA and OP of the PM extract. DHA concentration is the chosen unit for the AA assay and is determined using a DHA calibration curve. The AA assay was originally developed as an assay for the concentration of trace metals, however, it has also been shown to be sensitive to quinones (Campbell, 2021; Mudway et al., 2009; Simonetti et al., 2018).

Being originally developed for trace metal determination, AA measured OP (OP^{AA}) is particularly sensitive to dusts with containing higher concentrations of metals and metalloids. These include brake dust and pellet ash (produced from wood pellet stoves used for residential heating), which are rich in Fe, Mn, Sr, Ca, P, Rb, and Se. However, Mudway et al., 2009 reported significant AA depletion when the assay was carried out with diethylene triamine pentaacetic acid (DPTA) present which is a transition metal chelator, showing that

organic radicals could also play an important role in AA consumption (Conte et al., 2017; Mudway et al., 2009).

Results from AA studies have shown significant spatial and temporal variations, as well as variation depending on the size fraction of PM being measured, with Mudway et al., 2009 showing an increased AA response from PM_{10} compared to $PM_{2.5}$ samples collected during the same time frame on Marylebone Road in London. On a study of various sites around the Netherlands, selected for their distinct differences in PM characteristics Strak et al., 2012 found a 50 % higher AA response from two roadside sites compared to an urban background site. However, there was no significant difference between the roadside sites and a farm site (Mudway et al., 2009; Strak et al., 2012).

In a study measuring various OP assays across multiple sites in the Netherlands, Janssen et al., 2014 reported that OP^{AA} was insignificantly correlated with $PM_{2.5}$ and PM_{10}. AA was highest at an underground train station site that also had the highest concentrations of PM. Of the outdoor sites, the highway site showed the highest AA with the rural farm site showing the lowest AA activity. AA activity was attributed to traffic emissions, specifically PAHs, elemental carbon, Fe, and Cu. The comparison of the AA assay to the other assays in this study are discussed in later sections, as these assays are introduced (Janssen et al., 2014).

Campbell et al., 2020 reported significant seasonal variation in the impact of $PM_{2.5}$ concentration on AA volume normalised consumption (AA_v) during a winter and a summer campaign in Beijing, China. The winter showed a drastically higher $PM_{2.5}$ / AA_v correlation and over an order of magnitude greater gradient than during the summer.

2.1.2 2-7-dichlorofluoroscin/hydrogen peroxidase (DCFH) assay

DCFH is a fluorescent-based probe used to measure PM bound ROS. It is the most commonly used fluorescent probe for this purpose and works based on the oxidative conversion of DCFH to the fluorescent compound dichlorofluorescin (DCF). This oxidation takes place in the presence of horseradish peroxidase. DCF is detected using fluorescence spectroscopy at an excitation and emission wavelengths of 488 and 530 nm, respectively (Rui et al., 2016; Yang et al., 2013).

While DCFH now mostly refers to the chemical assay this fluorescence probe was originally developed to be applied to rat alveolar macrophage cell assays. Where the macrophage cells are exposed to PM extracts, then the DCFH probe enters the cell to measure ROS. This has the benefit over the chemical method by being able to measure ROS produced through cellular inflammation rather just the particle bound ROS at the cost of added complexity, reducing throughput (Decesari et al., 2017; Rui et al., 2016).

DCFH is particularly sensitive to hydrogen peroxide and the organic peroxides found in SOA. It is commonly used for measuring particle-bound ROS instead of the redox active species of the other assays. Simonetti et al., 2018 reported that DCFH is also sensitive to the water-soluble fractions of the crustal components of PM. This resulted in high intrinsic DCFH to the water-soluble fraction of brake dust, road dust, and soil. However, DCFH was less selective towards different PM fractions in this study than the AA assay (Campbell et al., 2020; Simonetti et al., 2018).

Zhou et al., 2018 tested whether iron of different oxidation states negatively impacted the DCFH signal, it was found that at most ambient iron concentrations Fe^{2+} significantly lowers the DCFH value. This was attributed to soluble Fe^{2+} substantially consuming H_2O_2 to form

hydroxyl radicals (OH·), which in turn will further react with H_2O_2. Fe^{3+} was not found to significantly impact DCFH (Zhou et al., 2018).

Campbell et al., 2020 reported significant seasonal variation for DCFH in Beijing. As with the other assays in this study (such as AA) the winter campaign had significantly higher levels of volume normalised DCFH than the summer. However, the DCFH values for each campaign were significantly correlated with $PM_{2.5}$ concentration leading to the suggestion that DCFH sensitive species such as peroxides and particle-bound ROS might be consistent between seasons. This is further supported by higher intrinsic DCFH values being observed on days with high $PM_{2.5}$ concentrations (Campbell et al., 2020).

2.1.3 Electron Parametric Resonance (EPR) spectroscopy

EPR is a method that is used to speciate and quantify radical species that are bound to aerosol particle surfaces or the radicals that form upon the extraction of particles into an aqueous solution. It has the benefits of being selective for specific radicals by using spin-trap reagents and does not require PM to be extracted from the filter (Campbell et al., 2020).

Electron parametric resonance actually refers to the detection technique employed in this assay. EPR is a spectroscopic technique used to determine the structure of radicals, by measuring the magnetic moment associated with unpaired electrons. This is similar to the way in which NMR works where the orientation of hydrogen atom magnetic moments are measured in a magnetic field. However, unpaired electrons have a much larger magnetic moment than protons and as such, the magnets used in EPR to detect the difference between the possible quantum states can be ~30 times weaker than those required in NMR (Clayden et al., 2001).

The EPR assay was originally developed to characterise the production of OH· under reducing conditions similar to those found in the lungs by using the EPR measurement technique with particle suspensions in the presence of hydrogen peroxide and 5,5-dimethyl-1-pyrroline-*N*-oxide (DMPO) which acts as a spin trap. Spin traps are used to scavenge reactive free radicals which have a lifetime too short to measure and form a more stable adduct with them, allowing for their measurement using EPR. PM mass loaded filters and PM water suspensions retain their ability to generate OH· *in vitro* through the reaction of particle bound metals and hydrogen peroxide present in lungs produced either exogenously or endogenously. This has the benefit over using metal concentration for mitigation policies as EPR gives a measure of metal bioavailability and reactivity (Dąbrowski, 2017; T. Shi et al., 2003; Shlyonsky et al., 2016).

Künzli et al., 2006 performed a study comparing OP measured using the EPR assay to the consumption of several physiologic antioxidants in the respiratory tract lining fluid, using 716 $PM_{2.5}$ samples from 20 locations across Europe. EPR was significantly correlated with AA, supporting the use of radical generation as a measure of oxidative stress in the lungs. However, the study reported substantial variation in OP and was unable to find a specific cause for the observed OP values (Künzli et al., 2006).

There has been epidemiological support for the impact of hydroxyl radicals on lung function. Schaumann et al., 2004 reported the results of a study into two areas southwest of Berlin in Germany. Hettstedt, an area with a smelter area, and a non-industrialised area nearby (Zerbst). The study consisted of sampling $PM_{2.5}$ simultaneously from both areas and then introducing the same mass of $PM_{2.5}$ (100 µg) into contralateral lung segments of 12 volunteers. It was found that $PM_{2.5}$ from both areas increased the number of leukocytes 24

hours later, however only Hettstedt PM resulted in a significant influx of monocytes. This coincided with an increased hydroxyl radical generation measured by EPR, leading to the suggestion that the higher concentration of metals in $PM_{2.5}$ collected in the smelting region could be responsible for the increased inflammation (Schaumann et al., 2004).

Campbell et al., 2020 reported significant seasonal variation in $PM_{2.5}$ EPR in Beijing, China. With the winter campaign showing a very strong correlation between EPR normalised for the volume of air sampled and $PM_{2.5}$ concentration but with a wide variability in gradient (± 70 %), the summer campaign showed no significant correlation. In this study, the superoxide radical (O_2^- ·) was chosen to represent EPR instead of the traditional OH· and as such, no metals measured were significantly correlated with OP measured by EPR. In this study none of the ~100 compositional measurements of $PM_{2.5}$ could explain the variation observed in the EPR data (Campbell et al., 2020). EPR measurements of OH· are commonly driven by various metals concentrations in the PM, most notably Cu (T. Shi et al., 2003).

2.1.4 Respiratory Tract Lining Fluid (RTLF) assay

The respiratory tract lining fluid (RTLF) protects the pulmonary epithelial cells from oxidation by redox active species breathed in. Instead, these species react with antioxidant enzymes and low molecular weight antioxidants found in the RTLF. The RTLF assay combines multiple antioxidants found in the RTLF to get a more detailed look at the lungs response to $PM_{2.5}$ induced ROS production. This is, in effect, a combination of several different assays, each of which uses one antioxidant present in the lungs: AA, urate (UA), and reduced glutathione (GSH) (Szigeti et al., 2016).

The assay involves the direct addition of PM loaded filter punches to a synthetic RTLF containing equal molarity of AA, UA, and GSH, under biological conditions of pH 7.40 and 37

°C. This mixture is incubated for 4 hours and subsequently centrifuged at 13,000 rpm for an hour. The remaining AA and UA are determined using high performance liquid chromatography (HPLC) with an electrochemical detector; GSH is quantified using UV visible spectrophotometry at 412 nm. Results from this assay can be reported in terms of OP for AA (OP^{AA}), UA (OP^{UA}), and GSH (OP^{GSH}), or the measurements can be combined into OP^{total} (Moreno et al., 2016).

Künzli et al., 2006 reported that OP assessed by the RTLF assay was significantly correlated to OP assed via the EPR assay when measuring OP from 716 $PM_{2.5}$ filters collected from 20 centres around Europe over the course of a year. The RTLF (and EPR) assay was shown to be sensitive to bioavailable metals. This is due to the consumption of AA and GSH through the reduction of oxidised metal ions such as Cu(II), Cr(VI), and Fe(III). AA and GSH are further consumed by the superoxide formed from this reaction (Künzli et al., 2006; Moreno et al., 2016).

In a study on oxidative potential in the Barcelona subway station Moreno et al., 2016 found weaker correlations between RTLF OP and metals, with only Cu showing a spearman correlation >0.6 ($p = 0.64$ for OP^{GSH}). OP in the subway was found to be lower than that of ambient outdoor air; however, there was wide variability in the OP between stations. The lowest OP values was found at the only station fitted with platform screen doors. This could be due to higher correlations found between OP^{total} and metallic trace elements like Cu and Sb. These are linked with brake dust and erosion of overhead pantographs, which the platform screen doors may help to block from the platform (Moreno et al., 2016).

Szigeti et al., 2016 found lower OP^{AA} and OP^{GSH} values for indoor air in office buildings around Europe than for outdoor air. The OP values showed significant spatial and seasonal

difference, with Hungary having the highest OP and Finland the lowest. However, Hungary had more office buildings sampled (n = 5) than Finland (n = 3). OP^{AA} and OP^{GSH} showed weaker correlation with indoor $PM_{2.5}$ compared to outdoor, possibly due to lower trace metal concentrations indoors (T Szigeti et al., 2016).

2.1.5 Dithiothreitol (DTT) assay

The dithiothreitol (DTT) assay uses DTT as a chemical surrogate for antioxidants found within the lungs and cells, such as nicotinamide adenine dinucleotide phosphate (NADPH) or glutathione. DTT mimics the redox cycling of these antioxidants when exposed to PM through an irreversible reaction where redox active species within PM oxidises DTT to its disulphide form. This reaction results in the formation of ROS as electrons are transferred from DTT to oxygen, these superoxide radicals then form hydrogen peroxide as shown in Figure 1-11. The assay is performed under biologically relevant conditions (pH 7.40 and 37 °C). The rate of DTT consumption is periodically measured by the fast reaction of DTT with 5,5'-dithiobis(2-nitrobenzoic acid) (DTNB), which oxidises the remaining DTT and produces the coloured product 2-nitro-5-thiobenzoic acid (TNB), this is measured at 412 nm (Charrier & Anastasio, 2012; Fang et al., 2015; Janssen et al., 2014; Li et al., 2009; Pietrogrande et al., 2018).

Before aliquots of the DTT reaction are oxidised by the DTNB solution, the reaction is quenched by adding it to 10 % v/v trichloroacetic acid (TCA). TCA quenches the reaction by reacting with the remaining DTT, turning it into its disulphide form without producing TNB. The DTNB solution is made up using a 0.4 M TRIS-HCl buffer at a pH of 8.9 containing 20 mM ethylenediaminetetraacetate (EDTA) which acts as a pH buffer. EDTA is now often excluded from the DTT assay as Charrier & Anastasio, 2012 reported that it significantly suppressed

the DTT response to quinones and metals, which were also found to be much more important for DTT depletion in the absence of EDTA (Borlaza et al., 2018a; Charrier & Anastasio, 2012; Curbo et al., 2013; T Fang et al., 2015; Mudway et al., 2009; Verma et al., 2012).

The dithiothreitol oxidation assay was originally developed to be more sensitive to quinone-catalysed oxidation than other oxidation assays. However, over time more studies have looked into the effects of different species on DTT oxidation. It is now understood that certain transition metals and SOA also have a significant impact on DTT oxidation (Charrier & Anastasio, 2012; Cho et al., 2005b; Kumagai et al., 2002; Mudway et al., 2009; Puthussery et al., 2020).

Cho et al., 2005 performed the first study using the DTT assay to determine particulate matter oxidative potential. It was highlighted that the main species responsible for DTT consumption were quinones, organic and elemental carbon, and to a lesser extent PAHs. Metals were considered to play a minor role in the redox process as it was found that Cu(II) and Fe(III) only increased the DTT consumption of the quinone 9,10-phenanthroquinone (PQN) by 10 %. However, Mudway et al., 2009 reported a significant reduction in the rate of DTT oxidation when the metal chelator DTPA was added, suggesting that metals have a more important role in DTT oxidation. As mentioned earlier Charrier & Anastasio, 2012 found that EDTA suppresses the response of quinones and metals in the DTT assay, when this was removed it was estimated that metals accounted for ~80 % of DTT consumption. Copper and manganese were suggested as the most redox active metal species. The remaining 20 % of DTT consumption was assigned to quinones and other redox active

species that were not measured (Charrier & Anastasio, 2012; Cho et al., 2005b; Mudway et al., 2009).

In a comparison study of OP^{AA}, OP^{DTT}, and OP^{EPR} Janssen et al., 2014 reported that AA was significantly correlated with DTT and EPR at r_s values of 0.86 and 0.96 respectively for multiple sites in the Netherlands. However, OP^{AA} was insignificantly correlated with $PM_{2.5}$ and PM_{10} concentrations, whereas OP^{DTT} was strongly correlated to both. This is due to the OP results in this study only being reported as volume normalised results. Campbell et al., 2020 reported that mass normalised AAm and DTTm were inversely correlated with $PM_{2.5}$ concentration (Campbell et al., 2020; Janssen et al., 2014).

Zeng et al., 2021 performed a study looking at OP^{DTT} differences between indoor and outdoor air when indoor PM was dominated by transport from outside. This was done by sampling different PM size fractions in an empty apartment building in Chicago, to remove the potential for local sources indoors. It was found that PM concentration and DTTv were considerably lower indoors than outdoors; however, the DTTm values were mostly higher indoors than outdoors. Increased intrinsic toxicity indoors was positively correlated with a higher temperature and lower relative humidity. Some of the suggested reasons behind the increased DTTm indoors relative to outdoors was the evaporation of volatile chemical components of PM, and / or humidity / temperature partitioning of PM-bound redox active species (Zeng et al., 2021).

2.1.6 Summary

A limitation of all of the above-described OP assays is that as acellular assays they only measure the 'intrinsic' OP of particles, such as redox active metals, quinone, and radicals. Any other biological pathways for oxidative stress are not measured by these assays. Table

2-1 shows a breakdown of the pros and cons of the various assays, with the species they are most selective for. Other limitations to the assays that were not mentioned previously include: the need for particle extraction for all assays aside from EPR. The quenching of the fluorescence signal in the ascorbic acid and DCFH assays. The inherent variability in all assays, the interference of the dark colour of PM on photometric methods (AA, DCFH, DTT, and partially RTLF), and interference caused by PM binding to reagents (Cho et al., 2004; Mudway et al., 2004, 2005).

Table 2-1: Breakdown of some pros and cons of the various different OP assays, along with the species they are most selective towards.

Pros	Cons	Notable species the assay is selective towards
Ascorbic acid assay		
Measurements made by fluorescence spectroscopy (readily available instrument)	Has been shown to have a better response to PM_{10} over $PM_{2.5}$	Trace metals and quinones
2-7-dichlorofluoroscin/hydrogen peroxidase assay		
Has the ability to measure ROS through cellular inflammation in addition to particle bound ROS (if used with cells)	The acellular assay only measures particle-bound ROS and not ROS produced by redox active species	Hydrogen peroxide and the organic peroxides found in SOA
Electron parametric resonance spectroscopy		
Selective to specific radicals by using spin-trap reagents. Does not require PM extraction from the filter. Measures metal bioavailability and reactivity.	Requires a specialised X-band EPR spectrometer to perform	Hydroxyl radicals, superoxide radicals, and other radicals based on choice of spin-trap
Respiratory tract lining fluid assay		

Combination of several OP assays, allowing it to be selective for more species than other assays. More biologically relevant as antioxidants are found within lungs.	Requires HPLC with electrochemical detector for analysis, a very expensive instrument. Multiple antioxidants adds complexity, slowing down assay.	Trace metals and quinones
Dithiothreitol assay		
Relatively simple assay with a common detection method (UV-visible photometry). Largest body of published studies to compare results to.	Uses a surrogate of antioxidants found in the lungs.	Metals, organic carbon, PAH, and quinones

To select the most appropriate OP assay for this project, three requirements were identified for the OP assay to reduce the number of possibilities. These were:

1. For the assay to be fast enough to enable a high throughput of filters to be analysed, as the various field campaigns resulted in a large number of filters.
2. The assay had to either be compatible with the available laboratory space, equipment, and instruments within the three accessible laboratories or the needed equipment had to be within budget to acquire.
3. The assay had to have a well-established body of evidence for its use in the literature.

The RTLF assay has the benefit of being a more biologically relevant OP assay (than the previously described single antioxidant assays) due to the use of multiple antioxidants, which appear in the RTLF. However, this multiple antioxidant approach adds complexity,

resulting in a much slower throughput of samples. This also results in the need of two detection method: UV visible spectrophotometry and HPLC with an electrochemical detector, the latter of which was not available and prohibitively expensive (Moreno et al., 2016; Szigeti et al., 2016).

The EPR assay was shown to be a good method for measuring the bioavailability and reactivity of metal species through the generation of hydroxyl radicals. However, this assay was mostly shown to be sensitive only to metals and carbon-based PM (when used with superoxide spin-traps), whereas other assays were also shown to be sensitive to quinones, SOA, and PAH. The EPR assay was removed from consideration owing to the need of a specialised X-band EPR spectrometer to perform (Campbell et al., 2020; Dąbrowski, 2017; Miller et al., 2009; T. Shi et al., 2003; Shlyonsky et al., 2016).

The DCFH assay has the ability to measure ROS produced through cellular oxidation if used with rat alveolar macrophage cells, however this drastically reduces the throughput of samples being analysed. The DCFH assay can be performed on other cell types and is also widely used without cells to measure particle bound ROS. There was available equipment to perform this assay, however it was determined that the body of literature to compare to for this assay was less than for the AA and DTT assays (Campbell et al., 2020; Rui et al., 2016; A. Yang et al., 2013).

The AA and DTT assays are possibly the most similar OP assays considered here, with Janssen et al., 2014 showing they are significantly correlated with each other at $r_s = 0.86$. Both of these assays appear to have a similar throughput for samples and both could be carried out with the available equipment. The DTT assay was ultimately chosen for this

project as it had the larger amount of published data to compare to (Campbell et al., 2020; Mudway et al., 2009; Simonetti et al., 2018).

2.2 Initial DTT experiments using Arizona testing dust

The following sections cover the development / implementation of the DTT assay to produce a standard operation protocol to measure the OP of filters collected during the APHH field campaigns. This was necessary due to the lack of detailed methods published in the literature, which resulted in poor repeatability in analysis during initial tests. Initially the experimental protocol used for the DTT assay was the protocol published by Cho et al., 2005. The DTT protocol consisted of mixing 0.7 mL of $PM_{2.5}$ extract, 0.2 mL potassium buffer, and 0.1 mL DTT at 37 ^{o}C. At five time points between 0–40 minutes, 100 µL aliquots of this reaction mixture was removed and added to 1.5 mL amber glass vials containing 0.2 mM DTNB. This mixture is then vigorously shaken to ensure all remaining DTT reacts with DTNB to form the coloured product: TNB. The solution would then immediately be measured by UV-vis at 412 (the strongest absorption wavelength for TNB) and 700 nm chosen as the baseline absorbance for TNB and the potassium buffer.

The first DTT test experiment performed was using four samples of an ISO fine Arizona test dust (ATD) to substitute $PM_{2.5,}$ due to the lack of access to spare PM loaded filters. ATD is a mixture of Arizona and California dust which is 70-80 % quartz. The particle size range of ATD is 0.97-176 µm and is widely used in filter testing. The mass of ATD in the four experiments ranged from 36 – 141 µg. The experiments were run for 30 minutes, taking DTT aliquots at 10-minute intervals to stop the experiment. Trichloroacetic acid (TCA) and TRIS-HCl were not used during this experiment. This first experiment produced a linear regression plot with good linearity (R^2 = 0.91 – 0.98). The DTT activity also showed good repeatability

with a coefficient of variation (% CV) of 8.4 % (2.84 ± 0.048 nmol DTT min^{-1}). However, the next few repeats of ATD over the course of a few months showed lower DTT activity. There was also extreme unpredictability in the linearity of the repeat experiments with some time points being significantly higher or lower than the line of best fit. Initially this was put down to a malfunctioning sonic bath for extraction, as the temperature would rise above 30 ^{o}C potentially removing volatile compounds from the extract. However, this unpredictability in the linear regression analyses continued during much of the method development process, an example of these linear regression plots is shown in Figure 2-12.

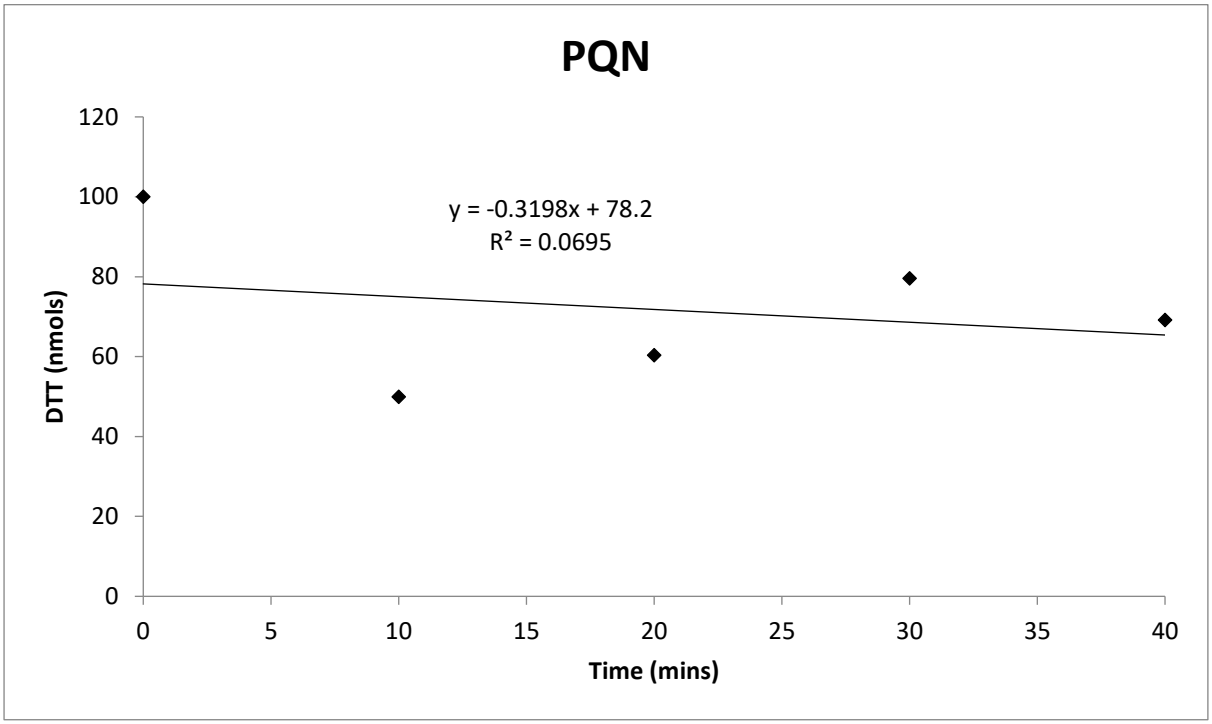

Figure 2-12: Linear regression plot showing the non-linear nature often observed during DTT method developments.

A different sonic bath was used for the extraction step so that the temperature issue could be removed and the DTT was prepared and stored in the dark to prevent potential photolysis, as some papers had included this step. However, this did not improve the uncertainty seen in the experimental results. Next, TCA was introduced to consume the remaining DTT, stopping the reaction, and TRIS-HCl to lower the pH to prevent the signal

from TNB at 412 nm from being overwhelmed by the TNB^{2-} signal. However, it was found that the introduction of TCA removed the colour from the TNB product unless at least 0.5 mL of 0.5 M k-buffer was used.

At this stage, it was decided to try a different protocol to see if an improved result could be obtained. The Fang et al., 2015 protocol was chosen (as opposed to the original Cho et al., 2005 protocol), where the time points used to stop the experiment increased from 4 to 5 and the times were changed from 0, 10, 20, and 30 minutes to 4, 13, 23, 32, and 41 minutes. It was thought that the removal of the zero minute time could improve the results, as stopping the reaction immediately after starting required more time than other times points i.e. to changed pipette tips. Previously a modified form of the Beer-Lambert equation was used to calculate DTT consumption:

$$\text{Concentration } 2 = \frac{\text{Absorbance } 2}{\text{Absorbance } 1} \times \text{Concentration } 1$$

Where absorbance and concentration refers to the absorbance and concentration of DTT in the reaction at time zero, with absorbance 2 being the measured absorbance at each time point. This new method required the use of the equation of the straight line from a calibration instead, as the concentration of DTT at 4 minutes (the first time point in the new method) was not known. The first experiment using this method did not produce good results. The amount of DTT being consumed during these experiments was concerning (47.2 ± 0.90 % DTT depletion, n = 3), as Cho et al., 2005 had suggested keeping DTT depletion below 20 % unless linearity is still strong. To limit the impact of this excessive DTT depletion

on linearity the DTT protocol published by Verma et al., 2012 was tried. Notable differences in this method were the lower overall experiment time (20 minutes vs 40 minutes) and an increase in the number of data points to seven. Although this did not improve results sufficiently (45.8 ± 2.1 % DTT depletion, n = 3) to be worth the added complexity and work involved, some aspects of this method were retained such as subtracting a background measurement at 700 nm. The background measurement accounted for 5.68 ± 1.0 % of the signal at 412 nm.

The University of Illinois group (J. Puthussery, pers. comm., 2017) provided more information on the DTT assay that is not published but required for successfully performing the assay. Their recent testing showed that TCA and TRIS-HCl were not necessary if the coloured TNB product was measured immediately after the reaction aliquot was added to DTNB. From this point, TCA and TRIS-HCl were not used in either testing or final DTT experiments.

J. Puthussery also stated that it was important to maintain the ratio of sample (whether PM extract, blank, or PQN), potassium phosphate buffer, and DTT at 7:2:1 in the reaction tube. The concentration of DTT in the reaction tube must also be 100 µM to have a rate of reaction comparable to literature. Having a similar mass of $PM_{2.5}$ in the reaction tube is also necessary to ensure consistency between DTT experiments, Cho et al., 2005 stated that this should be between 5 – 40 µg $PM_{2.5}$ mL^{-1}, during this study extraction volume and filter punches were adjusted to maintain as close to 20 µg $PM_{2.5}$ mL^{-1} within the reaction as possible.

2.3 Assessing impacts of light and additional chemical species

2.3.1 Impact of light exposure on the DTT assay

To determine the impact of photodegradation on chemicals involved in the DTT assay two sets of filter blanks were analysed. The first set using chemicals that had been prepared in foil covered volumetric flasks and the second set in normal volumetric flasks. The light restricted samples had much lower rates of DTT depletion with a lower uncertainty: 0.385 ± 0.014 nmol DTT min^{-1} than the light exposed blanks: 0.714 ± 0.34 nmol DTT min^{-1}. Therefore, it was decided to prepare and store the DTT and DTNB stocks and working solutions in amber glass bottles and volumetric flasks to reduce the impact of photodegradation on the assay results.

2.3.2 Optimising the PQN positive standard method

To determine the most stable concentration for the stock solution for PQN, two concentrations were chosen to be tested: 2 and 5 mM PQN in DMSO. Both stock solutions resulted in a good DTT degradation over time correlation (R^2 = 0.990 – 0.999) and similar gradients of ~ -0.01 µM DTT min^{-1}. 5 mM stock solution was chosen for the final protocol due to ease of making the dilutions for the PQN working solution.

To try to limit the amount of glassware and time required to perform the positive standards with PQN, two dilution strategies were tested. The first, a “short” dilution, involved 1 into 50/100 dilution steps. To see whether these large dilutions had a negative impact on the PQN repeatability and linearity, a second “long” dilution was also used. In this one, the maximum dilution step would be 5 in 100. Figure 2-13 shows the linear regressions for DTT depletion over time from these two dilution methods. Both show good linearity and similar

gradients at 0.91 – 0.97 nmol DTT min^{-1}. Therefore, the final dilution method used dilution steps up to 1 in 100.

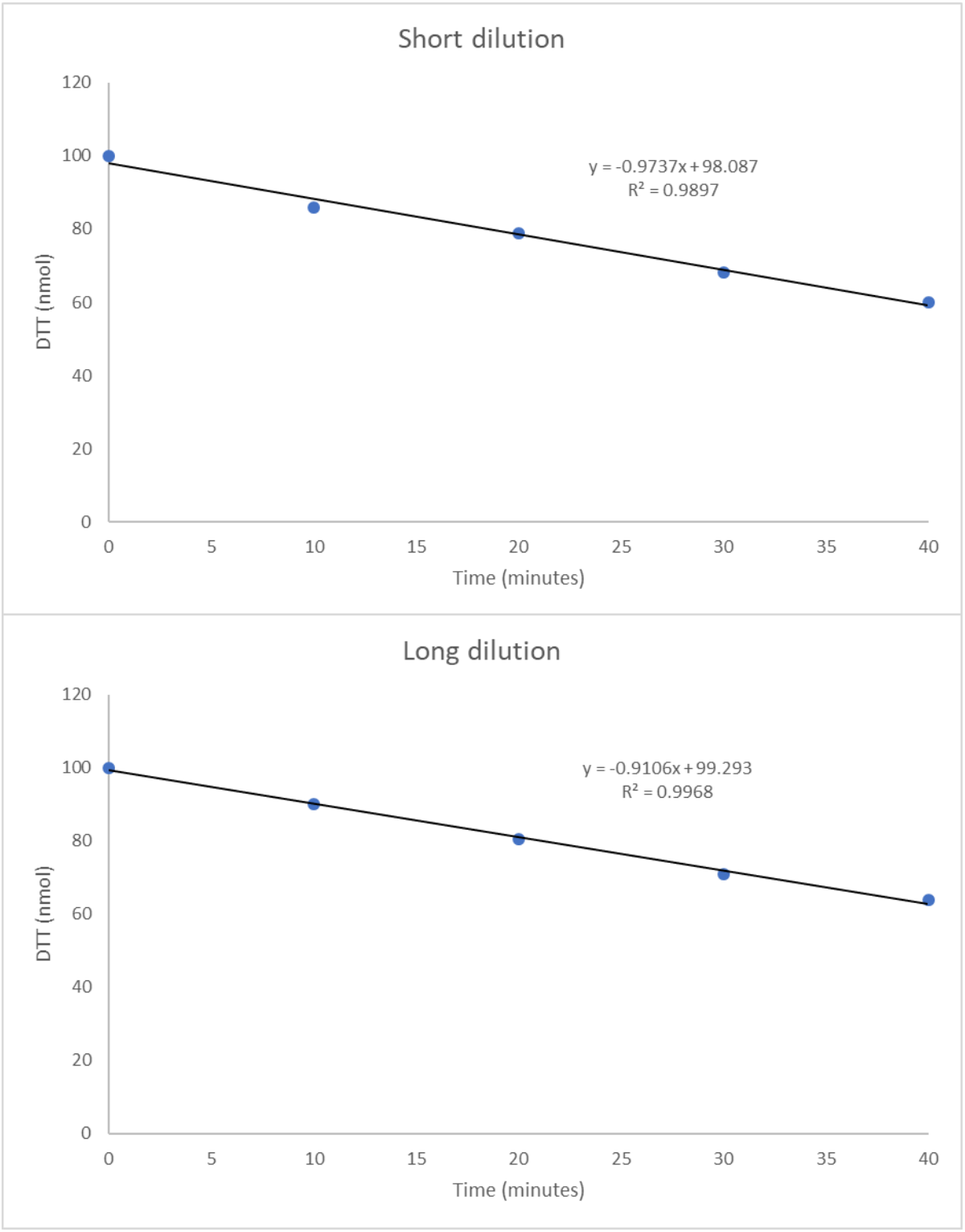

Figure 2-13: The DTT depletion over time when exposed to 0.7 mL 0.2 µM PQN positive standard. The top graph had dilution steps up to 1 in 100; the bottom graph had dilution steps up to 5 in 100.

Various concentrations of PQN working solution were tested to see which one would be optimal to ensure that DTT results were consistent over multiple days. Multiple PQN concentrations ranging from 0.3 – 0.05 µM were tested, linearity was only acceptable ($R^2 \geq 0.95$) for PQN concentrations ≤ 0.15 µM. The PQN concentration chosen for positive standard throughout this project was 0.05 µM, this represents 5 – 50 times the concentration found in ambient PM measured by Charrier et al., 2015 in Fresno, California. Particulate-phase PQN was first measured by Cho et al., 2004 in diesel exhaust particles and ambient $PM_{2.5}$ samples collected in several locations across California at a median concentration of 0.32 ng m^{-3} PQN (for the ambient samples).

The PQN concentration of 0.05 µM was chosen due to good repeatability and use in the literature. Alternatively 0.24 µM (J. Wang et al., 2018) and 0.1 µM (Jiang et al., 2016) are also used in the literature. The PQN standard was run periodically throughout method development and PM laden filter analysis; they were considered acceptable if the R^2 value ≥ 0.95. The gradients were consistent throughout this period at 0.76 ± 0.12 µM DTT min^{-1} (n = 27), this is consistent with other studies using the same concentration of PQN which obtained gradients of 0.74 ± 0.10 µM DTT min^{-1} (n = 7, Patel & Rastogi, 2018) and 0.71 ± 0.09 µM DTT min^{-1} (Charrier & Anastasio, 2012).

2.4 The causes of the unusual DTT results obtained previously

The three largest factors found during method development that negatively impacted results from the DTT assay were the caps used on the DTNB vials, acid washing equipment, and proper storage of DTT. One cause of erratic DTT results was found to be the material inside the caps of these vials. It was made of a foil covered cardboard insert, with repeated use bits of cardboard would contaminate the reaction mixture, causing the absorbance to

change at random. This problem was solved by replacing these vial caps with rubber-lined caps, which would not come loose. This decreased the amount of uncertainty in the results, as example PQN using the old caps: R^2 = 0.94 ± 0.05, gradient = -1.00 ± 0.18 nmol DTT min^{-1} (17.5 % CV, n = 3) compared to the new caps: R^2 = 1.00 ± 0.002, gradient = -0.821 ± 0.033 nmol DTT min^{-1} (4.02 % CV, n = 4).

Due to equipment and laboratory space limitations, all work on the DTT protocol aside from filter extraction was performed in an earth science laboratory. Therefore, contamination of equipment used in the DTT assay with redox active species, such as metals in sediment dust was a major concern. Through testing on the final DTT protocol, it was found that the DTT activity of blank filters would rise significantly, unless all glassware involved in the assay was acid washed overnight in nitric acid. As glassware was stored in a cupboard after washing, it was also necessary to rinse all glassware with milli-q water just prior to use. However, this was not possible for the 1.5 mL amber glass vials, as the small neck size would trap water due to water tension. These small vials were dried completely after acid washing in a laminar flow fume hood to prevent dust contamination. The fume hood was chosen as contamination was introduced through oven drying of the glassware, as soil and sediment samples were dried in the same oven.

The main reason behind the increasingly non-linear DTT consumption plots (as can be seen in Figure 2-12) was the improper storage of DTT. All chemical originally ordered did not have specific storage instructions included. Therefore, all chemicals used in the DTT assay were stored in a cool, dry cupboard. After several iterative method changes to improve DTT reliability and repeatability, it was decided to order new chemicals to ensure defective reagents were not the cause. The new batch of DTT came with storage instruction to be

refrigerated immediately upon delivery. Through non-literature forum searches it was found that DTT reacts readily with oxygen in the air if not refrigerated and should only be removed to stabilise the temperature for stock preparation, which should be refrigerated.

After implementing these three practices, the repeatability and linearity of our DTT analysis improved significantly, for example $PM_{2.5}$ samples analysed had a gradients of 0.542 ± 0.13 (R^2 = 0.77 ± 0.2, n = 4). Different $PM_{2.5}$ samples analysed after implementing these practices showed gradients of 1.18 ± 0.023 (R^2 = 1.0 ± 0.0008, n = 3). These were changes were implemented along with other practices such as using the correct concentration of DTT, the right range of PM mass in reaction, not using TCA and TRIS-HCl etc. These were all used to construct our own DTT protocol based on the University of Illinois (Puthussery et al., 2018) method with adaptations from the literature and previous assessments in this chapter.

2.5 Updating extraction procedure to a two-step methanol and DI water extraction

After incorporating all of the measures outlined in the previous sections the results from the DTT assay for PQN, filter blanks, and PM extracts were consistently linear (R^2 = 0.99 ± 0.01, 0.96 ± 0.05, and 0.98 ± 0.04 for PQN, filter blanks, and PM extracts respectively, n = 14, 24, and 10) and with acceptable repeatability of below 15 % coefficient of variation. However, when performing the assay on $PM_{2.5}$ laden filters an issue arose often where the activity of the PM extract would be close to and sometimes lower than that of the filter blank: 0.339 ± 0.090 for PM (n = 10) and 0.362 ± 0.18 nmol DTT min^{-1} for the filter blanks (n = 24). The lack of reliable mass data on the $PM_{2.5}$ loaded filters used likely had an impact on the activity obtained, if the PM mass in reaction was too low.

The extraction method used up until now was a DI water extraction where the PM-loaded filter was sonicated for 15 minutes. However, this single step extraction only dissolved water-soluble species for DTT analysis. Verma et al., 2012 and Gao et al., 2017 both reported significantly lower DTT responses from the water-soluble fraction of PM compared to the water-insoluble fraction. Methanol was used in these studies as the water-insoluble extraction fluid, being a very efficient solvent. The methanol to water DTT ratio in these studies was reported as 1.6 ± 0.4. Therefore it was decided to incorporate a two-step extraction method based on the method in Gao et al., 2017, where the filter punches would be extracted in methanol then dried to ~1-2 mL by nitrogen blowdown before having DI water added and extracted again. This allows for the analysis of both the water-soluble and insoluble fractions in the same DTT analysis.

Due to the lack of spare $PM_{2.5}$ loaded filters and $PM_{2.5}$ samplers, the methanol and DI water extraction method was tested on PM_{10} loaded filters collected at Bristol Road Observation Site (BROS) on the University of Birmingham campus, a roadside site approximately 10 m away from a junction. These filters gave much higher DTT activity than previously tested $PM_{2.5}$ filters using DI water alone, and had good repeatability. The two methanol extracted PM samples gave DTT activities of 0.828 ± 0.0069 (R^2 > 0.99, n = 2) and 1.04 ± 0.0059 nmol DTT min^{-1} (R^2 = 0.99 ± 0.01, n = 2). This was significantly higher than the previously measured DI water extractions which gave activities of 0.391 ± 0.085 (R^2 = 0.99 ± 0.008, n = 4) and 0.285 ± 0.072 nmol DTT min^{-1} (R^2 = 0.99 ± 0.002, n = 2). Although direct comparisons are limited due to the different PM size fractions analysed it should be noted that the filter blank activity for the water extract was higher than one of the PM samples at 0.324 nmol DTT min^{-1} (R^2 = 0.99). The two-step extraction using methanol and water also had the benefit of capturing both water-soluble and water-insoluble (which were previously not

extracted from filters) species in the extraction. Therefore, it was decided to perform the two-step extraction method on all of the filters analysed.

2.6 Testing finalised DTT protocol on samples collected at the Bristol road observation site (BROS) on the University of Birmingham campus

To validate the final DTT assay method for use on $PM_{2.5}$ loaded filters from Beijing and Delhi seven $PM_{2.5}$ filters were collected at BROS between 12-19.12.2018 for 24 hours each. These PM loaded filters along with a field filter blank were measured for mass and volume normalised DTT using the final DTT protocol. Each filter extract was measured in triplicate to ensure the results were consistent. The linearity was good for all filters at R^2 = 0.96 – 1.00 (0.99 ± 0.01, n = 24), the DTT activity of the field blank was 0.464 ± 0.06 nmol DTT min^{-1} with a 13 % CV.

The $PM_{2.5}$ mass in reaction was kept consistent across all mass loaded filters: 20.3 ± 0.18 µg $PM_{2.5}$. The DTT activity of the mass loaded filters was consistently higher than the filter blank value at 0.955 – 1.60 nmol DTT min^{-1} (1.19 ± 0.24 nmol DTT min^{-1}, n = 21) with coefficient of variations of 2.7 – 10.3 %. These $PM_{2.5}$ results along with the consistent PQN and calibration analysis showed that the DTT protocol produced reliable results.

2.7 Assessing dependence on reagent and sample age

To improve the throughput and reliability of the final DTT assay, the stability of different aspects of the assay were tested. These being the lifespan of the DTT stock and working solutions to allow more assays to be run between remaking solutions. The stability of the $PM_{2.5}$ extracts was also tested to optimise the number of filters that could be extracted at

the same time, as this occurred in a different laboratory to the DTT assay and required a day to prepare the final extracts.

The 10 mM DTT stock solution was shown to be stable for at least 3 months when stored in an amber glass bottle and refrigerated between DTT analyses through several PQN positive standard DTT analysis. These PQN results were included with other PQN results in the previous subsection on PQN optimisation and consistently fell within literature values as shown in that section. The stability of the DTT working solution was tested at the same time as the PQN dilution steps were being tested. Figure 2-14 shows the DTT linear regression for PQN when using a freshly made DTT working solution compared to the same working solution after an hour. As can be seen the linearity and gradient have both reduced significantly, likely due to the DTT reacting with oxygen in the air. Therefore, it was decided to make a fresh DTT working solution before every DTT analysis to ensure consistent results.

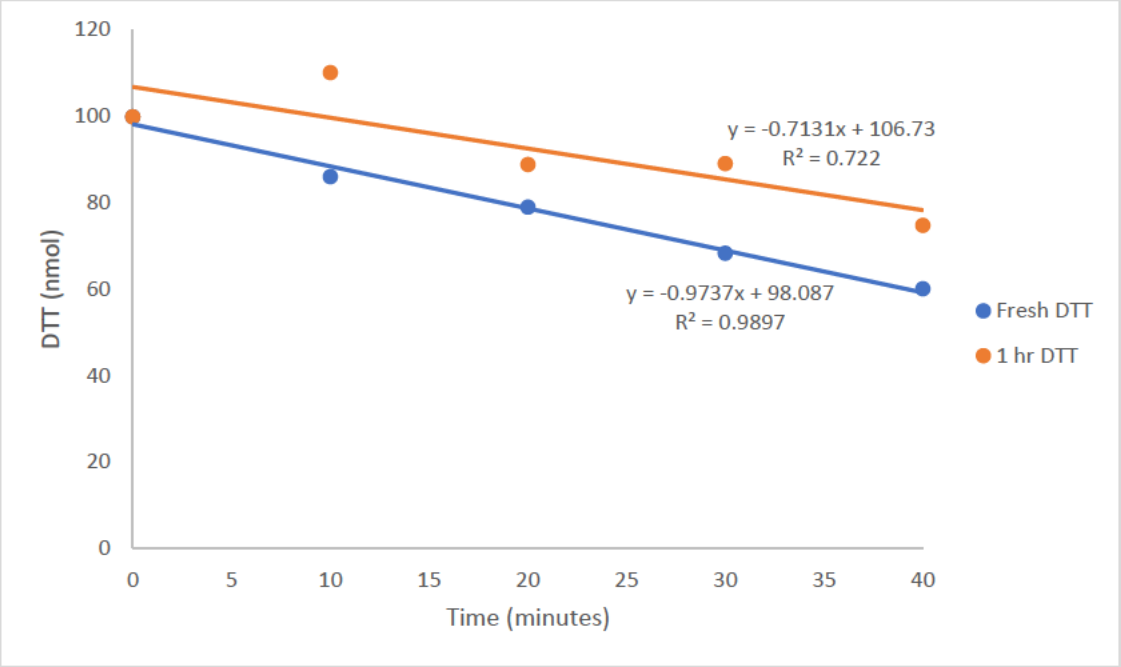

Figure 2-14: DTT depletion linear regression when exposed to 0.7 mL 0.2 µM PQN positive standard. The blue line shows the depletion of a freshly made DTT working solution, the orange line shows the depletion of the same working solution after 1 hour.

The impact of $PM_{2.5}$ extract age was tested on five $PM_{2.5}$ loaded filters from the Beijing winter campaign. The extracts were tested the day after extraction and then again just over a week later. Both days of analysis showed good linearity at $R^2 \geq 0.99$, with the filter blank activities being 0.818 ± 0.069 nmol DTT min^{-1} (CV 8.5 %, n = 2) for the fresh extracts and 0.755 ± 0.064 nmol DTT min^{-1} (CV 8.4 %, n = 3) for the week old extracts. The first $PM_{2.5}$ extract showed a DTT activity of 1.30 ± 0.039 nmol DTT min^{-1} (CV 3.0 %, n = 3) for the fresh extract, the aged extract was only analysed once but was within the uncertainty of the original triplicate value (1.316 nmol DTT min^{-1}). The other four PM loaded filters showed a 0.0362 ± 0.0021 nmol DTT min^{-1} reduction in DTT activity over the 9 days. Due to the lack of significant DTT loss during this test it was decided to analyse filters using the DTT assay up to a week after the date of extraction.

2.8 Finalised DTT protocol used for all samples

2.8.1 Chemicals, glassware and equipment

Chemicals (all from Sigma Aldrich):

- 9,10-Phenanthrenequinone, ≥99 % (PQN)
- 5,5'-Dithiobis(2-nitrobenzoic acid), 99 % (DTNB)
- DL-Dithiothreitol, ≥98 % (DTT)
- Potassium phosphate dibasic, ≥98 % (k-buffer)
- Potassium phosphate monobasic, ≥ 98 % (k-buffer)
- Nitrogen (oxygen free) from BOC
- Methanol, ≥99.9% from Fisher chemical

NB: DTT is stored in a fridge (5 ^{o}C) and allowed to settle at room temperature before opening.

Glassware (all glassware is acid washed overnight, rinsed in milli-q water and dried in a laminar hood. Immediately prior to use, all equipment is rinsed in milli-q water):

- Volumetric flasks; 25, 50, 100, and 250 mL. A-grade.
- Beakers; 25, 50, and 100 mL.
- Centrifuge tubes; 15 and 50 mL.
- Glass pipettes; 1, 2, 5, 25, and 50 mL. B-grade.
- Amber glass bottles; 1.5, 50, and 100 mL.
- Plastipak syringes; 10 mL.
- Polystyrol/polystyrene cuvettes; 10x4x45 mm.
- Acrodisc syringe filters; 0.45 µm membrane.
- Auto-pipettes; 20-200 µL, 0.1-1 mL, and 1-10 mL.

Equipment;

- Grant JB series, water bath.
- Jenway 6850 UV/vis. Spectrophotometer, dual beam (6850 PRISM software).
- Stuart orbital shaker.
- Hanna pH 210 microprocessor pH meter.
- 10 % HNO_3 acid bath.
- Laminar flow hood.

2.8.2 Stock preparation

- 10 mM DTT stock: 0.154 g of DTT was quantitatively transferred to a 100 mL volumetric flask and dissolved in DI water. It was stored in amber glass bottles in a fridge.
- 10 mM DTNB: 0.396 g of DTNB was quantitatively transferred to a 100 mL volumetric flask and dissolved in methanol; the stock was then transferred to an amber glass bottle with glass stopper (wrapped in aluminium foil to block light) and stored in a fridge.
- 0.5 M potassium phosphate buffer:

  0.5 M dipotassium phosphate (dibasic) was prepared by quantitatively transferring 8.71 g K_2HPO_4 into a 100 mL volumetric flask and dissolving in DI water.

  0.5 M monopotassium phosphate (monobasic) was prepared by quantitatively transferring 1.701 g KH_2PO_4 into a 100 mL volumetric flask and dissolving in DI water. The monobasic solution was added to the dibasic solution until the pH stabilised at 7.40 and stored at room temperature in an acid washed glass bottle.
- 0.05 µM PQN preparation (working solution), the 5 mM PQN stock was stored in a volumetric flask in a fridge (defrosted using a 37 ^{o}C water bath before use). The dilution steps are shown in Figure 2-15:

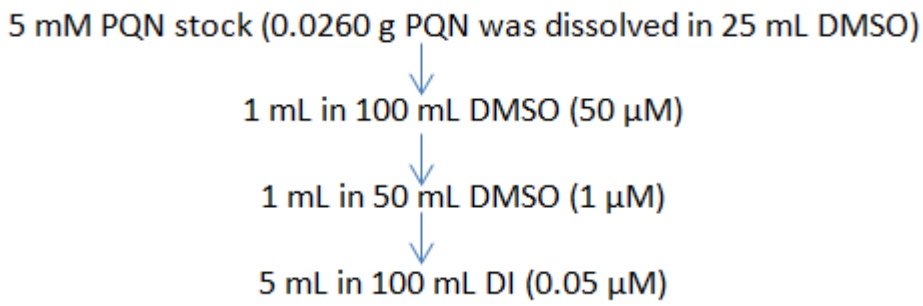

Figure 2-15: Dilution steps for preparing the PQN working solution from the 5 mM PQN stock solution.

2.8.3 $PM_{2.5}$ filter extraction

Rectangle (1 x 1.5 cm, SA 150 mm^2) and circular (0.8 cm Ø, SA 50 mm^2) punches were taken from each filter to ensure that ~20 µg $PM_{2.5}$ was present in each reaction (two rectangle punches were used for filter blanks). The equation for deriving the total mass of $PM_{2.5}$ in the reaction is:

$$\frac{\frac{Total\ PM\ on\ filter\ (\mu g)}{Filter\ SA\ (mm^2)} \times \sum SA\ of\ punches\ \ (mm^2)}{Final\ extract\ V\ (mL)} \times V\ of\ sample\ in\ reaction\ (mL)$$

Where SA = surface area and V = volume. For 47 mm Teflon filters the equation would be:

$$\frac{\frac{Total\ PM\ on\ filter\ (\mu g)}{1256\ mm^2} \times \sum SA\ of\ punches\ \ (mm^2)}{10\ mL} \times 0.7\ mL = PM\ in\ reaction\ (\mu g)$$

NB: The filter-cutting surface and punches were cleaned using dichloromethane prior to use and between filters to avoid cross contamination.

These punches were extracted in 5 mL methanol for 15 minutes via sonication; the extracts were then dried to ~1-2 mL using nitrogen blowdown. These extracts were then made up to 10 mL (volumes differed by ±5 mL in order to get the $PM_{2.5}$ in reaction to ~20 µg) using DI water and then extracted again for 15 minutes via sonication. The PM extract was then filtered through a 0.45 µm syringe filter, this filter extract was used in the same volume as PQN and filter blanks (0.7 mL).

SA of Teflon filter is 1256 mm^2 due to this being the area of the filter that is exposed to $PM_{2.5}$. The remaining portion of the filter is used to clamp the filter into the filter cradle.

2.8.4 DTT assay

- 0.2 mM DTNB preparation: a 50x dilution of the 10 mM DTNB stock was prepared by transferring 0.4 mL 10 mM DTNB into 19.6 mL DI water in a 50 mL amber glass bottle. 0.7 mL of 0.2 mM DTNB was transferred to 1.5 mL amber glass vials (5 vials per DTT run, one for each time point). (for other DTNB volumes: 29.4 mL DI & 0.6 mL DTNB, 39.2 mL DI & 0.8 mL DTNB)
- 0.7 mL of sample (PQN, PM extract, or filter blank,) was transferred to an acid washed centrifuge tube with 0.2 mL 0.5 M k-buffer, this solution was heated to 37 ^{o}C in a water bath. Just prior to starting the experiment a 1 mM DTT solution was prepared from the 10 mM DTT stock (5 mL 10 mM DTT stock made up in a 50 mL amber glass volumetric flask).
- 100 µL of 1 mM DTT was added to the sample / k-buffer solution. The solution was shaken and 100 µL of this solution was immediately transferred to an amber glass vial containing 0.2 mM DTNB, the coloured product of this reaction was immediately analysed using a dual-beam UV-vis.
- At various time points (0, 10, 20, 30, and 40 minutes) 100 µL of the reaction solution was transferred to the 0.2 mM DTNB vials, each vial was immediately analysed using UV-vis. Three measurements were taken for each time point at 412 and 700 nm (700 nm is the background reading).
- Two DTT runs are carried out at the same time, the second run is offset from the first by 5 minutes so that samples are analysed every 5 minutes. The second run uses the same 1 mM DTT as the first run but the DTT in the beaker is replaced by DTT in the volumetric flask. If more than two runs are being carried out the 1 mM DTT will be remade for each set of two runs.

During the DTT experiments, each day 2 filter blank DTT analysis were carried out along with 3 repeats of the first filter sample. To ensure the results were repeatable the results for that day were only kept if the coefficient of variation for both of these were below 15%. To account for day-to-day drift, periodically PQN positive standards were run through the DTT experiment.

2.8.5 Calibration

For the calibration, the solutions were not added to the water bath for heating and instead various concentrations of DTT solution were used. 0.7 mL of DI water and 0.2 mL 0.5 M k-buffer was added to five acid washed centrifuge tubes. Each tube had 100 µL of a different DTT concentration added and then had 100 µL removed and added to 0.2 mM DTNB, the DTT concentrations were:

- 100 µM: 5 mL in 50 mL DI
- 80 µM: 4 mL in 50 mL DI
- 60 µM: 3 mL in 50 mL DI
- 40 µM: 2 mL in 50 mL DI
- 20 µM: 1 mL in 50 mL DI
- 0 µM: 0.8 mL of DI water was used to take the place of DTT

The absorbance for each concentration was recorded in the same way as for samples and had the background reading at 700 nm and DI water absorbance subtracted from the absorbance at 412 nm. Figure 2-16 shows an example DTT calibration curve, the intercept is non-zero likely due to absorption by the presence of the k-buffer.

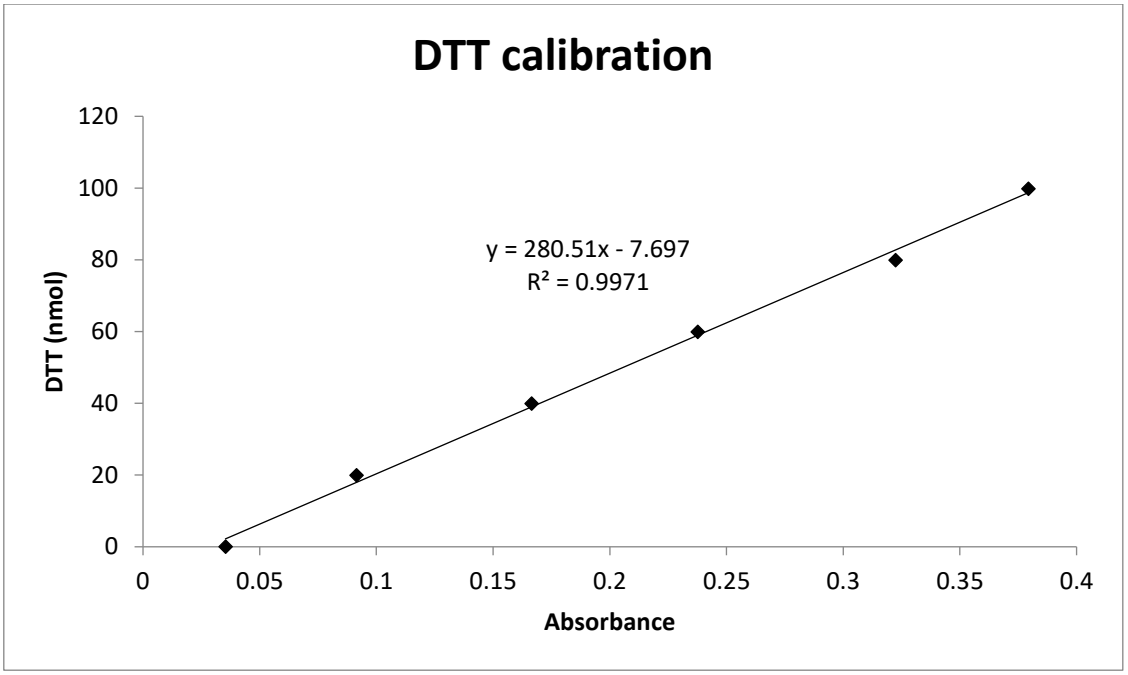

Figure 2-16: Example DTT calibration graph. Six DTT concentrations were chosen between 0-100 nmol (0, 20, 40, 60, 80, and 100). These were measured using the DTT assay under the same conditions as normal samples but were not heated and used milli-q water in place of PM extract. The small absorbance at 0 nmol DTT is likely due to the k-buffer in solution.

The equation of the straight line is used to determine DTT concentration from absorbance, from Figure 2-16 this would be: DTT (nmol) = 280.51 * absorbance – 7.697. Due to good repeatability of the DTT calibrations, they were performed less frequently than the PQN positive standard analysis. The average calibration equation for all calibration graphs was:

$$y = (284 \pm 9.0)x - (6.66 \pm 0.87)\ (\mathrm{R}^2 = (1.00 \pm 0.004), n = 5)$$

2.8.6 Analysing results

- All absorbance values at 412 nm have the background reading at 700 nm subtracted. The average DI water reading is also subtracted and then the average absorbance of each time point determined.

- The DTT concentration is determined from the absorbance at each time point by using the calibration equation: DTT (nmol) = 280.51 * absorbance – 7.697 or a rearranged form of Beer's law: C1 = (A1 / A2) * C2 (this only works if the absorbance at time 0 is reliable).
- DTT concentration (nmol, y-axis) is then plotted against time (min, x-axis). For a DTT run to be considered a success, the R^2 value should be above 0.95. The slope of the line is the DTT consumption rate: X nmol DTT min^{-1}, if the reaction volume is 1 mL, then X µM DTT min^{-1} is equivalent to X nmol DTT min^{-1}.
- DTT results are given in either units that are per unit mass of $PM_{2.5}$: pmol DTT min^{-1} μg^{-1} of $PM_{2.5}$ or per m^3 of sampled air: nmol DTT min^{-1} m^{-3}. Mass corrected DTT consumption is a measure of the intrinsic oxidative potential of the sampled PM, and is useful when comparing the OP of different $PM_{2.5}$ composition. Volume corrected DTT is a more health centred metric for the air encountered (inhaled), giving an OP value for a volume of air. DTTm and DTTv was calculated using the following equations:

$$DTT_v\ (\text{nmol min}^{-1}\ \text{m}^{-3}) = \frac{r_s\ (\text{nmol min}^{-1}) - r_b\ (\text{nmol min}^{-1})}{V_t\ (\text{m}^3) \times \frac{A_h\ (\text{cm}^2)}{A_t\ (\text{cm}^2)} \times \frac{V_s\ (\text{mL})}{V_e\ (\text{mL})}}$$

$$DTT_m\ (\text{nmol min}^{-1}\ \mu\text{g}^{-1}) = \frac{r_s\ (\text{nmol min}^{-1}) - r_b\ (\text{nmol min}^{-1})}{M_t\ (\mu\text{g}) \times \frac{A_h\ (\text{cm}^2)}{A_t\ (\text{cm}^2)} \times \frac{V_s\ (\text{mL})}{V_e\ (\text{mL})}}$$

Where r_s and r_b are the DTT consumption rates of sample and blank, respectively. V_t and M_t are the total sampling air volume and the total particle mass (with filter blank correction), respectively. A_h and A_t are the area of the punch and total filter, respectively. V_s and V_e are the sample volume participating in the reaction and extraction volume, respectively.

- To ensure results from the DTT experiment are correct, three criteria should be met:
    1. Linearity of the results should be 0.95 or higher (R^2)
    2. Coefficient of variation (%CV) 15 % or less for duplicate filter blank and PM loaded filter analysis
    3. Intermittent PQN positive standard analysis must remain consistent with previous measurements

Figure 2-17, Figure 2-18, and Figure 2-19 show example DTT depletion linear regression plots for a $PM_{2.5}$ extract, PQN positive standard, and a filter blank, respectively.

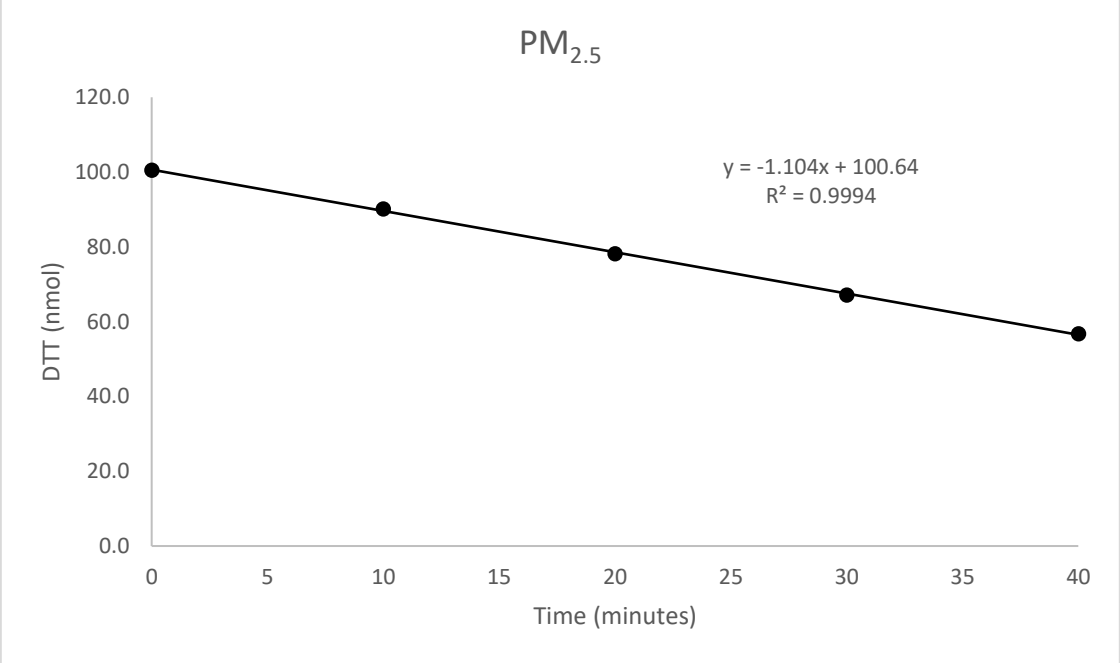

Figure 2-17: Example $PM_{2.5}$ DTT depletion linear regression plot. This $PM_{2.5}$ sample was collected during the Delhi winter campaign.

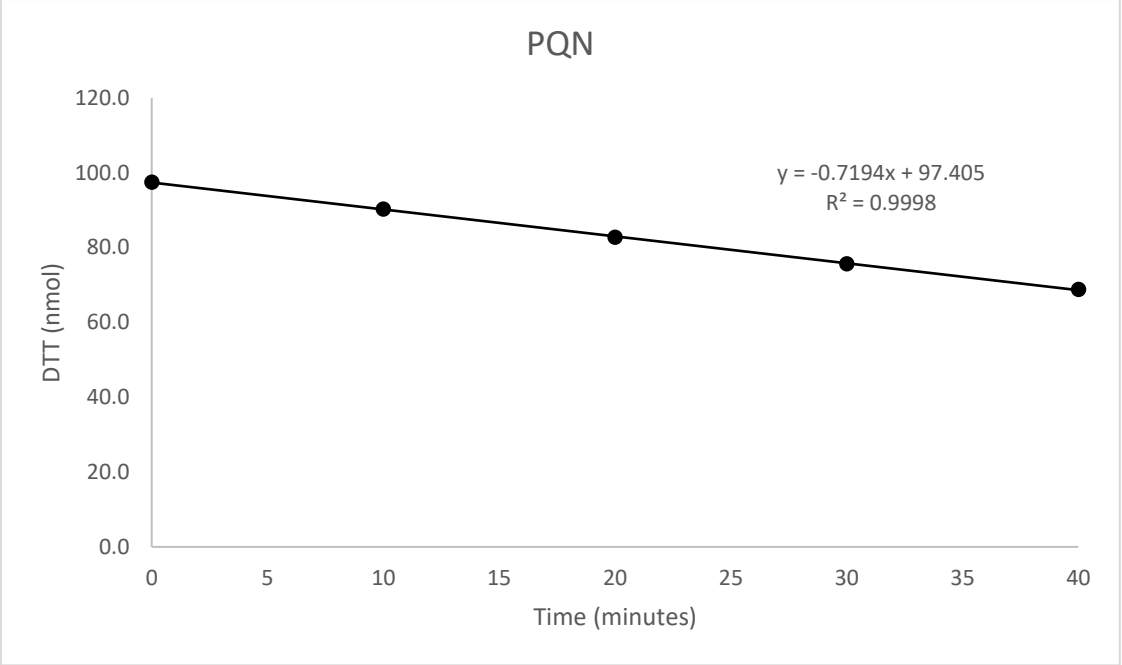

Figure 2-18: Example of a PQN positive standard DTT depletion linear regression.

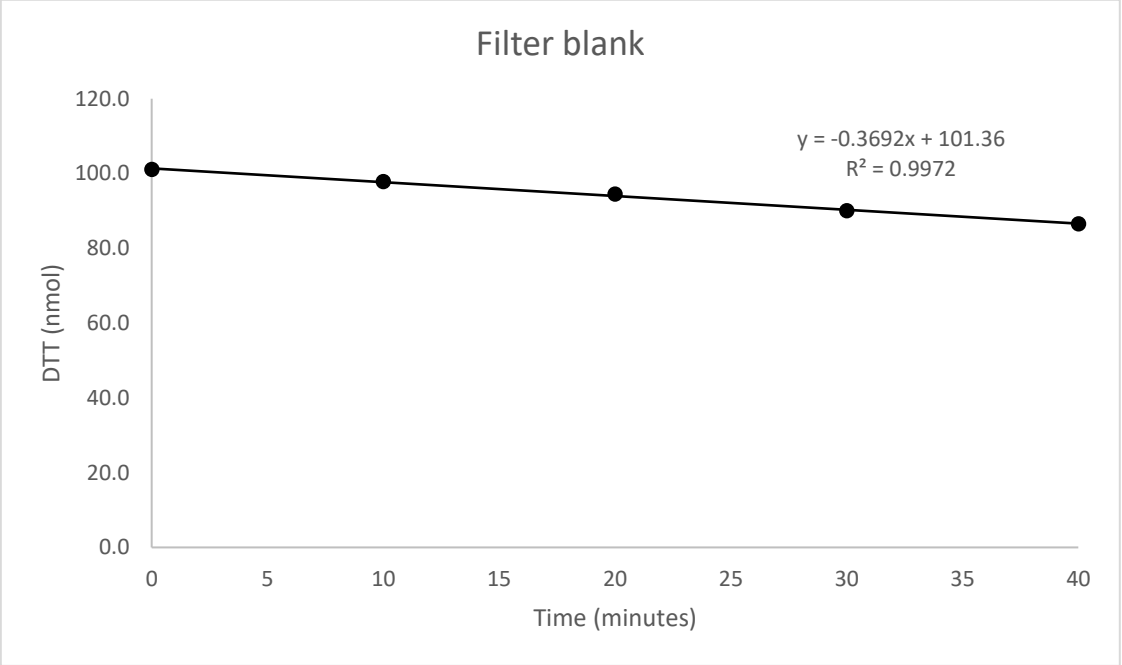

Figure 2-19: Example of a filter blank DTT depletion linear regression.

2.9 Conclusion

This chapter covered the background to various OP assays and the rationale behind choosing the DTT assay. The method development for the DTT assay was presented, along with the quality assurance steps for the final protocol. This protocol was applied to all $PM_{2.5}$

samples collected during this project. The results of this analysis in presented in later chapters of this thesis.

3 METHODOLOGY

This chapter presents the remaining methodology that was not covered in the method development section such as details on the various sampling campaigns in Birmingham, Beijing, and Delhi. The analytical tests performed on $PM_{2.5}$ loaded filters is also presented, along with details of the statistical tests performed on DTT values, PM composition data, and meteorological / gas-phase data. This analysis and its results is covered in chapters 4 – 6.

3.1 Offline sampling campaigns

3.1.1 Beijing – Sampling location characteristics

Beijing, the capital of China, is located at the northern tip of the North China Plain. Beijing has a continental climate with hot, humid summers and cold, dry, windy winters. The city lies on flat land with mountains to the north and west forming a semi-circular basin. This topography causes pollutants to get trapped during the summer by hot and humid high pressure systems from monsoons in the south. During the winter northerly winds regularly carry pollutants away from the city to the plains to the south. The location of the $PM_{2.5}$ samplers during the Beijing campaigns was on a roof in the Institute for Atmospheric Physics Tower Site (IAP), which is located between the second and third ring roads, north of the city centre. The height of the samplers was approximately 10 metres above ground level, and there are main road networks and commercial areas nearby (see Figure 3-20). The site is described as an urban background site and the two sampling campaigns were carried out during the winter of 2016 (09/11/16 – 11/12/16) and summer of 2017 (21/05/17 –

24/06/17) (Cheng et al., 2016; *Geography: Beijing*, 2020; National Bureau of Statistics of China, 2004; Z. Shi et al., 2019).

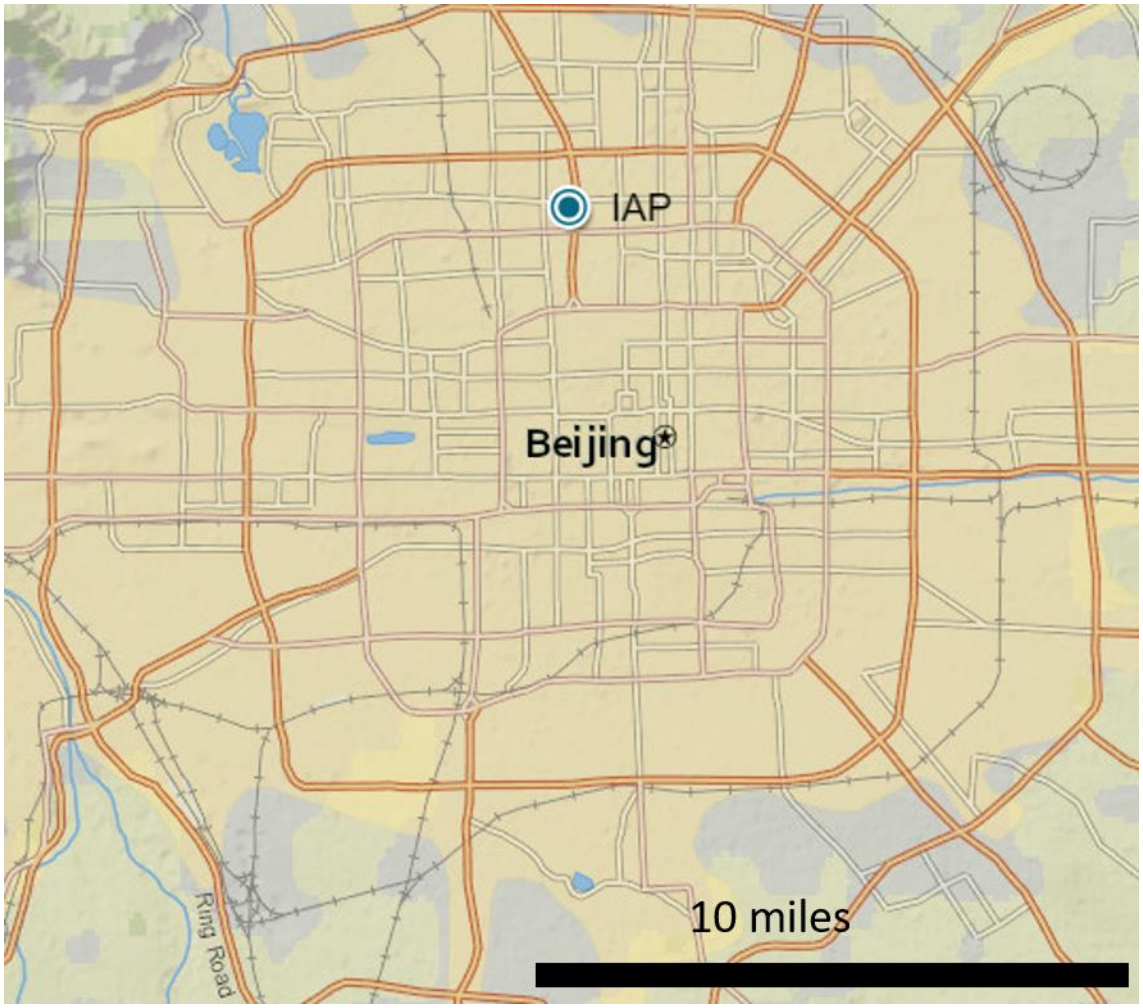

Figure 3-20: Map of Beijing, China showing the location of the Institute of Atmospheric Physics (IAP) site where all measurements for this campaign were made.

3.1.2 Delhi – Sampling location characteristics

Delhi, the capital and National Capital Territory of India is located in the Indo-Gangetic Plain. Air quality in Delhi is often the worst in the world (GBD MAPS Working Group, 2018), particularly in the autumn and winter due to high primary emissions, low wind speeds, and low boundary layer depth. Along with local sources, regional biomass burning emissions contribute significantly to the poor air quality in Delhi. PM sampling for the Delhi campaigns was carried out at the Indian Institute of Technology, Delhi (IIT). This site is described as an

urban background site located in the south of the city as shown in Figure 3-21. There were three periods of intensive sampling carried out at this site during 2018, split into winter (18/01/18 – 09/02/18), summer (30/04/18 – 03/06/18), and autumn (18/10/18 – 09/11/18) campaigns. Meteorological data was measured at the Indira Ghandi international airport, which was located roughly 5 km west of IIT. The AMS data was measured at Lodhi road, which was 10 km north of IIT (Bikkina et al., 2019; Census Organization of India, 2020; Puthussery et al., 2020; UNCCD COP 14, 2020).

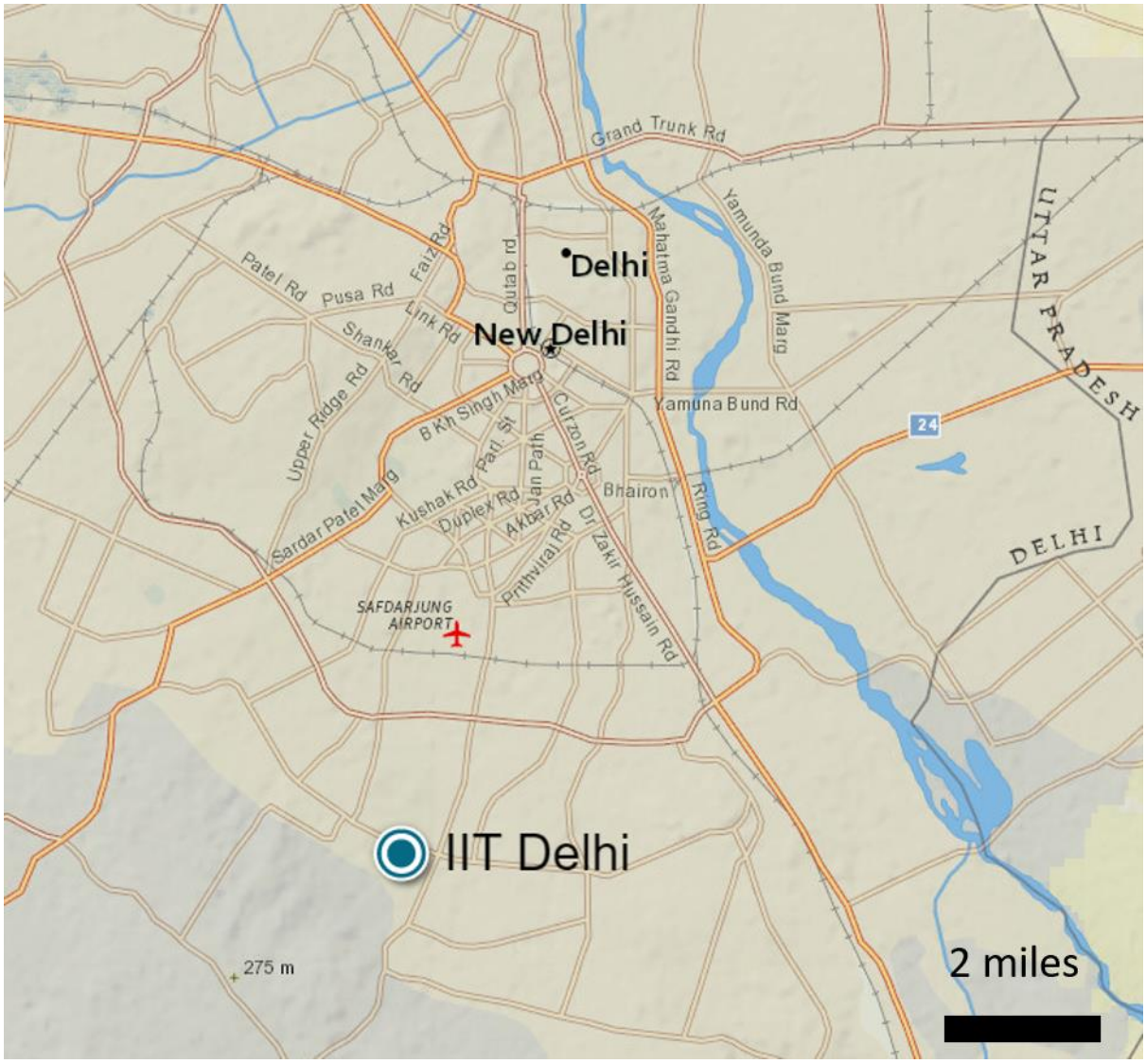

Figure 3-21: Map of New Delhi, India showing the location of the Indian Institute of Technology Delhi (IIT Delhi), where all measurements for Delhi that are shown in this thesis were conducted.

3.1.3 Birmingham – Sampling location characteristics

The Birmingham campaign was significantly different from the other two campaigns in this project. The short sampling campaign in Birmingham was intended as a real world test to confirm that the finalised DTT protocol was working correctly. Sampling was carried out for seven days during the winter of 2018: 03/12/18 – 09/12/18.

$PM_{2.5}$ sampling was conducting using a high volume $PM_{2.5}$ sampler at the Bristol road observation site (BROS) in the university of Birmingham campus. The site is described as roadside, being about 2 meters above and 5 meters away from the junction of Bristol and Bournbrook roads. For all seven days of sampling, construction work was taking place at the junction, on the road closest to the $PM_{2.5}$ sampler. This construction work closed a lane of Bristol road nearest the sampler, causing consistent traffic jams at the junction for the majority of the sampling period.

Due to a lack of available equipment, TEOM $PM_{2.5}$ measurements were not conducted at the BROS site. Instead the average $PM_{2.5}$ concentration from both of the two nearest air pollution monitoring stations were used to calculate mass loading on the filters. These stations were the A4540 roadside and Ladywood sites as shown in Figure 3-22.

Figure 3-22: Map showing the location of the $PM_{2.5}$ sampling site at the Bristol road observation site (BROS) in the University of Birmingham, Birmingham, UK. As well as the air pollution monitoring stations at Ladywood (2.39 miles from BROS) and A4540 roadside (3.00 miles from BROS). The Ladywood and A4540 roadside sites are 1.85 miles from each other.

3.1.2 $PM_{2.5}$ samplers

3.1.2.1 High volume samplers

Tisch environmental high volume air samplers were used to collect $PM_{2.5}$ onto baked quartz filters during the Beijing and Birmingham campaigns. These samplers were run for 23 / 24 hours (Beijing / Birmingham) per filter at a flow rate of 40 m^3 hr^{-1}. PM loaded filters were stored in a -80 °C freezer prior to transport back to the UK and during long term storage in the University of Birmingham.

3.1.2.2 DIGITEL $PM_{2.5}$ sampler

The Delhi field campaigns used DIGITEL aerosol samplers to sample $PM_{2.5}$ onto quartz filters at a flow rate of 30 m^3 hr^{-1}. These filters were sampled for 12 hours from 9 am to 9 pm

during the day and 9 pm to 9 am during the night. Filters were also stored in a -80 °C freezer before being transported back to UK and decanted into local freezers.

3.1.2.3 Minivol® TAS-5.0 (Air Metrics)

The TAS-5.0 Minivol sampler was used during the Delhi autumn campaign to accompany the DIGITEL sampler. The minivol samples $PM_{2.5}$ by drawing air through a particle size separator (impactor) at a constant flow rate of 5 L min^{-1}. The particulate matter is caught on the filter, which is secured by a cassette; the 47 mm diameter (Ø) filter is weighed pre- and post-exposure using a six-figure microbalance. The Teflon filters were conditioned in the temperature and humidity controlled weighing room overnight before measurements on the six-figure balance.

3.2 Physical and chemical analysis performed on $PM_{2.5}$ loaded filters

3.2.1 Dithiothreitol (DTT) assay

The development and operational protocol of the DTT assay was covered in detail in Chapter 2 Method Development. The DTT protocol used for analysis of the Birmingham, Beijing, and Delhi samples is outlined in section 2.8 of the method development chapter. Throughout this thesis the term intrinsic toxicity is used to refer to the OP of $PM_{2.5}$ particles (DTTm).

3.2.2 Online $PM_{2.5}$ measurements

Online $PM_{2.5}$ measurements for all campaigns was determined using TEOM instruments with filter equilibrating and weighing conditions in line with the United States Federal Reference Method (RH = 30 – 40 %, temperature = 20 – 23 °C) (U.S. EPA, 2016b; Jingsha Xu et al., 2020). TEOM $PM_{2.5}$ concentrations were used to determine the mass loading on the quartz

filters due to the lack of gravimetric data available for these filters from Beijing. Delhi quartz filters also used TEOM measurements to be in line with the data obtained for the Birmingham and Beijing campaigns.

3.2.3 Water soluble ions analysis

Water soluble ions were analysed for $PM_{2.5}$ samples collected during the Beijing and Delhi campaigns. The ions selected are commonly associated with a broad range of sources including coal and biomass combustion, crustal materials, and non-exhaust vehicle emissions. The ions analysed were: K^+, Na^+, NH_4^+, Ca^{2+}, NO_3^-, SO_4^{2-}, Cl^-, PO_4^{3-}, and Mg^{2+}.

This method is described in Xu et al., 2020. Briefly, half of PM loaded PTFE filters were extracted in 10 mL ultrapure water and analysed for inorganic ions using ion chromatography (Dionex, Sunnyvale, CA, USA). Analytical uncertainty was < 5 %. Measurements were corrected for field blank values. The detection limits of the measured ions range from 0.010 – 0.240 μg m^{-3} (for K^+ and NO_3^-, respectively). Quality assurance was carried out by analysing a Certified Reference Material (CRM).

3.2.4 Trace metal analysis

Metals are often used as indicators of various sources of $PM_{2.5}$ such as crustal material, re-suspended road dust, vehicle emissions (both exhaust and non-exhaust), and biomass burning (Das et al., 2015; Duan & Tan, 2013; Rai, Slowik, Furger, Haddad, et al., 2021). The analysis of metals for this project was carried out using Inductively Coupled Plasma Mass Spectrometry (ICP-MS) and X-Ray Fluorescence (XRF) spectroscopy.

These methods are described in Xu et al., 2020. Trace metals in $PM_{2.5}$ were analysed by extracting half the PTFE filter using diluted aqua regia (HNO_3 and HCl) and analysed using ICP-MS and XRF. Measurements were corrected for field blank values. The detection limits

for ICP-MS ranged from 0.003 – 0.221 µg m^{-3} (for Ti and Al, respectively). The detection limits for XRF ranged from 0.0004 – 0.077 µg m^{-3} (for As and Sb, respectively). Quality assurance was carried out by analysing a CRM.

3.2.5 Polycyclic Aromatic Hydrocarbon (PAH) and n-alkane analysis

Polycyclic aromatic hydrocarbons (PAH) are most commonly markers for unburned fuel from motor vehicles and biomass burning (Shirmohammadi et al., 2016). PAH are carcinogenic and often measured as part of air quality management protocols (European Communities, 2001). PAH during this project were analysed using Gas Chromatography with a Mass Spectrometer (GC-MS) detection method.

This method is described in Xu et al., 2020. Various n-alkanes, polycyclic aromatic hydrocarbons, fatty acids, and cholesterol was measured using GC-MS. Briefly, 9 cm^2 of PM loaded quartz filter was extracted using dichloromethane and methanol, this was concentrated using rotary evaporation and nitrogen blow down. A combination of 50 µL N,O-bis-(trimethylsilyl)trifluoroacetamide (BSTFA) in 1 % trimethylsilyl (TMS) chloride and 10 µL pyridine was added to the extracts and allowed to react for 3 hours at 70 °C. After cooling to room temperature the extracts were diluted with 140 µL C13 n-alkane internal standard for quality assurance and analysed using GC-MS. Recovery rates were in the range of 70 – 100 % based on spiked standards analysed using the same methods. Analysed field blanks showed no target compounds detected.

3.3 Statistical analysis

3.3.1 Linear regression analysis

The linear regression analysis used to determine the DTT oxidative potential of $PM_{2.5}$ samples was performed using Microsoft Excel. The linear regression plots included in this thesis were produced using the ggplot2 package in r-studio for easier control over the visual design and data manipulation. The Pearson correlation coefficient was used on these plots with the accompanying p-value. The standard error in the gradient was determined using the broom and tidyr packages in r-studio. R-studio was also used for the linear regression analysis for DTTm and $PM_{2.5}$ component species.

Correlation analysis involving the correlation of DTTm with $PM_{2.5}$ composition species had the units of these composition species converted from the standard (µg or ng) m^{-3} to (µg or ng) μg^{-1} $PM_{2.5}$. This was done by multiplying the composition specie concentration by the average $PM_{2.5}$ concentration during the sampling period. The composition species used in this analysis were used as indicators for different sources of PM, these sources are shown in Table 3-1. The $PM_{2.5}$ data were obtained from the TEOM measurements made near the $PM_{2.5}$ samplers. Average $PM_{2.5}$ concentrations for the sampling time was determined using the swfscMisc package in r-studio. This resulted in the gradients of these correlation plots having the units: pmol DTT min^{-1} μg^{-1} / ng^{-1} of each species, allowing for easier cross campaign comparison of the impact of each compositional specie on DTTm.

Table 3-1: Breakdown of which PM composition species are indicative of which sources.

Composition species	Indicated source	Reference
Aluminium, barium, cerium, NO_x, and water-soluble manganese	Vehicle emissions	Chen et al., 2001; Bhaskar & Mehta, 2010; Boningari & Smirniotis, 2016; Cao et al., 2012; Gunthe et al., 2021; Jain et al., 2020; R. Li et al., 2019; Monaci & Bargagli, 1996; Peel et al., 2013; Rai et al., 2021; Seigneur, 2019; U.S. EPA, 2016
Aluminium, potassium, and silicon	Crustal material and road dust	Z. Liu et al., 2018; Rai et al., 2021
Arsenic, chlorine, copper, lead, tin, and zinc	Primary emission group	Rai et al., 2021
Barium, calcium, iron, nickel, and strontium	Non-exhaust vehicle emissions	Z. Liu et al., 2018; Rai et al., 2021
Calcium, iron, strontium, and titanium	Crustal materials, road dust, and construction	Cao et al., 2012; Rai et al., 2021
Chlorine	Sea salt, road salt, and plastic-containing waste burning	Chen et al., 2001; Bhaskar & Mehta, 2010; Gunthe et al., 2021; R. Li et al., 2019; Monaci & Bargagli, 1996; Rai et al., 2021; Yao et al., 2002
Copper	Industrial emissions and coal / waste burning	Bhaskar & Mehta, 2010; Charrier et al., 2015; Gunthe et al., 2021; Rai et al., 2021
Elemental carbon	Coal combustion, vehicle emission, and biomass burning	Chen et al., 2001; Bhaskar & Mehta, 2010; Gunthe et al., 2021; R. Li et al., 2019; Monaci & Bargagli, 1996

Iron and manganese	Brake wear	Cao et al., 2012; Rai et al., 2021
Magnesium	Soil erosion, industrial sources, construction, and suspended road dust	Z. Liu et al., 2018; J. Wang et al., 2018
n-alkanes (even numbered)	Vehicle emissions and coal combustion	Lyu et al., 2019; Oros & Simoneit, 2000
n-alkanes (odd numbered)	Biomass burning and plant wax	Lyu et al., 2019; Oros & Simoneit, 2000
Nickel and vanadium	Residual oil and coal combustion	Das et al., 2015; Duan & Tan, 2013; Z. Liu et al., 2018
Organic carbon and potassium	Biomass burning	Jain et al., 2020; Z. Liu et al., 2018; Rai et al., 2021
PAH	Unburned fuel from motor vehicles and biomass burning	Shirmohammadi et al., 2017
Sodium	Sea salt and road salt	Z. Liu et al., 2018; Rai et al., 2021
Water-soluble chromium	Vehicle emissions and oil burning	Cao et al., 2012; Rai et al., 2021

3.3.2 Linear regression matrix

In order to visualise the Pearson correlation coefficient between DTTm and different aspects of $PM_{2.5}$ composition, considering the large number of measured species, correlograms (a graph of correlation matrix values) were produced using the R-studio package corrplot. Generally, species whose correlation with DTTm values showed an r value ≤ 0.5 and / or a p number > 0.05 were excluded from the matrix. The matrices were ordered according to the correlation coefficient, using a hierarchical clustering method. Any correlation in the matrix

below the 95 % confidence interval was included however, it was marked as unreliable (red cross over the value).

3.3.3 Source apportionment

The source apportionment method used is detailed in Xu et al., 2020. Briefly, the sources of OC and $PM_{2.5}$ (two separate analyses) were apportioned using the chemical mass balance model (US EPA CMB8.2), utilising a linear least squares solution. The principal sources determined for OC were vegetative detritus, biomass burning, gasoline vehicles, industrial coal combustion, residential coal combustion, cooking, and other OC.

3.3.4 Multiple linear regression

Multiple linear regression (MLR) analysis was carried out on the various sources described by the source apportionment analysis for the Beijing campaigns and select species representing different sources in Delhi. This was done using the tidyverse package in r-studio. After each application of the MLR analysis, the least significant species or source was removed; with the MLR analysis being rerun until only significant results remain based on the p-value (95 % confidence interval). The R^2 value was used to determine the proportion of variance in DTTm that could be predicted by the species / sources.

3.3.5 Pairwise unpaired t-test

To determine where samples or combinations of samples showed statistically significantly different concentrations of $PM_{2.5}$ or DTTm and DTTv values, a pairwise unpaired t-test analysis was performed. This was done using the dplyr package in r using a Benjamini & Hochberg p-value adjustment. This adjustment decreases the false positive rate in t-tests by determining a critical value to compare p-values to, based on the rank of p-values (in

ascending order), the total number of tests performed, and the false discovery rate. The t-test results were considered significant at a 95 % confidence interval.

3.3.6 Cluster analysis

Cluster analysis is a statistical method which organises data into groups or clusters based on how closely associated the different values are. It is an unsupervised learning algorithm which can find commonality in the variability of one or more parameters (Pietrogrande et al., 2018b).

Clustering analysis was performed on the DTTm and composition data to determine possible trends in the combined data or within campaigns. The clustering analysis was performed using r-studio and several packages. The data was treated by removing missing data and scaling the data. Hierarchical clustering was performed using the average, single, complete, and ward clustering methods. The ward method produced the best agglomerative coefficient for all scenarios, so was used for all clustering.

3.4 Contributions to the work presented here

The determination of $PM_{2.5}$ chemical composition, gas-phase data, and $PM_{2.5}$ sampling (only for Delhi) during the Beijing and Delhi campaigns were performed by other people, the breakdown is:

- All $PM_{2.5}$ composition species and TEOM measurements made during the Beijing field campaigns was carried out by the University of Birmingham.
- Gas-phase and meteorological data for the Beijing campaigns was measured by the University of York.

- Hydroxyl radicals measured during the Beijing campaigns was provided by the University of Leeds.
- $PM_{2.5}$ sampling and gas-phase data during the Delhi campaigns was performed by Louisa Kramer, Leigh Crilley, and Salim Alam of the University of Birmingham.
- $PM_{2.5}$ composition species measured during the Delhi campaigns was provided by Salim Alam of the University of Birmingham.
- AMS-PMF data for the Delhi campaigns was collected and analysed by Ernesto Villegas and James Allan of the Centre for Ecology & Hydrology (CEH) and the University of Manchester.

4 DATA REPORTING FOR BEIJING AND BIRMINGHAM

This chapter presents the $PM_{2.5}$ mass concentration, DTTm, DTTv, and chemical composition results for the Beijing and Birmingham campaigns, along with a brief narrative discussion of the trends observed in these data. Detailed statistical analysis of these data will be covered in Chapter 6.

4.1 Summary of the $PM_{2.5}$ sampling in Beijing and Birmingham

Beijing experiences frequent haze events during the winter, typically characterised by stagnant meteorological conditions and large emissions of primary air pollutants. Many papers have attributed this largely to a combination of primary emissions, notably from local coal-fired district heating during the winter months, and chemical processing of aerosol particles which increases their hygroscopicity and hence growth of haze. The summer generally has considerably lower concentrations of most pollutants such as $PM_{2.5}$ (during the campaigns discussed here winter: 99.2 ± 74, summer: 36.5 ± 17 μg m^{-3}), organic carbon (winter: 20.9 ± 12, summer: 6.44 ± 2.3 μg m^{-3}), PM-bound metals, and NO (winter: 41.9 ± 29, summer: 4.90 ± 5.5 ppb), however, some pollutants such as ozone are significantly higher during the summer (winter: 8.60 ± 5.8, summer: 55.5 ± 19 ppb) (Cheng et al., 2016; Guo et al., 2014; L. Jiang & Bai, 2018; Lu et al., 2020).

Table 4- provides a summary of the $PM_{2.5}$ samples that were collected during each campaign in Beijing and Birmingham. In total 80 filters were collected and analysed for DTT OP from these campaigns, including five higher time resolution filters collected during the Beijing

summer campaign. These filters were collected to gain insight into the development of OP throughout the day.

Table 4-1: Summary of $PM_{2.5}$ filter collection during the Beijing field campaigns and week of Birmingham sampling. Only filters that were analysed for DTT are included. The $PM_{2.5}$ data for Birmingham is the average reading of the A4540 roadside and Ladywood air pollution monitoring sites. All blank filters are field blanks that were loaded in the PM samplers.

Campaign	Filter type	Sampling dates	Number of filters analysed	Number of blank filters	Sampling time (hrs)	Avg. $PM_{2.5}$ ($\mu g\ m^{-3}$ TEOM)
Beijing winter	Quartz	09/11/16 – 11/12/16	33	2	23	99.2 ± 74
Beijing summer	Quartz	21/05/17 – 24/06/17	35	2	23	36.5 ± 17
Beijing summer high time resolution	Quartz	19-20/06/17	5	1	4 during the day, 8 overnight (00:00 – 08:00 20/06/17)	29.0 ± 8.4
Birmingham	Quartz	03/12/18 – 09/12/18	7	1	24	5.74 ± 2.6

4.2 Summary of wider composition data available for Beijing and Birmingham campaigns

As the $PM_{2.5}$ sampling and OP analysis in this project (with the exception of Birmingham) was part of the larger APHH programme, a wide array of $PM_{2.5}$ composition, meteorological, and gas data was made available to analyse. Table 4-1 provides the breakdown of the various data available for the Beijing field campaigns, along with the operators / institutions who collected the data and instruments used. Excluding $PM_{2.5}$ concentration and OP data, 115 species were measured for the winter campaign and 116 for the summer campaign.

In addition to these measurements J. Xu (2020, pers. comm., 22 June) provided source apportionment results obtained from the Beijing campaigns using the Chemical Mass Balance (CMB) model, performed on organic carbon and $PM_{2.5}$. $PM_{2.5}$ sources were determined using the OC / $PM_{2.5}$ ratio to convert OC sources to $PM_{2.5}$. For OC the sources were:

- Vegetative detritus.
- Biomass burning.
- Gasoline vehicles.
- Diesel vehicles.
- Industrial coal combustion.
- Residential coal combustion.
- Cooking.
- Other organic carbon.

The $PM_{2.5}$ source apportionment had the same sources as OC plus SNA (sulphate, nitrate, and ammonium) and geological minerals.

Table 4-2: All of the available composition data for $PM_{2.5}$, gases, and meteorological data during the Beijing field campaigns. 1 = University of Birmingham, 2 = Imperial College London, 3 = Institute of Atmospheric Physics, Chinese Academy of Sciences.

Campaign	Data description	Data provided by	Instrument	Species measured
Beijing winter and summer	OC / EC and ions	Tuan Vu[1,2], Di Liu[1], and Jingsha Xu[1]	DRI and Ion chromatography	OC, EC, K^+, Na^+, NH_4^+, Ca^{2+}, NO_3^-, SO_4^{2-}, Cl^-
	Metals		XRF and ICP-MS	Si, Al, Cu, Fe, Ti, V, Cr, Mn, Co, Ni, Zn, As, Sr, Ba, Pb, Cd, Sb
	Biomass tracers		GC-MS	Galactosan, mannosan, levoglucosan
	PAHs			Phenanthrene, anthracene, fluoranthene, pyrene, benzo(b)fluorine, benz(a)anthracene, chrysene / triphenylene, benzo(b)fluoranthene, benzo(k)fluoranthene, benzo(e)pyrene, **benzo(a)pyrene**, perylene, Indeno(1,2,3-cd)pyrene, dibenz(a,h)anthracene, benzo(ghi)perylene, coronene, picence, retene, cholesterol
	n-alkanes			C24, C25, C26, C27, C28, C29, C30, C31, C32, C33, C34
	Cooking markers			Palmitic acid, stearic acid
	Vehicle exhaust markers			17a (H) -22, 29, 30-Trisnorhopane (C27a), 17b (H), 21a (H) - Norhopane (C30ba)
	SOA tracers	Di Liu[1]		2-methylthreitol, 2-methylerythritol, 2-methylglyceric acid, cis-2-methyl-1,3,4-trihydroxy-1-butene, 3-methyl-2,3,4-trihydroxy-1-butene, trans-2-methyl-1,3,4-trihydroxy-1-butene, HGA, PNA, PA, MBTCA, β-caryophyllinic acid, 3-Acetylpentanedioic acid, 3-Acetyl hexanedioic acid, 3-Isopropylpentanedioic acid, 2,3-Dihydroxy-4-oxopentanoic acid, HDMGA, C5-alkene triols, 2-methyltetrols
	AMS data	Jingsha Xu[1]	AMS	Org, NH_4, NO_3, SO_4, Chl, COA, Summer only; HOA, OOA1, OOA2, OOA3, Winter only; CCOA, BBOA, OPOA, LOOA, MOOOA
	Gas data	University of		O_3, CO, NO, NO_2, NO_y, NO_z

		York		
	Hydroxyl radical	University of Leeds	FAGE	OH (molecules cm^{-3})
	Meteorology data	University of York		Wind speed, wind direction, relative humidity, temperature
Beijing summer	Gas data	IAP[3]		methanol, acetonitrile, acetaldehyde, acrolein, acetone, isoprene, methyl vinyl ketone and methacrolein, methyl ethyl ketone, benzene, toluene, C2-benzenes, C3-benzenes, monoterpenes
Beijing winter	Water soluble metals	Tuan Vu[1,2]	ICP-MS	Cu, Mn, Fe, Zn, As, Pb, Co, Ni, Cr, Cd, Sb

For the sampling at BROS in Birmingham, no PM composition analyses were performed. $PM_{2.5}$ concentration, gaseous composition and meteorological data were therefore obtained from the two closest air pollution monitoring sites: the A4540 (roadside) and Ladywood (background) sites in Birmingham. The breakdown of data obtained from these stations and data coverage / quality are provided in Table 4-.

Table 4-3: The level of data coverage and verification for different air pollutants measured by the A4540 roadside and Ladywood air pollution monitoring sites during the winter sampling in Birmingham.

Pollutant	Status at A4540	Status at Ladywood	Verified
O_3	Complete coverage	No data	A4540 - Verified
NO	Complete coverage	No data	A4540 – Verified
NO_2	Complete coverage	No data	A4540 – Verified
NO_x	Complete coverage	No data	A4540 – Verified
PM_{10}	Complete coverage	Complete coverage	A4540 – Verified Ladywood - verified
$PM_{2.5}$	Complete coverage	Complete coverage	A4540 – Verified Ladywood – verified
Non-volatile $PM_{2.5}$	Complete coverage	Complete coverage	A4540 – Verified Ladywood – verified
Volatile $PM_{2.5}$	Complete coverage	Complete coverage	A4540 – Verified Ladywood – verified
Wind direction (deg)	Missing 14.5 hrs data for first sample	Missing first 2 filters and 13.5 hours for 3rd filter	A4540 – Not verified Ladywood – not verified
Wind speed (m s^{-1})	Missing 14.5 hrs data for first sample	Missing first 2 filters and 13.5 hours for 3rd filter	A4540 – Not verified Ladywood – not verified
Temperature (°C)	Missing 14.5 hrs data for first sample	Missing first 2 filters and 13.5 hours for 3rd filter	A4540 – Not verified Ladywood – not verified

4.3 OP^{DTT} results for Beijing and Birmingham

The average $PM_{2.5}$ concentration, and corresponding mean volume normalised and intrinsic toxicity are shown in Table 4-. The $PM_{2.5}$ concentration observed during the Beijing campaigns are consistent with previously reported literature for cities within the North China Plain (NCP): 113.8 ± 62.7 and 50 – 410 μg m^{-3} reported for Beijing and 113.8 – 120.1 ± 50.5 – 88.3 μg m^{-3} for Jinzhou, Tianjin, and Yantai (Q. Liu et al., 2014; W. J. Liu et al., 2018b; S. Y. Yu et al., 2018). Birmingham $PM_{2.5}$ concentrations were similar to those reported for other developed cities such as Los Angeles (5 – 10 μg m^{-3}) or Atlanta (5 – 25 μg m^{-3}) (Hu et al., 2008; Verma et al., 2012).

Table 4-4: Summary table of the $PM_{2.5}$, DTTm, and DTTv results obtained for field campaigns in Beijing and Birmingham. Total filters = 80.

Campaign	Filter type	Avg. $PM_{2.5}$ ± SD (μg m^{-3})	Avg. DTTv ± SD (nmol DTT min^{-1} m^{-3})	DTTv range	Avg. DTTm ± SD (pmol DTT min^{-1} μg^{-1} $PM_{2.5}$)	DTTm range	Number of filters
Beijing winter	Quartz	99.2 ± 74	3.04 ± 1.9	0.59 – 6.68	37.0 ± 14	11.4 – 73.7	33
Beijing summer	Quartz	36.5 ± 17	0.896 ± 0.40	0.38 – 2.22	26.4 ± 9.2	11.6 – 46.1	35
Beijing summer high time resolution	Quartz	29.0 ± 8.4	1.01 ± 0.38	0.74 – 1.65	34.3 ± 5.2	28.1 – 39.6	5
Birmingham	Quartz	5.74 ± 2.6	0.217 ± 0.16	0.092 – 0.509	35.6 ± 13	23.8 – 56.3	7

For the Beijing measurements, the intrinsic toxicity as evaluated by the DTT assay was statistically significantly higher during the winter campaign than summer as shown by a unpaired t-test at a 99.9 % confidence interval (Figure 6-2). The intrinsic toxicity observed in Birmingham is not statistically significantly different from either of the Beijing campaigns.

Both campaigns have DTTm values that are consistent with those observed in other studies across the world, with similar values to:

- Patiala, India at 27 ± 8 pmol DTT min^{-1} μg^{-1} $PM_{2.5}$ (Patel & Rastogi, 2018a).
- Orinda, United States at 38 ± 21 pmol DTT min^{-1} μg^{-1} $PM_{2.5}$ (Ntziachristos et al., 2007).
- Los Angeles, United States at 19 ± 4 pmol DTT min^{-1} μg^{-1} $PM_{2.5}$ (Hu et al., 2008).
- Atlanta, Unites States at 34 ± 9 and 10 – 50 pmol DTT min^{-1} μg^{-1} $PM_{2.5}$ across two studies (T Fang et al., 2015; Verma et al., 2012).
- Mexico City, Mexico at 25 – 40 pmol DTT min^{-1} μg^{-1} $PM_{2.5}$ (De Vizcaya-Ruiz et al., 2006).
- Jinzhou, Tianjin, and Yantai, China at 35 ± 18, 49 ± 16, and 30 ± 16 pmol DTT min^{-1} μg^{-1} $PM_{2.5}$, respectively (W. J. Liu et al., 2018b).

Birmingham has similar DTTv values to other developed cities such as Atlanta (0.1 – 0.8 and 0.18 – 0.6 nmol DTT min^{-1} m^{-3}) and Chicago (0.05 – 0.60 nmol DTT min^{-1} m^{-3}) (T. Fang et al., 2015; T. Fang et al., 2016; Zeng et al., 2021). The Beijing summer campaign has some overlap in DTTv with these developed cities, however, the Beijing DTTv values mostly exceeded the DTTv seen in places such as Atlanta and Chicago. The Beijing campaigns fall more into the range observed by Borlaza et al., 2018 in Gwangju, South Korea and Manila, Philippines at 0.1 – 7.5 nmol DTT min^{-1} m^{-3}. W. J. Liu et al., 2018 reported slightly higher values for cities around the Bohai Sea in the North China Plain (4.4 ± 2.6, 6.8 ± 3.4, and 4.2 ± 2.7 nmol DTT min^{-1} m^{-3} for Jinzhou, Tianjin, and Yantai); however, this is likely due to higher $PM_{2.5}$ concentration observed during that study.

4.4 Time series of $PM_{2.5}$ concentration, DTTm, and DTTv values for Beijing and Birmingham

4.4.1 Beijing time series

Figure 4-23 shows the time series for $PM_{2.5}$ concentration, DTTv, and DTTm for the Beijing winter campaign. Frequent haze events are common during the winter in Beijing, owing to stagnant meteorological conditions and large emissions of air pollutants. These haze events are preceded by nucleation of gaseous pollutants and rapidly increasing number concentration of ultrafine particles before particle growth. This can been seen in Figure 4-23 as the cycle of clean days leading into haze events with much higher $PM_{2.5}$ concentrations (Cheng et al., 2016; Guo et al., 2014).

Generally, DTTv follows the pattern observed in the $PM_{2.5}$ time series indicating that $PM_{2.5}$ concentration is often a good indicator of human toxicity exposure. However, there are instances where the pattern shown between days in the $PM_{2.5}$ data is not observed in the DTTv data or the relative difference between days does not match. For example, during the period of 24 – 27/11/2016, while both $PM_{2.5}$ and DTTv are elevated, the $PM_{2.5}$ shows a significant increase from ~100 μg m^{-3} to ~200 μg m^{-3} before plateauing, however, in the DTTv data the toxicity decreases steadily over these 3 days. This decrease in volume-normalised toxicity coincides with a drop in the intrinsic toxicity between the cleaner and more polluted days.

An example of when the change in DTTv is significantly different from the change in $PM_{2.5}$ concentration is seen on the 28 – 29 November. There is a relatively small change in $PM_{2.5}$

concentration (75.3 ± 28 to 120 ± 31 μg m^{-3}) but a much larger difference seen in the DTTv values: 2.07 ± 0.25 to 6.20 ± 0.39 nmol DTT min^{-1} m^{-3}.

The time series for the Beijing summer campaign is shown in Figure 4-24; this campaign had much lower concentrations of $PM_{2.5}$ than during the winter campaign with less variability in the absence of haze events. The DTTv values generally follow the trend of the $PM_{2.5}$ concentrations during this campaign with some exceptions. One example of a deviation between the two being the 27th May and 17th June (the two highest $PM_{2.5}$ concentration days) which had similar $PM_{2.5}$ concentrations of 85.7 ± 28 and 78.1 ± 21 μg m^{-3}, however, due to the higher toxicity of PM sampled on the 17th much higher DTTv values resulted of 2.22 ± 0.22 compared to 1.28 ± 0.12 nmol DTT min^{-1} m^{-3} on the 27th.

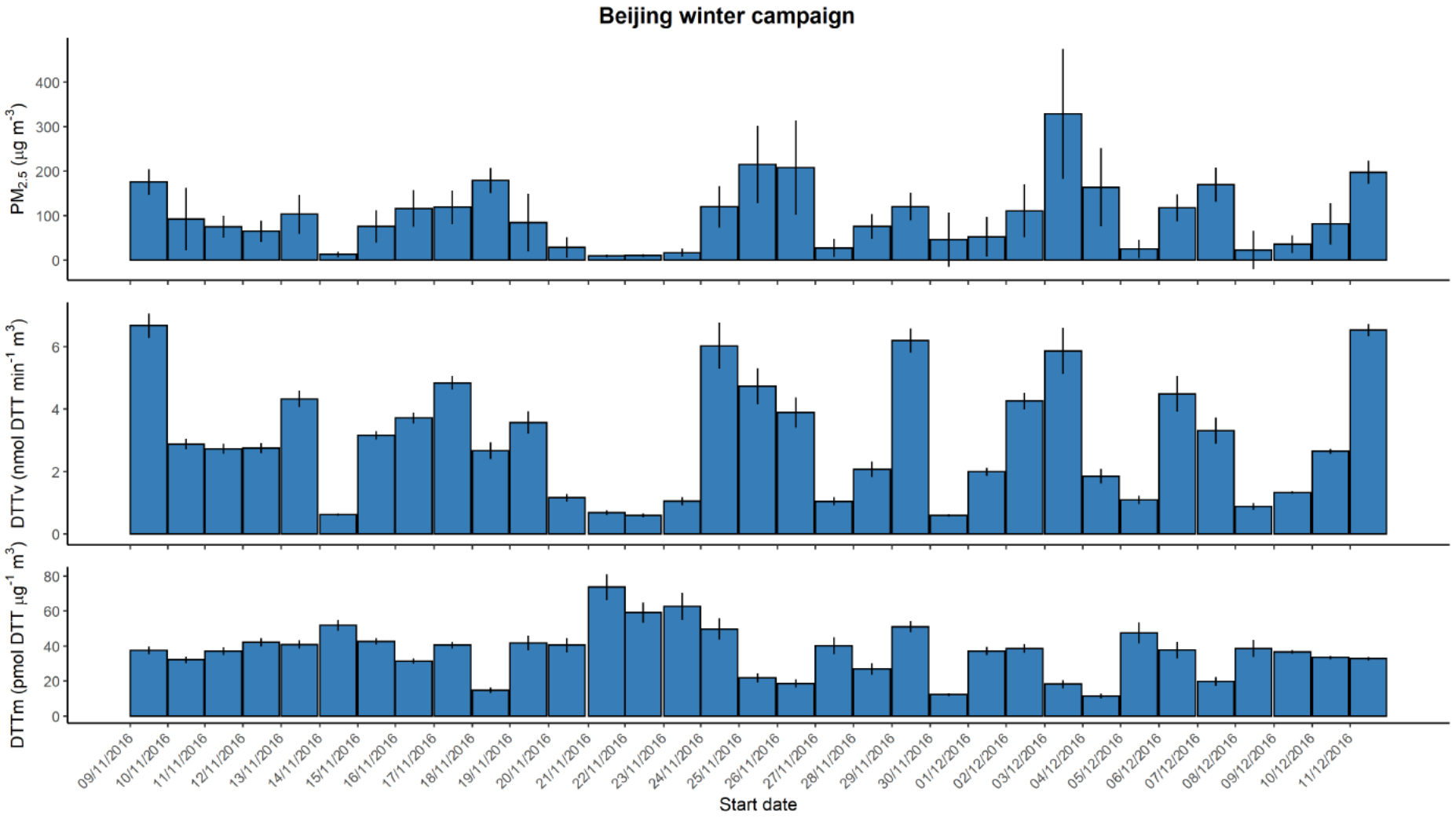

Figure 4-23: Time series of TEOM $PM_{2.5}$ (µg m^{-3}), DTTm (pmol DTT min^{-1} $µg^{-1}$), and DTTv (nmol DTT min^{-1} m^{-3}) for the Beijing winter campaign, n = 33. The error bars shown represent one standard deviation.

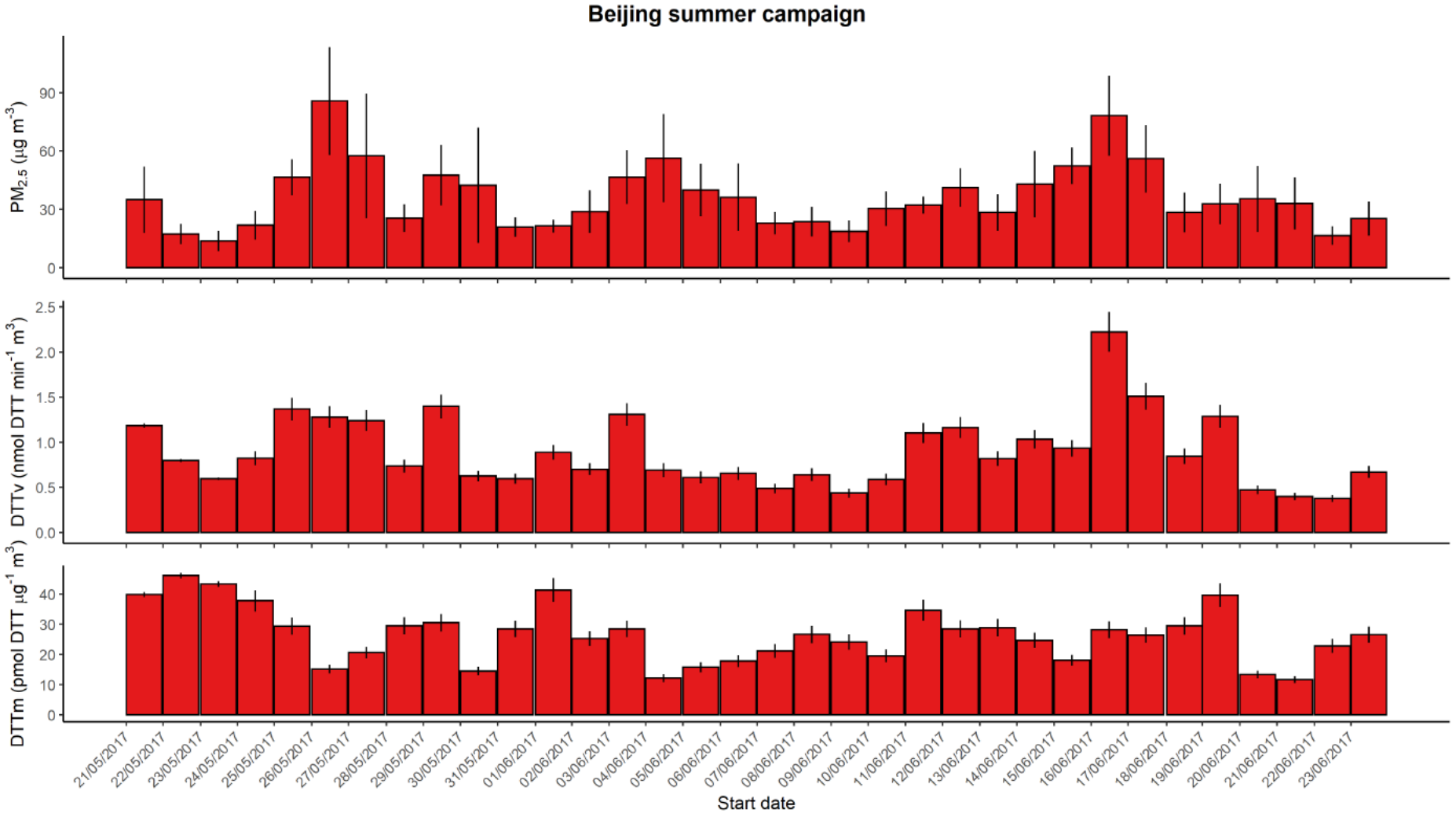

Figure 4-24: Time series of TEOM $PM_{2.5}$ (µg m^{-3}), DTTm (pmol DTT min^{-1} $µg^{-1}$), and DTTv (nmol DTT min^{-1} m^{-3}) for the Beijing summer campaign, n = 35. The error bars shown represent one standard deviation.

4.4.2 Birmingham time series

The time series for the trial week of sampling in Birmingham is shown in Figure 4-25, $PM_{2.5}$ and DTTv show the highest values during the beginning of the week before becoming nearly constant from Thursday to Sunday (06 – 09 December). Although the $PM_{2.5}$ concentration and DTTv values seen in the Birmingham samples are the lowest observed within the three locations / 6 campaigns presented in this thesis, the intrinsic toxicity (DTTm) was still similar to values from the other campaigns. At first glance this implies that intrinsic toxicity is relatively uniform across different regions / cities with more changes seen within campaigns (day-to-day variability) that across multiple cities (location-dependent differences).

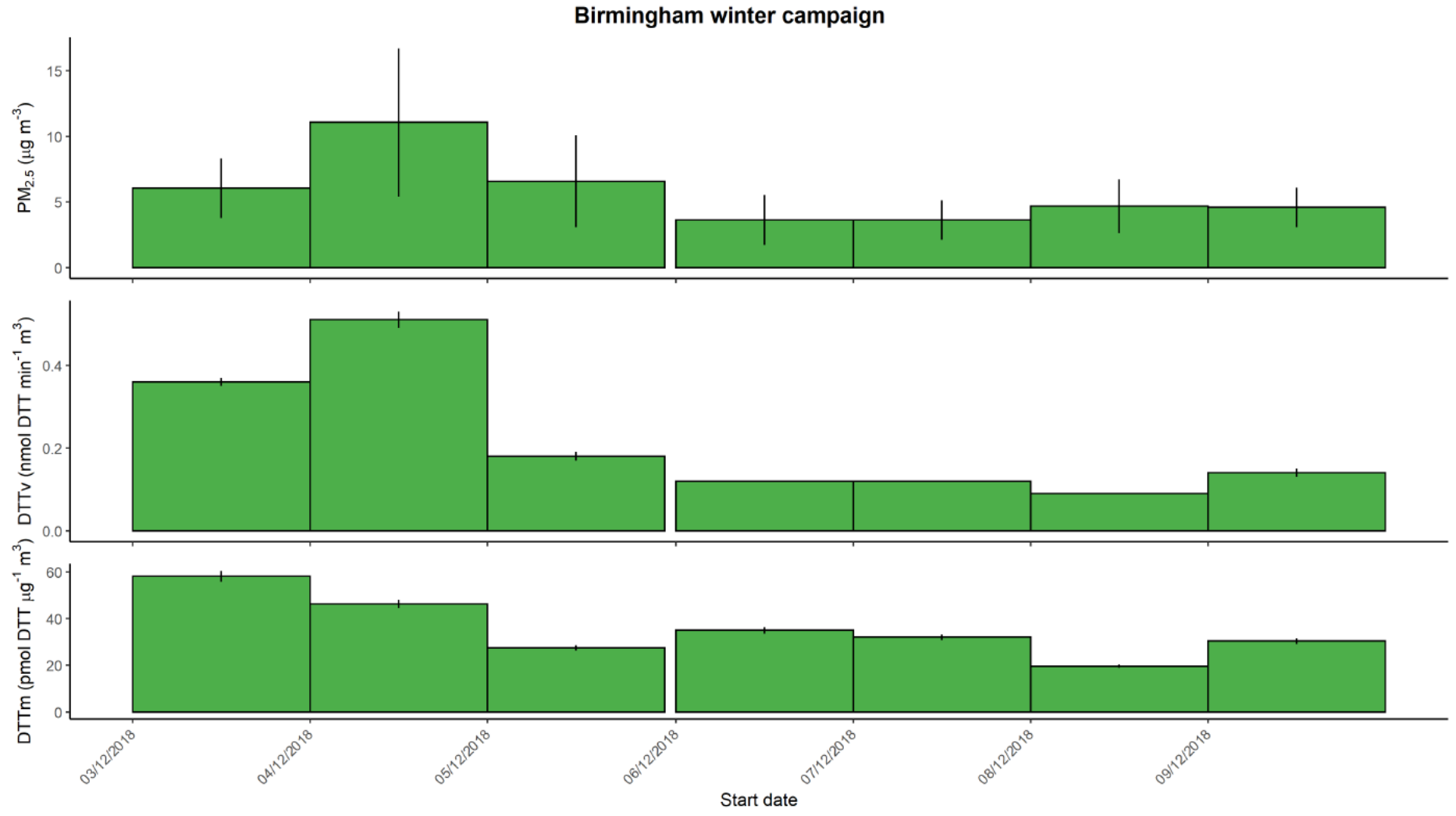

Figure 4-25: Time series of TEOM $PM_{2.5}$ (µg m^{-3}), DTTm (pmol DTT min^{-1} $µg^{-1}$), and DTTv (nmol DTT min^{-1} m^{-3}) for the Birmingham sampling, n = 7.

4.5 High time resolution sampling during the Beijing summer campaign

As part of the Beijing summer campaign, higher time resolution $PM_{2.5}$ sampling was carried out during several (anticipated) $PM_{2.5}$ pollution events. High time resolution PM samples from one of these days were analysed for DTT toxicity, across a time period which overlaps the sampling time of one of the 23-hour samples. The results of this analysis are shown in Figure 4-26. This day was chosen out of the three high-time-resolution-sampling days due to it having the higher DTTm values.

The DTTv values obtained are largely in the range seen throughout the rest of the Beijing summer campaign, apart from between 8pm and midnight, where the DTTv is significantly higher than most other values obtained for this season. The average DTTv value for the campaign is 0.896 ± 0.40 compared to 1.65 ± 0.15 nmol DTT min^{-1} m^{-3} for the 8pm to midnight sample. This appears to be driven by both higher $PM_{2.5}$ concentration and intrinsic toxicity during this time, as can be seen in Figure 4-26.

The average value for $PM_{2.5}$ concentration, DTTm and DTTv values of the high resolution filters overlap within uncertainty with those for the 23-hour sample that sampled during the same time period (this sample started at 9 am compared to 8 am for the high time resolution samples). $PM_{2.5}$ concentration for the 23-hour sample was 28.4 ± 10 µg m^{-3} (29.0 ± 6.1 for the high time resolution samples), DTTv value was 0.845 ± 0.085 nmol DTT min^{-1} m^{-3} (1.01 ± 0.091), and the DTTm value was 29.4 ± 2.9 pmol DTT min^{-1} μg^{-1} $PM_{2.5}$ (34.3 ± 3.1). The DTTv values from the high time resolution sampling were slightly higher than for the 23-hour sample, likely due to the higher DTTm values also observed. This may be due to more

volatile compounds being present in the high time resolution filters as all filters were frozen immediately after collection.

This higher resolution data can also show how changes in intrinsic toxicity can change potential human health effects from PM exposure, even when $PM_{2.5}$ concentrations are constant, as is seen during the 12:00 – 16:00 and 16:00 – 20:00 sampling times. The $PM_{2.5}$ concentration is approximately constant through this time at 26.3 ± 2.8 and 27.0 ± 2.9 μg m^{-3}, whereas the DTTv (1.04 ± 0.094 to 0.757 ± 0.068 nmol DTT min^{-1} m^{-3}) decreases significantly as a result of the lower intrinsic toxicity, which changed from 39.6 ± 3.6 to 28.1 ± 2.5 pmol DTT min^{-1} μg^{-1} $PM_{2.5}$. The impact of PM composition on changes to intrinsic toxicity similar to this are discussed in chapter 6.

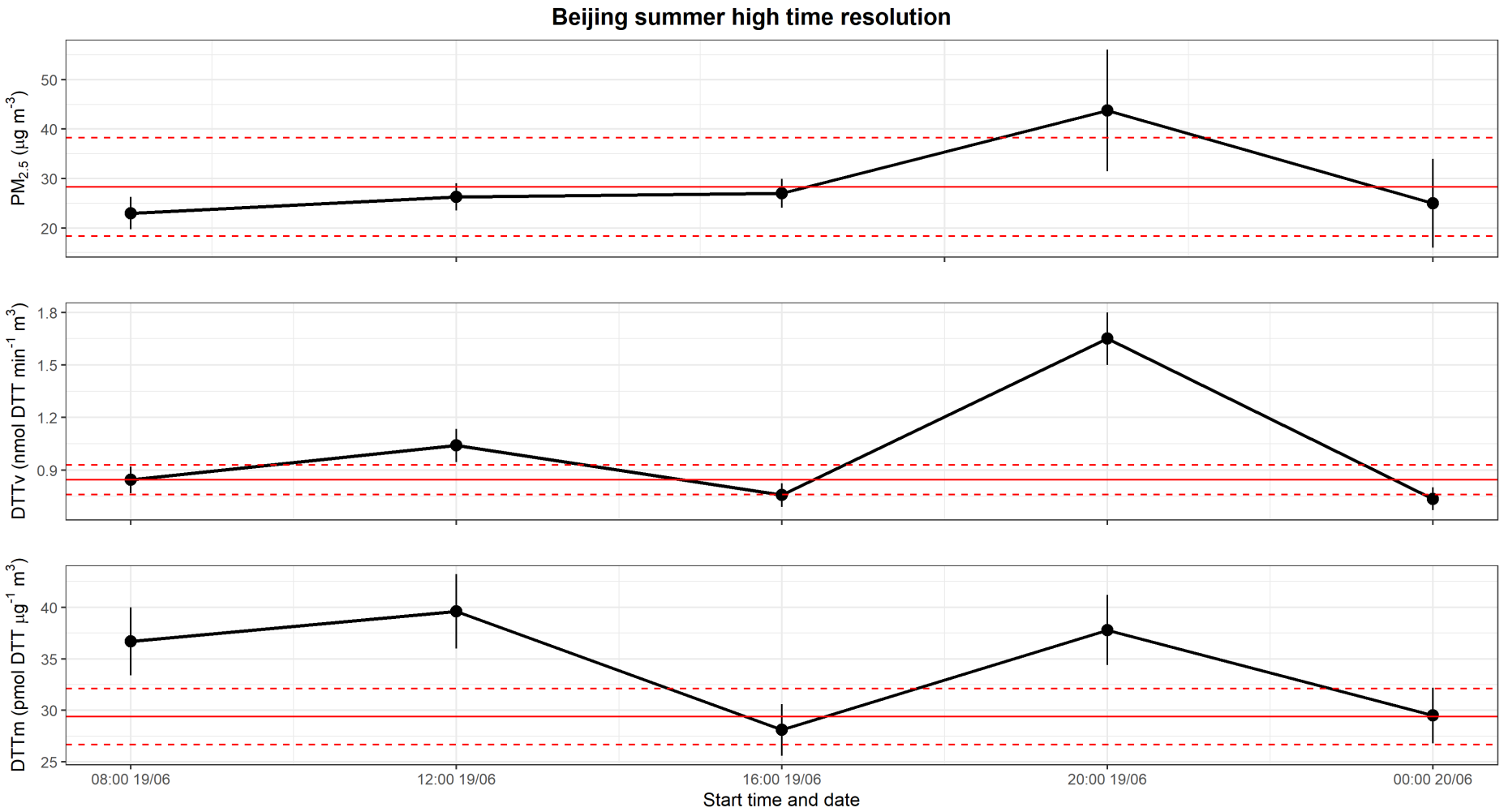

Figure 4-26: Time series of TEOM $PM_{2.5}$ (µg m^{-3}), DTTm (pmol DTT min^{-1} $µg^{-1}$), and DTTv (nmol DTT min^{-1} m^{-3}) for the 5 high time resolution filters collected during the Beijing summer campaign. Sampling times were 4 hour for the first 4 filters and 8 hours for the final filter. The red lines indicate the values ± SD for the 23 hour filter sampled during the same time. All times shown are the start of sampling, the 23 hour filter started sampling at 9 am and finished at 8 am on the 20th, the same time as the high resolution filters.

4.6 Overview of the $PM_{2.5}$ composition, gas, and meteorological data for Beijing

Due to the large number of meteorological, gas- and particle-phase composition data obtained during the Beijing campaigns it is necessary to select representative compounds for several groups for conciseness. In this section the rationale for the selection of these species is explained. Other groups such as OC / EC and metal concentrations within PM samples are reported in full, due to the lack of a single representative species for many metal groups, and the anticipated importance of these species to OP measured by DTT.

Mean gas- and particle-phase composition data for the Beijing field campaigns is shown in Table 4-. Some measurements are omitted for clarity. All measurements of soluble ions and metals that were performed in both campaigns have been included; generally, the winter campaign shows higher concentrations of most species than the summer campaign. However, there is significant overlap between mean concentration values for many species, likely due to the cleaner days in the winter proceeding haze events.

Benzo(a)pyrene (BaP) was chosen as the marker for all PAH due to its common use as a PAH marker by researchers and states inside the European Union (Cherrie et al., 2011). BaP has been shown to be a good marker for carcinogenic PAH relevant for air quality management, with a high correlation between BaP and other PAH under various circumstances and localities (Cherrie et al., 2011; European Communities, 2001).

To account for SOA three aerosol-phase compounds indicative of the degradation products of specific VOCs were chosen as SOA tracers for oxidation of isoprene, monoterpenes, and sesquiterpenes. These tracers were C_5-alkene triols (*cis*-2-methyl-1,3,4-trihydroxy-1-butene,

3-methyl-2,3,4-trihydroxy-1-butene, and *trans*-2-methyl-1,3,4-trihydroxy-1-butene), PNA (*cis*-pinonic acid), and CPA (β-caryophyllinic acid), respectively. Yuan et al., 2018 showed that in the Pearl River Delta these SOA tracers showed significant seasonal differences to each other, therefore multiple tracers were chosen as a representative sampling of the different SOA tracer data.

The n-alkanes measured during the Beijing campaigns were all alkanes between C24 and C34. Studies have shown that even and odd n-alkanes have different sources and generally smaller chain n-alkanes are more indicative of coal combustion and vehicle emissions. Therefore it was decided to use one even and one odd numbered lower chain length n-alkane to represent the n-alkane group (C24 and C25), both of these showed much higher concentrations during the winter than summer. This is likely due to primary emissions from coal combustion during the winter for heat and energy production, as Lyu et al., 2019 reported for the same samples collected during the winter campaign (W. Li et al., 2010; Lyu et al., 2019; Oros & Simoneit, 2000).

Ozone is much more abundant during the summer campaign, likely due to the increased photolysis of NO_2 and the much lower concentrations of NO, which is a sink for O_3 through a fast titration reaction producing NO_2 and O_2. This may suggest an increased influence from exhaust emissions during the winter campaign, along with the slightly higher concentrations of certain metal species associated with vehicles during the winter such as iron, manganese, nickel, and strontium. However, it may also be exacerbated by different meteorological conditions resulting in higher ozone concentrations during the summer campaign from similar emissions (Ball, 2014; Flynn, 2003; Mollenhauer & Tschoeke, 2010b; Pison & Menut, 2004; Rai, Slowik, Furger, Haddad, et al., 2021).

Table 4-5: Summary table showing the concentrations of some of the compositional species available for the Beijing winter and summer campaigns. The values are reported as the mean ± SD.

Data description	Species / Parameter	Beijing winter	Beijing summer
OC / EC and ions (µg m^{-3})	OC	20.9 ± 12	6.44 ± 2.3
	EC	3.38 ± 2.0	0.901 ± 36
	K^+	1.30 ± 1.0	0.374 ± 0.35
	Na^+	0.421 ± 0.24	0.205 ± 0.16
	NH_4^+	8.23 ± 5.6	3.62 ± 3.1
	Ca^{2+}	0.334 ± 0.11	0.178 ± 0.11
	NO_3^-	12.5 ± 9.4	7.16 ± 4.9
	SO_4^{2-}	8.53 ± 7.1	6.87 ± 4.0
	Cl^-	4.05 ± 2.2	0.469 ± 0.42
Metals (ng m^{-3})	Si	908 ± 669	534 ± 350
	Al	598 ± 446	230 ± 143
	Cu	17.8 ± 13	6.13 ± 5.1
	Fe	679 ± 434	486 ± 199
	Ti	36.9 ± 32	21.4 ± 10
	V	2.12 ± 2.0	5.05 ± 6.4
	Cr	23.6 ± 15	4.74 ± 2.6
	Mn	42.6 ± 30	27.3 ± 14
	Co	0.458 ± 0.25	0.937 ± 1.2
	Ni	4.66 ± 3.0	2.05 ± 2.0
	Zn	301 ± 193	116 ± 64
	As	9.64 ± 6.5	9.59 ± 8.2
	Sr	3.11 ± 1.5	1.83 ± 1.4
	Ba	9.35 ± 7.8	12.0 ± 10
	Pb	84.6 ± 67	33.6 ± 26
	Cd	22.2 ± 16	9.29 ± 7.4
	Sb	9.02 ± 6.5	54.0 ± 43
Biomass tracer (ng m^{-3})	Galactosan	40.2 ± 25	1.52 ± 0.80
PAH (ng m^{-3})	Benzo(a)pyrene	10.1 ± 10	0.0267 ± 0.021
n-alkanes (ng m^{-3})	C24	63.6 ± 49	1.36 ± 0.64
	C25	63.6 ± 48	2.88 ± 1.5
Cooking marker (ng m^{-3})	Palmitic acid	345.1 ± 254	25.2 ± 12
SOA tracers (ng m^{-3})	C_5-alkene triols	0.908 ± 0.5	0.507 ± 0.20
	PNA	3.80 ± 1.6	3.17 ± 1.1
	CPA	15.4 ± 12	3.93 ± 2.5
Gas data (ppb)	O_3	8.60 ± 5.8	55.5 ± 19
	NO	41.9 ± 29	4.90 ± 5.5
	NO_2	36.9 ± 14	22.0 ± 6.3
Meteorology data (m s^{-1}, %, °C)	Wind speed	2.64 ± 1.1	3.66 ± 0.80
	Relative humidity	43.0 ± 15	44.3 ± 19
	Temperature	8.00 ± 3.4	25.1 ± 3.6

In this chapter details of the number of samples collected for the Birmingham and Beijing campaigns and the various compositional data obtained from Beijing is outlined. The time series of $PM_{2.5}$ concentration, DTTm and DTTv values obtained in this work are shown. Finally the meteorological, gas- and particle-phase averaged data are shown for each of the Beijing campaigns. These data, along with the $PM_{2.5}$ concentration and DTT measurements, will be used for the data analysis reported in chapter 6, which aims to determine the impact of various meteorological and $PM_{2.5}$ compositional impacts on OP as determined by the DTT assay in the Beijing and Delhi campaigns.

5 DATA REPORTING FOR DELHI

This chapter presents the $PM_{2.5}$ concentration, DTTm, DTTv, and compositional species concentrations for the Delhi campaigns. A brief narrative discussion of the trends observed in the data is also covered, however, detailed statistical analysis of this data will be covered in Chapter 6.

5.1 Summary of the $PM_{2.5}$ sampling in Delhi

Sampling for the Delhi campaigns described here was carried out at the Indian Institute of Technology, Delhi (IIT). Measurements were also made in Old Delhi at the Indira Gandhi Delhi Technical University for Women (IGDTUW) but are not presented in this thesis. The IIT site is located in the south of the city, roughly 5 km east of the Indira Ghandi international airport (IGI airport). The sampling site is described as an urban background site. Air pollution sources in Delhi are dominated by regional seasonal biomass burning and local fossil fuel combustion during the winter and autumn, and vehicular emissions during the summer. Delhi also experiences sporadic extreme pollution events during some special events, most notably the Diwali festival (also known as the festival of light), where there is widespread use of firecrackers and fireworks along with the lighting of candles and oil lamps in most houses (Bikkina et al., 2019; Foster & Kumar, 2011a; Singh & Sharma, 2012).

Table 5-2 provides a summary of the $PM_{2.5}$ samples that were collected during the Delhi campaigns. In total 156 filters were collected and analysed for DTT OP from these campaigns, including 18 filters that were collected on Teflon filters using a Minivol $PM_{2.5}$ sampler (the remainder sampled onto quartz filters). With the $PM_{2.5}$ loaded filters collected

during the Beijing and Birmingham campaigns, the total number of filters analysed for DTT OP during this project was 236.

Table 5-2: Summary of $PM_{2.5}$ filter collection during the Delhi field campaigns. Only filters that were analysed for DTT are included. All blank filters are field blanks that were loaded in the PM samplers.

Campaign	Filter type	Sampling dates	Number of filters analysed	Number of blank filters	Sampling time (hrs)	Avg. $PM_{2.5}$ ($\mu g\ m^{-3}$ TEOM)
Delhi winter	Quartz	18/01/18 – 09/02/18	42	5	12	168 ± 60
Delhi summer	Quartz	30/04/18 – 03/06/18	66	5	12	122 ± 49
Delhi autumn	Teflon	19/10/18 – 09/11/18	18	7	Variable from 12 - 36	249 ± 92
Delhi autumn	Quartz	18/10/18 – 05/11/18	30	3	12	199 ± 68

5.2 Summary of composition data available for Delhi

The $PM_{2.5}$ filters collected during the Delhi campaigns were also analysed for a variety of compositional species. Meteorological data was acquired from the IGI airport measurement site, and online PM composition data (AMS) was provided by J. Allan & E. Villegas (2020, pers. comm., 2 June). Table 5- provides a breakdown of the various data available for the Delhi field campaigns, along with the operators who collected the data and the instruments used. Excluding $PM_{2.5}$ concentration, metal oxides, and OP data, 49 species were measured for the Delhi campaigns.

Table 5-7: All of the available composition data for $PM_{2.5}$, gases, and meteorological data during the Delhi field campaigns. 1 = University of Birmingham, 2 = Indira Gandhi International Airport, 3 = University of Manchester, and 4 = UK Centre for Ecology & Hydrology.

Campaign	Data description	Data provided by	Instrument	Species measured
Delhi winter, summer, and autumn	OC / EC	Salim Alam[1]	DRI	OC, EC
	Ions		IC	PO_4^{3-}, NO_3^-, SO_4^{2-}, Cl^-, K^+, Ca^{2+}, Mg^{2+}, NH_4^+, Na^+
	Metals		ICP-MS	Li, Na, Mg, Al, K, Ca, Ti, V, Cr, Mn, Fe, Co, Ni, Cu, Zn, As, Sr, Cd, Sn, Sb, Ba, Ce, Pb
	Soil dust		ICP-MS	MgO, Al_2O_3, CaO, Ti_2O_3, Fe_2O_3, SiO_2 (from XRF)
	Gas data	University of Birmingham		O_3, NO, NO_2, NOx
	Meteorology data	IGI airport data[2]		Wind speed, wind direction, ceiling height, visibility, temperature, dew point, relative humidity
Delhi summer	AMS-PMF	Ernesto Villegas[3], James Allan[3], and CEH[4]	HRAMS at Lodhi road	HOA, LVOOA, BBOA, COA, SVOOA
Delhi winter	AMS-PMF		ACSM at Lodhi road	HOA, LVOOA, BBOA, oPOA, COA
Delhi autumn	AMS-PMF		cToFAMS at Lodhi road	HOA, LVOOA, BBOA, oPOA, SVOOA

5.3 OP^{DTT} results for Delhi

The average $PM_{2.5}$ concentration, and volume normalised and intrinsic toxicity are shown in Table 5-. The $PM_{2.5}$ concentrations observed during the Delhi campaigns are consistent with previously reported literature for cities within the Indo-Gangetic Plain (IGP): 150 ± 53 μg m^{-3} reported for Patiala and 131 ± 79 (17 – 417) μg m^{-3} reported for Delhi (Jain et al., 2020; Patel & Rastogi, 2018b). The high $PM_{2.5}$ concentration observed during the collection of Teflon filters within the autumn campaign is due to the Diwali festival. During the festival houses are lit with oil lamps and large quantities of fireworks are set off, especially in urban areas (Singh & Sharma, 2012).

Table 5-8: Summary table of the $PM_{2.5}$ concentration, DTTm, and DTTv results obtained for field campaigns in Delhi. Total filters = 156.

Campaign	Filter type	Avg. $PM_{2.5}$ ± SD (μg m^{-3})	Avg. DTTv ± SD (nmol DTT min^{-1} m^{-3})	DTTv range	Avg. DTTm ± SD (pmol DTT min^{-1} μg^{-1} $PM_{2.5}$)	DTTm range	Number of filters
Delhi winter	Quartz	168 ± 60	5.62 ± 1.4	2.32 – 8.49	35.2 ± 10	17.8 – 54.0	42
Delhi summer	Quartz	122 ± 49	4.19 ± 1.7	1.86 – 9.12	35.8 ± 11	8.1 – 76.3	66
Delhi autumn	Teflon	249 ± 92	NA	NA	29.2 ± 9.2	14.2 – 63.4	18
Delhi autumn	Quartz	199 ± 68	6.83 ± 1.2	4.36 – 9.89	37.1 ± 12	23.1 – 65.8	30

The DTTm values obtained during the Delhi campaigns show weak seasonal variability with statistically insignificant differences (t-test p-value = 0.57 – 0.81). The DTTm values obtained during the Delhi campaigns are also statistically significantly similar to those obtained during the Beijing winter and Birmingham campaigns, however, DTTm values for the Beijing summer campaign are (statistically) significantly lower. Like the Beijing campaigns, the Delhi

campaigns have DTTm values that are consistent with those observed in other studies across the world, with similar values to:

- Delhi, India at 5 – 65 pmol DTT min^{-1} μg^{-1} $PM_{2.5}$ (Puthussery et al., 2020).
- Patiala, India at 27 ± 8 pmol DTT min^{-1} μg^{-1} $PM_{2.5}$ (Patel & Rastogi, 2018a).
- Orinda, United States at 38 ± 21 pmol DTT min^{-1} μg^{-1} $PM_{2.5}$ (Ntziachristos et al., 2007).
- Los Angeles, United States at 19 ± 4 pmol DTT min^{-1} μg^{-1} $PM_{2.5}$ (Hu et al., 2008).
- Atlanta, Unites States at 34 ± 9 and 10 – 50 pmol DTT min^{-1} μg^{-1} $PM_{2.5}$ across two studies (T Fang et al., 2015; Verma et al., 2012).
- Mexico City, Mexico at 25 – 40 pmol DTT min^{-1} μg^{-1} $PM_{2.5}$ (De Vizcaya-Ruiz et al., 2006).
- Jinzhou, Tianjin, and Yantai, China at 35 ± 18, 49 ± 16, and 30 ± 16 pmol DTT min^{-1} μg^{-1} $PM_{2.5}$, respectively (W. J. Liu et al., 2018b).

The DTTv values for every Delhi campaign are statistically significantly higher than those obtained during the Beijing or Birmingham campaigns. Pairwise t-test results show that each of the Delhi campaign DTTv values are significantly different from each other, with the autumn campaign showing the highest values followed by the winter, with the summer campaign having the lowest values (confidence interval ≥99.9 %). The Delhi campaigns have much higher DTTv values than those seen in developed cities such as Atlanta and Chicago (0.1 – 0.8 nmol DTT min^{-1} m^{-3}), being more similar to values reported by Liu et al., 2018 during heavily polluted episodes in cities around the Bohai Sea in the North China Plain (4.4 ± 2.6, 6.8 ± 3.4, and 4.2 ± 2.7 nmol DTT min^{-1} m^{-3} for Jinzhou, Tianjin, and Yantai) (T. Fang et al., 2015; T. Fang et al., 2016; Zeng et al., 2021).

5.3.1 OP^{DTT} results split diurnally

The diurnal variability of OP measured by DTT and $PM_{2.5}$ concentration and composition is possible to determine for the Delhi campaigns as filter sampling time was 12 hours. Table 5-93 shows the average $PM_{2.5}$ concentration, and volume normalised and intrinsic toxicity for the Delhi campaigns, split diurnally for each. DTTm values during the autumn and winter campaigns along with $PM_{2.5}$ concentration during the winter campaign are the only instances of statistically significant diurnal variability. During the autumn and winter campaigns the DTTm values are significantly higher during the day compared to nights.

Interestingly, the DTTv values for the winter campaign do not (statistically significantly) show diurnal variation, however the $PM_{2.5}$ concentration is significantly higher at night than during the day (201 ± 59 μg m^{-3} at night and 134 ± 38 μg m^{-3} during the day, pairwise t-test with 95 % confidence interval). This is likely due to the day having higher intrinsic toxicity than during the night, reducing the impact of $PM_{2.5}$ concentration on the DTTv value at night.

Table 5-93: Summary table of the diurnal PM2.5 and DTT values during the Delhi field campaigns.

Campaign	Day / night	Avg. $PM_{2.5}$ ± SD (µg m^{-3})	Avg. DTTv ± SD (nmol DTT min^{-1} m^{-3})	DTTv range	Avg. DTTm ± SD (pmol DTT min^{-1} μg^{-1} $PM_{2.5}$)	DTTm range	Number of filters
Delhi winter	Day	134 ± 38	5.36 ± 1.0	3.63 – 7.70	41.0 ± 8.1	26.7 – 54.0	21
	Night	201 ± 59	5.88 ± 1.8	2.32 – 8.49	29.5 ± 9.0	17.8 – 47.0	21
Delhi summer	Day	116 ± 49	3.84 ± 1.7	1.86 – 9.12	34.4 ± 13	8.08 – 76.3	31
	Night	127 ± 49	4.54 ± 1.6	2.07 – 8.53	37.1 ± 8.9	20.9 – 63.1	32
Delhi autumn	Day	168 ± 54	6.95 ± 0.90	5.47 – 8.70	44.4 ± 11	25.8 – 65.8	14
	Night	204 ± 56	6.72 ± 1.4	4.36 – 9.89	34.3 ± 10	23.1 – 56.3	16

5.4 Time series of $PM_{2.5}$ concentration, DTTm, and DTTv values for Delhi

Figure 5-27 shows the time series for $PM_{2.5}$ concentration, DTTv and DTTm values for the Delhi winter campaign. Air quality in Delhi is often among the worst observed in the world, particularly in the autumn and winter where low wind speeds and low boundary layer depth exacerbate the impact of local emission sources and that of crop burning taking place in neighbouring states whose emissions are transported into Delhi. This can be seen in Figure 5-27 where 12-hour averaged $PM_{2.5}$ concentration is rarely below 100 µg m^{-3} with a peak approaching 400 µg m^{-3}. The $PM_{2.5}$ concentration during the second half of the campaign shows a diurnal cycle, with higher concentrations at night than during the day. This is likely due to the lower boundary layer during the night (Bikkina et al., 2019; Puthussery et al., 2020).

Generally, DTTv shows less variation than is seen in the $PM_{2.5}$ concentration and DTTm values, indicating that changes in $PM_{2.5}$ concentration does not always result in changing the OP of the air mass. Changes in DTTv during this campaign appears to also be primarily driven by the intrinsic toxicity of the $PM_{2.5}$. There are several examples where $PM_{2.5}$ concentration increases but the DTTv decreases. There are also instances where the $PM_{2.5}$ concentration is the same but the DTTv value changes, for example on the 25/01/2018 where the $PM_{2.5}$ concentrations during the day and night are 119 ± 28 and 123 ± 48 μg m^{-3}, however, the DTTv value decreases from 3.63 ± 0.18 during the day to 2.32 ± 0.12 nmol DTT min^{-1} m^{-3} at night. This is most likely due to the corresponding DTTm decreasing from 30.3 ± 1.5 to 18.7 ± 0.96 pmol DTT min^{-1} μg^{-1} $PM_{2.5}$.

The autumn campaign also has several days where DTTm appears to have more of an impact on DTTv values than $PM_{2.5}$ concentration, as can be seen in Figure 5-28. The 27th October had significantly higher $PM_{2.5}$ concentration than the 20th October at 266 ± 45 compared to 126 ± 46 μg m^{-3}, however, the DTTv value was lower at 6.86 ± 0.60 compared to 7.28 ± 0.11 nmol DTT min^{-1} m^{-3}. This lower OP of the airmass during a more polluted day is due to the intrinsic toxicity being much lower on the 27th at 25.8 ± 2.3 compared to 56.8 ± 0.85 pmol DTT min^{-1} μg^{-1} $PM_{2.5}$ on the 27th October.

The Diwali festival occurred on the 7th November, this day along with the two preceding days had the highest average $PM_{2.5}$ concentrations of any days sampled during this project, with peak concentrations as high as 800 μg m^{-3}. Diwali showed the lowest DTTm value (14.2 ± 1.3 pmol DTT min^{-1} μg^{-1} $PM_{2.5}$) during the autumn campaign, being comparable to the lowest DTTm values obtained for the Beijing campaigns (Beijing winter: 11.4 ± 1.4, summer: 11.6 ± 1.2 pmol DTT min^{-1} μg^{-1} $PM_{2.5}$). This is despite Diwali having significantly higher $PM_{2.5}$

concentration at 300 ± 236 compared to 163.8 ± 88 and 33.0 ± 13 μg m^{-3} during the Beijing winter and summer. However, the samples collected during Diwali were on a Teflon filter substrate rather than the quartz filters used throughout the other campaigns.

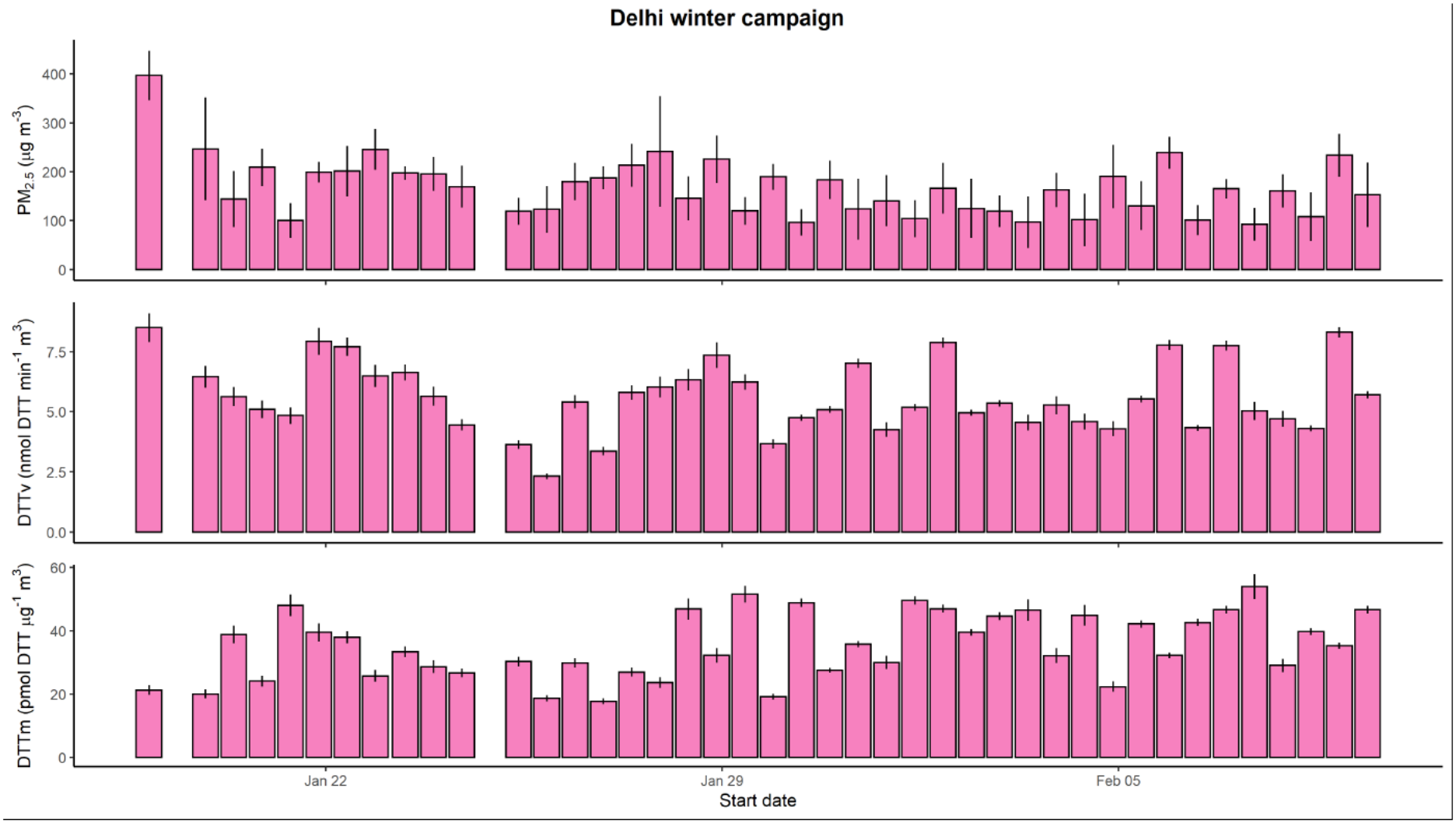

Figure 5-27: Time series of TEOM $PM_{2.5}$ (µg m^{-3}), DTTm (pmol DTT min^{-1} $µg^{-1}$), and DTTv (nmol DTT min^{-1} m^{-3}) for the Delhi winter campaign, n = 42. The error bars shown represent one standard deviation.

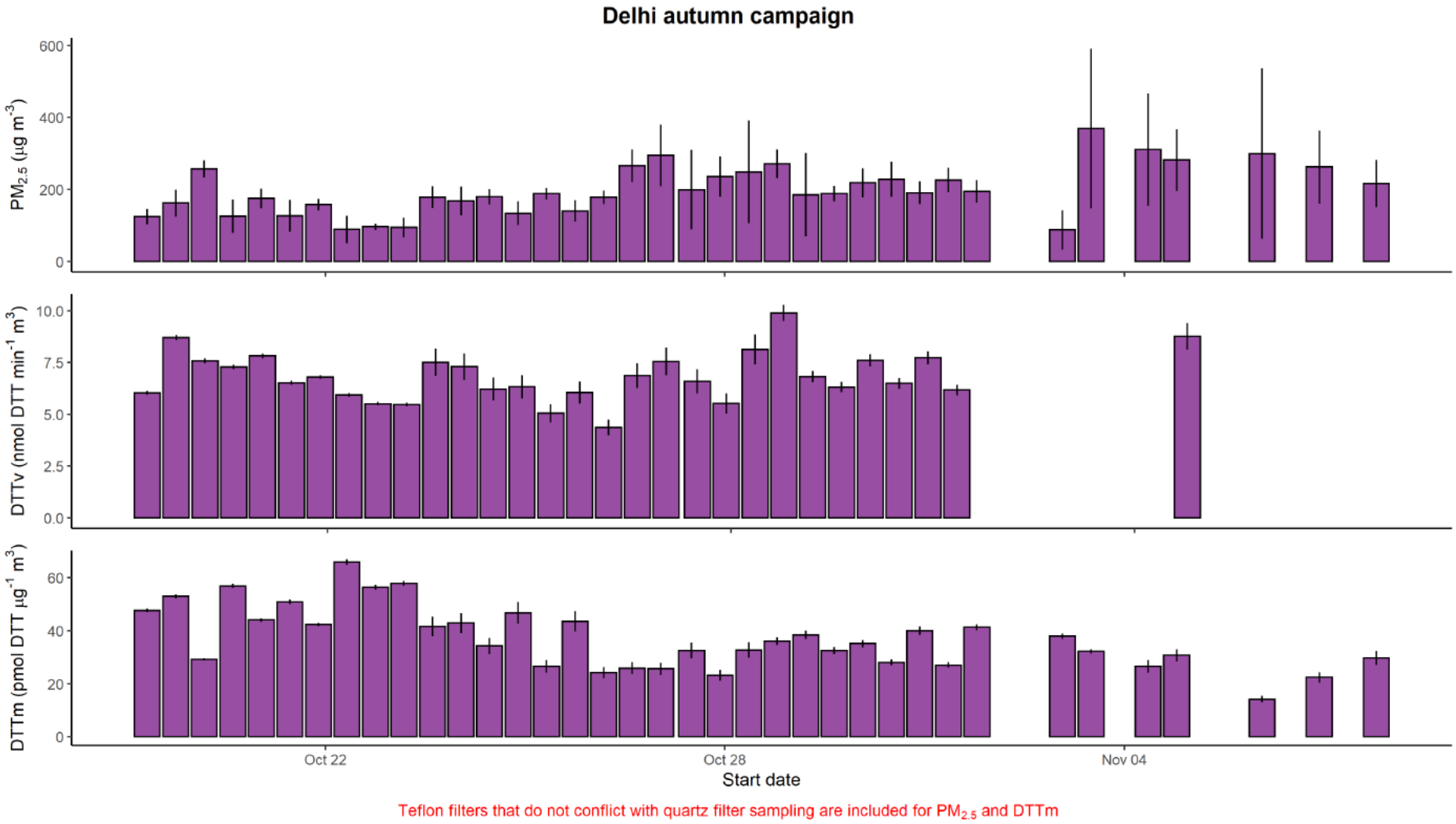

Figure 5-28: Time series of TEOM $PM_{2.5}$ (µg m^{-3}), DTTm (pmol DTT min^{-1} $µg^{-1}$), and DTTv (nmol DTT min^{-1} m^{-3}) for the Delhi autumn campaign, n = 48. The error bars shown represent one standard deviation. $PM_{2.5}$ concentration and DTTm values for Teflon filters are included where there is a time gap for quartz filters. Missing columns in DTTv panel are due to issues determining DTTv values for Teflon filters, possibly due to filters getting clogged during sampling.

Figure 5-29 shows the time series for $PM_{2.5}$ concentration, DTTv and DTTm values for the Delhi summer campaign. Unlike the winter and autumn campaigns, biomass burning does not significantly contribute to $PM_{2.5}$ concentration during the summer. Instead vehicular emissions are thought to be the major source during this season. This campaign shows less diurnal variability than the other two, with the only apparent diurnal variation in $PM_{2.5}$ concentration and DTTv values being during the week of the 23-30/05/2018.

The DTTv values during this campaign show more variation than during the other Delhi campaigns. The peaks in DTTv values are not correlated with high $PM_{2.5}$ concentration days, most notably on the night of the 5th May which had a DTTv value of 8.42 ± 0.63 nmol DTT min^{-1} m^{-3}, among the highest values observed during this campaign. The $PM_{2.5}$ concentration, however, was only slightly above average at 145 ± 23 (average = 122 ± 49 µg m^{-3}).

The DTTm values obtained during this campaign do not show as much of an inverse relationship with $PM_{2.5}$ concentration as is seen during the winter and autumn campaigns. This campaign does show the highest DTTm value obtained from any field campaign in this study at 76.3 ± 5.7 pmol DTT min^{-1} μg^{-1} $PM_{2.5}$. It is notable that the concentration of all composition species for this sample is below average. Only the ozone concentration and meteorological parameters (wind speed, relative humidity, ceiling height, and visibility) were above average during this sampling period, with this period having the greatest visibility of the campaign (4.92 km).

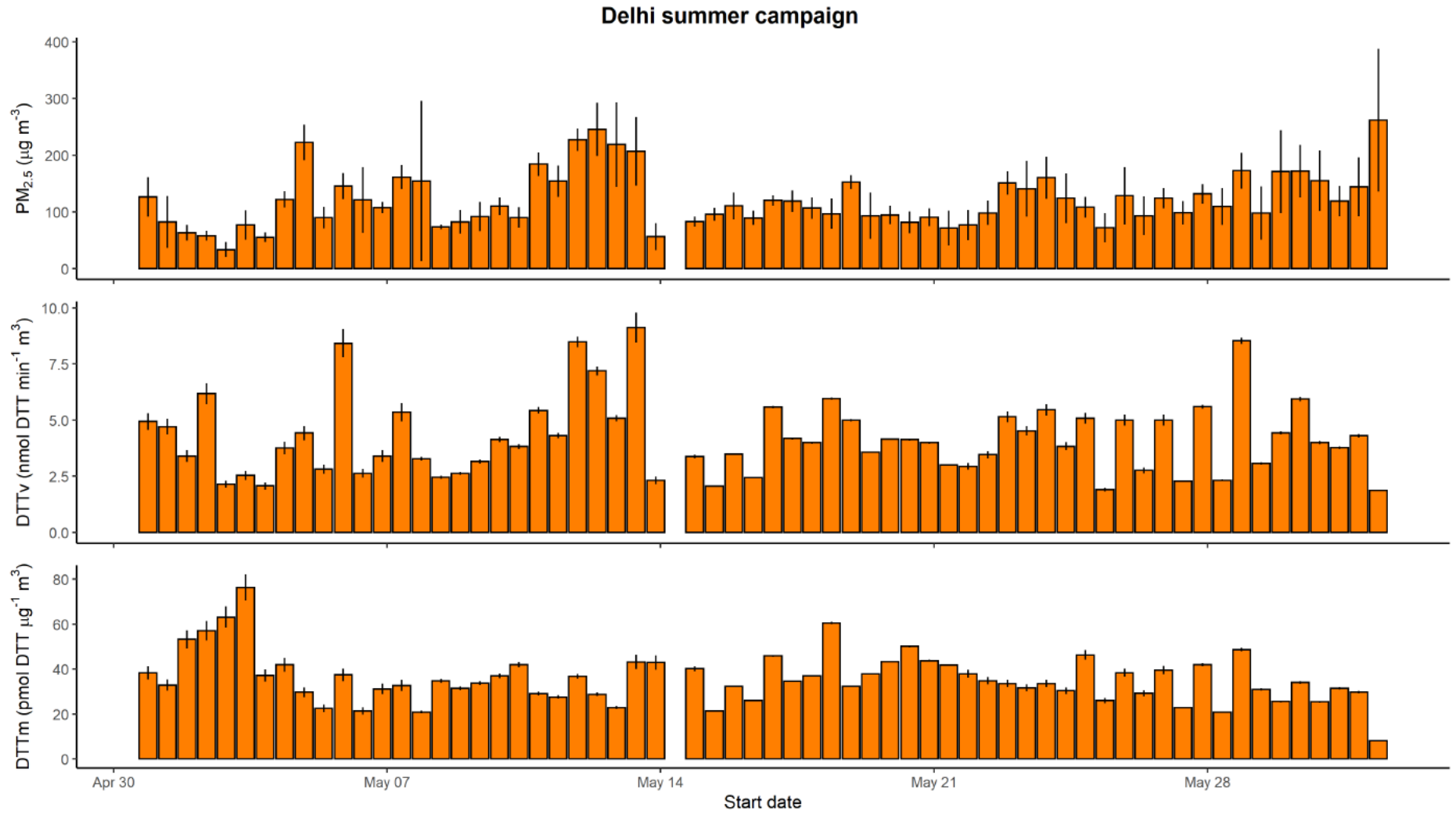

Figure 5-29: Time series of TEOM $PM_{2.5}$ (µg m^{-3}), DTTm (pmol DTT min^{-1} $µg^{-1}$), and DTTv (nmol DTT min^{-1} m^{-3}) for the Delhi summer campaign, n = 66. The error bars shown represent one standard deviation.

5.5 Overview of the $PM_{2.5}$ composition, gas, and meteorological data for Delhi

Mean gas- and particle-phase composition data for the Delhi field campaigns is shown in Table 5-4. Generally, Delhi shows less seasonal variation in $PM_{2.5}$ components than seen in the Beijing campaigns Table 4-5. Many species show significant overlap within uncertainty (1 SD) across all campaigns such as OC (43.9 ± 16 to 64.6 ± 27 μg m^{-3}), Na (0.767 ± 0.44 to 0.872 ± 0.45 ng m^{-3}), and O_3 (20.6 ± 16 to 33.1 ± 22 ppb). Meteorologically the winter and autumn campaigns are more similar to each other than the summer campaign, with generally lower temperatures, higher relative humidity, and lower wind speeds. The wind direction for the winter campaign was predominantly western, generally from the Haryana and Punjab states. The summer and autumn campaign had more varied wind directions.

The colder winter and autumn campaigns generally have higher OC/EC and ion concentrations on average compared to the summer campaign, however, the summer campaign does have similar concentrations of Ca^{2+}, Mg^{2+}, and Na^{+} which are most associated with crustal materials, soil / road dust, and construction activity (Jain et al., 2020; Rai, Slowik, Furger, Haddad, et al., 2021).

The concentration of many metal species peaked during the summer campaign. Concentrations of species associated with crustal materials, soil / road dust, and construction activity such as Fe, Mg, Al, Ca, Mn, and Sr were much higher during the summer campaign than the winter and autumn campaigns. One of the few metal species significantly higher during the autumn and winter campaign was Pb, which is associated with vehicle emissions (A. Chen et al., 2001; Bhaskar & Mehta, 2010; Gunthe et al., 2021; Monaci & Bargagli, 1996; Rai et al., 2021).

There is a statistically significantly higher concentration of O_3 during the summer campaign compared to the colder campaigns (two-tailed t-test 95 % confidence interval). Notably there is a significantly higher concentration of NO during the autumn than winter campaign, however, there is no significant difference in O_3 concentration. O_3 is consumed rapidly near sources of NO by a fast titration reaction, this is seen during the Beijing campaigns as the summer has a significantly higher concentration of O_3 than the winter while having significantly lower concentration of NO. Lower NO during the Delhi winter campaign is likely due to calm conditions and a low boundary layer height, which amplifies O_3 titration by freshly emitted NO (Ball, 2014).

Table 5-40: Summary table showing the concentrations of the compositional species available for the Delhi campaigns. The values are reported as the mean ± SD.

Data description	Species / Parameter	Delhi winter	Delhi summer	Delhi autumn
OC / EC and ions (μg m^{-3})	OC	43.9 ± 16	44.5 ± 16	64.6 ± 27
	EC	17.0 ± 8.9	9.20 ± 4.0	14.9 ± 5.5
	PO_4^{3-}	1.52 ± 0.81	1.46 ± 0.32	0.606 ± 0.51
	NO_3^-	24.1 ± 9.1	7.36 ± 2.4	12.3 ± 4.8
	SO_4^{2-}	19.3 ± 10	9.96 ± 3.8	13.6 ± 5.2
	Cl^-	33.1 ± 23	3.49 ± 3.7	4.02 ± 3.4
	K^+	2.46 ± 0.75	3.65 ± 0.95	6.21 ± 3.9
	Ca^{2+}	2.68 ± 1.5	5.99 ± 1.7	5.48 ± 1.2
	Mg^{2+}	0.497 ± 0.14	2.24 ± 0.23	2.53 ± 0.48
	NH_4^+	24.1 ± 10	3.56 ± 2.7	8.99 ± 14
	Na^+	1.61 ± 0.20	2.47 ± 0.43	2.24 ± 1.2
Metals (ng m^{-3})	Li	0.00107 ± 0.0012	0.00696 ± 0.0037	0.00181 ± 0.0013
	Na	0.767 ± 0.44	0.778 ± 0.696	0.872 ± 0.45
	Mg	0.818 ± 0.69	4.23 ± 2.1	0.981 ± 0.68
	Al	2.38 ± 1.9	12.5 ± 6.6	2.16 ± 1.4
	K	3.81 ± 0.92	7.05 ± 2.6	4.48 ± 1.6
	Ca	2.09 ± 1.8	8.18 ± 3.6	2.89 ± 1.9
	Ti	0.112 ± 0.091	0.529 ± 0.26	0.0219 ± 0.061
	V	0.00681 ± 0.0038	0.0226 ± 0.010	0.00724 ± 0.0033
	Cr	0.0179 ± 0.036	0.0225 ± 0.021	0.0190 ± 0.025
	Mn	0.0636 ± 0.036	0.209 ± 0.092	0.0857 ± 0.037
	Fe	2.13 ± 1.6	9.86 ± 4.7	2.66 ± 1.6

	Co	0.00124 ± 0.00094	0.00547 ± 0.00646	0.000829 ± 0.00066
	Ni	0.00803 ± 0.011	0.0222 ± 0.010	0.00817 ± 0.0039
	Cu	0.0383 ± 0.023	0.127 ± 0.26	0.0139 ± 0.064
	Zn	0.520 ± 0.22	0.636 ± 0.39	0.617 ± 0.20
	As	0.00643 ± 0.0042	0.00813 ± 0.0051	0.00685 ± 0.0028
	Sr	0.0238 ± 0.024	0.0765 ± 0.041	0.0216 ± 0.014
	Cd	0.00596 ± 0.011	0.00647 ± 0.023	0.0176 ± 0.019
	Sn	0.0288 ± 0.023	-0.00460 ± 0.032	0.0124 ± 0.021
	Sb	0.0174 ± 0.012	0.0122 ± 0.015	0.0189 ± 0.022
	Ba	0.0319 ± 0.023	0.0591 ± 0.051	0.128 ± 0.11
	Ce	0.00816 ± 0.0079	0.0316 ± 0.026	0.00326 ± 0.0036
	Pb	0.542 ± 0.49	0.217 ± 0.28	0.416 ± 0.29
AMS-PMF (ng m^{-3})	HOA	19.9 ± 12	2.87 ± 2.6	34.6 ± 20
	LVOOA	3.99 ± 1.2	4.69 ± 3.1	7.31 ± 2.2
	BBOA	7.87 ± 4.8	1.82 ± 1.4	4.78 ± 3.0
	COA	3.64 ± 1.3	1.73 ± 1.5	NA
	oPOA	12.0 ± 3.9	NA	15.1 6.2
	SVOOA	NA	1.66 ± 1.2	7.63 ± 3.8
Gas data (ppb)	O_3	20.6 ± 16	33.1 ± 22	22.3 ± 17
	NO	50.0 ± 50	57.5 ± 71	91.2 ± 78
	NO_2	62.1 ± 21	60.5 ± 31	81.5 ± 25
	NOx	113 ± 62	109 ± 98	170 ± 79
Meteorology data (m s^{-1}, degrees, m, °C, %)	Wind speed	2.1 ± 0.85	3.10 ± 1.1	1.29 ± 0.60
	Wind direction	252 ± 62	181 ± 83	197 ± 84
	Ceiling height	19000 ± 5800	16100 ± 7000	20800 ± 2500
	Visibility	1680 ± 830	3360 ± 560	2380 ± 540
	Temperature	14.7 ± 3.1	34.5 ± 3.3	24.2 ± 1.6
	Dew point	8.03 ± 2.2	13.7 ± 5.0	13.9 ± 1.6
	Relative humidity	66.5 ± 17	32.7 ± 13	55.9 ± 7.7

In this chapter details of the number of samples collected for the Delhi campaigns and the various compositional data obtained from these has been outlined. The time series of $PM_{2.5}$ concentration, DTTm and DTTv values are shown. Finally, the meteorological, gas- and particle-phase mean data are shown for each campaign. These data, along with the $PM_{2.5}$

concentration and DTT data from this chapter and from chapter 5, are applied in the detailed analysis reported in chapter 6, which determines the impact of various metrological and $PM_{2.5}$ compositional impacts on OP determined by the DTT assay in Beijing and Delhi.

6 $PM_{2.5}$ COMPOSITION EFFECTS ON OP^{DTT} AND INTER-CAMPAIGN COMPARISONS

This chapter presents a detailed statistical analysis of the data presented in chapters 4 and 5 for Birmingham, Beijing, and Delhi. The impacts of $PM_{2.5}$ concentration on DTTv and DTTm are described, before the PM compositional drivers of DTTm will be explored for each campaign in turn. Diurnal variation in the species driving DTTm for the Delhi campaigns is investigated. Finally, the pooled PM composition data for all campaigns are analysed and discussed.

6.1 Overview of $PM_{2.5}$ concentrations and OP^{DTT} values across campaigns

This project analysed $PM_{2.5}$ composition and characteristics from various locations around the globe and during different seasons. Wide variability in the concentrations of $PM_{2.5}$ was seen across the different field campaigns. Figure 6-30 shows an overview of the $PM_{2.5}$ concentration, DTTv, and DTTm for each of the campaigns. Birmingham had by far the lowest $PM_{2.5}$ concentration (5.74 ± 2.6 μg m^{-3}) and subsequently, DTTv values.

The measurements from Beijing show a very clear seasonal difference in $PM_{2.5}$ concentration with the winter (99.2 ± 74 μg m^{-3}) having significantly higher concentrations than the summer (36.5 ± 17 μg m^{-3}). This seasonal variability is also seen in the DTTv (and to a lesser extent DTTm data) with the highest values observed during the winter.

Delhi also shows seasonal variability, however, it is less pronounced than in Beijing. The summer campaign has the lowest $PM_{2.5}$ concentration and DTTv values but there is a lot of overlap in values with the other seasons as shown in Table 5-3. The autumn and winter campaigns generally have similar $PM_{2.5}$ concentrations and DTTv values; however, during the autumn, there is a large increase in $PM_{2.5}$ during the Diwali festival but there is a lack of DTTv data for this festival. This was due to the large difference in the sampler flow rates for Teflon and quartz filters collected. The summer campaign in Delhi shows the largest variability in DTTm, containing both the minimum and maximum values obtained during this thesis (including Birmingham, which was much less polluted than the other cities sampled) at 8.10 and 76.3 pmol DTT min^{-1} μg^{-1} $PM_{2.5}$.

Values for DTTm are more similar across locations and seasons than the other two measurements ($PM_{2.5}$ and DTTv), with a lot of overlap in values between campaigns. The Beijing summer campaign has the lowest DTTm at 26.4 ± 9.2 pmol DTT min^{-1} μg^{-1} $PM_{2.5}$ with the other campaigns having mean values between 35.2 ± 10 and 37.1 ± 12 pmol DTT min^{-1} μg^{-1} $PM_{2.5}$. There is a lot more DTTm variability within campaigns than between different locations and seasons, suggesting that broadly the PM components that the DTT assay is sensitive to are not location or season specific.

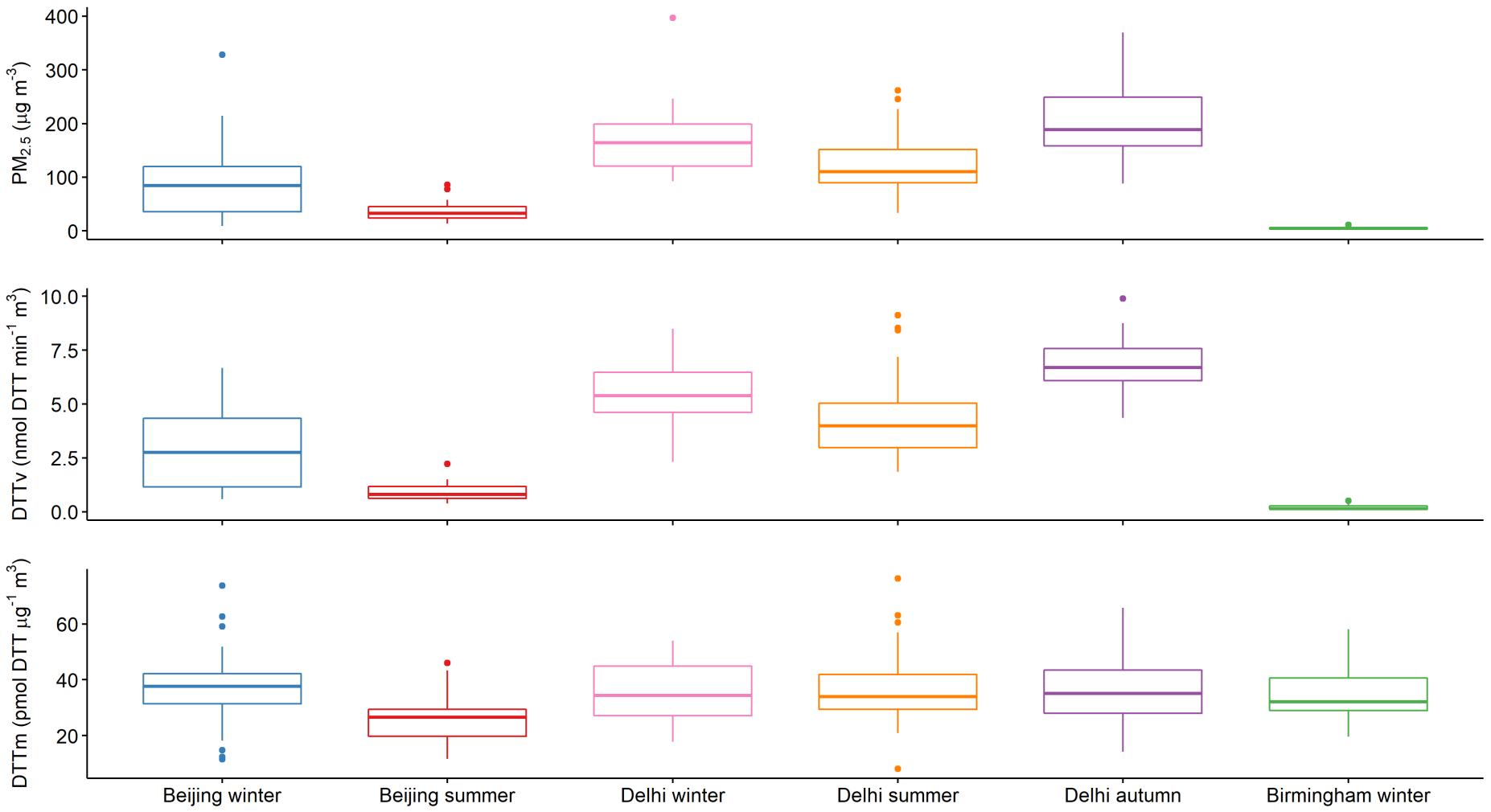

Figure 6-30: $PM_{2.5}$ concentration, DTTm and DTTv values for every field campaign.

6.2 Comparison of $PM_{2.5}$ concentration, DTTm and DTTv values across campaigns – statistical significance

Unpaired t-tests were performed on the $PM_{2.5}$ concentrations, DTTv and DTTm values from all of the campaigns, with the Delhi campaigns separated diurnally, to determine which campaigns / seasons were significantly different from each other. Figure 6-31 shows the t-test results as a series of box plots for DTTm, where the red lines between "boxes" / campaigns show significant difference. The plots for DTTv and $PM_{2.5}$ concentration are in the appendices for clarity and instead will be explained in text (Figure S1 and Figure S2).

The t-test results for $PM_{2.5}$ concentration show nine instances where $PM_{2.5}$ concentration is insignificantly different between two campaigns (based on an adjusted p-value using the Benjamini & Hochberg method, 95 % confidence interval). However, only four instances show insignificantly different mean DTTv values between campaigns, meaning there are five instances where the $PM_{2.5}$ concentration is insignificantly different while DTTv is significantly different. This shows that $PM_{2.5}$ concentration, in this study, is not a good predictor of the toxicity of the air mass (based of DTTv values). The five instances where the mean DTTv is significantly different between campaigns while the mean $PM_{2.5}$ concentrations is similar between the same campaigns are shown in Table 6-.

Table 6-11: Unpaired t-test results for campaigns where $PM_{2.5}$ concentration is significantly similar whilst DTTv is different. The units are DTTv = nmol DTT min^{-1} m^{-3} and $PM_{2.5}$ = µg m^{-3}. The p-values are adjusted using the Benjamini & Hochberg method.

Group 1	DTTv	$PM_{2.5}$	Group 2	DTTv	$PM_{2.5}$	p-value (DTTv)	p-value ($PM_{2.5}$)
Beijing winter	3.04 ± 1.9	99.2 ± 74	Delhi summer day	3.84 ± 1.7	116 ± 49	0.03	0.2
Delhi autumn day	6.95 ± 0.90	168 ± 54	Delhi winter day	5.36 ± 1.0	134 ± 38	<0.01	0.07
Delhi summer day	3.84 ± 1.7	116 ± 49				<0.01	0.2
Delhi summer night	4.54 ± 1.6	127 ± 49				0.04	0.6
Delhi autumn day	6.95 ± 0.90	168 ± 54	Delhi winter night	5.88 ± 1.8	201 ± 59	0.03	0.07

Notably, of the five instances shown in Table 6- only one pairing (Delhi autumn day and Delhi winter night campaigns) has significantly different DTTm values (Figure 6-31, p-value <0.01). The autumn days have significantly higher intrinsic toxicity than the winter nights, likely increasing the toxicity of the air mass even with similar $PM_{2.5}$ concentrations.

There is also one instance of the inverse of the above. During the Delhi winter, the days have significantly lower $PM_{2.5}$ concentrations than the nights (p-value <0.001), whilst the DTTv shows an insignificant difference (p-value 0.2). This is likely due to the significantly

higher intrinsic toxicity observed during the day in this campaign (41.0 ± 8.1 day and 29.5 ± 9.0 pmol DTT min^{-1} μg^{-1} $PM_{2.5}$ at night, p-value <0.01).

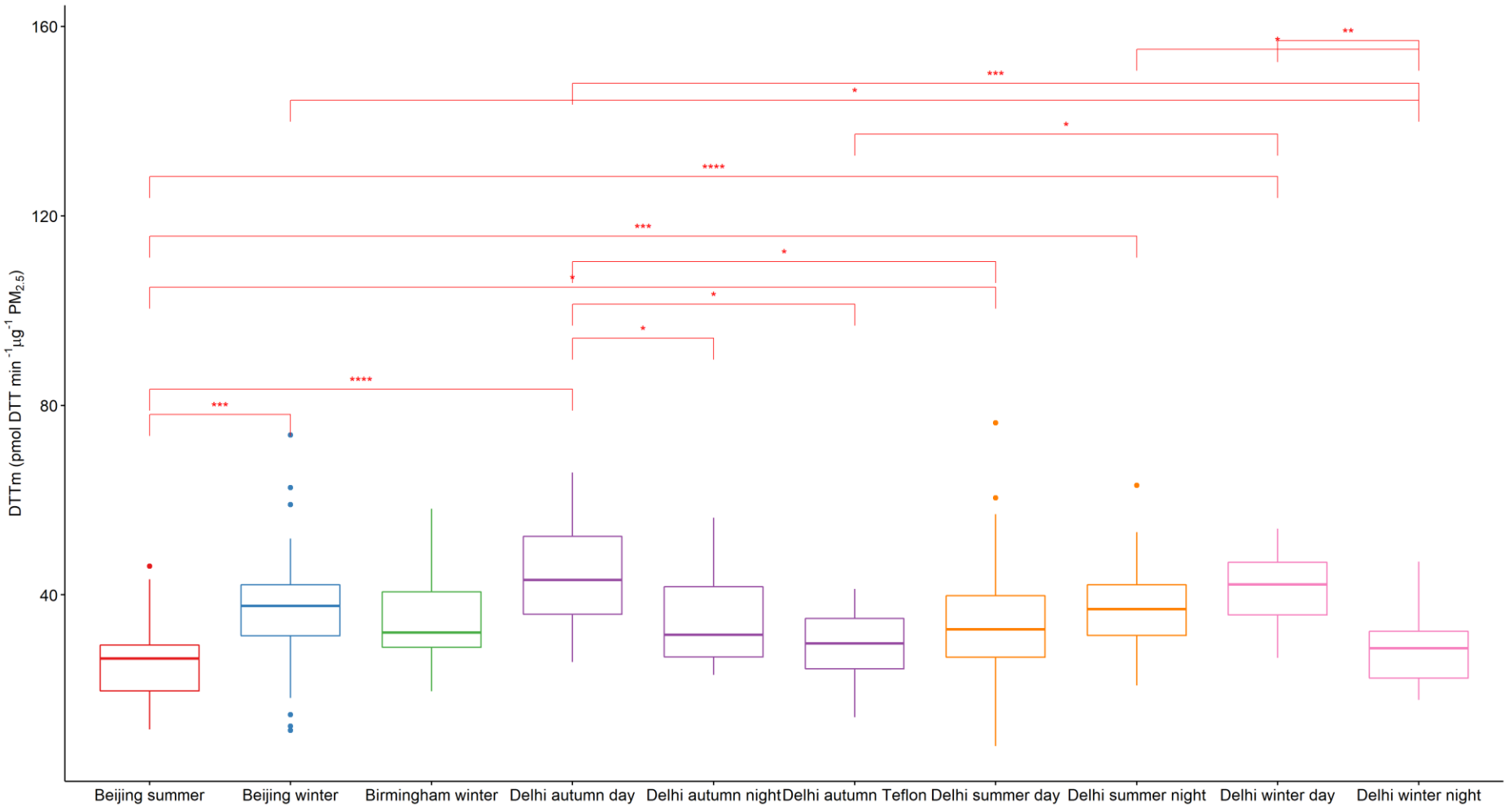

*Figure 6-31: Box plots and pairwise unpaired T-test of DTTm results for all field campaigns; where day / night samples have been separated. P-value adjustment was done using Benjamini & Hochberg (BH) method. The red bars represent statistically significantly different campaigns. The asterisks represent the significance levels and are * = 95 %, ** = 99 %, *** = 99.9 %, **** = 99.99 %.*

6.3 Impact of $PM_{2.5}$ concentration on OP^{DTT}

$PM_{2.5}$ concentration has been shown in literature to often be strongly correlated with – and likely a key determinant of – volume normalised OP (DTTv), with Fang et al., 2015 showing that the Pearson correlation coefficient varied between 0.49 – 0.88 for various seasons and sampling locations across Atlanta, Georgia. Wang et al., 2018 showed that there can be significant diurnal variability in the impact of $PM_{2.5}$ on DTTv with the daytime correlation (r_s = 0.83, $p < 0.0001$) being significantly higher than nighttime (r_s = 0.33, p = 0.077) in Hangzhou city, China. The gradient between DTTv and $PM_{2.5}$ reported by Wang et al., 2018 during the daytime was also three times higher than during the night (day = 0.0111, night = 0.0037 nmol DTT min^{-1} μg^{-1} $PM_{2.5}$), without a significant increase in $PM_{2.5}$ or DTTv during the day, implying a strong compositional change between day and night. However, due to the insignificant correlation at night, the gradient should be treated with caution.

This positive correlation between DTTv and $PM_{2.5}$ is seen across multiple OP chemical assays. Campbell et al., 2020 (paper attached in the appendices) published the results for four OP assays performed during the Beijing campaigns discussed in this thesis; DTT (the measurements shown in this thesis), ascorbic acid (AA), 7-dichlorofluoroscein/hydrogen peroxidase assay (DCFH), and electron parametric spectroscopy (EPR). Every OP assay showed stronger correlation between $PM_{2.5}$ and volume normalised toxicity during the winter campaign compared to summer with all Spearman correlations (r_s) for the winter being significant (DTTv; r_s = 0.81, AAv; r_s = 0.89, DCFHv; r_s = 0.96, EPRv; r_s = 0.89). The $PM_{2.5}$ contribution to volume-normalised toxicity is to be expected considering volume-normalised toxicity is essentially intrinsic toxicity multiplied by $PM_{2.5}$ concentration.

This trend can also be seen when combining all data across the various field campaigns reported in this thesis, as shown in Figure 6-32 where r_p (Pearson correlation coefficient, hereafter represented by the symbol r) = 0.82. For ease of viewing the uncertainty in the $PM_{2.5}$ concentrations is not shown, as this varied considerably, especially during longer sampling times. Instead a bootstrap analysis using 100,000 resamples of the data within uncertainty was performed to determine correlation within uncertainty, giving r = 0.79 ± 0.044. This test performs multiple linear regression analyses (100,000 in this case) using random values for $PM_{2.5}$ concentration within the uncertainty range; the r-values obtained form a normal distribution where the peak represents the most common r-value for the data.

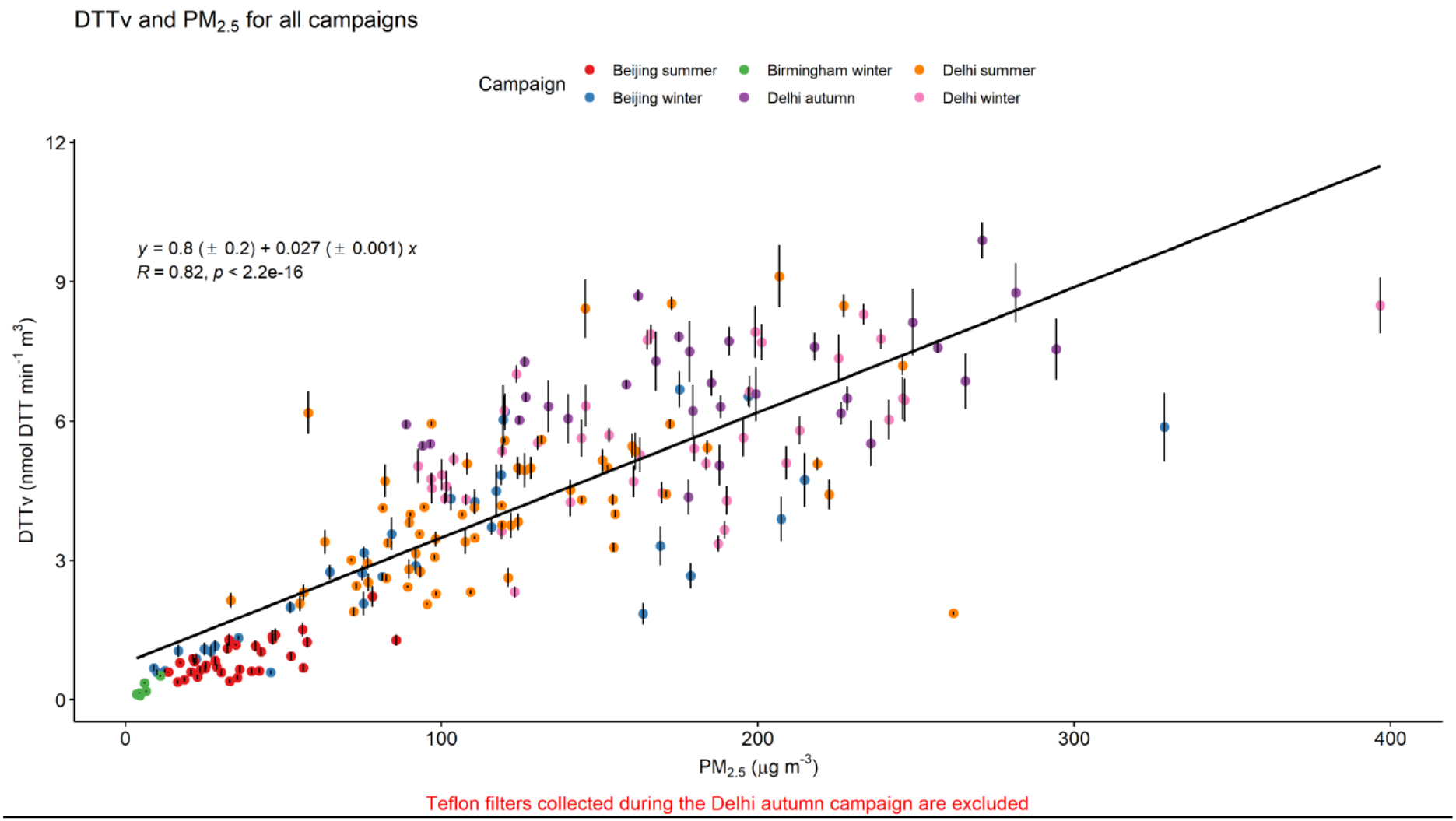

Figure 6-32: $PM_{2.5}$ vs DTTv correlation plot for all campaign data (N = 209) excluding the Teflon filters collected in Delhi (due to DTTv values being significantly different depending on filter material). The uncertainties in DTTv values represent 1 SD, the uncertainties for $PM_{2.5}$ concentration were omitted for clarity.

This high correlation between the combined $PM_{2.5}$ concentration and DTTv invites the obvious question; if $PM_{2.5}$ concentration is well correlated with DTTv why not just use $PM_{2.5}$ concentration to estimate toxicity? While this relationship holds for lower $PM_{2.5}$ concentrations, it has become apparent in the data obtained during this project that as the $PM_{2.5}$ concentration rises the correlation changes. This can be seen in Figure 6-32 when the $PM_{2.5}$ concentration increases the data points become less well correlated within uncertainty. To show this effect more clearly the combined dataset is split into a low and high $PM_{2.5}$ concentration groups (separated at the median $PM_{2.5}$ value, 110.6 μg m^{-3}) so that each group contains the same number of data points, the correlation plots for these two groups can be seen in Figure 6-33.

The low $PM_{2.5}$ concentration group shows a very similar correlation value to the combined group at r = 0.85 compared to 0.82, however, the high $PM_{2.5}$ group shows an insignificant correlation ($r \leq 0.6$) at r = 0.41. The gradient is also higher in the low $PM_{2.5}$ group, this is an estimation of DTTm. DTTm is slightly higher for the low $PM_{2.5}$ group at 36.3 ± 13 compared to 32.9 ± 9.8 pmol DTT min^{-1} μg^{-1} $PM_{2.5}$ at high $PM_{2.5}$, based on the average experimental values for DTTm for each group. However, this difference is not statistically significant at a 95 % confidence interval (Welch t-test p-value = 0.03). This difference in the ability of $PM_{2.5}$ to drive volume-normalised toxicity at different concentrations shows that under severely polluted environments, $PM_{2.5}$ is not a good catchall metric for determining human toxicity exposure (DTTv).

The drivers for this lower correlation at higher $PM_{2.5}$ concentrations are explored in Figure 6-34, where correlations between the intrinsic toxicity values DTTm, and $PM_{2.5}$ are shown for low and high $PM_{2.5}$ concentrations.

At lower $PM_{2.5}$ concentrations, intrinsic toxicity (DTTm) is approximately constant with respect to $PM_{2.5}$ concentration with a low Pearson correlation coefficient ($r = 0.11$) and insignificant p-value ($p = 0.26$), therefore the DTTv value is proportional to $PM_{2.5}$ concentration. However, at higher concentrations a weak negative correlation between DTTm and $PM_{2.5}$ ($r = -0.46$, $p < 0.01$) is shown, indicating that during these highly polluted sampling times something is depressing the intrinsic toxicity of the particles to the point where the air mass toxicity overall can be reduced. An example of this is provided by two night-time samples collected during the Delhi winter campaign on the nights of 18-19/01/2018 (night 1) and 01-02/02/18 (night 2). Night 1 had $PM_{2.5}$ concentrations over twice those of night 2 at 397 ± 51 μg m^{-3} compared to 166 ± 52 μg m^{-3}, however, the DTTv value for both nights are similar at 8.49 ± 0.60 and 7.87 ± 0.21 nmol DTT min^{-1} m^{-3} respectively. This is due to the $PM_{2.5}$ on night 2 having over twice the intrinsic toxicity of those on night 1, 21.3 ± 1.5 compared to 47.0 ± 1.3 pmol DTT min^{-1} μg^{-1} $PM_{2.5}$ respectively. This shows that in extreme PM events $PM_{2.5}$ concentration can be a bad indicator of OP toxicity, with particle composition playing a much more important role. This is explored further later in this chapter for Beijing, Delhi, and their combined datasets in sections 6.5 to 6.7.

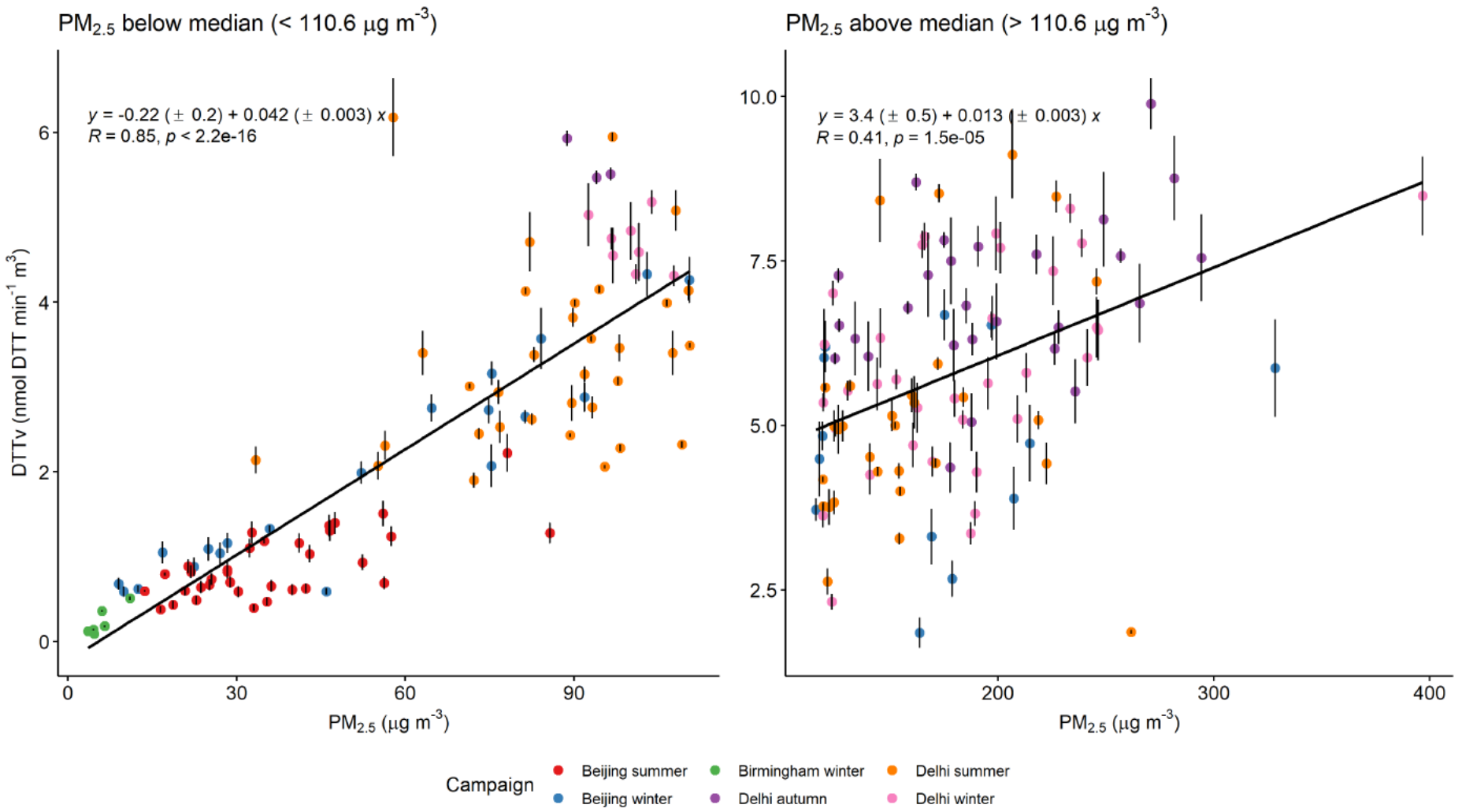

Figure 6-33: $PM_{2.5}$ vs DTTv correlation plots for all campaign data where the data has been split by $PM_{2.5}$ median (110.6 μg m^{-3}) into low $PM_{2.5}$ (N = 105) and high $PM_{2.5}$ (N = 104).

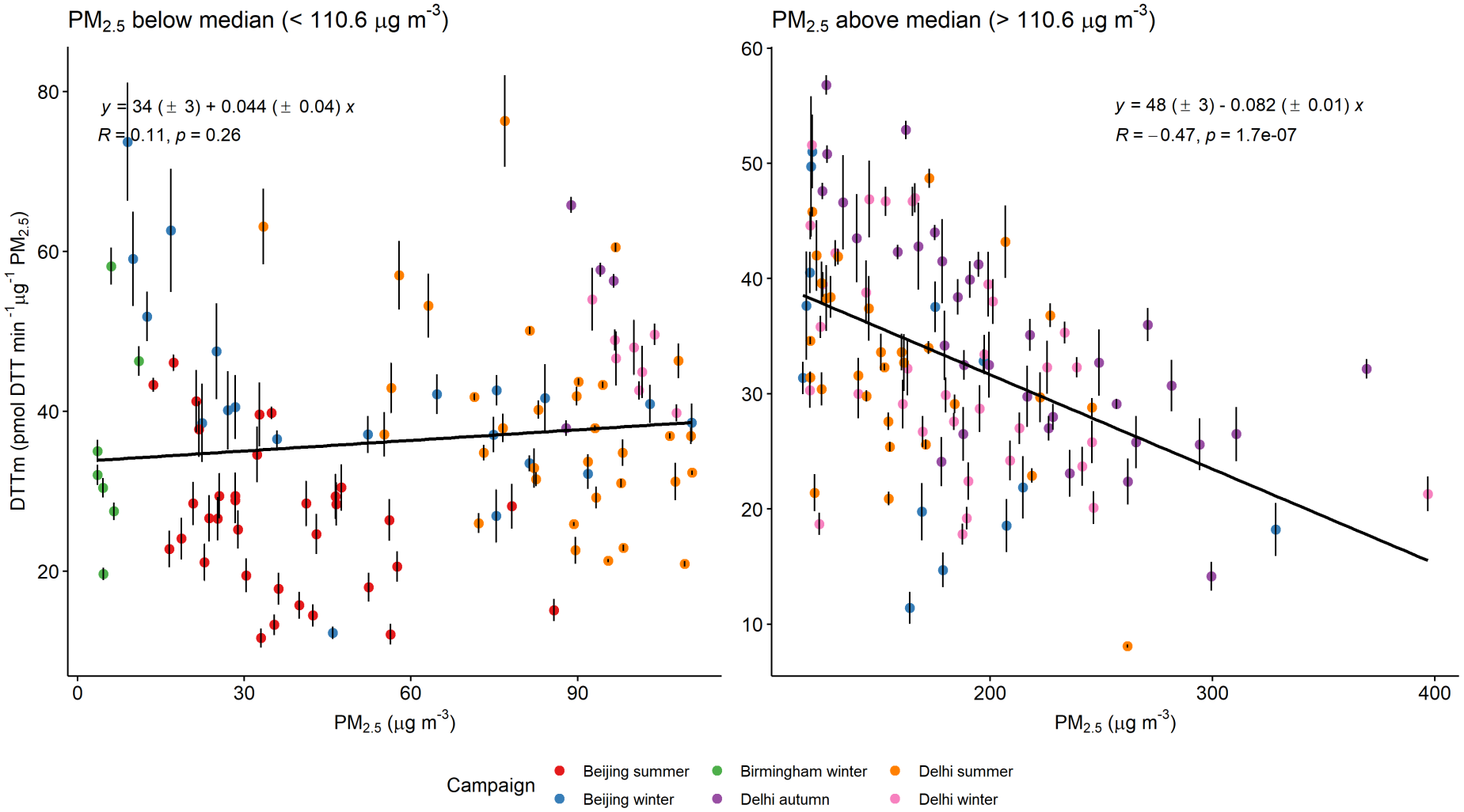

Figure 6-34: PM2.5 vs DTTm correlation plots for all campaign data where the data has been split by PM2.5 median (110.6 µg m-3) into low PM2.5 (N = 108) and high PM2.5 (N = 108). Seven Delhi autumn Teflon filters have been included in this plot.

6.3.1 Seasonal variability in $PM_{2.5}$ / DTT correlation

There is also seasonal and location variability in the correlation between DTT and $PM_{2.5}$. As mentioned earlier in this chapter, Campbell et al., 2020 reported that four acellular OP assays showed a higher correlation for volume normalised toxicity and $PM_{2.5}$ concentration in the winter compared to the summer in Beijing. This is shown in Figure 6-35 A and B, where data from both the winter and summer campaigns show high correlation between DTTv and $PM_{2.5}$ but the winter campaign has a higher correlation coefficient than the summer. This indicates that there was significantly higher intrinsic PM toxicity, as assessed by these assays, during the winter campaign as can be seen in Figure 6-31.

The Birmingham campaign showed the strongest correlation between DTTv and $PM_{2.5}$ ($r = 0.9$), with DTTv being almost entirely driven by $PM_{2.5}$ concentration. This is likely due to the sampling site being a roadside site and therefore, most of the $PM_{2.5}$ sampled would be largely vehicle exhaust emissions and road dust, with limited composition variability expected. This was also a short single season sampling period, limiting the ability to discern variations in PM sources and composition. Simonetti et al., 2018 showed that DTT is sensitive to species associated with non-exhaust vehicle emissions such as iron and nickel.

All Delhi campaigns show an insignificant correlation ($r < 0.60$, Figure 6-35) between DTTv and $PM_{2.5}$ concentration, with the autumn campaign showing the lowest correlation at $r = 0.49$. The summer and winter campaigns have the same correlation ($r = 0.56$), despite the winter having significantly higher $PM_{2.5}$ concentrations (winter = 168 ± 44, summer = 122 ± 31 μg m^{-3}). This is due to the winter campaign having a much stronger anti-correlation coefficient between DTTm and $PM_{2.5}$ than the summer (winter $r = -0.63$, summer $r = -0.43$). This is also the case for the Beijing campaigns where the correlation coefficients for the

winter and summer are almost identical to those seen during the Delhi winter and summer campaigns. This results in similar correlation coefficients between DTTv and $PM_{2.5}$ for the Beijing campaigns, despite the significantly higher $PM_{2.5}$ concentration during the winter.

Puthussery et al., 2020 reported a significant correlation between DTTv and PM_1 measurements obtained using a 1-hour time resolution online DTT instrument in Delhi between 03/02/2019 – 09/02/2019. This resulted in an r_s number of 0.66 with a higher gradient of 0.075 nmol DTT min^{-1} μg^{-1} PM_1 compared to the winter measurement presented here at 0.014 nmol DTT min^{-1} μg^{-1} $PM_{2.5}$. The DTTv values measured here were significantly higher than those reported by Puthussery et al., 2020 at 5.62 ± 1.4 (2.32 to 8.49) nmol min^{-1} m^{-3} compared to their 1.57 ± 0.7 (0.49 to 3.60). This is likely due to higher average PM concentrations during the sampling campaigns reported here ($PM_{2.5}$: 167.7 ± 44 $\mu g\ m^{-3}$ compared to PM_1: 105 ± 60 $\mu g\ m^{-3}$) and higher intrinsic toxicity during these campaigns. It is also possible that there is a compositional difference between the PM_1 and $PM_{2.5}$, Puthussery et al., 2020 provide a correlation plot between their PM_1 measurements and $PM_{2.5}$ concentration measured at the US consulate (R^2 = 0.71, y = 0.75x + 17.92). Puthussery et al., 2020 do not report DTTm values, however, through estimations from figures in the paper most values fall between 10 – 20 pmol min^{-1} μg^{-1} PM_1 compared to 35.2 ± 10 pmol min^{-1} μg^{-1} $PM_{2.5}$ for the campaigns reported here. Lastly, they indicate that caution needs to be exercised when comparing filter based DTT analysis to the near real-time measurements in their paper.

Delhi autumn shows the least impact from $PM_{2.5}$ concentration on DTTv, due to this campaign exhibiting the strongest anti-correlation between intrinsic toxicity and $PM_{2.5}$ (r = -0.77), while having the highest $PM_{2.5}$ concentration (198.6 ± 60 $\mu g\ m^{-3}$).

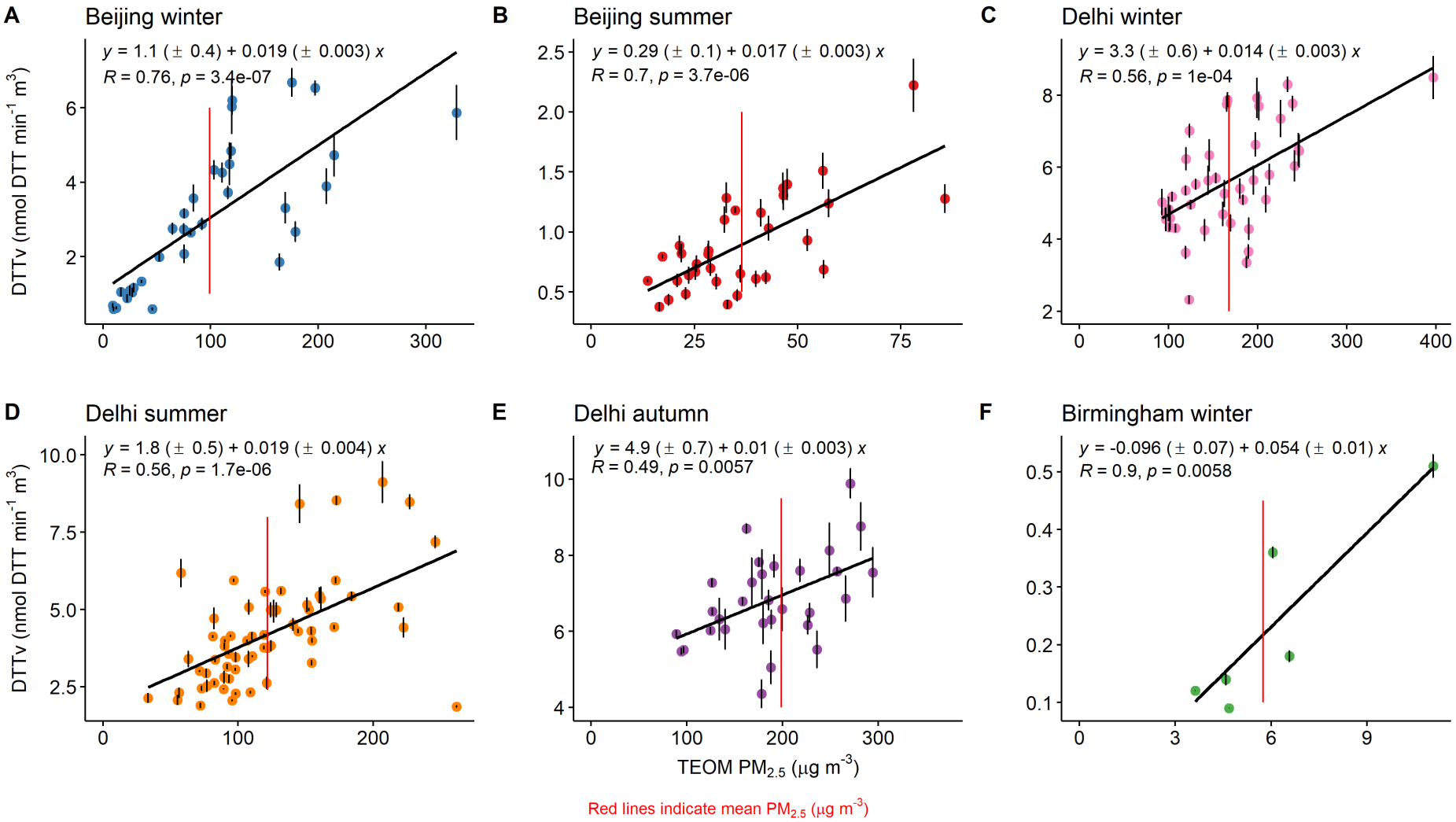

Figure 6-35: $PM_{2.5}$ vs DTTv correlation graphs split into field campaigns. Mean ± SD $PM_{2.5}$ ($\mu g\ m^{-3}$) for each campaign: A = 99.2 ± 42, B = 36.5 ± 12, C = 168 ± 44, D = 122 ± 31, E = 199 ± 60, F = 5.74 ± 2.6.

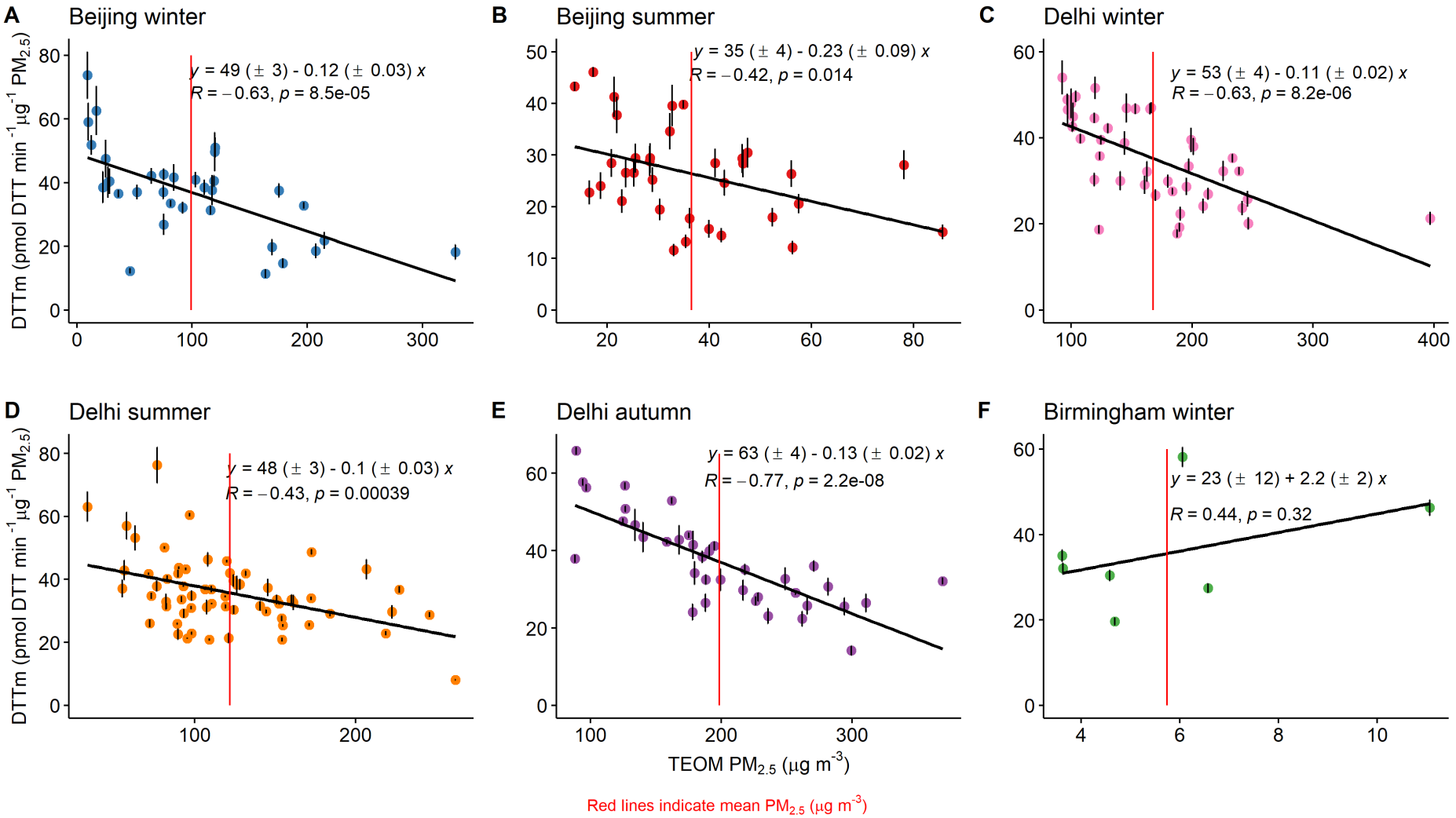

Figure 6-36: PM2.5 vs DTTm correlation graphs split into field campaigns.

6.3.2 Diurnal variation in $PM_{2.5}$ / DTT correlations

As the sampling in the Delhi campaigns was carried out for 12 hours with filters being changed at 09:00 and 21:00, the data allow for the impacts of diurnal variation in $PM_{2.5}$ OP across the seasons in Delhi to be analysed. As can be seen in Figure 6-37 the Delhi winter samples show a similar DTTv / $PM_{2.5}$ correlation diurnally, with r = 0.58 and 0.57 for day and night respectively, this also applies to the gradient (0.015 ± 0.005 and 0.017 ± 0.006 nmol DTT min^{-1} μg^{-1} $PM_{2.5}$) and y-intercept (3.3 ± 0.7 and 2.5 ± 1 nmol DTT min^{-1} m^{-3}). This is despite the nighttime samples having a much higher $PM_{2.5}$ concentration than during the day (201.0 ± 45 μg m^{-3} at night compared to 134.4 ± 43 μg m^{-3} during day). The reason for this is that the daytime samples have a much stronger negative DTTm – $PM_{2.5}$ correlation than the night (as can be seen in Figure 6-38). As a result, DTTv values during the winter do not significantly vary diurnally (Figure S1) despite the higher $PM_{2.5}$ concentration during the night.

Figure 6-37 shows that during the autumn campaign the correlation of $PM_{2.5}$ concentration and DTTv is diurnally similar (for both correlation coefficient and gradient), with no significant difference in DTTv values. This is despite the days having significantly higher DTTm values than at night (Figure 6-31) and the $PM_{2.5}$ concentrations being statistically similar. This is likely due to the DTTm during the day being much more sensitive to $PM_{2.5}$ concentration than during the night. Figure 6-38 shows that the autumn days have the strongest $PM_{2.5}$ / DTTm anti-correlation (r = -0.93 and -0.71 during the day and night, respectively), with a larger inverse gradient than during the night (-0.2 ± 0.02 and -0.12 ± 0.03 pmol DTT min^{-1} m^{-3}).

The summer campaign appears to be the most diurnally homogenous campaign in Delhi, with the $PM_{2.5}$ concentration, DTTv, and DTTm values being the same, within uncertainty, diurnally. The DTTv / DTTm correlations do not significantly differ diurnally, with the gradients and y-intercepts being the same, within uncertainty (Figure 6-37 and Figure 6-38).

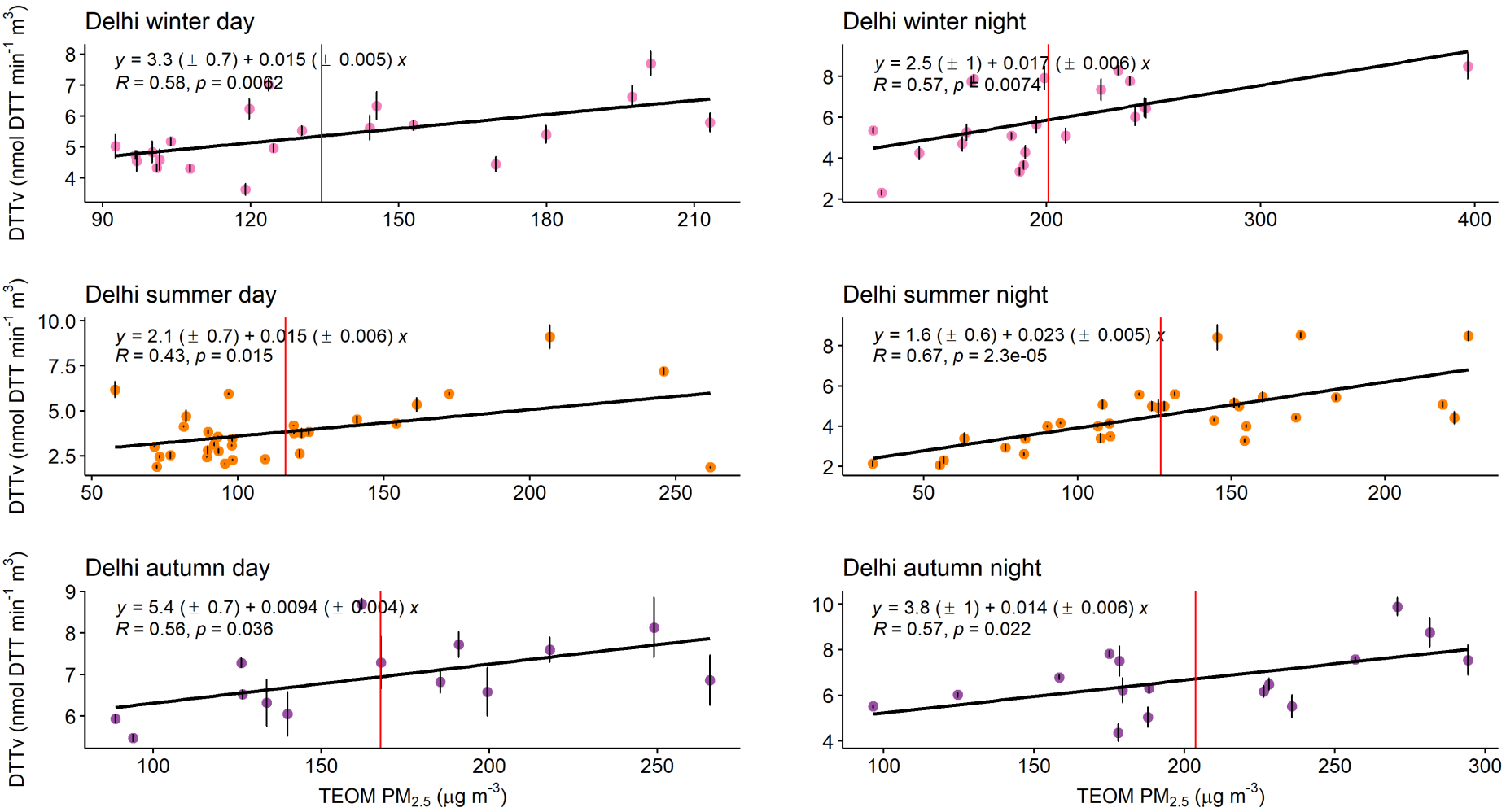

Figure 6-37: $PM_{2.5}$ vs DTTv correlation graphs for Delhi where the data has been split diurnally into day / night for each campaign. The mean $PM_{2.5}$ ± SD (µg m^{-3}) during the day (night) for each campaign: Delhi winter = 134.4 ± 43 (201.0 ± 45), Delhi summer = 116.3 ± 33 (127.1 ± 30), Delhi autumn = 167.7 ± 56 (203.8 ± 35).

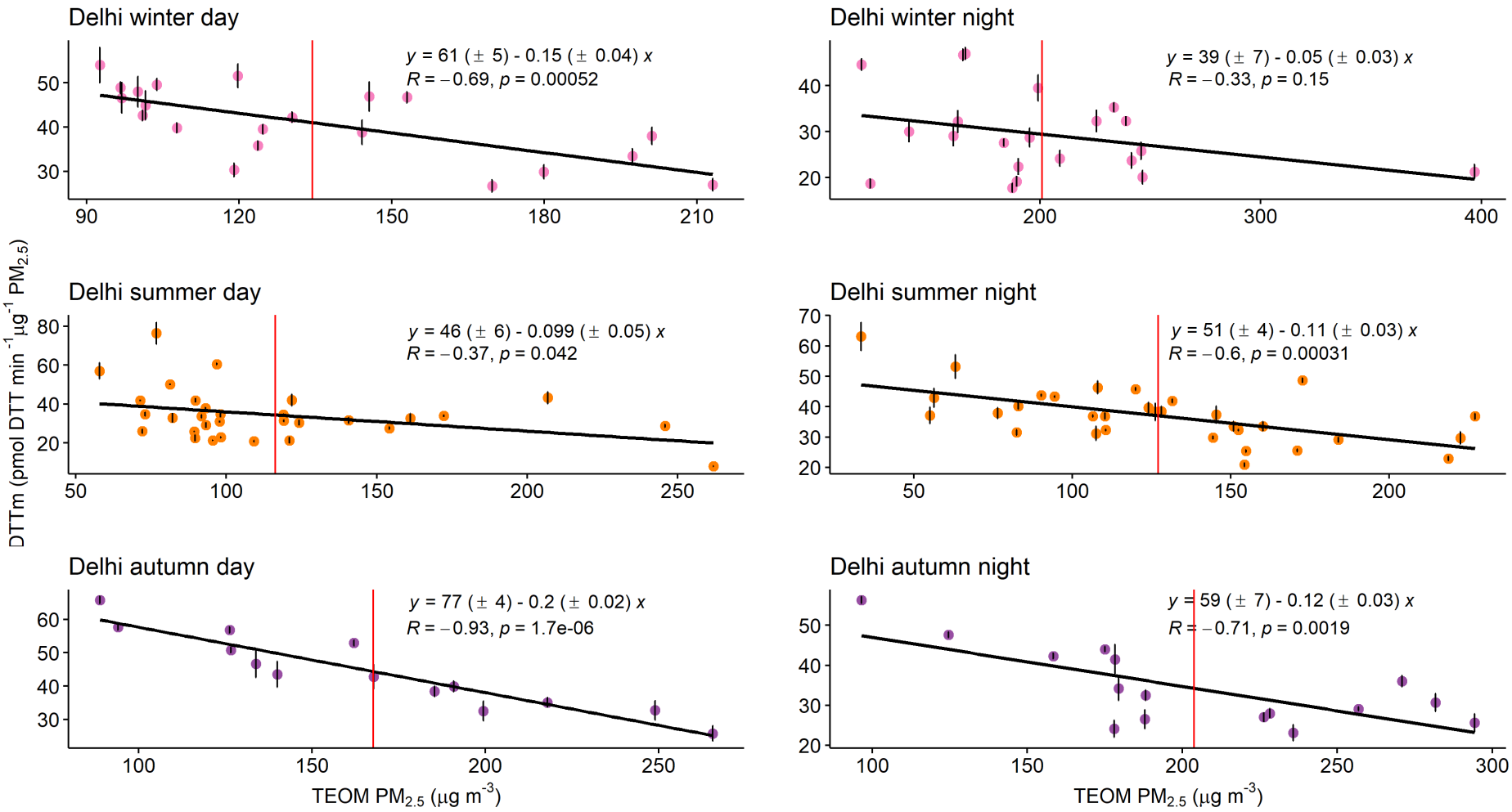

Figure 6-38: PM2.5 vs DTTm correlation graphs for Delhi where the data has been split diurnally into day / night for each campaign

6.4 Drivers of intrinsic toxicity, as measured by DTTm, for the Beijing campaigns and Birmingham

6.4.1 Beijing Winter campaign

Figure 6-39 shows a correlation matrix of statistically significantly correlated $PM_{2.5}$ components with DTTm. The significance level chosen for all correlation matrixes in this chapter is a p-value ≤ 0.05 and r ≥ 0.5, unless otherwise stated. The "crossed out" correlations are species for which no significant correlation was found (those with a p-number ≥ 0.05). Considering the correlations in turn from the strongest (highest r value): calcium (r = 0.71) and strontium (r = 0.69) are well correlated with DTTm and are typically crustal in origin, being a good marker for suspended road dust and construction. The strong correlation with iron (r = 0.69) and manganese (0.66, 0.59 for water-soluble) may be indicative of brake wear. Water-soluble chromium (r = 0.70) has been found in the emissions from vehicles and oil burning. These five elements put together indicates a reasonably strong influence upon DTTm from various vehicle emission sources to $PM_{2.5}$ toxicity in Beijing; road dust resuspension, brake wear, and direct emissions. The focus here has been on the species with the strongest correlations (Cao et al., 2012; Rai, Slowik, Furger, Haddad, et al., 2021).

To assess the relative impact of different chemical species on the intrinsic toxicity during the various field campaigns the gradients of the linear regression of the chemical species and DTTm were used. Examples of these plots / regression analyses is shown in Figure 6-40, with the standard error for the gradient being shown in the caption. The units for these gradients are pmol DTT min^{-1} ng^{-1} of the species plotted, for clarity these units are written as

$DTTm^{species}$ in the following text. For example, for iron in Figure 6-40 this would be 1.5 ± 0.28 $DTTm^{Fe}$, to compare to other species.

DTTm showed a much stronger dependence upon (higher gradients) several of the vehicle source markers than for the other species measured, these markers include water-soluble chromium and manganese, and strontium, which had gradients of 235 ± 43 $DTTm^{WS\text{-}Cr}$, 99.4 ± 24 $DTTm^{WS\text{-}Mn}$, and 169 ± 32 $DTTm^{Sr}$. Water-soluble chromium has a much higher gradient than total chromium (22.6 ± 5.6 $DTTm^{Cr}$).

Chlorine was well correlated with DTTm (r = 0.61) in this campaign, chlorine is often associated with sea salt (unlikely in Beijing due to the large distance from the sea) or road salt (this is possible as this campaign experienced a few days below freezing). Chlorine could also be indicative of the contribution of coal combustion; however, chlorine shows an insignificant correlation with sulphate, which is normally correlated where the main source is coal combustion, especially in locations with limited use of flue-gas desulphurisation. In terms of gradient chlorine had the second to lowest impact upon OP, at 0.39 ± 0.095 $DTTm^{Cl^-}$ (Rai, Slowik, Furger, Haddad, et al., 2021; Yao et al., 2002).

Organic carbon has a higher correlation with intrinsic toxicity during the Beijing winter campaign (r = 0.68) than most of the other campaigns, with the exception of Delhi autumn (r = 0.78). However, in the Delhi autumn campaign there is the possibility of this being driven by widespread agricultural burning not seen during any of the other campaigns. This is also observed in the gradients where the DTT – OC gradient for the Beijing winter campaign is slightly higher than most campaigns but within uncertainty (0.108 ± 0.021 $DTTm^{OC}$ compared to 0.0524 – 0.0874 ± 0.02 $DTTm^{OC}$ for the other campaigns), whereas the

Delhi autumn campaign is significantly higher at 0.153 ± 0.023 $DTTm^{OC}$ (Jain et al., 2020; Rai et al., 2021).

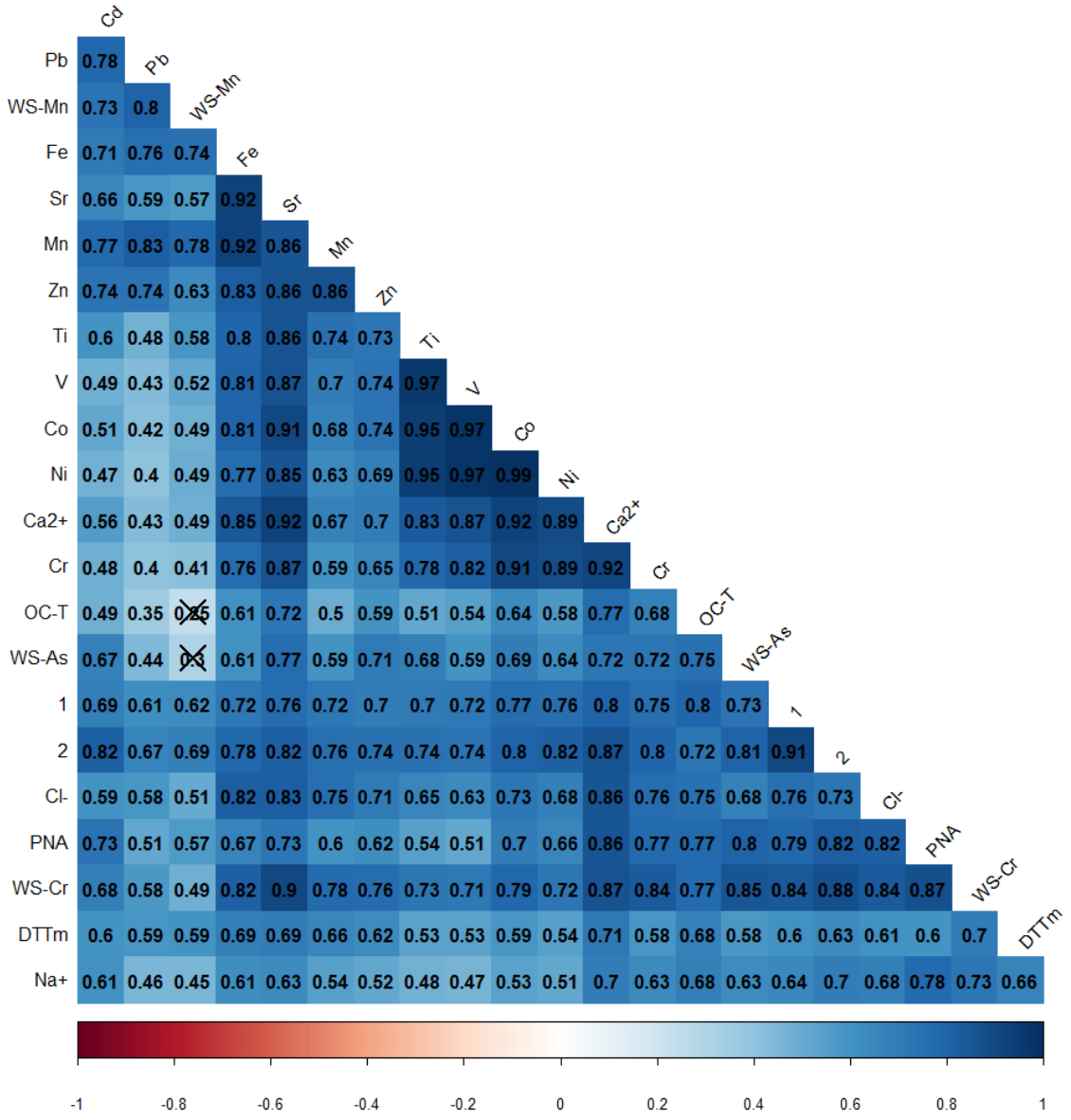

Figure 6-39: Pearson correlation matrix of DTTm and mass-normalised $PM_{2.5}$ composition species for the Beijing winter campaign. All species with a p-value > 0.05 and/or r ≤ 0.5 with DTTm have been excluded. Crossed out boxes represent p > 0.05. 1 = cis-2-methyl-1,3,4-trihydroxy-1-butene and 2 = 3-methyl-2,3,4-trihydroxy-1-butene.

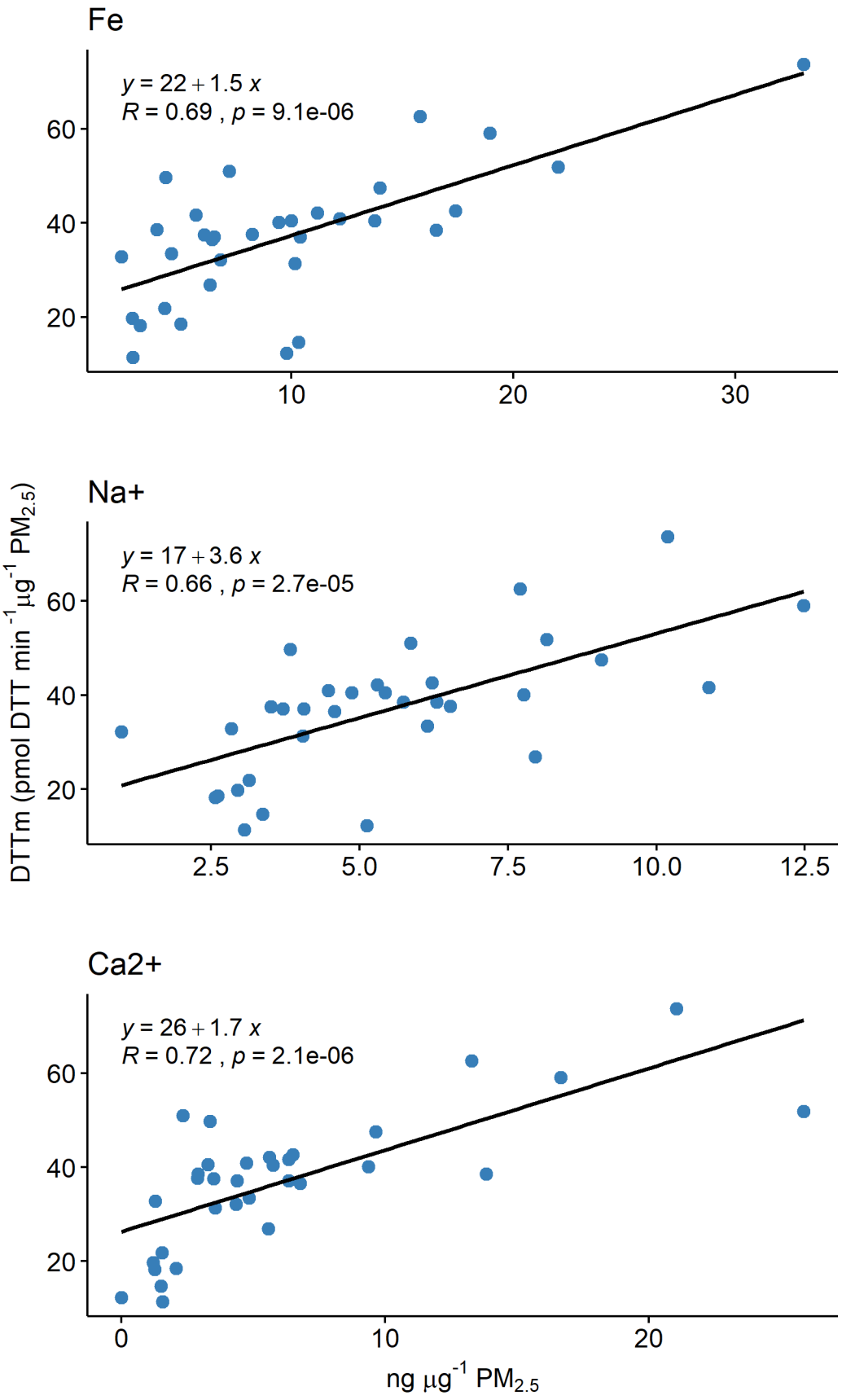

Figure 6-40: Linear regression plots of three highly correlated $PM_{2.5}$ species with intrinsic DTT toxicity. The standard error for the gradients shown are Fe = 1.50 ± 0.28, Na^{+} = 3.58 ± 0.73, and Ca^{2+} = 1.65 ± 0.30 pmol DTT min^{-1} ng^{-1}.

6.4.2 Beijing Summer campaign

DTTm values from the Beijing summer campaign generally showed weaker correlations with compositional species than was observed in the other campaigns. As can be seen in Figure 6-41, the majority of the species that have a significant correlation (p-value < 0.05) have an r number ≤ 0.6. As discussed in earlier sections Figure 6-31 shows that PM samples from this (Beijing summer) campaign have significantly lower intrinsic toxicity than those from most other campaigns. This may be due to the lack of significant influence from most metal species, which dominate all other campaigns. Generally, the Beijing summer campaign showed the lowest concentration for most of these metal species, Table 6- shows the average concentrations for four metal species that correlate well with DTTm in other campaigns:

Table 6-12: Average concentrations of Fe, Al, Mg, and Sr for the Beijing and Delhi campaigns. The uncertainty represents 1 S.D.

Campaign	Fe (μg m^{-3})	Al (μg m^{-3})	Mg (μg m^{-3})	Sr (ng m^{-3})
Beijing winter	0.679 ± 0.43	0.598 ± 0.45	NA	3.11 ± 1.5
Beijing summer	0.486 ± 0.20	0.223 ± 0.15	0.110 ± 0.064	1.45 ± 1.4
Delhi winter	2.13 ± 1.6	2.38 ± 1.9	0.818 ± 0.69	23.8 ± 24
Delhi summer	9.86 ± 4.7	12.5 ± 6.6	4.23 ± 2.1	76.5 ± 41
Delhi autumn	2.66 ± 1.6	2.16 ± 1.4	0.981 ± 0.68	21.6 ± 14

Unlike the winter campaign, the DTT values for samples from the Beijing summer show significant correlations with the concentrations of almost all n-alkanes. According to the gradients, the greatest influence from these n-alkanes on intrinsic toxicity is from the even numbered alkanes, with larger chain alkanes having more of an influence than short chains. The highest gradient for these being 821 ± 164 $DTTm^{C34}$ going down to 124 ± 29 $DTTm^{C26}$, at

which point the odd numbered alkanes appear ranging from 121 ± 31 $DTTm^{C33}$ to 51.5 ± 15 $DTTm^{C25}$.

Lyu et al., 2019 reported that the major sources of n-alkanes during the APHH campaign were local vehicular exhaust and coal combustion. This study only looked at the winter campaign, however, the contribution of coal combustion is supported by the C_{max} at C_{29} with a secondary peak at C_{25} (Lyu et al., 2019; Oros & Simoneit, 2000). Generally, the higher molecular weight odd-numbered n-alkanes are associated with biogenic sources such as plant wax or biomass burning. Vehicular emissions are more associated with shorter chain length even-number n-alkanes (Li et al., 2010).

Table 6-5 shows the correlations between DTTm and species for which the datasets were incomplete, which prevented them from being including in the correlation matrix. Three PAH: chrysene, coronene, and indeno(1,2,3-cd)pyrene were well correlated with DTTm and had some of the highest gradients per unit mass: 1177 ± 383 $DTTm^{chrysene}$, 1382 ± 411 $DTTm^{coronene}$, and 1683 ± 520 $DTTm^{indeno(1,2,3\text{-}cd)pyrene}$. The major source for these PAH is unburned fuel from motor vehicles and biomass burning (Shirmohammadi et al., 2016).

Table 6-5: Highly correlated $PM_{2.5}$ species with DTTm from the Beijing summer campaign, which do not have a complete dataset. All species with a p-value > 0.05 and/or $r_p \leq 0.5$ have been excluded.

Species	r	p-value	n
Ni	0.60	0.01	16
Chrysene	0.50	<0.01	31
Indeno(1,2,3-cd)pyrene	0.64	<0.01	17
Coronene	0.77	<0.01	10
C34	0.74	<0.01	23
17b (H), 21a (H) - Norhopane	0.84	<0.01	8

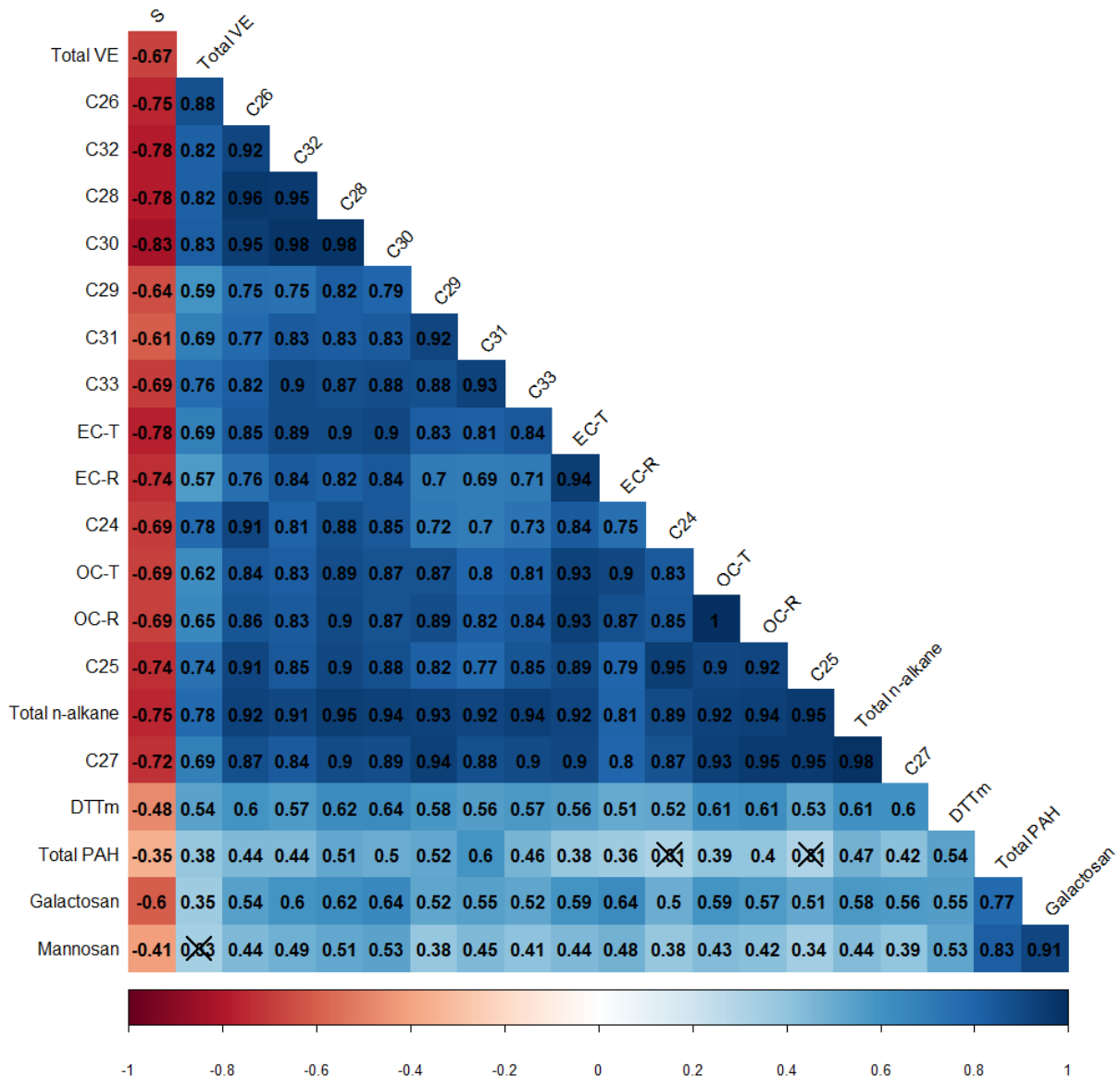

Figure 6-41: Pearson correlation matrix of DTTm and mass-normalised PM2.5 composition species for the Beijing summer campaign. All species with a p-value > 0.05 and/or r ≤ 0.5 has been excluded (aside from S), as well has any specie with an incomplete dataset (n = 34). Crossed out boxes represent p > 0.05. Total VE represents combined vehicle emission markers.

6.4.3 Multiple linear regression analysis on source apportionment results for Beijing

To assess the relative impact of different PM sources on intrinsic toxicity in Beijing a multiple linear regression (MLR) analysis was performed on pooled source apportionment results for both campaigns. The background to the source apportionment analysis was covered in Chapter 4. Initially, the MLR analysis was performed on each campaigns OC and $PM_{2.5}$ derived source apportionment. However, insignificant results were obtained for all sources aside from other organic carbon for the winter and cooking for the summer. Therefore, the MLR analysis was performed on the combined dataset from both campaigns.

The analysis was carried out with the most insignificant results based on p-value being dropped iteratively until only significant results ($p < 0.05$) remained. For example, for the OC source apportionment, the insignificant sources were vegetative detritus ($p = 0.91$), gasoline vehicles ($p = 0.65$), residential coal combustion ($p = 24$), and industrial coal combustion ($p = 0.12$). The result obtained from the OC source apportionment was:

$$DTTm = (5.15 \pm 3.4) + (337 \pm 71) * Cooking + (261 \pm 47) * BB + (168 \pm 30) * Other\ OC$$

Where BB = biomass burning. These sources account for 52 % of the variance based on the adjusted R-squared value. The $PM_{2.5}$ derived source apportionment results yielded the same order of sources, with other organic matter replace OC:

$$DTTm = (5.62 \pm 3.6) + (252 \pm 54) * Cooking + (111 \pm 21) * BB + (70.3 \pm 13) * Other\ OM$$

The insignificant results for many of the sources in Beijing is rather surprising, specifically for vehicle related sources and geological minerals. The strong correlations seen for metals linked to non-exhaust / exhaust vehicle emissions and geological minerals during the winter campaign and multiple n-alkanes during the summer campaign support these sources being important drivers of PM OP in Beijing. Organic carbon was well correlated with intrinsic toxicity during both campaigns, however, many other species showed considerably higher species corrected intrinsic toxicity ($DTTm^{species}$) such as $DTTm^{C34}$ being roughly four orders of magnitude higher than $DTTm^{OC}$ during the summer.

6.4.3 Species contributing to oxidative potential in Birmingham

The two monitoring sites that were used to gather $PM_{2.5}$ data to calculate DTTm in Birmingham: The A4540 roadside and Ladywood AURN stations also measure other air pollutants. Measurements were averaged over both sites, given their distance from the PM sampling site, the resulting correlation matrix for all Birmingham species is shown in Figure 6-42. There is an unusually strong correlation between DTTv and $PM_{2.5}$ for Birmingham (r = 0.9) compared to the other campaigns: Beijing winter and summer: 0.75 and 0.68; Delhi winter, summer, and autumn: 0.52, 0.63, and 0.49. All with a p-value ≤ 0.01. This is likely due to the influence of traffic emissions and road dust, with this sampling site being the only roadside site, sampled for a shorter duration, and hence the single-source dominance for the Birmingham measurements. This is supported by the high correlations between DTTm and NO_x species in Figure 6-42.

Out of the NO_x species, NO_2 showed the most influence on DTTm at 0.722 ± 0.24 $DTTm^{NO2}$ compared to 0.421 ± 0.14 $DTTm^{NO}$ and 0.206 ± 0.065 $DTTm^{NOX}$. As discussed in the introduction, NO_2 has been shown to react with antioxidants in the lungs. However, there is still uncertainty as to whether the effects of NO_x exposure is independent of other traffic related pollutants (Boningari & Smirniotis, 2016; Peel et al., 2013; U.S. EPA, 2016). As this is the only campaign to show significant positive correlations with NO_x, these other traffic related pollutants might be the cause of the DTT degradation. Unfortunately, due to the lack of compositional data this cannot be confirmed.

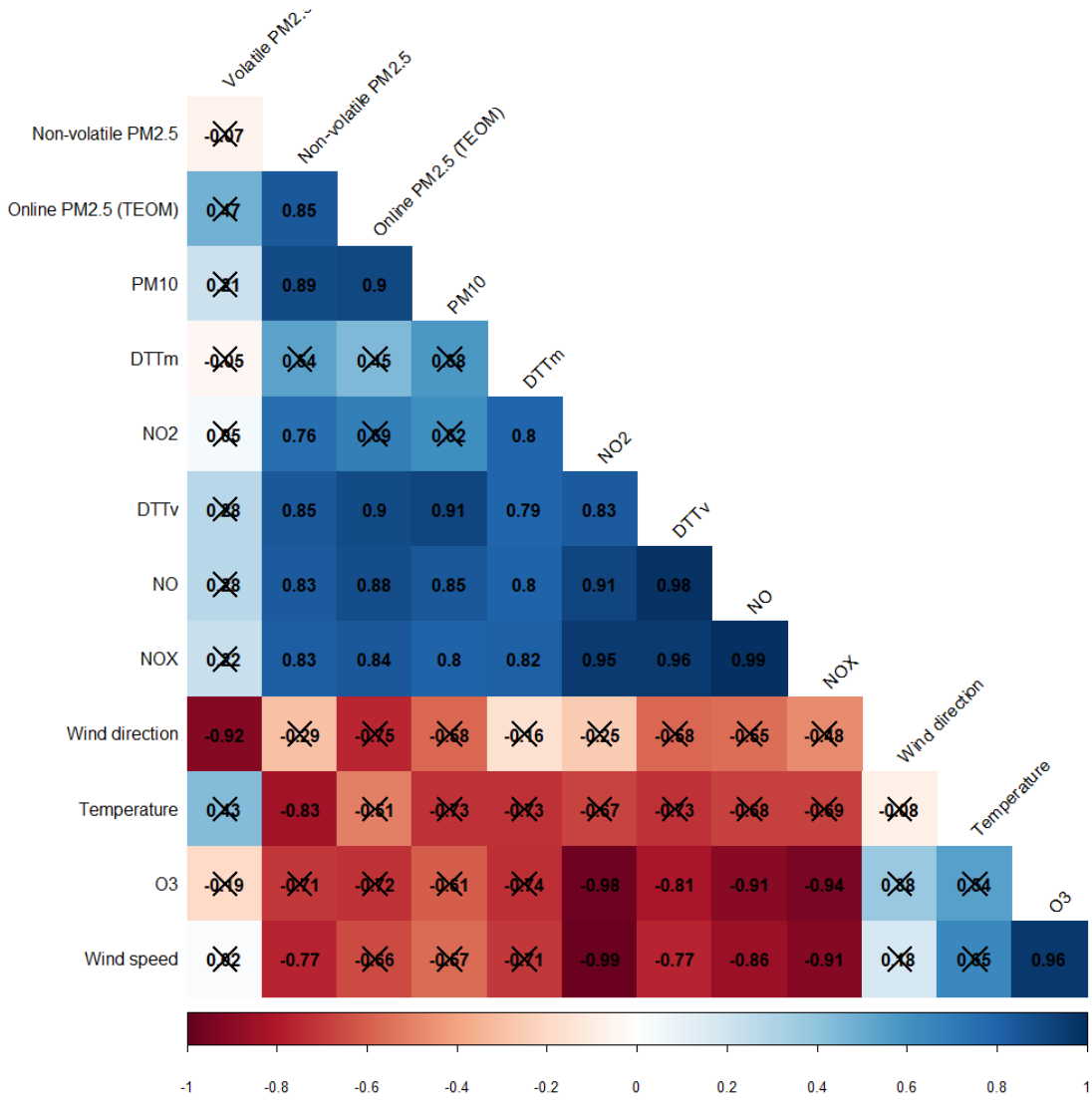

Figure 6-42: Correlation matrix for filters collected during the Birmingham winter sampling. The data was obtained from the A4350 roadside and Ladywood monitoring sites. The tolerance value was set at p <0.05, number of observations = 7.

6.5 Correlation analysis of the Delhi campaigns

6.5.1 Winter campaign

DTTm during the Delhi winter campaign is well correlated with the concentrations of a broad range of metals, with r numbers ranging from 0.6 – 0.77. Species assigned to non-exhaust vehicle emissions (Ba, Sr, Ca, and Fe) and biomass (K) burning by Rai et al., 2021 are well correlated with DTTm, having high gradients relative to other species, specifically 27.9 ± 5.5 $DTTm^{Sr}$ and 1.95 ± 0.37 $DTTm^{potassium}$.

Some species were measured using multiple techniques such as ion chromatography (IC), ICP-MS, and XRF. During this campaign calcium, potassium, and magnesium showed a significant correlation with DTTm when detected using IC and ICP-MS. However, the IC derived measurements all had a stronger correlation than ICP-MS as seen in Figure 6-43 and up to a four times larger gradient (1.02 ± 0.18 $DTTm^{Mg}$ and 4.15 ± 0.64 $DTTm^{magnesium}$). This is despite both detection methods showing similar concentrations of magnesium (0.497 ± 0.14 and 0.818 ± 0.69 μg m^{-3} for IC and ICP-MS, respectively).

Many of the strongly correlated ($r \geq 0.6$) species during this campaign are characteristic of suspended road dust / construction (calcium r = 0.74, strontium r = 0.65, and barium r = 0.60) and brake wear (iron r = 0.68). Magnesium (r = 0.72) can have several different sources including dust from soil erosion, industrial sources, construction, and resuspension by traffic (W. J. Liu et al., 2018b; J. Wang et al., 2018).

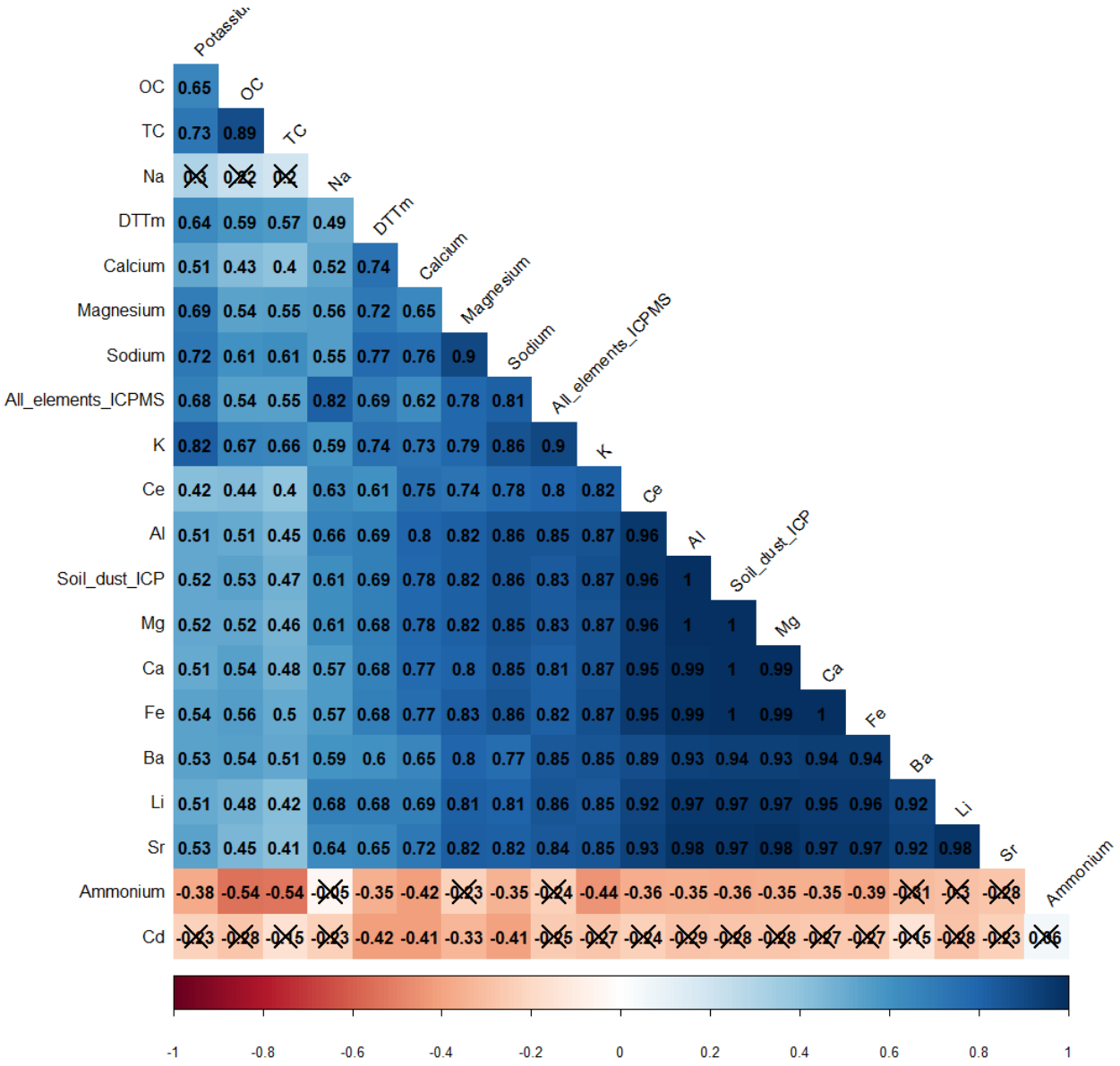

Figure 6-43: Pearson correlation matrix of DTTm and mass-normalised PM2.5 composition species for the Delhi winter campaign. All species with a p-value > 0.05 and/or r ≤ 0.5 has been excluded (except for anti-correlated species), as well as the XRF analysed metals due to an incomplete dataset. Crossed out boxes represent p > 0.05.

6.5.1.1 Positive matrix factorisation Aerosol Mass Spectrometry (AMS) data for Delhi winter campaign

AMS data was collected during the winter campaign near to the IIT site at Lodhi road. However, the AMS data collection period only overlapped with that of nine of the PM filters used here, so it was not included in the above correlation analysis. For all nine filters the only significant correlation with DTTm was cooking-emission related organic aerosol (COA)

which had a significant negative correlation (r = -0.8), the other SOA tracers: traffic-related hydrocarbon-like organic aerosol (HOA), low-volatility oxygenated organic aerosol (LVOOA), biomass burning organic aerosol (BBOA), and oxidised primary organic aerosol (OPOA) were all also negatively correlated but with a p-number >0.05. Due to the small dataset, the AMS data could not be split diurnally. The AMS data is for non-refractory PM_1 rather than the $PM_{2.5}$ measured during the DTT assay (Palm et al., 2018; J. Xu et al., 2014).

6.5.1.2 Metals analysed using XRF

Metal species during this campaign were analysed using XRF along with ICP-MS, due to the lower number of observations for the XRF data these were excluded from the correlation matrix analysis, as the matrix requires the same number of observations for all species. The correlation and gradient results for the XRF metals with DTTm are shown in Table 6-146. The sources for these species are expected to be primarily crustal material and road dust (Al, Si, K, Ca, Ti, and Fe), non-exhaust vehicle emissions (Ni), and biomass burning (K). This is in line with the correlations seen in Figure 6-43 (W. J. Liu et al., 2018b; Rai, Slowik, Furger, Haddad, et al., 2021).

Table 6-146: Highly correlated XRF detected metal species with DTTm from the Delhi winter campaign. All species with a p-value > 0.05 and/or $r_p \leq 0.5$ have been excluded. The gradients are shown with the standard error; the units are pmol DTT min^{-1} ng^{-1} of each metal specie.

Specie	r	p-value	n	Gradient
Soil dust	0.78	<0.01	12	0.145 ± 0.036
Al	0.67	0.02	12	1.38 ± 0.48
Si	0.79	<0.01	12	0.908 ± 0.22
K	0.58	0.05	12	0.795 ± 0.35
Ca	0.84	<0.01	12	1.54 ± 0.32
Ti	0.85	<0.01	10	30.6 ± 6.6
Fe	0.74	<0.01	12	1.58 ± 0.46
Ni	0.87	<0.01	9	148 ± 32

6.5.2 Summer campaign

The Delhi summer campaign has the least number of strong correlations ($r \geq 0.6$) of PM components with DTTm values out of any campaign, with the correlation coefficients for most species whose concentrations are significantly correlated with DTTm being below r = 0.60. While organic carbon and potassium are significantly correlated with DTTm during this campaign (r = 0.59 and 0.66), both show generally lower gradients (0.0524 ± 0.012 $DTTm^{OC}$ and 0.747 ± 0.17 $DTTm^{potassium}$) than seen in the winter (0.0803 ± 0.018 $DTTm^{OC}$ and 1.95 ± 0.37 $DTTm^{potassium}$) and autumn (0.153 ± 0.023 $DTTm^{OC}$ and 0.867 ± 0.28 $DTTm^{potassium}$) campaigns. These lower gradients likely mean that biomass burning has less of an impact during the summer campaign than during the other Delhi campaigns.

IC detected sodium correlates well with DTTm during this campaign at r = 0.60. Sodium is often associated with sea / road salt, however, a high correlation with potassium (r = 0.81) suggests that they have the same anthropogenic source. Notably, sodium detected by ICP-MS shows a negative correlation with all species in the correlation matrix in Figure 6-44.

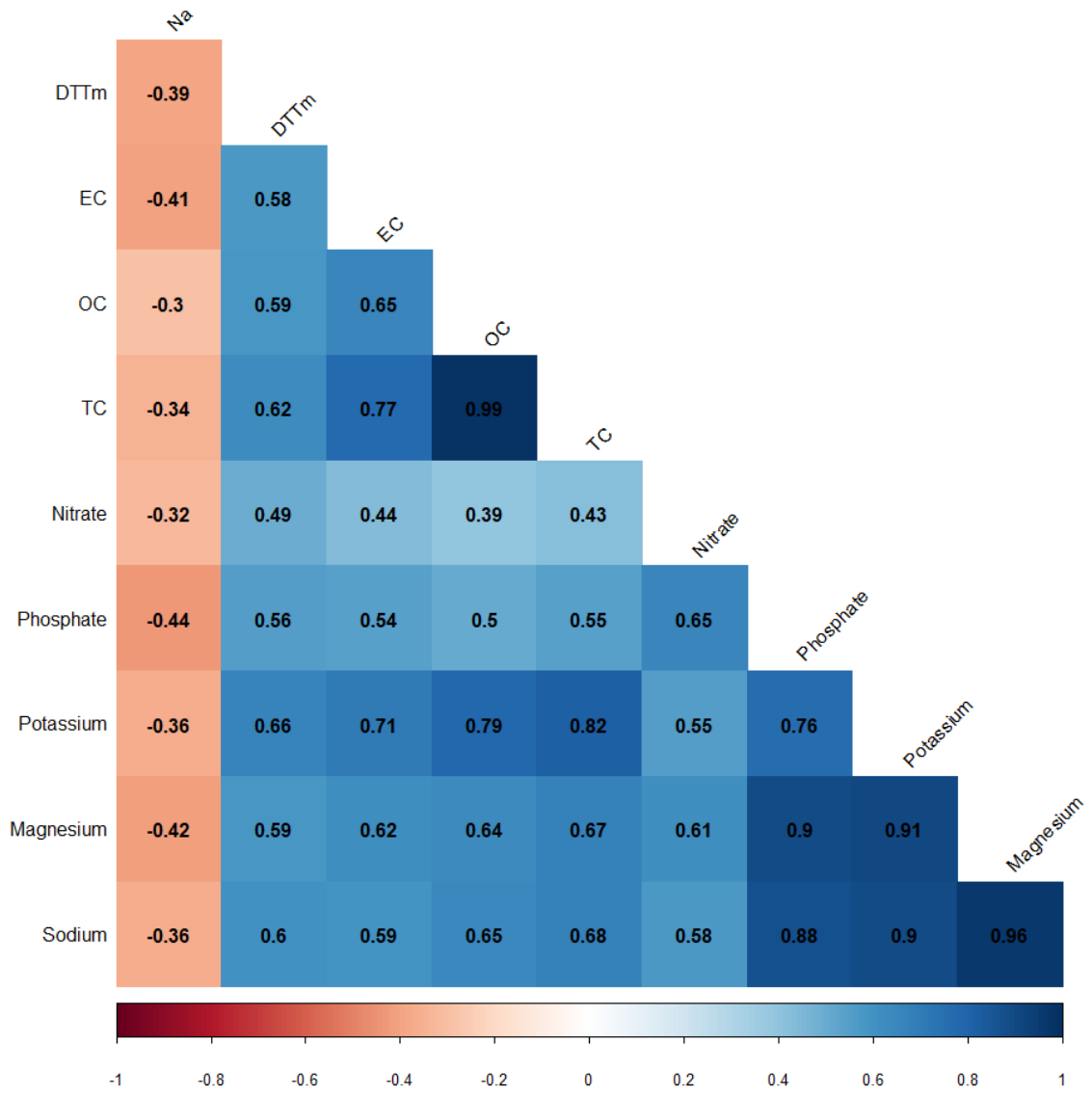

Figure 6-44: Pearson correlation matrix of DTTm and mass-normalised $PM_{2.5}$ composition species for the Delhi summer campaign. All species with a p-value > 0.05 and/or r ≤ 0.5 has been excluded (except for Na and nitrate), n = 63.

As with the winter campaign, there are gaps in the data obtained by XRF so this data was analysed separately and is shown in Table 6-7. Similar to the correlation analysis of the other species, these metal species show considerably weaker correlations with DTTm for the Delhi summer data, compared to the other campaigns. However, correlations of DTTm to species associated with crustal materials / road dust and biomass burning are strongly correlated with high gradients, similar to the correlations from the winter campaign.

Interestingly this is the only campaign during this study that shows a significantly positive correlation of DTTm with copper, which DTT has been shown to be sensitive to in previous studies (Charrier et al., 2015; J. Wang et al., 2018). In Delhi Cu is mostly associated with industrial emissions and coal / waste burning, however, copper is the only species from this source to be significantly correlated with DTTm and therefore the influence of these sources is likely not that significant upon the toxicity of PM as measured by the DTT assay (Rai, Slowik, Furger, Haddad, et al., 2021).

Table 6-75: Highly correlated XRF detected metal species with DTTm from the Delhi summer campaign. All species with a p-value > 0.05 and/or $r_p \leq 0.5$ have been excluded. The gradients are shown with the standard error; the units are pmol DTT min^{-1} ng^{-1} of each metal. All elements refers to the collation of all XRF metals and soil dust is the combination of metal oxides.

Specie	r	p-value	n	Gradient
All elements	0.62	<0.01	25	0.406 ± 0.11
Soil dust	0.51	<0.01	25	0.0496 ± 0.018
Na	0.59	<0.01	22	1.23 ± 0.38
Al	0.57	<0.01	25	0.572 ± 0.17
Si	0.49	0.01	25	0.253 ± 0.093
P	0.53	<0.01	25	7.24 ± 2.4
S	0.50	0.01	25	0.394 ± 0.14
K	0.63	<0.01	25	0.782 ± 0.20
Ti	0.57	<0.01	25	10.5 ± 3.2
Cr	0.54	0.02	19	53.6 ± 20
Fe	0.59	<0.01	25	1.08 ± 0.31
Ni	0.71	<0.01	14	72.0 ± 21
Cu	0.52	<0.01	25	15.4 ± 5.3
W	0.64	<0.01	25	18.6 ± 4.6

6.5.3 Autumn campaign

The Delhi autumn campaign is characterised by high correlations between metal species and DTTm values, with most having an r value above 0.8 (apart from potassium, sodium, and nickel), as shown in Figure 6-45. These are much stronger correlations than is observed in the other campaigns which generally have r numbers in the range of 0.5 – 0.7. In terms of the species that are well correlation with intrinsic toxicity the Beijing and Delhi winter campaigns are most similar to this one, with all having significant correlations with calcium, iron, sodium, and strontium.

The Delhi autumn campaign is the only campaign for which DTTm showed a significant correlation with vanadium (Beijing winter had a correlation at $r < 0.6$). The correlation was very strong at $r = 0.90$ with the second highest gradient at 306 ± 28 $DTTm^{V}$. Higher levels of vanadium and nickel ($r = 0.77$, 255 ± 39 $DTTm^{Ni}$) are normally associated with residual oil or coal combustion, which Liu et al., 2018 assigned to shipping activities. However, in Delhi it is more likely associated with residential heating (Das et al., 2015; Duan & Tan, 2013).

The positive response to calcium ($r = 0.9$ for IC and 0.86 for ICP-MS), titanium ($r = 0.85$, however detection limit may be an issue here), strontium ($r = 0.87$), and iron ($r = 0.89$) indicate a strong source from crustal materials, road dust, and construction. Iron is also released from brake wear, adding to the non-exhaust vehicle emissions. Rai et al., (2021) reported that these four elements along with silicon were indicators of crustal materials and road dust, in Delhi during the winter of 2019. Manganese ($r = 0.89$) and nickel may be indicators of brake wear from vehicles, however nickel has multiple sources and could equally be from industrial emissions or oil burning.

The highest observed gradient for this campaign was for cerium at 344 ± 41 $DTTm^{Ce}$ (r = 0.85). The most likely source for cerium in Delhi is from vehicle exhaust, as the substrate in catalytic converters are covered by either aluminium oxide or cerium oxide and will wear off with time. This may also explain the strong correlation seen for aluminium (r = 0.89), however, construction and crustal materials are also a significant source of aluminium (Jain et al., 2020; Seigneur, 2019).

Magnesium detected both by IC and ICP-MS showed a strong correlation at r = 0.88 each. The IC detected magnesium did have a higher gradient at 2.11 ± 0.21 $DTTm^{Mg}$ compared to 1.48 ± 0.16 $DTTm^{Mg}$ for ICP-MS. The source for magnesium is crustal origin, either from soil or road dust (Jain et al., 2020). Jain et al., 2020 assigned the source for sodium as sodium and magnesium salt source, as Delhi is far enough from the sea to make a marine source unlikely. The source for these salts can be diverse including sea salt, rivers / other waterways, and soil / road dust. Interestingly, sodium detected by ICP-MS had a considerably weaker correlation than for IC, at r = 0.54 compared to 0.83 for IC. However, the gradients were similar at 1.73 ± 0.50 and 1.67 ± 0.21 $DTTm^{Na}$, respectively.

Potassium, a marker for biomass burning shows a weaker correlation than seen in species with a crustal origin. The relationship between DTTm and concentrations of potassium also has a lower gradient than many of the other road dust / construction species at 0.994 ± 0.23 (r = 0.64) and 0.867 ± 0.28 (r = 0.51) $DTTm^{K}$, for ICP-MS and IC detection respectively. This suggests that although biomass burning contributes significantly to $PM_{2.5}$ mass during the post-monsoon and winter periods in Delhi, it does not contribute to the oxidative potential of $PM_{2.5}$ as much as other sources (Jain et al., 2020; Rai, Slowik, Furger, Haddad, et al., 2021).

Interestingly, in the Rai et al., 2021 study where elements were assigned source groups based on their enrichment factor and $PM_{2.5}$ / PM_{10} ratio, none of the elements in the primary emission group are significantly correlated with intrinsic toxicity during this campaign. This implies that primary particle emissions have less of an impact on the toxicity in this campaign. This may explain the sharp drops in DTTm observed during extremely heavily polluted days (in the order of 200-350 µg m^{-3}) as primary emissions would dominate on these days. This would be particularly true for Diwali as the roads were closed off, limiting road dust resuspension. Therefore, most of the $PM_{2.5}$ would derive from fireworks, kerosene lamps, and residential heating (the most common fuel types for heating in Delhi are wood, crop residue, dung cakes, and coal). This group is also associated with industrial and coal / waste burning so these are less likely to be influencing DTTm as much as other sources. All species that are associated with the primary emission group (Cu, As, Zn, Sn, Pb, and Cl) presented by Rai , et al., 2021 show insignificant correlations with DTTm (Mondal et al., 2021).

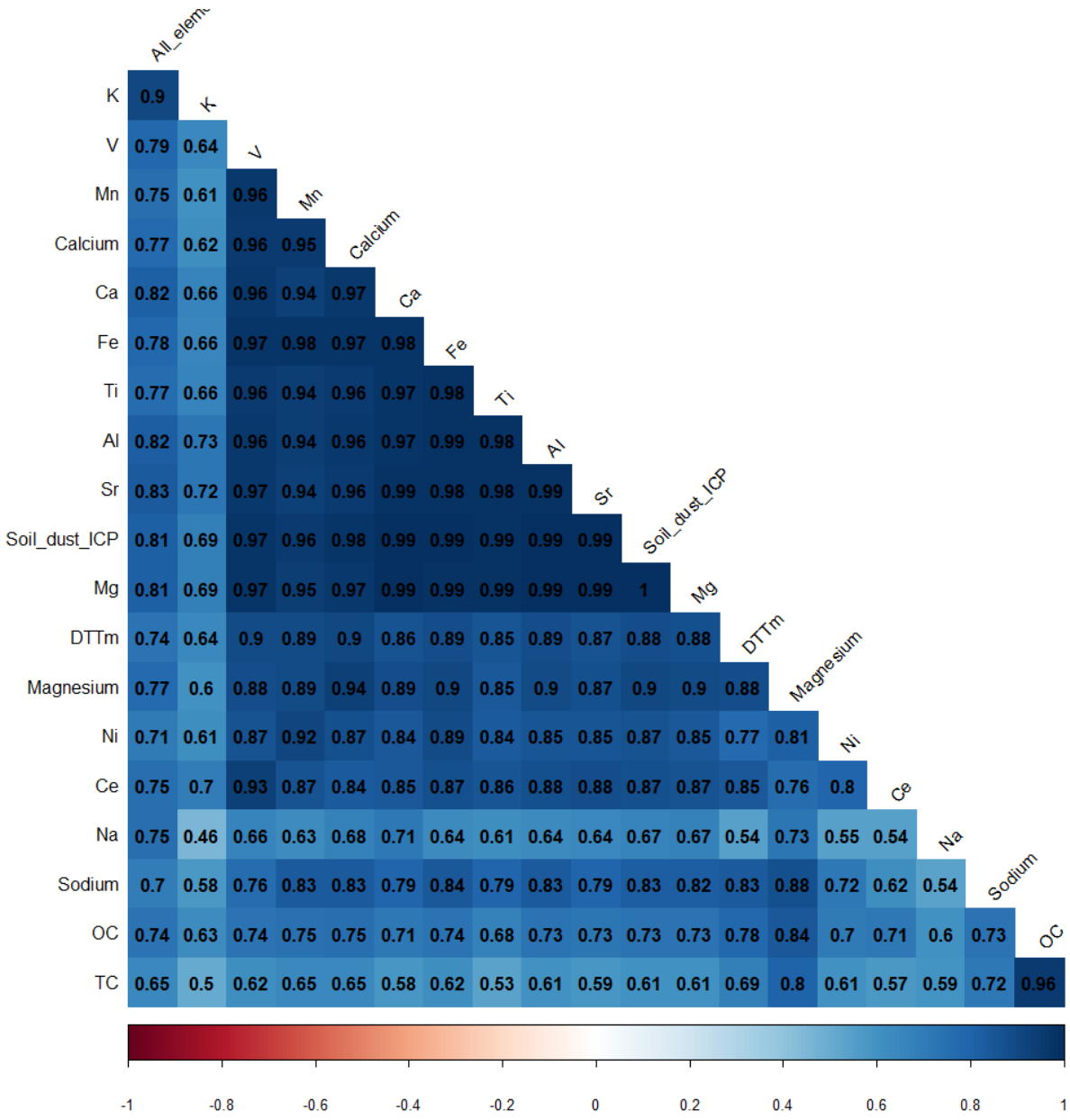

Figure 6-45: Pearson correlation matrix of DTTm and mass-normalised $PM_{2.5}$ composition species for the Delhi autumn campaign. All species with a p-value > 0.05 and/or r ≤ 0.5 has been excluded (n = 30). Potassium and ammonium are not in the figure due to having 29 and 28 observations, respectively. Potassium: r = 0.51 and ammonium: r = -0.62 both at p < 0.01.

6.5.4 Multiple linear regression analysis on select elements for different sources in Delhi

Due to the lack of source apportionment results for the Delhi campaigns at the time of writing, species were chosen to represent (approximate) the different source groups expected, as outlined in Rai et al., 2021. These groups are based on $PM_{2.5}$ / PM_{10} ratios and

titanium derived PM_{10} enrichment factors, various species were assigned to different sources in Delhi. The species chosen to represent these groups were:

- Strontium for crustal materials and road dust
- Nickel for non-exhaust traffic emissions
- Potassium for biomass combustion
- Chlorine or tin for industrial emissions

No sources for the mixed industrial / traffic emissions group were shown in Rai et al., 2021. There were no data available for nickel (non-exhaust traffic emissions) for the Delhi winter campaign, so iron was chosen for this category / campaign, as there is some overlap between road dust and non-exhaust emissions for this element. For the winter campaign potassium and iron accounted for 51 % of the variance in DTTm (DTTm = 16.2 + 936 * K^+ + 329 * Fe, units = pmol DTT min^{-1} μg^{-1} $PM_{2.5}$). This shows that road dust / brake wear and biomass burning are a large influence on intrinsic toxicity during the winter campaign in Delhi.

For the Delhi summer campaign potassium, iron, and strontium account for 53 % of variance, with strontium having an inverse relationship with intrinsic toxicity (DTTm = 13.7 + 768 * K^+ + 115 * Fe + -18542 Sr). As with the winter campaign, biomass burning appears to contribute significantly more to DTTm than non-exhaust traffic emissions.

The Delhi autumn campaign shows significant results for iron alone, accounting for 78 % of the variance (DTTm = 28.3 + 622 * Fe). This suggests that DTTm of PM from this campaign is dominated by non-exhaust traffic emissions / road dust. However, there is diurnal variability during this campaign, with the day showing strontium being significant, accounting for 86 %

of variance alone (DTTm = 30.1 + 65535 * Sr) and the night showing iron accounting for 80 % of variance (DTTm = 24.0 + 1169 * Fe).

As biomass burning is the dominant source of $PM_{2.5}$ during the autumn campaign this increased contribution from biomass burning to $PM_{2.5}$ may explain why DTTm decreases with increasing $PM_{2.5}$ concentration faster than is the case in any other campaign. This would reduce the overall share of crustal material / road dust in the $PM_{2.5}$ (Jain et al., 2020; Rai, Slowik, Furger, Haddad, et al., 2021).

6.6 Diurnal correlation analysis for Delhi campaigns

6.6.1 Delhi winter diurnal variation

Samples collected during the nights during the Delhi winter campaign shows higher concentrations of $PM_{2.5}$ than during the day (also apparent in the autumn), likely due to the lower boundary layer, limiting mixing and dilution, while emissions continue. However, the intrinsic toxicity is significantly lower at night / higher during the day (Figure 6-31). This causes the night-time samples to show similar DTTv values to the day (5.88 ± 1.8 and 5.36 ± 1.0 nmol DTT min^{-1} m^{-3}) even though the $PM_{2.5}$ concentration is significantly higher at night (201 ± 59 and 134 ± 38 µg m^{-3}). This lower DTTm at night is likely due to the weak contribution of species to DTTm during the night, with all correlations apart from lithium (r = 0.62) being insignificant (r = < 0.6). Figure 6-46 shows the correlation matrix for the daytime-only winter campaign filters. Compared with the correlations assessed for the complete dataset (day and night) potassium has a higher correlation during the day, with the correlation for ICP-MS-derived potassium only being significant during the day (r = 0.86, 0.43 at night) and the r-number for IC potassium increasing from 0.74 for the combined dataset to 0.82 for the daytime samples. This implies a possible increased contribution from

solid fuel burning of coal and wood to DTTm during the day, although for both potassium forms the concentration is higher at night than during the day (2.06 and 3.68 μg m^{-3} during the day for IC and ICP-MS respectively; 2.83 and 3.94 μg m^{-3} for the night).

Broadly the other species that correlated well in the overall winter analysis are the same as during the day with only sodium (r = 0.74 and 0.49 for IC and ICP-MS increasing to 0.82 and 0.57) and calcium (ICP-MS increasing from 0.72 to 0.84 but IC remaining the same) increasing their correlations.

Many species have overlapping gradients within uncertainty during the day and night, however, the nights generally show weak correlations, limiting the usefulness of direct comparisons. Some vehicle / road dust markers do show higher gradients at night than during the day such as iron (night: 2.07 ± 0.89 $DTTm^{Fe}$ and r = 0.50, day: 0.372 ± 0.094 $DTTm^{Fe}$ and r = 0.68), strontium (94.6 ± 40 $DTTm^{Sr}$ and r = 0.51, 20.1 ± 6.2 and r = 0.61), and magnesium (4.27 ± 1.9 $DTTm^{Mg}$ and r = 0.49, 0.863 ± 0.22 and r = 0.68). However, the uncertainties are larger at night with weaker correlations but still implying an increased contribution of certain species to DTTm at night.

The reason for lower DTTm at night may rather be factors that are reducing intrinsic toxicity such as relative humidity and organic aerosols (OA). Relative humidity can reduce PM OP through condensation onto atmospheric particles, increasing particle size and reducing the relative impact of more reactive species. W. Xu et al., 2015 also reported that higher relative humidity increasing uptake of SO_2 onto particle surfaces, decreasing DTT activity through consumption of oxidative active sites. Three OA and relative humidity were negatively correlated with DTTm during the winter nights as shown in Table S1 (in the appendices). These were hydrocarbon-like OA (HOA), biomass burning OA (BBOA), and cooking OA (COA).

Zhang et al., 2005 reported that the spectra for HOA was very similar to that of directly sampled vehicle exhaust, showing diurnal variation with a peak during morning rush hour before decreasing with the rising boundary layer. As OA often accounts for a significant proportion of PM mass, the relatively high negative gradients of these OA species with DTTm values could account for the substantially lower DTTm observed during high pollution events, which sometimes reduce the OP of the air mass to below that of cleaner days (Bressi et al., 2016; W. Xu et al., 2015; Q. Zhang et al., 2005).

DTTm values in samples collected during both the day and night showed a negative correlation with relative humidity (-0.442 ± 0.089 and -0.366 ± 0.16 $DTTm^{RH}$, day and night, respectively) and positive correlation with temperature (2.45 ± 0.63 and 1.99 ± 0.92 $DTTm^{T}$). This is likely due to this combination facilitating the resuspension of crustal material / road dust, which has been shown to contribute to DTT activity during this campaign. The range of relative humidity values during this campaign were 48.4 – 92.0 % and temperature was 10.8 – 20.0 °C. Therefore the influence of relative humidity (9.97 – 48.9 pmol DTT min^{-1} μg $PM_{2.5}$) and temperature (11.6 – 61.6 pmol DTT min^{-1} μg $PM_{2.5}$) on DTTm could be substantial during the winter in Delhi based on the gradients and dynamic range (Altuwayjiri et al., 2021; Yang et al., 2021).

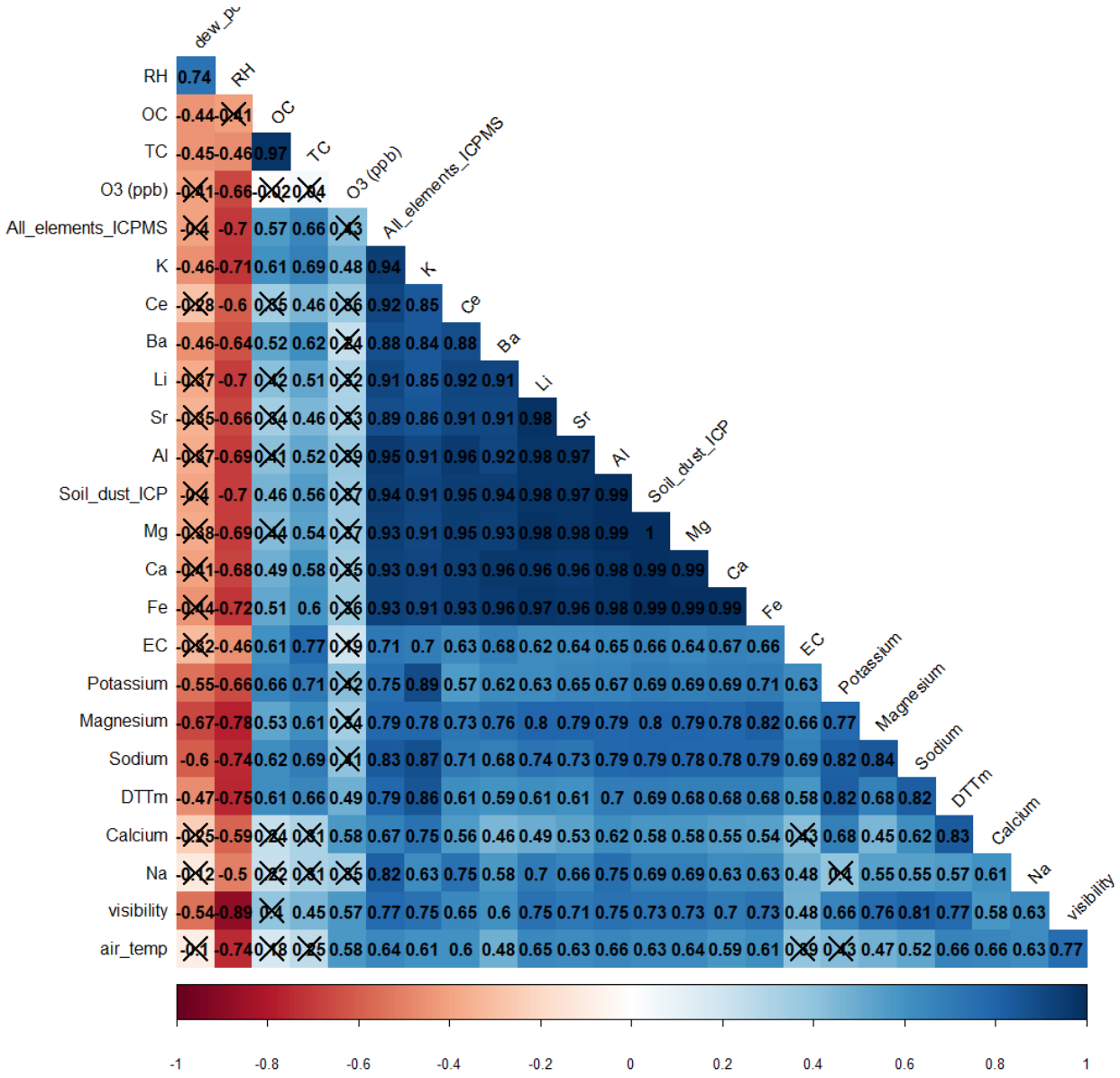

Figure 6-46: Pearson correlation matrix of DTTm and mass-normalised PM2.5 composition species for the Delhi winter daytime samples. All species with a p-value > 0.05 and/or r ≤ 0.5 has been excluded (n = 21). Elements that are listed by name and symbol were measured using both IC and ICP-MS, with the name showing the IC result and the symbol showing the ICP-MS result.

6.6.2 Delhi summer diurnal variation

The Delhi summer campaign showed the least amount of diurnal variation, with $PM_{2.5}$ concentration, DTTm, and DTTv not varying significantly as shown in, Figure S-2, Figure 6-31, and Figure S-1 (Figures denoted with an S are in the appendices), respectively. Most compositional species also show little diurnal variation during this campaign, with some species showing higher correlations at night but higher gradients during the day such as

tungsten: 27.1 ± 9.4 $DTTm^{W}$ and r = 0.64 during the day, 14.0 ± 3.0 $DTTm^{W}$ and r = 0.84 at night.

6.6.3 Delhi autumn diurnal variation

The Delhi autumn campaign, like the winter, has significantly higher DTTm during the day than at night. However, unlike during the winter, samples collected during the nights during the autumn show a large number of species that are well correlated with DTTm (Figure 6-48). Surprisingly the species associated with non-exhaust vehicle emission, crustal material, and road dust (Al, Ca, Ce, Fe, Mn, Sr, and Ti) all have higher gradients during the night than during the day as seen in tables Table S2 and Table S3 (in the appendices).

The gradient for vanadium shows diurnal variation, being higher at night compared to the day (night: 458 ± 79, day: 287 ± 32 $DTTm^{V}$). This is most likely due to the increased presence of heavy goods vehicles during the night in Delhi. Vanadium is often associated with fossil fuel combustion such as coal or oil (Das et al., 2015; Duan & Tan, 2013).

The influence of biomass burning during the autumn campaign appears to be diurnal. Potassium and BBOA are only significantly correlated with DTTm during the day. Potassium has significantly higher correlation coefficient with higher gradients during the day than seen in the combined data, with IC potassium being 1.56 ± 0.21 $DTTm^{K}$ and r = 0.91 (combined dataset: 0.867 ± 0.28 and r = 0.51, night: 0.320 ± 0.35 and r = 0.24), and ICP-MS potassium being 1.38 ± 0.14 $DTTm^{K}$ and r = 0.94 (0.994 ± 0.23 and r = 0.64, 0.419 ± 0.34 and r = 0.31).

BBOA along with several other OA (HOA, OPOA, and LVOOA) were significantly negatively correlated with DTTm during the autumn days, these are shown in Table S2 (in the appendices). BBOA showed a larger negative gradient during this campaign than during the

Delhi winter night at -2.78 ± 0.96 $DTTm^{BBOA}$ compared to -1.30 ± 0.46 $DTTm^{BBOA}$. This is consistent with the source-dependent MLR analysis reported in section 6.5.4, as DTTm during the autumn campaign is almost entirely driven by non-exhaust vehicle emissions (with iron accounting for 78 % of the variance) with no significant contribution from biomass burning. Other significant OA during the daytime were HOA, less-oxidised OA (LVOOA), and oxidised primary OA (OPOA) which was also negatively correlated during the night (Jingsha Xu et al., 2020).

The only other species and meteorological parameters that are significantly positively correlated with DTTm during the days are barium, wind speed, chloride, and elemental carbon as seen in Figure 6-47. Barium appears to have the most impact of the various elements with a gradient of 23.9 ± 3.9 $DTTm^{Ba}$, r = 0.87. Barium is present in diesel and petrol, being a valuable tracer for vehicle emissions. However, it is unusual that lead was not significant as this is a more common tracer for this source, dependent on fuel type. Wind speed impacts the transportation of air pollutants, during this campaign the wind speed was generally low (0.5 – 3.3 m/s). This positive correlation may indicate the importance of local transport of pollutants around Delhi or from the surrounding provinces to DTTm. Elemental carbon could be attributable to coal combustion, vehicular emission, or biomass burning. Elemental carbon concentrations are higher during the night (night: 18.7 ± 5.1, day: 11.2 ± 2.8 μg m^{-3}) when heavy goods vehicles are more common in Delhi. Gunthe et al., 2021 reported that the most likely source of chloride in the Delhi region is plastic-contained waste burning and other industry (A. Chen et al., 2001; Bhaskar & Mehta, 2010; Gunthe et al., 2021; R. Li et al., 2019; Monaci & Bargagli, 1996).

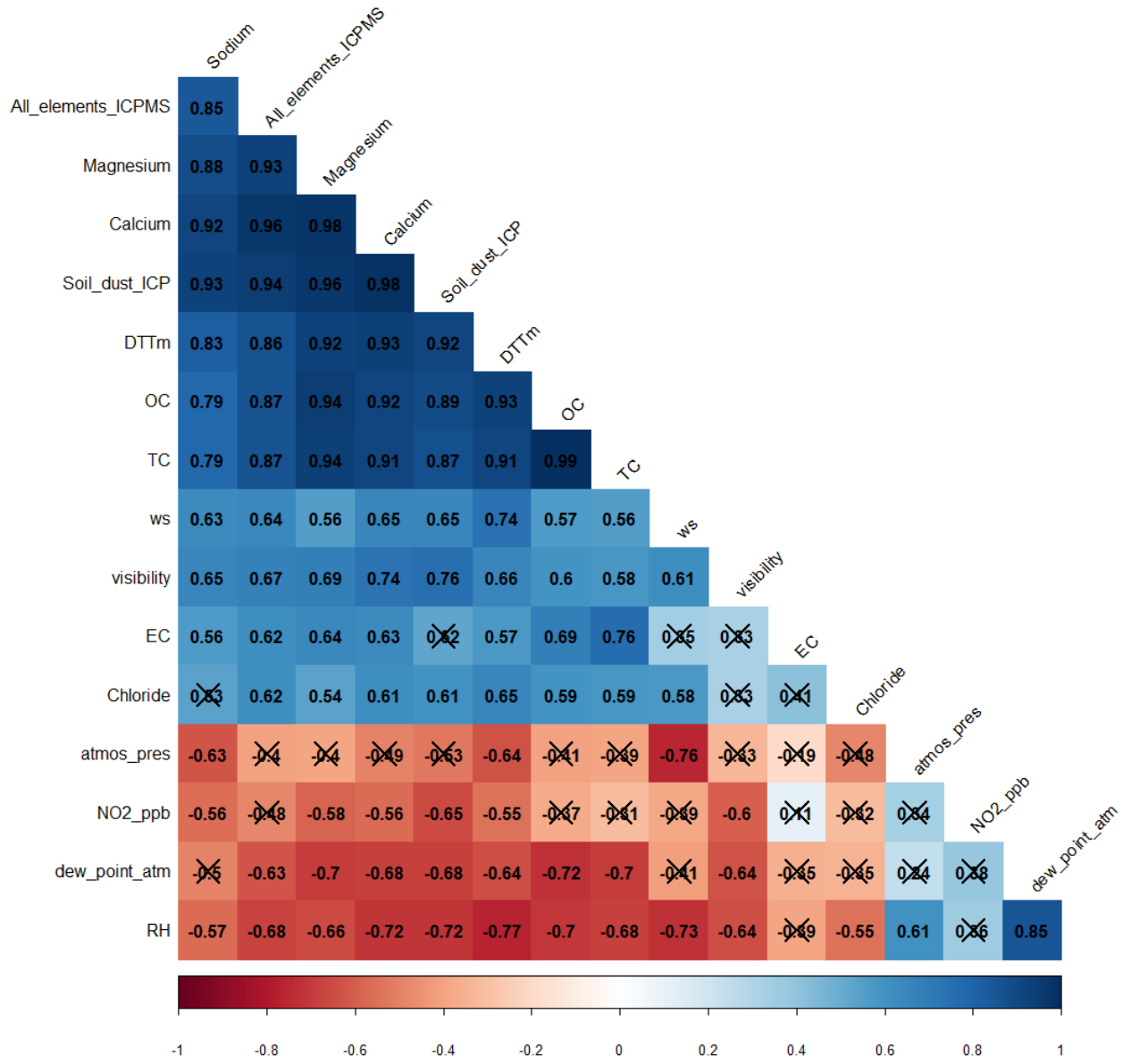

Figure 6-47: Pearson correlation matrix of DTTm and mass-normalised $PM_{2.5}$ species for the Delhi autumn daytime samples. All species with a p-value > 0.05 and/or r ≤ 0.5 has been excluded. As well as ICP-MS metal species for clarity, these species were: Na, Mg, Al, K, Ca, Ti, V, Mn, Fe, Ni, Sr, Ba, and Ce. Number of observations = 14.

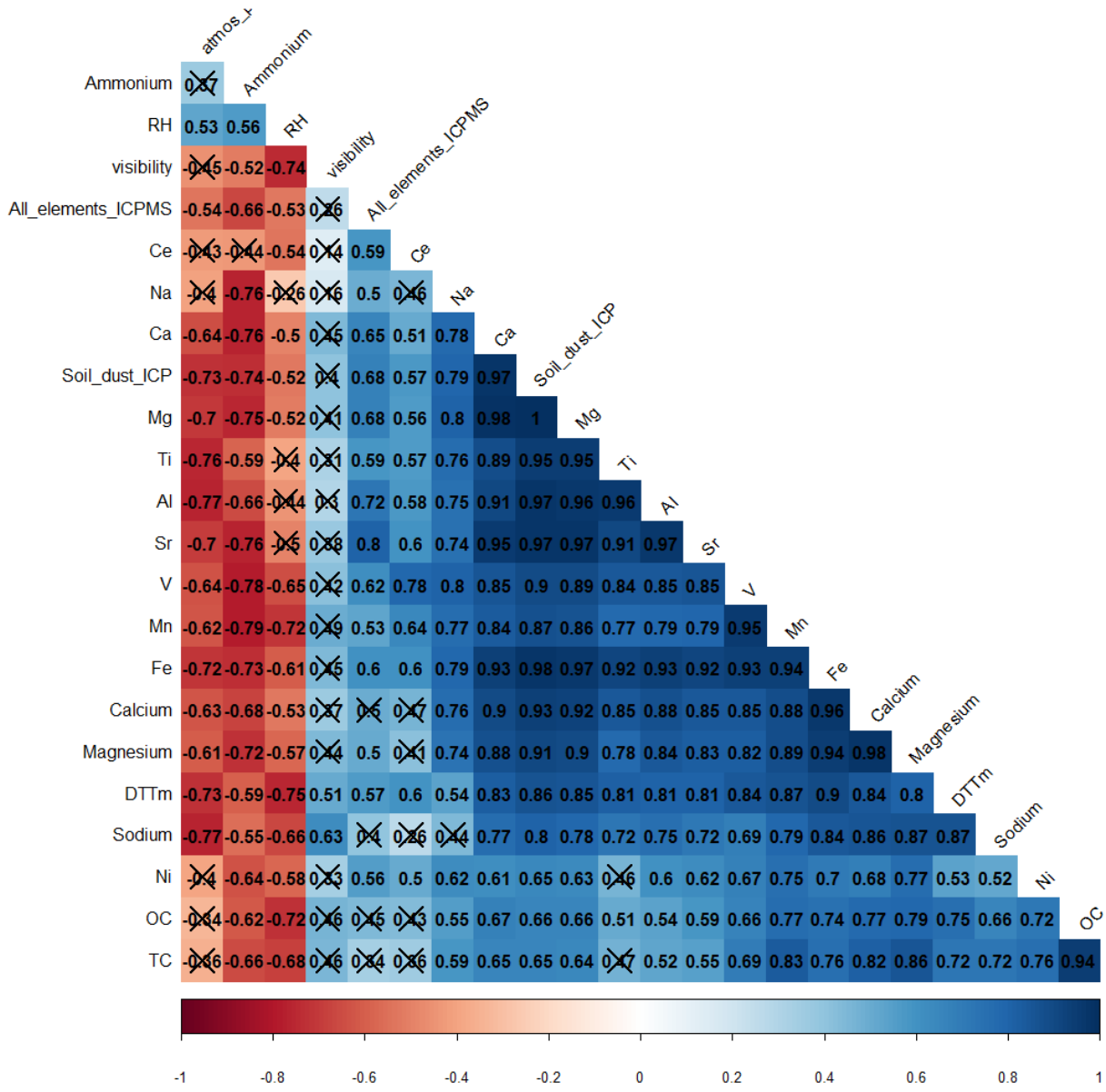

Figure 6-48: Pearson correlation matrix of DTTm and mass-normalised $PM_{2.5}$ species for the Delhi autumn night samples. All species with a p-value > 0.05 and/or r ≤ 0.5 has been excluded. oPOA was also excluded for having 15 observations (r = -0.60, p = 0.02). Number of observations = 16.

6.7 Compositional and meteorological impacts on OP^{DTT} from all campaigns combined

As discussed in the previous sections, the species which correlate well with intrinsic toxicity varies quite considerably between different seasons, locations, and diurnally. To investigate whether any species correlate strongly with DTTm when all data are combined a pairwise correlation analysis using the complete observations datasets was used. Only species that

were present in at least three campaigns were analysed. As the correlations were weaker than for the individual campaigns, all species with $r \leq 0.4$ were excluded, the results are shown in Table 6-8.

The only species with a significant correlation as defined in previous sections was organic carbon. This is not surprising as organic carbon was the only species to be significantly correlated with DTTm during every field campaign (excluding Birmingham where it was not measured). All of these campaigns showed a moderate correlation of $r = 0.59 – 0.68$, however during the Delhi autumn campaign the correlation was strong at $r = 0.78$. This campaign also had a considerably higher gradient than the other campaigns at 0.153 ± 0.023 $DTTm^{OC}$, likely due to the large amount of biomass burning and residential heating. The second highest gradient was the Beijing winter campaign at 0.108 ± 0.021 $DTTm^{OC}$ which was likely due to coal combustion, however, $DTTm^{OC}$ during this campaign was within the uncertainty of the Beijing summer and Delhi winter campaigns. The Delhi summer showed far lower organic carbon toxicity than any other campaign at 0.0524 ± 0.012 $DTTm^{OC}$. Organic carbon only showed diurnal variability during the Delhi winter, where it was only significantly correlated with DTTm during daytime.

The other species in Table 6-8 only show a weak to moderate correlation with intrinsic toxicity. Potassium is generally a marker for biomass burning. The weak correlation is likely due to potassium only being significantly correlated during the Delhi campaigns. Calcium, magnesium, and sodium are most associated with crustal materials, soil / road dust, and construction activity. Rivers and other waterways are also a possible source for sodium, however, this is unlikely in this case as sodium was also significantly correlated during the

Beijing winter campaign, a city without major waterways (Jain et al., 2020; Liu et al., 2018; Rai et al., 2021; J. Wang et al., 2018).

Table 6-86: Highly correlated species with DTTm from the combined data for all campaigns. All species with a p-value > 0.05 and/or $r_p \leq 0.4$ have been excluded. Only species with data for at least four campaigns were included. The gradients are shown with the standard error; the units are pmol DTT min^{-1} ng^{-1} of each specie. No Mg^{2+} data was available for the Beijing winter campaign.

Specie	r	p-value	n	Gradient ($DTTm^{species}$)
Na	0.45	<0.01	200	0.582 ± 0.082
Mg^{2+}	0.48	<0.01	167	0.545 ± 0.078
K^+	0.43	<0.01	201	0.419 ± 0.063
Ca^{2+}	0.43	<0.01	199	0.214 ± 0.032
OC	0.59	<0.01	202	0.0591 ± 0.0057

6.8 Conclusion

This study has showed that $PM_{2.5}$ concentrations show significant variation across localities, seasons, and diurnally. While at lower concentrations (~ < 100 µg m^{-3}), $PM_{2.5}$ predicted the OP toxicity of the air mass (DTTv) well with an r number of 0.85. At higher concentrations, this correlation breaks down, leading to instances where campaigns with statistically similar $PM_{2.5}$ concentrations have significantly different DTTv, as shown in Table 6-. In some examples where the $PM_{2.5}$ concentration is very high such as during the Delhi autumn campaign, DTTv overlaps within uncertainty between two nights while the $PM_{2.5}$ concentration is almost twice as high (DTTv = 7.87 ± 0.21 and 8.49 ± 0.60 nmol DTT min^{-1} m^{-3}, $PM_{2.5}$ = 166 ± 52 and 397 ± 51 µg m^{-3}). At the same time DTTm varies dramatically, showing that during these extreme events particle composition, instead of mass concentration alone, predicts the oxidative capacity of the air mass. There is also more

DTTm variability within campaigns than between different locations and seasons; this suggests that species the DTT is most sensitive to may not be location or season specific.

All campaigns measured during this project showed significant correlations between vehicle related emissions and DTTm. Crustal materials, re-suspended road dust, and non-exhaust vehicle emissions were significantly correlated with DTTm during the Beijing winter and all Delhi campaigns. Coal combustion emissions also contribute to DTTm during the Beijing winter along with residential heating during the Delhi autumn and direct vehicle emissions during the Beijing summer campaign.

DTTv values during the Delhi winter campaign showed no significant diurnal variation. However, $PM_{2.5}$ concentrations were significantly higher during the night than day. This was most likely due to the significantly higher intrinsic toxicity observed during the day during sampling (41.0 ± 8.1 day and 29.5 ± 9.0 pmol DTT min^{-1} μg^{-1} $PM_{2.5}$ at night, p-value <0.01).

The Delhi summer campaign is the only campaign in this study to show a moderate positive correlation between DTTm and Cu (r = 0.52, gradient = 15.4 ± 5.3 $DTTm^{Cu}$). DTT has been shown in previous studies to be sensitive to Cu. In Delhi it is mostly associated with industrial emissions and coal / waste burning, however, Cu is the only species from this group to be moderately correlated ($r \geq 0.5$) with DTTm. Therefore, it is likely this source does not significantly contribute to PM OP as measured by the DTT assay in this study.

Multiple linear regression analysis on source apportionment results for the combined Beijing campaigns assigned 52 % of the variance to cooking emissions, biomass burning, and other organic carbon sources. MLR analysis was also carried out on various source marker species for the Delhi campaigns. During the winter and summer, roughly 50 % of variance in DTTm was assigned to biomass burning and brake wear.

Biomass burning during the Delhi autumn campaign does not appear to significantly contribute to DTTm. OC and K are significantly positively correlated with DTTm during the autumn campaign (r = 0.78 and 0.64 for OC and K). However, the gradients for these species (0.153 ± 0.023 $DTTm^{OC}$ and 0.994 ± 0.23 $DTTm^{K}$) are much lower than seen for many of the non-vehicle exhaust emissions and crustal materials (i.e. 344 ± 41 $DTTm^{Ce}$ and 72.7 ± 7.8 $DTTm^{Sr}$). The influence of OC and K are also likely diminished by the negative correlation observed for BBOA (-2.78 ± 0.96 $DTTm^{BBOA}$). The MLR analysis performed for the autumn campaign showed that the variance in DTTm is almost entirely explained by non-exhaust vehicle emissions (iron accounts for 78 % of variance in DTTm). Biomass burning is the dominant source of $PM_{2.5}$ during the autumn campaign; therefore, this may explain why DTTm decreases with increasing $PM_{2.5}$ concentration faster in this campaign than the other campaigns. The increased contribution of biomass emissions to $PM_{2.5}$ concentration would reduce the overall share of crustal material / non-exhaust vehicle emissions in the $PM_{2.5}$ (Jain et al., 2020; Rai et al., 2021).

7 CONCLUSIONS AND RECOMMENDATIONS FOR FUTURE WORK

7.1 Conclusions

The aim of this project was to determine the impact of $PM_{2.5}$ concentration on the oxidative potential (OP) of the air mass (DTTv), and the effect of PM chemical composition on the intrinsic OP of $PM_{2.5}$ particles. These factors were investigated through several intensive periods of $PM_{2.5}$ measurement in Birmingham, Beijing, and Delhi. The OP of the $PM_{2.5}$ sampled was determined using a DTT protocol developed during this project to produce accurate results (with a good repeatability) with the equipment and laboratory space available.

Linear regression analysis of DTTv values as a function of $PM_{2.5}$ concentration combined from all campaigns showed that DTTv was well correlated ($r = 0.85$) with $PM_{2.5}$ at lower $PM_{2.5}$ concentrations (~ < 100 μg m^{-3}). However, at higher $PM_{2.5}$ concentrations this relationship breaks down ($r = 0.41$), leading to instances where $PM_{2.5}$ concentrations are significantly different but the DTTv values are similar, for example during two nights in the Delhi autumn campaign the $PM_{2.5}$ concentrations were 166 ± 52 and 397 ± 51 μg m^{-3} with DTTv values of 7.87 ± 0.21 and 8.49 ± 0.60 nmol DTT min^{-1} m^{-3}.

The $PM_{2.5}$ samples collected during the Beijing and Delhi campaigns were also analysed for a broad range of chemical composition species. These were used alongside meteorological and gas-phase data collected during these campaigns to determine which species and PM sources most affected the intrinsic OP of $PM_{2.5}$ particles (DTTm). This was achieved through linear regression and t-test analyses, where the gradients of DTTm and composition species determined the relative impact of these species.

All campaigns showed significant correlations between vehicle related emissions and DTTm. Crustal material, re-suspended road dust, and non-exhaust vehicle emissions were significantly correlated with DTTm during the Beijing winter and all Delhi campaigns. These sources showed the highest gradients during all campaigns, notably Ce (358 ± 34 $DTTm^{Ce}$), Cr (235 ± 43 $DTTm^{Cr}$), Ni (255 ± 39 $DTTm^{Ni}$), and Sr (94.6 ± 40 $DTTm^{Sr}$). Biomass burning emissions were the dominant source of $PM_{2.5}$ during the Delhi autumn campaign, however, the gradients of DTTm with respect to concentration for these species (OC, K, and biomass burning OA) were lower than for other species. This likely explains the lower than expected DTTv values seen during extreme the $PM_{2.5}$ pollution events during this campaign.

7.2 Limitations

This section highlights the key limitations of the analyses performed during this thesis. These are:

- That only one method for determining PM OP was used during this project. Different OP assays are sensitive to different components of $PM_{2.5}$ and as such a multiple assay study would capture more sources contributing to the OP of $PM_{2.5}$. This comparison for the Beijing OP data was carried out in Campbell et al., 2020, where

the DTT data obtained during this project was compared to AA, EPR, and DCFH assays. However, this comparison was not available for the Delhi campaigns.

- A limitation of all of the OP assays in the comparison paper is that as acellular assays they only measure the 'intrinsic' OP of particles, such as redox active metals, quinone, and radicals. Any other biological pathways for oxidative stress are not measured by these assays. There is a version of the DCFH assay using rat alveolar macrophage cells, which is better able to capture these biological processes, however, this was not possible to carry out during this project.
- As the $PM_{2.5}$ sampling during this campaign was offline, many more volatile species are likely to have not been captured and analysed in this project. The offline sampling also limited the ability to determine how OP changes throughout the day and night, however, diurnal variation was analysed.
- Most metal species analysed during this project were total metal concentration (with the exception of some water-soluble metal species for the Beijing winter campaign). This resulted in the sources most commonly associated with these metal species being very broad. Measuring the oxidation states of various metal species would allow for more precise source profiles, which would better aid mitigation efforts.
- Sampling during this project, while diverse in the number of cities and seasons sampled, only occurred at one location per city. Therefore, spatial variability in PM OP within cities is not possible to determine. Further work on this could possibly be added in the future as there was $PM_{2.5}$ sampling at an alternative site for both the Beijing and Delhi campaigns (Indira Gandhi Delhi Technical University for Women and the village of Pinggu, in Delhi and Beijing respectively). Fang et al., 2016

reported that OP can vary substantially between different locations in Atlanta, Georgia.

- The $PM_{2.5}$ concentrations observed during the winter and autumn campaigns in Delhi were so high that it was difficult to find literature values to compare results to. Only studies in the Indo Gangetic Plain in India and Bohai Sea region in China had $PM_{2.5}$ concentration in the range found within Delhi during this project. Similarly to $PM_{2.5}$ concentration, few studies showed DTTv values as high as those obtained during the Delhi campaigns.
- There were significant limitations in the ability to determine which species and meteorological conditions contribute to intrinsic toxicity in samples collected in Birmingham. This was due to composition data for these $PM_{2.5}$ samples not being available. The only data analysed were gas-phase and meteorological measurements obtained from nearby air pollution monitoring sites.
- Due to the lack of accurately weighed quartz filters used during this project, TEOM online $PM_{2.5}$ measurements were used to calculate $PM_{2.5}$ mass loading on filters. Gravimetric data was available for the Delhi campaigns, however, it was decided to also use TEOM data for these campaigns to keep a consistent method across all campaigns. Having gravimetric data for all $PM_{2.5}$ samples would have been preferable for added accuracy.
- Finally, the work presented within this thesis is based on the assumption that OP as measured by the DTT assay is useful as a predictor of toxicity within cells and negative health impacts in humans. Whilst many studies have shown links between DTT OP and negative health outcomes, such as in the Øvrevik, 2019 review of 29 studies where 22 found a link between DTT OP and at least one specific health

outcome. However, even in this example, the studies disagreed on which health outcomes were statistically significantly linked with only asthma / wheeze in humans consistently showing a connection. While OP appears to not be useful at predicting specific health outcomes, community wide it seems to be able to predict at least some health outcomes. However, with the positive correlation between DTTv and $PM_{2.5}$ concentration, it is unclear whether it is more valuable than particulate concentration alone at predicting these.

7.3 Recommendations for future work

Considering the research carried out in this project, the area most in need for further research is Delhi and generally, India more broadly. There is an expansive collection of high quality OP studies in the literature covering Beijing and other cities across China. These include detailed source apportionment studies, high time resolution sampling, and multiple year seasonal variability studies. Delhi, in contrast, has a considerably smaller number of OP studies with the literature search in this project only finding a handful of OP studies in the Indo Gangetic Plain region (Jain et al., 2020; Patel & Rastogi, 2018a; Puthussery et al., 2020; Rai, Slowik, Furger, El Haddad, et al., 2021). There are a number of areas that would benefit from further research:

- The current pool of very limited OP data for Delhi entirely consists of DTT measurements. A multiple OP assay comparison study such as Campbell et al., 2020 performed in Beijing would be very useful for understanding the impact of different species to OP in Delhi. This is due to the limitation of a single assay being more sensitive to certain species and potentially missing out important sources of PM OP in Delhi.

- An investigation into the OP of specific sources in Indian cities. The PM composition species analysed during this study were often associated with multiple different sources, making it impossible to determine which source contribute the most to intrinsic particle OP. For effective mitigation strategies it is important to better understand these sources. This may include sampling primary particles from specific emission sources or further analysing composition species such as looking at the oxidation states of measured metal species.
- Further exploration of the impact of biomass burning emissions on air mass OP in Delhi, especially during the autumn campaign. The incorporation of back trajectory analysis would also allow for the contribution of regionally transported emissions to be estimated.
- All OP studies found in the Indo Gangetic Plain at the time of writing consist of a single sampling site. Simultaneous sampling within a megacity core and in the surrounding satellite cities / towns would allow for a better spatial understanding of OP in these megacities. The satellite cities surrounding Delhi has weaker air pollution control legislation and as such the $PM_{2.5}$ composition in these cities is likely significantly different to that found within Delhi owing to the more polluting industries moving to these cities.
- Measurements of OP and composition species during extreme air pollution events in Delhi, most notably the Diwali festival of light. Limitations in available samplers restricted the ability of this project from exploring composition species influence during this event. However, $PM_{2.5}$ concentrations during the Diwali event in the autumn regularly exceeded 300 μg m^{-3} with values of over 600 μg m^{-3} also measured. This study showed that these extreme PM events coincided with very low intrinsic

toxicity values. Further study of the OP of the air mass and the PM compositional makeup during the Diwali event is required to determine the impact to human health from such extreme air pollution events in Delhi.

- Further air pollution chamber experiments to better understand the evolution of $PM_{2.5}$ OP over time from various sources. The current literature in this area primarily focuses on diesel exhaust particles and SOA tracers. However, this research project has shown the importance of other sources to particle OP, primarily crustal materials, non-exhaust vehicle emissions, and re-suspended road dust. The impact of high $PM_{2.5}$ concentration primary emissions, notably biomass burning emissions, should also be studied in further detail due to the low DTTm values of these particles in this study likely causes significantly lower DTTv values during extreme pollution events.

All of the above recommendations for future research are based on similar approaches to those taken within this project. The next steps to take this research beyond the approaches mentioned within this thesis would be to work on a cross disciplinary project, where the real world health impacts of pollution events are looked at in parallel to the OP of the PM (i.e. a panel study). This may involve personal pollution monitoring devices for individuals within these cities or collated hospital admission data for a certain time frame to compare to the OP differences observed.

The standout findings of this project were that intrinsic toxicity does not appear to drastically vary between the different sampling locations, however, sampling in Birmingham was roadside so different PM makeup could explain this similarity. This project is also the first OP study to sample multiple seasons in Delhi, finding that intrinsic

toxicity significantly reduces at higher $PM_{2.5}$ concentrations to the point of reducing the OP of the air mass to that of days with up to 100 μg m^{-3} lower $PM_{2.5}$ concentrations. The implications of this for regulation of pollutants would be to increase focus on low, as well as high pollution days. According to the research in this project the most important source to reduce would be non-exhaust vehicle emissions and suspended road dust, as this has consistently been shown to increase the OP of $PM_{2.5}$ more than other sources. The lack of significant correlations between OP and the most significant PM mass sources, specifically biomass burning, presents an interesting opportunity to look at these emissions in more detail through chamber experiments.

8 LIST OF REFERENCES

Altuwayjiri, A., Soleimanian, E., Moroni, S., Palomba, P., Borgini, A., De Marco, C., Ruprecht, A. A., & Sioutas, C. (2021). The impact of stay-home policies during Coronavirus-19 pandemic on the chemical and toxicological characteristics of ambient PM2.5 in the metropolitan area of Milan, Italy. *Science of the Total Environment*, *758*, 143582. https://doi.org/10.1016/j.scitotenv.2020.143582

An, X., Zhu, T., Wang, Z., Li, C., & Wang, Y. (2007). A modeling analysis of a heavy air pollution episode occurred in Beijing. *Atmospheric Chemistry and Physics*, *7*(12), 3103–3114. https://doi.org/10.5194/acp-7-3103-2007

Atony Chen, L. W., Doddridge, B. G., Dickerson, R. R., Chow, J. C., Mueller, P. K., Quinn, J., & Butler, W. A. (2001). Seasonal variations in elemental carbon aerosol, carbon monoxide and sulfur dioxide: Implications for sources. *Geophysical Research Letters*, *28*(9), 1711–1714.

Ayres, J. G., Borm, P., Cassee, F. R., Castranova, V., Donaldson, K., Ghio, A., Harrison, R. M., Hider, R., Kelly, F., Kooter, I. M., Marano, F., Maynard, R. L., Mudway, I., Nel, A., Sioutas, C., Smith, S., Baeza-Squiban, A., Cho, A., Duggan, S., & Froines, J. (2008). Evaluating the toxicity of airborne particulate matter and nanoparticles by measuring oxidative stress potential - A workshop report and consensus statement. *Inhalation Toxicology*, *20*(1), 75–99. https://doi.org/10.1080/08958370701665517

Ball, S. (University of L. (2014). *ECG Environmental Briefs Atmospheric chemistry at night* (Issue 3).

Bates, J. T., Weber, R. J., Abrams, J., Verma, V., Fang, T., Klein, M., Strickland, M. J., Sarnat, S. E., Chang, H. H., Mulholland, J. A., Tolbert, P. E., & Russell, A. G. (2015). Reactive Oxygen Species Generation Linked to Sources of Atmospheric Particulate Matter and Cardiorespiratory Effects. *Environmental Science and Technology*, *49*(22), 13605–13612. https://doi.org/10.1021/acs.est.5b02967

Bell, M., Davis, D. L., & Fletcher, T. (2004). A retrospective assessment of mortality from the London smog episode of 1952: The role of influenza and pollution. *Environmental Health Perspectives*, *112*(1), 6–8. https://doi.org/10.1289/ehp.6539

Bell, M. L., Zanobetti, A., & Dominici, F. (2014). Who is more affected by ozone pollution? A systematic review and meta-analysis. *American Journal of Epidemiology*, *180*(1), 15–28. https://doi.org/10.1093/aje/kwu115

Bhaskar, B. V., & Mehta, V. M. (2010). Atmospheric particulate pollutants and their relationship with meteorology in Ahmedabad. *Aerosol and Air Quality Research*, *10*(4), 301–315. https://doi.org/10.4209/aaqr.2009.10.0069

Bikkina, S., Andersson, A., Kirillova, E. N., Holmstrand, H., Tiwari, S., Srivastava, A. K., Bisht, D. S., & Gustafsson, Ö. (2019). Air quality in megacity Delhi affected by countryside biomass burning. *Nature Sustainability*, *2*(3), 200–205. https://doi.org/10.1038/s41893-019-0219-0

Bloss, W. (University of B. (2014). *ECG Environmental Briefs Atmospheric particulate matter*. *10*(4), 1–2. http://www.euro.who.int/__data/assets/pdf_file/0005/

Boningari, T., & Smirniotis, P. G. (2016a). Impact of nitrogen oxides on the environment and human health: Mn-based materials for the NOx abatement. *Current Opinion in Chemical Engineering*, *13*, 133–141. https://doi.org/10.1016/j.coche.2016.09.004

Boningari, T., & Smirniotis, P. G. (2016b). ScienceDirect Impact of nitrogen oxides on the environment and human health : Mn-based materials for the NO x abatement. *Current Opinion in Chemical Engineering*, *13*(x), 133–141. https://doi.org/10.1016/j.coche.2016.09.004

Borlaza, L. J. S., Cosep, E. M. R., Kim, S., Lee, K., Joo, H., Park, M., Bate, D., Cayetano, M. G., & Park, K. (2018a). Oxidative potential of fine ambient particles in various environments. *Environmental Pollution*, *243*, 1679–1688. https://doi.org/10.1016/j.envpol.2018.09.074

Borlaza, L. J. S., Cosep, E. M. R., Kim, S., Lee, K., Joo, H., Park, M., Bate, D., Cayetano, M. G., & Park, K. (2018b). Oxidative potential of fine ambient particles in various environments. *Environmental Pollution*, *243*, 1679–1688. https://doi.org/10.1016/j.envpol.2018.09.074

Bressi, M., Cavalli, F., Belis, C. A., Putaud, J. P., Fröhlich, R., Martins Dos Santos, S., Petralia, E., Prévôt, A. S. H., Berico, M., Malaguti, A., & Canonaco, F. (2016). Variations in the chemical composition of the submicron aerosol and in the sources of the organic fraction at a regional background site of the Po Valley (Italy). *Atmospheric Chemistry and Physics*, *16*(20), 12875–12896. https://doi.org/10.5194/acp-16-12875-2016

Brook, R. D., Rajagopalan, S., Pope, C. A., Brook, J. R., Bhatnagar, A., Diez-Roux, A. V., Holguin, F., Hong, Y., Luepker, R. V., Mittleman, M. A., Peters, A., Siscovick, D., Smith, S. C., Whitsel, L., & Kaufman, J. D. (2010). Particulate matter air pollution and cardiovascular disease: An update to the scientific statement from the american heart association. *Circulation*, *121*(21), 2331–2378. https://doi.org/10.1161/CIR.0b013e3181dbece1

Campbell, S. J. (2021). Supplement of Atmospheric conditions and composition that influence PM 2 . 5 oxidative potential in Beijing , China Section S1 : APHH site location. *Atmospheric Chemistry and Physics*, *21*, 5549–5573.

Campbell, S. J., Wolfer, K., Utinger, B., Westwood, J., Zhang, Z., Steimer, S. S., Vu, T. V, Xu, J., Straw, N., Thomson, S., Sun, Y., Liu, D., Li, L., Fu, P., Lewis, A. C., Harrison, R. M., Bloss, J., Loh, M., Miller, M. R., … Kalberer, M. (2020). Atmospheric conditions and composition that influence PM 2 . 5 oxidative potential in Beijing , China. *Atmospheric Chemistry and Physics*, *October*, 2–7.

Cao, J. J., Shen, Z. X., Chow, J. C., Watson, J. G., Lee, S. C., Tie, X. X., Ho, K. F., Wang, G. H., & Han, Y. M. (2012). Winter and Summer PM2.5 Chemical Compositions in Fourteen Chinese Cities. *Journal of the Air and Waste Management Association*, *62*(10), 1214–1226. https://doi.org/10.1080/10962247.2012.701193

Carnell, E., Vieno, M., Vardoulakis, S., Beck, R., Heaviside, C., Tomlinson, S., Dragosits, U., Heal, M. R., & Reis, S. (2019). Modelling public health improvements as a result of air

pollution control policies in the UK over four decades - 1970 to 2010. *Environmental Research Letters*, *14*(7). https://doi.org/10.1088/1748-9326/ab1542

Census Organization of India. (2020). *Delhi Population 2011 - 2020*.

Chang, X., Wang, S., Zhao, B., Xing, J., Liu, X., Wei, L., Song, Y., Wu, W., Cai, S., Zheng, H., Ding, D., & Zheng, M. (2019). Contributions of inter-city and regional transport to PM 2.5 concentrations in the Beijing-Tianjin-Hebei region and its implications on regional joint air pollution control. *Science of the Total Environment*, *660*, 1191–1200. https://doi.org/10.1016/j.scitotenv.2018.12.474

Charrier, J. G., & Anastasio, C. (2012). On dithiothreitol (DTT) as a measure of oxidative potential for ambient particles: evidence for the importance of soluble transition metals. *Atmospheric Chemistry and Physics*, *12*(5), 11317–11350. https://doi.org/10.1038/jid.2014.371

Charrier, J. G., Richards-Henderson, N. K., Bein, K. J., McFall, A. S., Wexler, A. S., & Anastasio, C. (2015). Oxidant production from source-oriented particulate matter - Part 1: Oxidative potential using the dithiothreitol (DTT) assay. *Atmospheric Chemistry and Physics*, *15*(5), 2327–2340. https://doi.org/10.5194/acp-15-2327-2015

Cheng, Y., Zheng, G., Wei, C., Mu, Q., Zheng, B., Wang, Z., Gao, M., Zhang, Q., He, K., Carmichael, G., Pöschl, U., & Su, H. (2016). Reactive nitrogen chemistry in aerosol water as a source of sulfate during haze events in China. *Science Advances*, *2*(12). https://doi.org/10.1126/sciadv.1601530

Cherrie, J. W., Ng, M. G., Searl, A., Shafrir, A., Iom, M. V. T., Mistry, R., Sobey, M., Warwick, O., & Entec, C. C. (2011). *Health , socio-economic and environmental aspects of possible amendments to the EU Directive on the protection of workers from the risks related to exposure to carcinogens and mutagens at work Hexavalent Chromium* (Issue P937/22).

Cho, A. K., Di Stefano, E., You, Y., Rodriguez, C. E., Schmitz, D. A., Kumagai, Y., Miguel, A. H., Eiguren-Fernandez, A., Kobayashi, T., Avol, E., & Froines, J. R. (2004). Determination of four quinones in diesel exhaust particles, SRM 1649a, and atmospheric PM2.5. *Aerosol Science and Technology*, *38*(SUPPL. 1), 68–81. https://doi.org/10.1080/02786820390229471

Cho, A. K., Sioutas, C., Miguel, A. H., Kumagai, Y., Schmitz, D. A., Singh, M., Eiguren-Fernandez, A., & Froines, J. R. (2005a). Redox activity of airborne particulate matter at different sites in the Los Angeles Basin. *Environmental Research*, *99*(1), 40–47. https://doi.org/10.1016/j.envres.2005.01.003

Cho, A. K., Sioutas, C., Miguel, A. H., Kumagai, Y., Schmitz, D. A., Singh, M., Eiguren-Fernandez, A., & Froines, J. R. (2005b). Redox activity of airborne particulate matter at different sites in the Los Angeles Basin. *Environmental Research*, *99*(1), 40–47. https://doi.org/10.1016/j.envres.2005.01.003

Chuang, H. C., Jones, T. P., Lung, S. C. C., & BéruBé, K. A. (2011). Soot-driven reactive oxygen species formation from incense burning. *Science of the Total Environment*, *409*(22), 4781–4787. https://doi.org/10.1016/j.scitotenv.2011.07.041

Clayden, J., Greevs, N., Warren, S., & Wothers, P. (2001). Organic Chemistry. In *Oxford*

University Press. https://doi.org/10.1007/s00897010513a

Colls, J., & Tiwary, A. (2009). *Air Pollution : Measurement, Modelling and Mitigation, Third Edition*. CRC Press LLC. http://ebookcentral.proquest.com/lib/bham/detail.action?docID=446716

COMEAP. (2018). *Associations of long-term average concentrations of nitrogen dioxide with mortality: A report by the Committee on the Medical Effects of Air Pollution*. https://assets.publishing.service.gov.uk/government/uploads/system/uploads/attachment_data/file/734799/COMEAP_NO2_Report.pdf

Connolley, W. M. (1996). The Antarctic temperature inversion. *International Journal of Climatology*, *16*(12), 1333–1342. https://doi.org/10.1002/(sici)1097-0088(199612)16:12<1333::aid-joc96>3.3.co;2-y

Conte, E., Canepari, S., Frasca, D., & Simonetti, G. (2017). Oxidative Potential of Selected PM Components. *Proceedings*, *1*(5), 108. https://doi.org/10.3390/ecas2017-04131

Curbo, S., Reiser, K., Rundlöf, A. K., Karlsson, A., & Lundberg, M. (2013). Is trichloroacetic acid an insufficient sample quencher of redox reactions? *Antioxidants and Redox Signaling*, *18*(7), 795–799. https://doi.org/10.1089/ars.2012.4949

Dąbrowski, J. M. (2017). Reactive Oxygen Species in Photodynamic Therapy: Mechanisms of Their Generation and Potentiation. In *Advances in Inorganic Chemistry* (Vol. 70, pp. 343–394). https://doi.org/10.1016/bs.adioch.2017.03.002

Dang, R., & Liao, H. (2019). Radiative Forcing and Health Impact of Aerosols and Ozone in China as the Consequence of Clean Air Actions over 2012–2017. *Geophysical Research Letters*, *46*(21), 12511–12519. https://doi.org/10.1029/2019GL084605

Das, R., Khezri, B., Srivastava, B., Datta, S., Sikdar, P. K., Webster, R. D., & Wang, X. (2015). Trace element composition of PM2.5 and PM10 from kolkata–a heavily polluted indian metropolis. *Atmospheric Pollution Research*, *6*(5), 742–750. https://doi.org/10.5094/APR.2015.083

De Vizcaya-Ruiz, A., Gutiérrez-Castillo, M. E., Uribe-Ramirez, M., Cebrián, M. E., Mugica-Alvarez, V., Sepúlveda, J., Rosas, I., Salinas, E., Garcia-Cuéllar, C., Martínez, F., Alfaro-Moreno, E., Torres-Flores, V., Osornio-Vargas, A., Sioutas, C., Fine, P. M., Singh, M., Geller, M. D., Kuhn, T., Miguel, A. H., … Froines, J. (2006). Characterization and in vitro biological effects of concentrated particulate matter from Mexico City. *Atmospheric Environment*, *40*(SUPPL. 2), 583–592. https://doi.org/10.1016/j.atmosenv.2005.12.073

Decesari, S., Sowlat, M. H., Hasheminassab, S., Sandrini, S., Gilardoni, S., Facchini, M. C., Fuzzi, S., & Sioutas, C. (2017). Enhanced toxicity of aerosol in fog conditions in the Po Valley, Italy. *Atmospheric Chemistry and Physics*, *17*(12), 7721–7731. https://doi.org/10.5194/acp-17-7721-2017

Drishti. (2020). *Temperature Inversion*. https://www.drishtiias.com/to-the-points/paper1/temperature-inversion

Du, Y., Xu, X., Chu, M., Guo, Y., & Wang, J. (2016). Air particulate matter and cardiovascular disease: The epidemiological, biomedical and clinical evidence. *Journal of Thoracic Disease*, *8*(1), E8–E19. https://doi.org/10.3978/j.issn.2072-1439.2015.11.37

Duan, J., & Tan, J. (2013). Atmospheric heavy metals and Arsenic in China: Situation, sources and control policies. *Atmospheric Environment*, *74*, 93–101. https://doi.org/10.1016/j.atmosenv.2013.03.031

Dutta, A. K. (1932). Heat of Dissociation of Oxygen. *Nature*, *129*(3252), 317. https://doi.org/10.1038/129317b0

Environmental Pollution Centers. (2020). *What is Air Pollution*. https://www.environmentalpollutioncenters.org/air/

European Communities. (2001). *Ambient Air Pollution by Polycyclic Aromatic Hydrocarbons (PAH): Position Paper*.

Fang, T, Verma, V., Guo, H., King, L. E., Edgerton, E. S., & Weber, R. J. (2015). A semi-automated system for quantifying the oxidative potential of ambient particles in aqueous extracts using the dithiothreitol (DTT) assay: Results from the Southeastern Center for Air Pollution and Epidemiology (SCAPE). *Atmospheric Measurement Techniques*, *8*(1), 471–482. https://doi.org/10.5194/amt-8-471-2015

Fang, Ting, Verma, V., Bates, J. T., Abrams, J., Klein, M., Strickland, M. J., Sarnat, S. E., Chang, H. H., Mulholland, J. A., Tolbert, P. E., Russell, A. G., & Weber, R. J. (2016). Oxidative potential of ambient watersoluble PM 2.5 in the southeastern United States: contrasts in sources and health associations between ascorbic acid (AA) and dithiothreitol (DTT) assays. *Atmos. Chem. Phys*, *16*, 3865–3879. https://doi.org/10.5194/acp1638652016

Fang, Ting, Verma, V., T Bates, J., Abrams, J., Klein, M., Strickland, J. M., Sarnat, E. S., Chang, H. H., Mulholland, A. J., Tolbert, E. P., Russell, G. A., & Weber, J. R. (2016a). Oxidative potential of ambient water-soluble PM2.5 in the southeastern United States: Contrasts in sources and health associations between ascorbic acid (AA) and dithiothreitol (DTT) assays. *Atmospheric Chemistry and Physics*, *16*(6), 3865–3879. https://doi.org/10.5194/acp-16-3865-2016

Fang, Ting, Verma, V., T Bates, J., Abrams, J., Klein, M., Strickland, J. M., Sarnat, E. S., Chang, H. H., Mulholland, A. J., Tolbert, E. P., Russell, G. A., & Weber, J. R. (2016b). Oxidative potential of ambient water-soluble PM2.5 in the southeastern United States: Contrasts in sources and health associations between ascorbic acid (AA) and dithiothreitol (DTT) assays. *Atmospheric Chemistry and Physics*, *16*(6), 3865–3879. https://doi.org/10.5194/acp-16-3865-2016

Fang, Z., Deng, W., Zhang, Y., Ding, X., Tang, M., Liu, T., Hu, Q., Zhu, M., Wang, Z., Yang, W., Huang, Z., Song, W., Bi, X., Chen, J., Sun, Y., George, C., & Wang, X. (2017). Open burning of rice, corn and wheat straws: Primary emissions, photochemical aging, and secondary organic aerosol formation. *Atmospheric Chemistry and Physics*, *17*(24), 14821–14839. https://doi.org/10.5194/acp-17-14821-2017

Feng, X., Wei, S., & Wang, S. (2020). Temperature inversions in the atmospheric boundary layer and lower troposphere over the Sichuan Basin, China: Climatology and impacts on air pollution. *Science of the Total Environment*, *726*, 138579. https://doi.org/10.1016/j.scitotenv.2020.138579

Finch, D. P., & Palmer, P. I. (2020). Increasing ambient surface ozone levels over the UK accompanied by fewer extreme events. *Atmospheric Environment*, *237*(June), 117627.

https://doi.org/10.1016/j.atmosenv.2020.117627

Flynn, G. (2003). The Kinetics of Atmospheric Ozone Ozone. In *Columbia University*. http://www.columbia.edu/itc/chemistry/chem-c2407/hw/ozone_kinetics.pdf

Forouzanfar, M. H., Alexander, L., Bachman, V. F., Biryukov, S., Brauer, M., Casey, D., Coates, M. M., Delwiche, K., Estep, K., Frostad, J. J., Astha, K. C., Kyu, H. H., Moradi-Lakeh, M., Ng, M., Slepak, E., Thomas, B. A., Wagner, J., Achoki, T., Atkinson, C., … Zhu, S. (2015). Global, regional, and national comparative risk assessment of 79 behavioural, environmental and occupational, and metabolic risks or clusters of risks in 188 countries, 1990-2013: A systematic analysis for the Global Burden of Disease Study 2013. *The Lancet*, *386*(10010), 2287–2323. https://doi.org/10.1016/S0140-6736(15)00128-2

Foster, A., & Kumar, N. (2011a). Health effects of air quality regulations in Delhi, India. *Atmospheric Environment*, *45*(9), 1675–1683. https://doi.org/10.1016/j.atmosenv.2011.01.005

Foster, A., & Kumar, N. (2011b). Health effects of air quality regulations in Delhi , India. *Atmospheric Environment*, *45*(9), 1675–1683. https://doi.org/10.1016/j.atmosenv.2011.01.005

Fritts, D. C., & Alexander, M. J. (2003). Gravity wave dynamics and effects in the middle atmosphere. *Reviews of Geophysics*, *41*(1), 1–64. https://doi.org/10.1029/2001RG000106

Gao, D., Fang, T., Verma, V., Zeng, L., & Weber, R. J. (2017). A method for measuring total aerosol oxidative potential (OP) with the dithiothreitol (DTT) assay and comparisons between an urban and roadside site of water-soluble and total OP. *Atmospheric Measurement Techniques*, *10*(8), 2821–2835. https://doi.org/10.5194/amt-10-2821-2017

GBD MAPS Working Group. (2016). Burden of Disease Attributable to Coal-Burning and Other Air Pollution Sources in China. Special Report 20. In *MA: Health Effects Institute*. https://www.healtheffects.org/system/files/GBDMAPS-ReportEnglishFinal1.pdf

GBD MAPS Working Group. (2018). Burden of Disease Attributable to Major Air Pollution Sources in India. *Special Report 21. Boston, MA:Health Effects Institute.*, *January*, 6.

Geography: Beijing. (2020). https://geography.name/beijing/

Global Health Metrics. (2020). Ambient ozone pollution — Level 3 risk. In *The Lancet* (Vol. 396).

Griffin, R. J. J. (2013). The Sources and Impacts of Tropospheric Particulate Matter. *Nature Education Knowledge*, *4*(5), 1. http://www.nature.com/scitable/knowledge/library/the-sources-and-impacts-of-tropospheric-particulate-102760478

Gschwandtner, G., Gschwandtner, K., Eldridge, K., Mobley, D., Gschwandtner, G., Gschwandtner, K., Eldridge, K., Gschwandtner, G., Gschwandtner, K., Eldridge, K., Carolina, N., Mann, C., & Mobley, D. (1986). Historic Emissions of Sulfur and Nitrogen Oxides in the United States from 1900 to 1980. *Journal of the Air Pollution Control Association*, *36*(2), 139–149. https://doi.org/10.1080/00022470.1986.10466052

Guan, Y., Kang, L., Wang, Y., Zhang, N. N., & Ju, M. T. (2019). Health loss attributed to PM 2.5 pollution in China's cities: Economic impact, annual change and reduction potential. *Journal of Cleaner Production*, *217*, 284–294. https://doi.org/10.1016/j.jclepro.2019.01.284

Guilbert, A., De Cremer, K., Heene, B., Demoury, C., Aerts, R., Declerck, P., Brasseur, O., & Van Nieuwenhuyse, A. (2019). Personal exposure to traffic-related air pollutants and relationships with respiratory symptoms and oxidative stress: A pilot cross-sectional study among urban green space workers. *Science of the Total Environment*, *649*, 620–628. https://doi.org/10.1016/j.scitotenv.2018.08.338

Gunthe, S. S., Liu, P., Panda, U., Raj, S. S., Sharma, A., Darbyshire, E., Reyes-Villegas, E., Allan, J., Chen, Y., Wang, X., Song, S., Pöhlker, M. L., Shi, L., Wang, Y., Kommula, S. M., Liu, T., Ravikrishna, R., McFiggans, G., Mickley, L. J., … Coe, H. (2021). Enhanced aerosol particle growth sustained by high continental chlorine emission in India. *Nature Geoscience*, *14*(2), 77–84. https://doi.org/10.1038/s41561-020-00677-x

Guo, S., Hu, M., Zamora, M. L., Peng, J., Shang, D., Zheng, J., Du, Z., Wu, Z., Shao, M., Zeng, L., Molina, M. J., & Zhang, R. (2014). Elucidating severe urban haze formation in China. *Proceedings of the National Academy of Sciences*, *111*(49), 17373–17378. https://doi.org/10.1073/pnas.1419604111

Gurjar, B. R., Molina, L. T., & Ojha, C. S. P. (2010). *Air pollution : health and environmental impacts*. CRC Press LLC.

Guttikunda, S. K., Goel, R., & Pant, P. (2014). Nature of air pollution, emission sources, and management in the Indian cities. *Atmospheric Environment*, *95*, 501–510. https://doi.org/10.1016/j.atmosenv.2014.07.006

Guttikunda, S. K., & Gurjar, B. R. (2012). Role of meteorology in seasonality of air pollution in megacity Delhi, India. *Environmental Monitoring and Assessment*, *184*(5), 3199–3211. https://doi.org/10.1007/s10661-011-2182-8

Health Effects Institute. (2019). State of Global Air 2019. *Health Effects Institute.*, 24. https://doi.org/https://www.stateofglobalair.org/sites/default/files/soga_2019_report.pdf

Hoek, G., Krishnan, R. M., Beelen, R., Peters, A., Ostro, B., Brunekreef, B., & Kaufman, J. D. (2013). Long-term air pollution exposure and cardio-respiratory mortality: A review. *Environmental Health: A Global Access Science Source*, *12*(1), 1–15. https://doi.org/10.1186/1476-069X-12-43

Hu, S., Polidori, A., Arhami, M., Shafer, M. M., Schauer, J. J., Cho, A., & Sioutas, C. (2008). Redox activity and chemical speciation of size fractioned PM in the communities of the Los Angeles-Long Beach harbor. *Atmospheric Chemistry and Physics*, *8*(21), 6439–6451. https://doi.org/10.5194/acp-8-6439-2008

Institute for Health Metrics and Evaluation. (2020). GBD Compare | Viz Hub. In *Global Burden of Disease 2017*. https://vizhub.healthdata.org/gbd-compare/

Jacobson, M. Z. (2005). *Fundamentals of Atmospheric Modeling* (2nd ed.). Cambridge University Press.

Jain, S., Sharma, S. K., Vijayan, N., & Mandal, T. K. (2020). Seasonal characteristics of aerosols (PM2.5 and PM10) and their source apportionment using PMF: A four year study over Delhi, India. *Environmental Pollution*, *262*, 114337. https://doi.org/10.1016/j.envpol.2020.114337

Janssen, N. A. H., Yang, A., Strak, M., Steenhof, M., Hellack, B., Gerlofs-Nijland, M. E., Kuhlbusch, T., Kelly, F., Harrison, R., Brunekreef, B., Hoek, G., & Cassee, F. (2014). Oxidative potential of particulate matter collected at sites with different source characteristics. *Science of the Total Environment*, *472*, 572–581. https://doi.org/10.1016/j.scitotenv.2013.11.099

Jiang, H., Jang, M., Sabo-Attwood, T., & Robinson, S. E. (2016). Oxidative potential of secondary organic aerosols produced from photooxidation of different hydrocarbons using outdoor chamber under ambient sunlight. *Atmospheric Environment*, *131*, 382–389. https://doi.org/10.1016/j.atmosenv.2016.02.016

Jiang, L., & Bai, L. (2018). Spatio-temporal characteristics of urban air pollutions and their causal relationships: Evidence from Beijing and its neighboring cities. *Scientific Reports*, *8*(1), 1–12. https://doi.org/10.1038/s41598-017-18107-1

Kelly, F J, Cotgrove, M., & Mudway, I. S. (1996). Respiratory tract lining fluid antioxidants: the first line of defence against gaseous pollutants. *Central European Journal of Public Health*, *4 Suppl*, 11–14.

Kelly, Frank J, & Fussell, J. C. (2012). Size, source and chemical composition as determinants of toxicity attributable to ambient particulate matter. *Atmospheric Environment*, *60*, 504–526. https://doi.org/10.1016/j.atmosenv.2012.06.039

Kulkarni, N. S., Prudon, B., Panditi, S. L., Abebe, Y., & Grigg, J. (2005). Carbon loading of alveolar macrophages in adults and children exposed to biomass smoke particles. *The Science of the Total Environment*, *345*(1–3), 23–30. https://doi.org/10.1016/j.scitotenv.2004.10.016

Kumagai, Y., Koide, S., Taguchi, K., Endo, A., Nakai, Y., Yoshikawa, T., & Shimojo, N. (2002). Oxidation of proximal protein sulfhydryls by phenanthraquinone, a component of diesel exhaust particles. *Chemical Research in Toxicology*, *15*(4), 483–489. https://doi.org/10.1021/tx0100993

Künzli, N., Jerrett, M., Mack, W. J., Beckerman, B., LaBree, L., Gilliland, F., Thomas, D., Peters, J., & Hodis, H. N. (2005). Ambient air pollution and atherosclerosis in Los Angeles. *Environmental Health Perspectives*, *113*(2), 201–206. https://doi.org/10.1289/ehp.7523

Künzli, N., Mudway, I. S., Götschi, T., Shi, T., Kelly, F. J., Cook, S., Burney, P., Forsberg, B., Gauderman, J. W., Hazenkamp, M. E., Heinrich, J., Jarvis, D., Norbäck, D., Payo-Losa, F., Poli, A., Sunyer, J., & Borm, P. J. A. (2006). Comparison of oxidative properties, light absorbance, and total and elemental mass concentration of ambient PM2.5 collected at 20 European sites. *Environmental Health Perspectives*, *114*(5), 684–690. https://doi.org/10.1289/ehp.8584

Li, H., You, S., Zhang, H., Zheng, W., Zheng, X., Jia, J., Ye, T., & Zou, L. (2017). Modelling of AQI related to building space heating energy demand based on big data analytics.

Applied Energy, *203*, 57–71. https://doi.org/10.1016/j.apenergy.2017.06.002

Li, K., Jacob, D. J., Liao, H., Shen, L., Zhang, Q., & Bates, K. H. (2019). Anthropogenic drivers of 2013–2017 trends in summer surface ozone in China. *Proceedings of the National Academy of Sciences of the United States of America*, *116*(2), 422–427. https://doi.org/10.1073/pnas.1812168116

Li, N., Sioutas, C., Cho, A., Schmitz, D., Misra, C., Sempf, J., Wang, M., Oberley, T., Froines, J., & Nel, A. (2003). Ultrafine particulate pollutants induce oxidative stress and mitochondrial damage. *Environmental Health Perspectives*, *111*(4), 455–460. https://doi.org/10.1289/ehp.6000

Li, P., Yan, R., Yu, S., Wang, S., Liu, W., & Bao, H. (2015). Reinstate regional transport of PM2.5 as a major cause of severe haze in Beijing. *Proceedings of the National Academy of Sciences of the United States of America*, *112*(21), E2739--E2740. https://doi.org/10.1073/pnas.1502596112

Li, Q., Wyatt, A., & Kamens, R. M. (2009). Oxidant generation and toxicity enhancement of aged-diesel exhaust. *Atmospheric Environment*, *43*(5), 1037–1042. https://doi.org/10.1016/j.atmosenv.2008.11.018

Li, R., Wang, Z., Cui, L., Fu, H., Zhang, L., Kong, L., Chen, W., & Chen, J. (2019a). Air pollution characteristics in China during 2015–2016: Spatiotemporal variations and key meteorological factors. *Science of the Total Environment*, *648*, 902–915. https://doi.org/10.1016/j.scitotenv.2018.08.181

Li, R., Wang, Z., Cui, L., Fu, H., Zhang, L., Kong, L., Chen, W., & Chen, J. (2019b). Air pollution characteristics in China during 2015–2016: Spatiotemporal variations and key meteorological factors. *Science of the Total Environment*, *648*, 902–915. https://doi.org/10.1016/j.scitotenv.2018.08.181

Li, W., Peng, Y., & Bai, Z. (2010). Distributions and sources of n-alkanes in PM2.5 at urban, industrial and coastal sites in Tianjin, China. *Journal of Environmental Sciences*, *22*(10), 1551–1557. https://doi.org/10.1016/S1001-0742(09)60288-6

Liu, Q., Baumgartner, J., Zhang, Y., Liu, Y., Sun, Y., & Zhang, M. (2014). Oxidative potential and inflammatory impacts of source apportioned ambient air pollution in Beijing. *Environmental Science and Technology*, *48*(21), 12920–12929. https://doi.org/10.1021/es5029876

Liu, W. J., Xu, Y. S., Liu, W. X., Liu, Q. Y., Yu, S. Y., Liu, Y., Wang, X., & Tao, S. (2018a). Oxidative potential of ambient PM2.5 in the coastal cities of the Bohai Sea, northern China: Seasonal variation and source apportionment. *Environmental Pollution*, *236*, 514–528. https://doi.org/10.1016/j.envpol.2018.01.116

Liu, W. J., Xu, Y. S., Liu, W. X., Liu, Q. Y., Yu, S. Y., Liu, Y., Wang, X., & Tao, S. (2018b). Oxidative potential of ambient PM2.5in the coastal cities of the Bohai Sea, northern China: Seasonal variation and source apportionment. *Environmental Pollution*, *236*, 514–528. https://doi.org/10.1016/j.envpol.2018.01.116

Liu, X. G., Li, J., Qu, Y., Han, T., Hou, L., Gu, J., Chen, C., Yang, Y., Liu, X., Yang, T., Zhang, Y., Tian, H., & Hu, M. (2013). Formation and evolution mechanism of regional haze: A case

study in the megacity Beijing, China. *Atmospheric Chemistry and Physics*, *13*(9), 4501–4514. https://doi.org/10.5194/acp-13-4501-2013

Liu, X. H., Zhang, Y., Cheng, S. H., Xing, J., Zhang, Q., Streets, D. G., Jang, C., Wang, W. X., & Hao, J. M. (2010). Understanding of regional air pollution over China using CMAQ, part I performance evaluation and seasonal variation. *Atmospheric Environment*, *44*(20), 2415–2426. https://doi.org/10.1016/j.atmosenv.2010.03.035

Liu, Z., Gao, W., Yu, Y., Hu, B., Xin, J., Sun, Y., Wang, L., Wang, G., Bi, X., Zhang, G., Xu, H., Cong, Z., He, J., Xu, J., & Wang, Y. (2018). Characteristics of PM2.5mass concentrations and chemical species in urban and background areas of China: Emerging results from the CARE-China network. *Atmospheric Chemistry and Physics*, *18*(12), 8849–8871. https://doi.org/10.5194/acp-18-8849-2018

Lu, X., Zhang, L., Wang, X., Gao, M., Li, K., Zhang, Y., Yue, X., & Zhang, Y. (2020). Rapid Increases in Warm-Season Surface Ozone and Resulting Health Impact in China since 2013. *Environmental Science and Technology Letters*, *7*(4), 240–247. https://doi.org/10.1021/acs.estlett.0c00171

Lyu, R., Shi, Z., Alam, M. S., Wu, X., Liu, D., Vu, T. V., Stark, C., Xu, R., Fu, P., Feng, Y., & Harrison, R. M. (2019). Alkanes and aliphatic carbonyl compounds in wintertime PM2.5 in Beijing, China. *Atmospheric Environment*, *202*(January), 244–255. https://doi.org/10.1016/j.atmosenv.2019.01.023

Mage, D., Ozolins, G., Peterson, P., Webster, A., Orthofer, R., Vandeweerd, V., & Gwynne, M. (1996). Urban air pollution in megacities of the world. *Atmospheric Environment*, *30*(5), 681–686. https://doi.org/10.1016/1352-2310(95)00219-7

Magnani, L., Gaydou, E. M., & Hubaud, J. C. (2000). Spectrophotometric measurement of antioxidant properties of flavones and flavonols against superoxide anion. *Analytica Chimica Acta*, *411*(1–2), 209–216. https://doi.org/10.1016/S0003-2670(00)00717-0

Mason, P. J., & Thomson, D. J. (2015). *Boundary Layer (Atmospheric) and Air Pollution* (G. R. North, J. Pyle, & F. B. T.-E. of A. S. (Second E. Zhang (Eds.); pp. 220–226). Academic Press. https://doi.org/https://doi.org/10.1016/B978-0-12-382225-3.00081-5

McClellan, R. O., & Miller, F. J. (1997). An overview of EPA's proposal revision of the particulate matter standards. *CIIT Activities*, *17*(4), 1–22.

Mentel, T. H. F., Bleilebens, D., & Wahner, A. (1996). A Study of Nighttime Nitrogen Oxide Oxidation Chamber-The Fate of N02, HN03, and 03 at Different Humidities. *Atmospheric Environment*, *30*(23), 4007–4020.

Miller, M. R., Borthwick, S. J., Shaw, C. A., McLean, S. G., McClure, D., Mills, N. L., Duffin, R., Donaldson, K., Megson, I. L., Hadoke, P. W. F., & Newby, D. E. (2009). Direct impairment of vascular function by diesel exhaust particulate through reduced bioavailability of endothelium-derived nitric oxide induced by superoxide free radicals. *Environmental Health Perspectives*, *117*(4), 611–616. https://doi.org/10.1289/ehp.0800235

Mollenhauer, K., & Tschoeke, H. (2010a). *Handbook of Diesel Engines*. Springer. https://doi.org/10.1007/978-3-540-89083-6

Mollenhauer, K., & Tschoeke, H. (2010b). *Handbook of Diesel Engines*. Springer. https://doi.org/10.1007/978-3-540-89083-6

Monaci, F., & Bargagli, R. (1996). Barium and other trace metals as indicators of vehicle emissions. *Water Air and Soil Pollution*, *100*, 89–98. https://doi.org/10.1023/A

Mondal, A., Saharan, U. S., Arya, R., Yadav, L., Ahlawat, S., Jangirh, R., Kotnala, G., Choudhary, N., Banoo, R., Rai, A., Yadav, P., Rani, M., Lal, S., Stewart, G. J., Nelson, B. S., Acton, W. J. F., Vaughan, A. R., Hamilton, J. F., Hopkins, J. R., … Mandal, T. K. (2021). Non-methane volatile organic compounds emitted from domestic fuels in Delhi: Emission factors and total city-wide emissions. *Atmospheric Environment: X*, *11*(February), 100127. https://doi.org/10.1016/j.aeaoa.2021.100127

Moon, J., Lee, W. K., Song, C., Lee, S. G., Heo, S. B., Shvidenko, A., Kraxner, F., Lamchin, M., Lee, E. J., Zhu, Y., Kim, D., & Cui, G. (2017). An Introduction To Mid-Latitude Ecotone: Sustainability and Environmental Challenges. *Sibirskij Lesnoj Zurnal (Sib. H. For. Sci.)*, *6*, 41–53. https://doi.org/10.15372/sjfs20170603

Moreno, T., Kelly, F. J., Dunster, C., Oliete, A., Martins, V., Reche, C., Minguillón, M. C., Amato, F., Capdevila, M., de Miguel, E., & Querol, X. (2016). Oxidative potential of subway PM2.5. *Atmospheric Environment*, *148*, 230–238. https://doi.org/10.1016/j.atmosenv.2016.10.045

Mudway, I. S., Duggan, S. T., Venkataraman, C., Habib, G., Kelly, F. J., & Grigg, J. (2005). Combustion of dried animal dung as biofuel results in the generation of highly redox active fine particulates. *Particle and Fibre Toxicology*, *2*, 6. https://doi.org/10.1186/1743-8977-2-6

Mudway, I. S., Fuller, G., Green, D., Dunster, C., & Kelly, F. J. (2009). *Quantifying the London Specific Component of PM 10 Oxidative Activity* (Issue November).

Mudway, I. S., Stenfors, N., Duggan, S. T., Roxborough, H., Zielinski, H., Marklund, S. L., Blomberg, A., Frew, A. J., Sandström, T., & Kelly, F. J. (2004). An in vitro and in vivo investigation of the effects of diesel exhaust on human airway lining fluid antioxidants. *Archives of Biochemistry and Biophysics*, *423*(1), 200–212. https://doi.org/10.1016/j.abb.2003.12.018

National Bureau of Statistics of China. (2004). About Beijing: Beijing Introduction. In *National Bureau of Statistics of China, 2012*. http://www.stats.gov.cn/english/18round/others/200403/t20040304_44593.html

National Research Council. (1998). The atmospheric sciences: entering the twenty-first century. In *The National Academies Press*. https://doi.org/10.17226/6021

National Research Council (US) Committee on Research Priorities for Airborne Particulate Matter. (1998). *Research Priorities for Airborne Particulate Matter I. Immediate Priorities and a Long-Range Research Portfolio*. National Academics Press (US).

NERC. (2014a). *Atmospheric Pollution and Human Health in a Chinese Megacity - Announcement of Workshop* (pp. 1–4). National Environment Research Council. https://webarchive.nationalarchives.gov.uk/20200930155405/https://nerc.ukri.org/research/funded/programmes/atmospollution/news/ao-workshop/ao/

NERC. (2014b). *Atmospheric Pollution and Human Health in a Chinese Megacity A UK-China Collaboration: Announcement of Opportunity (AO) - Call for Expressions of Interest* (pp. 1–13). National Environment Research Council. https://webarchive.nationalarchives.gov.uk/20200930155755/https://nerc.ukri.org/research/funded/programmes/atmospollution/news/ao/ao/

NERC. (2015). *Atmospheric Pollution and Human Health in a Chinese Megacity A UK-China Collaboration: Guidance for invited Full Proposals from UK applicants* (pp. 1–15). National Environment Research Council. https://webarchive.nationalarchives.gov.uk/20200930160032/https://nerc.ukri.org/research/funded/programmes/atmospollution/news/fullproposal/guidance/

NERC. (2016). *Atmospheric Pollution and Human Health in an Indian Megacity Guidance for post-workshop applications* (pp. 1–11). National Environment Research Council.

Ntziachristos, L., Froines, J. R., Cho, A. K., & Sioutas, C. (2007). Relationship between redox activity and chemical speciation of size-fractionated particulate matter. *Particle and Fibre Toxicology*, *4*, 1–12. https://doi.org/10.1186/1743-8977-4-5

Nuvolone, D., Petri, D., & Voller, F. (2018). The effects of ozone on human health. *Environmental Science and Pollution Research*, *25*(9), 8074–8088. https://doi.org/10.1007/s11356-017-9239-3

Oros, D. R., & Simoneit, B. R. T. (2000). Identification and emission rates of molecular tracers in coal smoke particulate matter. *Fuel*, *79*(5), 515–536. https://doi.org/10.1016/S0016-2361(99)00153-2

Øvrevik, J. (2019). Oxidative potential versus biological effects: A review on the relevance of cell-free/abiotic assays as predictors of toxicity from airborne particulate matter. *International Journal of Molecular Sciences*, *20*(19). https://doi.org/10.3390/ijms20194772

Palm, B. B., De Sá, S. S., Day, D. A., Campuzano-Jost, P., Hu, W., Seco, R., Sjostedt, S. J., Park, J. H., Guenther, A. B., Kim, S., Brito, J., Wurm, F., Artaxo, P., Thalman, R., Wang, J., Yee, L. D., Wernis, R., Isaacman-VanWertz, G., Goldstein, A. H., … Jimenez, J. L. (2018). Secondary organic aerosol formation from ambient air in an oxidation flow reactor in central Amazonia. *Atmospheric Chemistry and Physics*, *18*(1), 467–493. https://doi.org/10.5194/acp-18-467-2018

Parthasarathy, B., Sontakke, N. A., Monot, A. A., & Kothawale, D. R. (1987). Droughts/floods in the summer monsoon season over different meteorological subdivisions of India for the period 1871–1984. *Journal of Climatology*, *7*(1), 57–70. https://doi.org/10.1002/joc.3370070106

Patel, A., & Rastogi, N. (2018a). Oxidative potential of ambient fine aerosol over a semi-urban site in the Indo-Gangetic Plain. *Atmospheric Environment*, *175*(November 2017), 127–134. https://doi.org/10.1016/j.atmosenv.2017.12.004

Patel, A., & Rastogi, N. (2018b). Oxidative potential of ambient fine aerosol over a semi-urban site in the Indo-Gangetic Plain. *Atmospheric Environment*, *175*(November 2017), 127–134. https://doi.org/10.1016/j.atmosenv.2017.12.004

Peel, J. L., Haeuber, R., Garcia, V., Russell, A. G., & Neas, L. (2013). Impact of nitrogen and climate change interactions on ambient air pollution and human health. *Biogeochemistry*, *114*(1–3), 121–134. https://doi.org/10.1007/s10533-012-9782-4

Pietrogrande, M. C., Dalpiaz, C., Dell'Anna, R., Lazzeri, P., Manarini, F., Visentin, M., & Tonidandel, G. (2018a). Chemical composition and oxidative potential of atmospheric coarse particles at an industrial and urban background site in the alpine region of northern Italy. *Atmospheric Environment*, *191*(August), 340–350. https://doi.org/10.1016/j.atmosenv.2018.08.022

Pietrogrande, M. C., Dalpiaz, C., Dell'Anna, R., Lazzeri, P., Manarini, F., Visentin, M., & Tonidandel, G. (2018b). Chemical composition and oxidative potential of atmospheric coarse particles at an industrial and urban background site in the alpine region of northern Italy. *Atmospheric Environment*, *191*(August), 340–350. https://doi.org/10.1016/j.atmosenv.2018.08.022

Pison, I., & Menut, L. (2004). Quantification of the impact of aircraft traffic emissions on tropospheric ozone over Paris area. *Atmospheric Environment*, *38*(7), 971–983. https://doi.org/10.1016/j.atmosenv.2003.10.056

Pitts, J. N. J., Hammond, G. S., & Noyes, W. A. J. (1969). *Advances in Photochemistry* (Vol. 7). Interscience Publishers. https://doi.org/10.1063/1.2807549

Puthussery, J. V., Singh, A., Rai, P., Bhattu, D., Kumar, V., Vats, P., Furger, M., Rastogi, N., Slowik, J. G., Ganguly, D., Prevot, A. S. H., Tripathi, S. N., & Verma, V. (2020). Real-Time Measurements of PM 2.5 Oxidative Potential Using a Dithiothreitol Assay in Delhi, India. *Environmental Science & Technology Letters*. https://doi.org/10.1021/acs.estlett.0c00342

Puthussery, J. V., Zhang, C., & Verma, V. (2018). Development and field testing of an online instrument for measuring the real-time oxidative potential of ambient particulate matter based on dithiothreitol assay. *Atmospheric Measurement Techniques*, *11*(10), 5767–5780. https://doi.org/10.5194/amt-11-5767-2018

Quan, J., Tie, X., Zhang, Q., Liu, Q., Li, X., Gao, Y., & Zhao, D. (2014). Characteristics of heavy aerosol pollution during the 2012-2013 winter in Beijing, China. *Atmospheric Environment*, *88*, 83–89. https://doi.org/10.1016/j.atmosenv.2014.01.058

Rai, P., Slowik, J. G., Furger, M., El Haddad, I., Visser, S., Tong, Y., Singh, A., Wehrle, G., Kumar, V., Tobler, A. K., Bhattu, D., Wang, L., Ganguly, D., Rastogi, N., Huang, R. J., Necki, J., Cao, J., Tripathi, S. N., Baltensperger, U., & Prevot, A. S. H. (2021). Highly time-resolved measurements of element concentrations in PM10 and PM2.5: Comparison of Delhi, Beijing, London, and Krakow. *Atmospheric Chemistry and Physics*, *21*(2), 717–730. https://doi.org/10.5194/acp-21-717-2021

Rai, P., Slowik, J. G., Furger, M., Haddad, I. El, Visser, S., Tong, Y., Singh, A., Wehrle, G., Kumar, V., Tobler, A. K., Bhattu, D., & Wang, L. (2021). Highly time-resolved measurements of element concentrations in PM10 and PM 2.5: comparison of Delhi, Beijing, London, and Krakow. *Atmos. Chem. Phys*, *21*, 717–730. https://doi.org/https://doi.org/10.5194/acp-21-717-2021

Rattanavaraha, W., Rosen, E., Zhang, H., Li, Q., Pantong, K., & Kamens, R. M. (2011). The

reactive oxidant potential of different types of aged atmospheric particles: An outdoor chamber study. *Atmospheric Environment*, *45*(23), 3848–3855. https://doi.org/10.1016/j.atmosenv.2011.04.002

Rui, W., Guan, L., Zhang, F., Zhang, W., & Ding, W. (2016). PM2.5-induced oxidative stress increases adhesion molecules expression in human endothelial cells through the ERK/AKT/NF-$κ$B-dependent pathway. *Journal of Applied Toxicology*, *36*(1), 48–59. https://doi.org/10.1002/jat.3143

Sacks, J. D., Stanek, L. W., Luben, T. J., Johns, D. O., Buckley, B. J., Brown, J. S., & Ross, M. (2011). Particulate matter-induced health effects: Who is susceptible? *Environmental Health Perspectives*, *119*(4), 446–454. https://doi.org/10.1289/ehp.1002255

Sahu, S. K., & Kota, S. H. (2017). Significance of PM2.5 air quality at the Indian capital. *Aerosol and Air Quality Research*, *17*(2), 588–597. https://doi.org/10.4209/aaqr.2016.06.0262

Schaumann, F., Borm, P. J. A., Herbrich, A., Knoch, J., Pitz, M., Schins, R. P. F., Luettig, B., Hohlfeld, J. M., Heinrich, J., & Krug, N. (2004). Metal-rich ambient particles (particulate matter2.5) cause airway inflammation in healthy subjects. *American Journal of Respiratory and Critical Care Medicine*, *170*(8), 898–903. https://doi.org/10.1164/rccm.200403-423OC

Seigneur, C. (2019). *Air Pollution Concepts, Theory, and Applications* (1st ed., Issue November). Cambridge University Press. https://doi.org/10.1016/B978-0-12-809633-8.02081-1

Shi, T., Schins, R. P. F., Knaapen, A. M., Kuhlbusch, T., Pitz, M., Heinrich, J., & Borm, P. J. A. (2003). Hydroxyl radical generation by electron paramagnetic resonance as a new method to monitor ambient particulate matter composition. *Journal of Environmental Monitoring*, *5*(4), 550–556. https://doi.org/10.1039/b303928p

Shi, Z., Vu, T., Kotthaus, S., Harrison, R. M., Grimmond, S., Yue, S., Zhu, T., Lee, J., Han, Y., Demuzere, M., Dunmore, R. E., Ren, L., Liu, D., Wang, Y., Wild, O., Allan, J., Joe Acton, W., Barlow, J., Barratt, B., … Zheng, M. (2019). Introduction to the special issue "in-depth study of air pollution sources and processes within Beijing and its surrounding region (APHH-Beijing)." *Atmospheric Chemistry and Physics*, *19*(11), 7519–7546. https://doi.org/10.5194/acp-19-7519-2019

Shirmohammadi, F., Wang, D., Hasheminassab, S., Verma, V., Schauer, J. J., Shafer, M. M., & Sioutas, C. (2016). Oxidative potential of on-road fine particulate matter (PM2.5) measured on major freeways of Los Angeles, CA, and a 10-year comparison with earlier roadside studies. *Atmospheric Environment*, *148*, 102–114. https://doi.org/10.1016/j.atmosenv.2016.10.042

Shirmohammadi, F., Wang, D., Hasheminassab, S., Verma, V., Schauer, J. J., Shafer, M. M., & Sioutas, C. (2017). Oxidative potential of on-road fine particulate matter (PM2.5) measured on major freeways of Los Angeles, CA, and a 10-year comparison with earlier roadside studies. *Atmospheric Environment*, *148*, 102–114. https://doi.org/10.1016/j.atmosenv.2016.10.042

Shlyonsky, V., Boom, A., & Mies, F. (2016). Hydrogen Peroxide and Sodium Transport in the

Lung and Kidney. *BioMed Research International*, *2016*, 9512807. https://doi.org/10.1155/2016/9512807

Simonetti, G., Conte, E., Massimi, L., Frasca, D., Perrino, C., & Canepari, S. (2018). Oxidative potential of particulate matter components generated by specific emission sources. *Journal of Aerosol Science*, *126*(July), 99–109. https://doi.org/10.1016/j.jaerosci.2018.08.011

Singh, R. P., & Sharma, M. (2012). Enhancement of BC concentration associated with Diwali festival in India. *International Geoscience and Remote Sensing Symposium (IGARSS)*, 3685–3688. https://doi.org/10.1109/IGARSS.2012.6350616

Song, C., He, J., Wu, L., Jin, T., Chen, X., Li, R., Ren, P., Zhang, L., & Mao, H. (2017). Health burden attributable to ambient PM2.5 in China. *Environmental Pollution*, *223*, 575–586. https://doi.org/10.1016/j.envpol.2017.01.060

Strak, M., Janssen, N. A. H., Godri, K. J., Gosens, I., Mudway, I. S., Cassee, F. R., Lebret, E., Kelly, F. J., Harrison, R. M., Brunekreef, B., Steenhof, M., & Hoek, G. (2012). Respiratory health effects of airborne particulate matter: The role of particle size, composition, and oxidative potential-the RAPTES project. *Environmental Health Perspectives*, *120*(8), 1183–1189. https://doi.org/10.1289/ehp.1104389

Stull, R. (2017). Practical Meteorology - An Algebra-based Survey of Atmospheric Science. In *University of British Columbia*. https://www.eoas.ubc.ca/books/Practical_Meteorology/prmet/PracticalMet_WholeBook-v1_00b.pdf

Sun, Y., Jiang, Q., Wang, Z., Fu, P., Li, J., Yang, T., & Yin, Y. (2014). Investigation of the sources and evolution processes of severe haze pollution in Beijing in January 2013. *Journal of Geophysical Research: Atmospheres*, *119*, 4380–4398. https://doi.org/10.1002/2014JD021641.Received

Szigeti, Tamas, Dunster, C., Cattaneo, A., Cavallo, D., Spinazz??, A., Saraga, D. E., Sakellaris, I. A., de Kluizenaar, Y., Cornelissen, E. J. M., H??nninen, O., Peltonen, M., Calzolai, G., Lucarelli, F., Mandin, C., Bartzis, J. G., Z??ray, G., & Kelly, F. J. (2016). Oxidative potential and chemical composition of PM2.5 in office buildings across Europe - The OFFICAIR study. *Environment International*, *92–93*, 324–333. https://doi.org/10.1016/j.envint.2016.04.015

Szigeti, Tamás, Dunster, C., Cattaneo, A., Cavallo, D., Spinazzè, A., Saraga, D. E., Sakellaris, I. A., de Kluizenaar, Y., Cornelissen, E. J. M., Hänninen, O., Peltonen, M., Calzolai, G., Lucarelli, F., Mandin, C., Bartzis, J. G., Záray, G., & Kelly, F. J. (2016). Oxidative potential and chemical composition of PM2.5 in office buildings across Europe - The OFFICAIR study. *Environment International*, *92–93*, 324–333. https://doi.org/10.1016/j.envint.2016.04.015

The World Bank Group. (2020). *Databank | World Development Indicators*. https://databank.worldbank.org/WHO-Interim-Target-1/id/8030eb3e

Timmons, D., Zirogiannis, N., & Lutz, M. (2016). Location matters: Population density and carbon emissions from residential building energy use in the United States. *Energy Research and Social Science*, *22*, 137–146. https://doi.org/10.1016/j.erss.2016.08.011

Tuet, W. Y., Chen, Y., Fok, S., Champion, J. A., & Ng, N. L. (2017). Inflammatory responses to secondary organic aerosols (SOA) generated from biogenic and anthropogenic precursors. *Atmospheric Chemistry and Physics Discussion*, *March*, 1–42. https://doi.org/10.5194/acp-2017-262

U.S. EPA. (2016a). Integrated science assessment for oxides of nitrogen - health criteria (final report). In *Washington D.C.: EPA/600/R-08/071*. https://doi.org/10.1080/00107510412331283531

U.S. EPA. (2016b). *Monitoring PM2.5 in Ambient Air Using Designated Reference or Class I Equivalent Methods*.

UNCCD COP 14. (2020). *Information about Delhi*. United Nations Convention to Combat Desertification.

United Nations, Department of Economic and Social Affairs, P. D. (2019). (2018). World Urbanization Prospects: The 2018 Revision (ST/ESA/SER.A/420). In *New York: United Nations*. https://population.un.org/wup/Publications/Files/WUP2018-Report.pdf

Valavanidis, A., Vlachogianni, T., Fiotakis, K., & Loridas, S. (2013). Pulmonary oxidative stress, inflammation and cancer: Respirable particulate matter, fibrous dusts and ozone as major causes of lung carcinogenesis through reactive oxygen species mechanisms. *International Journal of Environmental Research and Public Health*, *10*(9), 3886–3907. https://doi.org/10.3390/ijerph10093886

Verma, V., Rico-Martinez, R., Kotra, N., King, L., Liu, J., Snell, T. W., & Weber, R. J. (2012). Contribution of water-soluble and insoluble components and their hydrophobic/hydrophilic subfractions to the reactive oxygen species-generating potential of fine ambient aerosols. *Environmental Science and Technology*, *46*(20), 11384–11392. https://doi.org/10.1021/es302484r

Viegi, G., Simoni, M., Scognamiglio, A., Baldacci, S., Pistelli, F., Carrozzi, L., & Annesi-Maesano, I. (2004). Indoor air pollution and airway disease. *The International Journal of Tuberculosis and Lung Disease : The Official Journal of the International Union against Tuberculosis and Lung Disease*, *8*(12), 1401–1415.

Visentin, M., Pagnoni, A., Sarti, E., & Pietrogrande, M. C. (2016). Urban PM2.5 oxidative potential: Importance of chemical species and comparison of two spectrophotometric cell-free assays. *Environmental Pollution*, *219*, 72–79. https://doi.org/10.1016/j.envpol.2016.09.047

Wallington, T. J., Atkinson, R., Winer, A. M., & Pitts, J. N. (1987). A study of the reaction NO3 + NO2 + M → N2O5 + M(M = N2, O2). *International Journal of Chemical Kinetics*, *19*(3), 243–249. https://doi.org/10.1002/kin.550190307

Wang, J., Lin, X., Lu, L., Wu, Y., Zhang, H., Lv, Q., Liu, W., Zhang, Y., & Zhuang, S. (2018). Temporal variation of oxidative potential of water soluble components of ambient PM2.5measured by dithiothreitol (DTT) assay. *Science of the Total Environment*, *649*, 969–978. https://doi.org/10.1016/j.scitotenv.2018.08.375

Wang, J., Lin, X., Lu, L., Wu, Y., Zhang, H., Lv, Q., Liu, W., Zhang, Y., & Zhuang, S. (2019). Temporal variation of oxidative potential of water soluble components of ambient

PM2.5measured by dithiothreitol (DTT) assay. *Science of the Total Environment*, *649*, 969–978. https://doi.org/10.1016/j.scitotenv.2018.08.375

Wang, Shaojian, Zhou, C., Wang, Z., Feng, K., & Hubacek, K. (2017). The characteristics and drivers of fine particulate matter (PM2.5) distribution in China. *Journal of Cleaner Production*, *142*, 1800–1809. https://doi.org/10.1016/j.jclepro.2016.11.104

Wang, Shunyao, Ye, J., Soong, R., Wu, B., Yu, L., Simpson, A. J., & Chan, A. W. H. (2018). Relationship between chemical composition and oxidative potential of secondary organic aerosol from polycyclic aromatic hydrocarbons. *Atmospheric Chemistry and Physics*, *18*(6), 3987–4003. https://doi.org/10.5194/acp-18-3987-2018

Wang, T., Nie, W., Gao, J., Xue, L. K., Gao, X. M., Wang, X. F., Qiu, J., Poon, C. N., Meinardi, S., Blake, D., Wang, S. L., Ding, A. J., Chai, F. H., Zhang, Q. Z., & Wang, W. X. (2010). Air quality during the 2008 Beijing Olympics: Secondary pollutants and regional impact. *Atmospheric Chemistry and Physics*, *10*(16), 7603–7615. https://doi.org/10.5194/acp-10-7603-2010

Wang, Y., Wild, O., Chen, X., Wu, Q., Gao, M., Chen, H., Qi, Y., & Wang, Z. (2020). Health impacts of long-term ozone exposure in China over 2013–2017. *Environment International*, *144*(April). https://doi.org/10.1016/j.envint.2020.106030

Watson, J. G. (2002). Visibility: Science and regulation. *Journal of the Air and Waste Management Association*, *52*(6), 628–713. https://doi.org/10.1080/10473289.2002.10470813

Weschler, C. J. (2006). Ozone's impact on public health: Contributions from indoor exposures to ozone and products of ozone-initiated chemistry. *Environmental Health Perspectives*, *114*(10), 1489–1496. https://doi.org/10.1289/ehp.9256

Willis, R. J., & Kratzing, C. C. (1974). Ascorbic Acid in Rat Lung. *Biochemical and Biophysical Research Communications*, *59*(4).

World Health Organisation. (2020a). *Ambient air pollution: Health impacts*. https://www.who.int/airpollution/ambient/health-impacts/en/

World Health Organisation. (2020b). *Metrics: Disability-Adjusted Life Year (DALY)*. https://www.who.int/healthinfo/global_burden_disease/metrics_daly/en/

World Health Organisation Regional Office For Europe. (2013). *Health effects of particulate matter*.

Xavier, P. K., Marzin, C., & Goswami, B. N. (2007). An objective definition of the Indian summer monsoon season and a new perspective on the ENSO-monsoon relationship. *Quarterly Journal of the Royal Meteorological Society*, *133*, 749–764. https://doi.org/10.1002/qj

Xie, Y., Dai, H., Zhang, Y., Wu, Y., Hanaoka, T., & Masui, T. (2019). Comparison of health and economic impacts of PM2.5 and ozone pollution in China. *Environment International*, *130*(March), 104881. https://doi.org/10.1016/j.envint.2019.05.075

Xu, F., Qiu, X., Hu, X., Shang, Y., Pardo, M., Fang, Y., Wang, J., Rudich, Y., & Zhu, T. (2018). Effects on IL-1B signaling activation induced by water and organic extracts of fine

particulate matter (PM2.5) in vitro. *Environmental Pollution*, *237*, 592–600. https://doi.org/10.1016/j.envpol.2018.02.086

Xu, J., Zhang, Q., Chen, M., Ge, X., Ren, J., & Qin, D. (2014). Chemical composition, sources, and processes of urban aerosols during summertime in northwest China: Insights from high-resolution aerosol mass spectrometry. *Atmospheric Chemistry and Physics*, *14*(23), 12593–12611. https://doi.org/10.5194/acp-14-12593-2014

Xu, Jingsha, Liu, D., Wu, X., Vu, T., Zhang, Y., Fu, P., Sun, Y., Xu, W., Zheng, B., Harrison, R., & Shi, Z. (2020). Source Apportionment of Fine Aerosol at an Urban Site of Beijing using a Chemical Mass Balance Model. *Atmospheric Chemistry and Physics Discussions*, *2*, 1–28. https://doi.org/10.5194/acp-2020-1020

Xu, W., Li, Q., Shang, J., Liu, J., Feng, X., & Zhu, T. (2015). Heterogeneous oxidation of SO2 by O3-aged black carbon and its dithiothreitol oxidative potential. *Journal of Environmental Sciences (China)*, *36*(1974), 56–62. https://doi.org/10.1016/j.jes.2015.02.014

Yang, A., Jedynska, A., Hellack, B., Kooter, I., Hoek, G., Brunekreef, B., Kuhlbusch, T. A. J., Cassee, F. R., & Janssen, N. A. H. (2013). Measurement of the oxidative potential of PM2.5 and its constituents: The effect of extraction solvent and filter type. *Atmospheric Environment*, *83*, 35–42. https://doi.org/10.1016/j.atmosenv.2013.10.049

Yang, F., Liu, C., & Qian, H. (2021). Comparison of indoor and outdoor oxidative potential of PM2.5: pollution levels, temporal patterns, and key constituents. *Environment International*, *155*, 106684. https://doi.org/10.1016/j.envint.2021.106684

Yang, Y., Qu, S., Cai, B., Liang, S., Wang, Z., Wang, J., & Xu, M. (2020). Mapping global carbon footprint in China. *Nature Communications*, *11*(1), 6–13. https://doi.org/10.1038/s41467-020-15883-9

Yao, X., Chan, C. K., Fang, M., Cadle, S., Chan, T., Mulawa, P., He, K., & Ye, B. (2002). The water-soluble ionic composition of PM2.5 in Shanghai and Beijing, China. *Atmospheric Environment*, *36*(26), 4223–4234. https://doi.org/10.1016/S1352-2310(02)00342-4

Yu, M., Li, Q., Hayes, M. J., Svoboda, M. D., & Heim, R. R. (2014). Are droughts becoming more frequent or severe in China based on the standardized precipitation evapotranspiration index: 1951-2010? *International Journal of Climatology*, *34*(3), 545–558. https://doi.org/10.1002/joc.3701

Yu, S. Y., Liu, W. J., Xu, Y. S., Yi, K., Zhou, M., Tao, S., & Liu, W. X. (2018). Characteristics and oxidative potential of atmospheric PM2.5 in Beijing: Source apportionment and seasonal variation. *Science of the Total Environment*, *650*, 277–287. https://doi.org/10.1016/j.scitotenv.2018.09.021

Yuan, Q., Lai, S., Song, J., Ding, X., Zheng, L., Wang, X., Zhao, Y., Zheng, J., Yue, D., Zhong, L., Niu, X., & Zhang, Y. (2018). Seasonal cycles of secondary organic aerosol tracers in rural Guangzhou, Southern China: The importance of atmospheric oxidants. *Environmental Pollution*, *240*(2), 884–893. https://doi.org/10.1016/j.envpol.2018.05.009

Zeng, Y., Yu, H., Zhao, H., Stephens, B., & Verma, V. (2021). Influence of environmental conditions on the dithiothreitol (DTT)-Based oxidative potential of size-resolved indoor

particulate matter of ambient origin. *Atmospheric Environment*, *255*(January), 118429. https://doi.org/10.1016/j.atmosenv.2021.118429

Zhang, Q., Worsnop, D. R., Canagaratna, M. R., & Jimenez, J. L. (2005). Hydrocarbon-like and oxygenated organic aerosols in Pittsburgh: Insights into sources and processes of organic aerosols. *Atmospheric Chemistry and Physics*, *5*(12), 3289–3311. https://doi.org/10.5194/acp-5-3289-2005

Zhang, R., Guo, S., Zamora, M. L., & Hu, M. (2015). Reply to Li et al.: Insufficient evidence for the contribution of regional transport to severe haze formation in Beijing. *Proceedings of the National Academy of Sciences of the United States of America*, *112*(21), E2741. https://doi.org/10.1073/pnas.1503855112

Zhao, P., & Zhang, M. (2018). The impact of urbanisation on energy consumption: A 30-year review in China. *Urban Climate*, *24*(November 2017), 940–953. https://doi.org/10.1016/j.uclim.2017.11.005

Zheng, S., Singh, R. P., Wu, Y., & Wu, C. (2017a). A Comparison of Trace Gases and Particulate Matter over Beijing (China) and Delhi (India). *Water, Air, and Soil Pollution*, *228*(5). https://doi.org/10.1007/s11270-017-3360-2

Zheng, S., Singh, R. P., Wu, Y., & Wu, C. (2017b). A Comparison of Trace Gases and Particulate Matter over Beijing (China) and Delhi (India). *Water, Air, and Soil Pollution*, *228*(5). https://doi.org/10.1007/s11270-017-3360-2

Zhou, J., Bruns, E. A., Zotter, P., Stefenelli, G., Prévôt, A. S. H., Baltensperger, U., El-Haddad, I., & Dommen, J. (2018). Development, characterization and first deployment of an improved online reactive oxygen species analyzer. *Atmospheric Measurement Techniques*, *11*(1), 65–80. https://doi.org/10.5194/amt-11-65-2018

APPENDICES

Figure S49 and Figure S50 show the t-test results for DTTv and $PM_{2.5}$ concentration across different campaigns and diurnally, as a series of box plots. The red lines between the "boxes" / campaigns show significant difference.

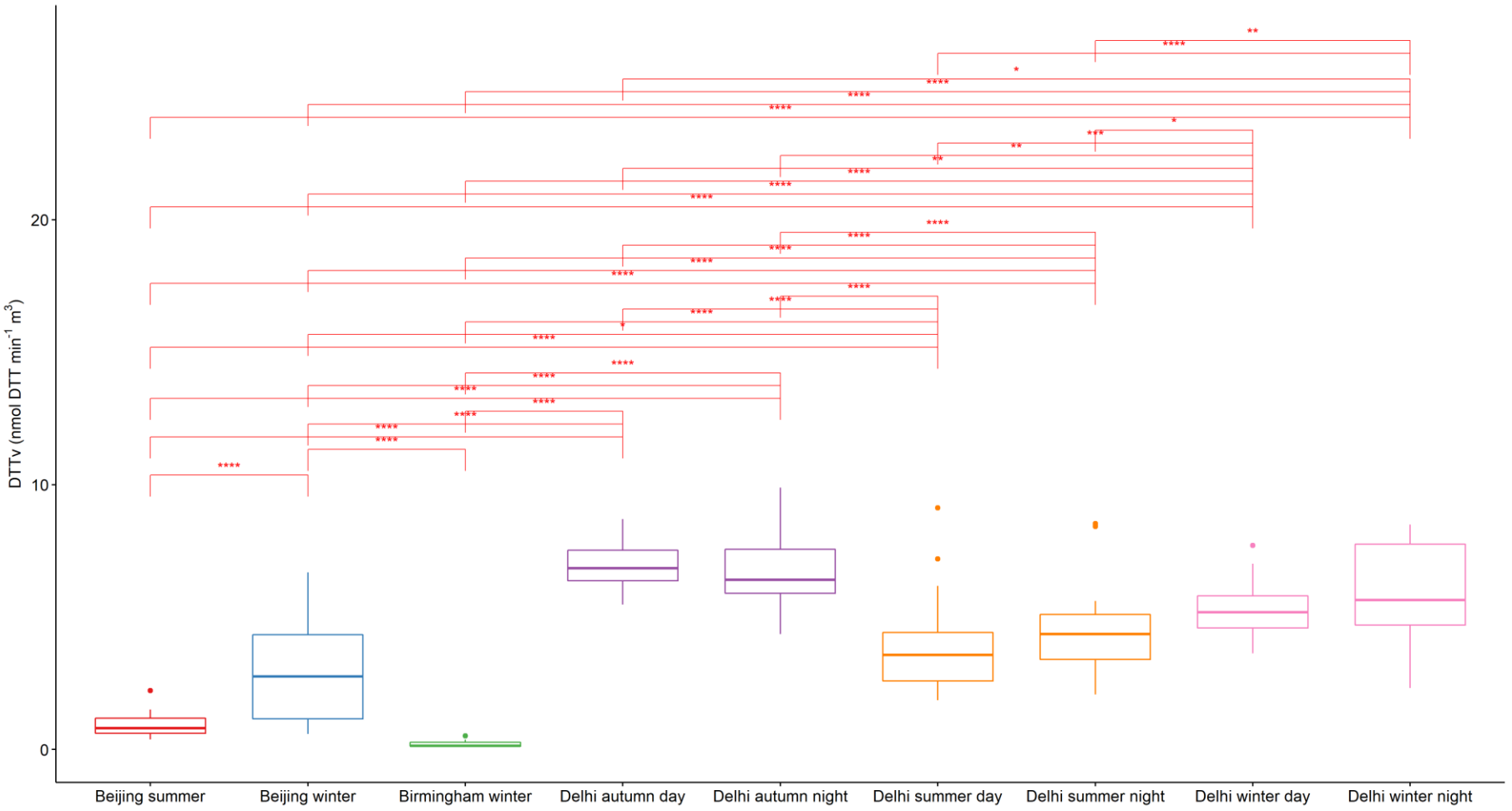

*Figure S49: Box plots and pairwise unpaired T-test of DTTv results for all field campaigns; where day / night samples have been separated. P-value adjustment was done using Benjamini & Hochberg (BH) method. The significance levels are * = 95 %, ** = 99 %, *** = 99*

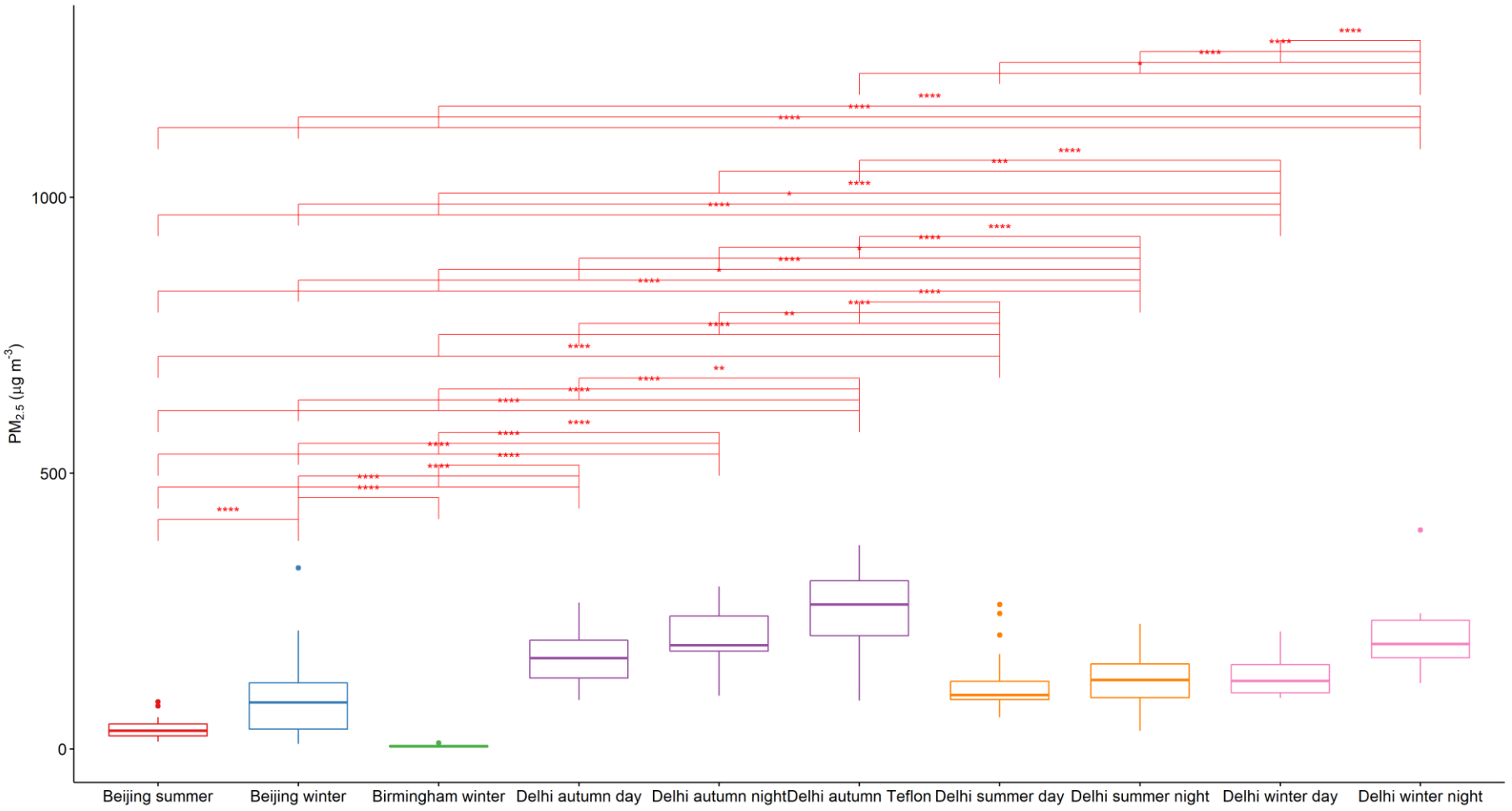

*Figure S50: Box plots and pairwise unpaired T-test of $PM_{2.5}$ results for all field campaigns; where day / night samples have been separated. P-value adjustment was done using Benjamini & Hochberg (BH) method. The significance levels are * = 95 %, ** = 99 %, *** = 99*

Table S9 shows the gradient, Pearson correlation coefficient, and p-values for different $PM_{2.5}$ composition species correlated with DTTm for the Delhi winter night samples.

Table S9: Highly correlated XRF detected metal species with DTTm for Delhi winter night samples. All species with a p-value > 0.05 and/or rp ≤ 0.5 have been excluded. The gradients are shown with the standard error; the units are pmol DTT min^{-1} ng^{-1} for metals, $°C^{-1}$ for temperature, $\%RH^{-1}$ for RH, m^{-1} for visibility, and μg^{-1} m^{3} for AMS species.

Specie	r	p-value	n	Gradient
All elements (ICPMS)	0.50	0.03	18	0.712 ± 0.31
Air temperature	0.45	0.04	21	1.99 ± 0.92
Visibility	0.50	0.02	21	0.00861 ± 0.0035
RH	-0.47	0.03	21	-0.366 ± 0.16
Magnesium	0.51	0.02	21	4.30 ± 1.7
Sodium	0.48	0.03	21	2.21 ± 0.93
Fe	0.50	0.03	18	2.07 ± 0.89
Li	0.62	<0.01	18	1439 ± 458
Mg	0.49	0.04	18	4.27 ± 1.9
Sr	0.51	0.03	18	94.6 ± 40
Ca (XRF)	0.90	0.04	5	3.22 ± 0.89
HOA	-0.76	0.02	9	-0.563 ± 0.18
BBOA	-0.73	0.02	9	-1.30 ± 0.46
COA	-0.80	0.01	9	-4.27 ± 1.2

Table S10 shows the gradient, Pearson correlation coefficient, and p-values for different $PM_{2.5}$ composition species correlated with DTTm for the Delhi autumn daytime samples.

Table S10: Highly correlated species with DTTm for Delhi autumn daytime samples that do not appear in the correlation matrix. All species with a p-value > 0.05 and/or $r_p \leq 0.5$ have been excluded. The gradients are shown with the standard error; the units are pmol DTT min^{-1} ng^{-1} for each specie.

Specie	r	p-value	n	Gradient
Ce	0.95	<0.01	14	358 ± 34
V	0.93	<0.01	14	287 ± 32
Ni	0.82	<0.01	14	248 ± 49
Sr	0.93	<0.01	14	65.5 ± 7.4
Mn	0.9	<0.01	14	24.3 ± 3.4
Ba	0.87	<0.01	14	23.9 ± 3.9
Wind speed	0.74	<0.01	14	21.9 ± 5.7
Ti	0.9	<0.01	14	19.8 ± 2.8
Chloride	0.65	0.01	14	2.52 ± 0.94
Magnesium	0.92	<0.01	14	2.02 ± 0.25
Potassium	0.91	<0.01	13	1.56 ± 0.21
Na	0.59	0.03	14	1.51 ± 0.59
K	0.94	<0.01	14	1.38 ± 0.14
Mg	0.91	<0.01	14	1.30 ± 0.17
All elements ICPMS	0.86	<0.01	14	0.760 ± 0.13
Al	0.93	<0.01	14	0.681 ± 0.075
Calcium	0.93	<0.01	14	0.648 ± 0.074
Fe	0.91	<0.01	14	0.555 ± 0.072
EC	0.57	0.03	14	0.511 ± 0.21
Ca	0.9	<0.01	14	0.492 ± 0.071
OC	0.93	<0.01	14	0.140 ± 0.016
TC	0.91	<0.01	14	0.122 ± 0.016
Soil dust ICPMS	0.92	<0.01	14	0.106 ± 0.013
visibility	0.66	0.01	14	0.0149 ± 0.0049
NO2	-0.55	0.04	14	-0.210 ± 0.092
Ammonium	-0.58	0.05	12	-0.284 ± 0.13
HOA	-0.65	0.02	13	-0.899 ± 0.32
RH	-0.77	<0.01	14	-1.46 ± 0.35
OPOA	-0.92	<0.01	13	-1.52 ± 0.20
BBOA	-0.66	0.01	13	-2.78 ± 0.96
LVOOA	-0.69	<0.01	13	-3.40 ± 1.1
Atmospheric pressure	-0.64	0.01	14	-4.88 ± 1.7
Dew point atmosphere	-0.64	0.01	14	-4.93 ± 1.7

Table S11 shows the gradient, Pearson correlation coefficient, and p-values for different $PM_{2.5}$ composition species correlated with DTTm for the Delhi autumn night samples.

Table S11: Highly correlated species with DTTm for Delhi autumn nighttime samples that do not appear in the correlation matrix. All species with a p-value > 0.05 and/or $r_p \leq 0.5$ have been excluded. The gradients are shown with the standard error; the units are pmol DTT min^{-1} ng^{-1} for each specie.

Specie	r	p-value	n	Gradient
V	0.84	<0.01	16	458 ± 79
Ce	0.6	0.01	16	287 ± 103
Ni	0.53	0.03	16	260 ± 111
Sr	0.81	<0.01	16	140 ± 28
Ti	0.81	<0.01	16	43.3 ± 8.3
Mn	0.87	<0.01	16	38.7 ± 5.9
Mg	0.85	<0.01	16	2.74 ± 0.45
Magnesium	0.8	<0.01	16	1.92 ± 0.38
Na	0.54	0.03	16	1.86 ± 0.78
Sodium	0.87	<0.01	16	1.75 ± 0.27
Fe	0.9	<0.01	16	1.17 ± 0.15
Al	0.81	<0.01	16	1.14 ± 0.22
Ca	0.83	<0.01	16	0.996 ± 0.18
Calcium	0.84	<0.01	16	0.929 ± 0.16
All elements ICPMS	0.57	0.02	16	0.638 ± 0.25
Soil dust ICPMS	0.86	<0.01	16	0.213 ± 0.033
OC	0.75	<0.01	16	0.178 ± 0.042
TC	0.72	<0.01	16	0.123 ± 0.032
Visibility	0.51	0.04	16	0.0112 ± 0.0051
Ammonium	-0.59	0.02	16	-0.217 ± 0.079
OPOA	-0.6	0.02	15	-1.01 ± 0.37
RH	-0.75	<0.01	16	-1.30 ± 0.30
Atmospheric pressure	-0.73	<0.01	16	-3.99 ± 1.0

ATMOSPHERIC CONDITIONS AND COMPOSITION THAT INFLUENCE $PM_{2.5}$ OXIDATIVE POTENTIAL IN BEIJING, CHINA

The contributions of this thesis' author to the Campbell et al., 2020 paper are DTT OP results for the Beijing winter and summer campaigns, including the quality assurance data associated with these measurements such as filter blank analysis, PQN positive standards, and calibration graphs. The complete DTT protocol presented in this thesis was also attached to the supplementary information of the paper. All other work on the paper, including statistical analysis and writing was performed by the other authors.

p221

https://doi.org/10.5194/acp-2020-1024
Preprint. Discussion started: 13 October 2020

Atmospheric Chemistry and Physics Discussions

Atmospheric conditions and composition that influence $PM_{2.5}$ oxidative potential in Beijing, China

Steven J. Campbell[1,2*], Kate Wolfer[1*], Battist Utinger[1], Joe Westwood[2], Zhi-hui Zhang[1,2], Nicolas Bukowiecki[1], Sarah S. Steimer[2§], Tuan V. Vu[3#], Jingsha Xu[3], Nicholas Straw[4], Steven Thomson[3], Atallah Elzein[5], Yele Sun[6], Di Liu[3,6], Linjie Li[6], Pingqing Fu[8], Alastair C. Lewis[5,7], Roy M. Harrison[3†], William J. Bloss[3], Miranda Loh[9], Mark R. Miller[4], Zongbo Shi[3] and Markus Kalberer[1,2]

[1]Department of Environmental Sciences, University of Basel, Basel, Switzerland
[2]Department of Chemistry, University of Cambridge, Cambridge, UK
[3]School of Geography Earth and Environmental Sciences, University of Birmingham, Birmingham, UK
[4]Centre for Cardiovascular Science, Queen's Medical Research Institute, University of Edinburgh, Edinburgh, UK
[5]Wolfson Atmospheric Chemistry Laboratories, Department of Chemistry, University of York, York, UK
[6]State Key Laboratory of Atmospheric Boundary Layer Physics and Atmospheric Chemistry, Institute of Atmospheric Physics, Chinese Academy of Sciences, Beijing, China
[7]National Centre for Atmospheric Science, University of York, York, UK
[8]Institute of Surface Earth System Science, Tianjin University, Tianjin, China
[9]Institute of Occupational Medicine, Edinburgh, UK

[§] Now at: Department of Environmental Science, Stockholm University, Stockholm, Sweden
[†]Also at: Department of Environmental Sciences / Center of Excellence in Environmental Studies, King Abdulaziz University, PO Box 80203, Jeddah, 21589, Saudi Arabia
[#]Now at School of Public Health, Imperial College London, London, UK

*Authors contributed equally to the manuscript

Correspondence to:

Abstract. Epidemiological studies have consistently linked exposure to $PM_{2.5}$ with adverse health effects. The oxidative potential (OP) of aerosol particles has been widely suggested as a measure of their potential toxicity. Several acellular chemical assays are now readily employed to measure OP, however, uncertainty remains regarding the atmospheric conditions and specific chemical components of $PM_{2.5}$ that drive OP. A limited number of studies have simultaneously utilised multiple OP assays with a wide range of concurrent measurements and investigated the seasonality of $PM_{2.5}$ OP. In this work, filter samples were collected in winter 2016 and summer 2017 during the atmospheric pollution and human health in a Chinese megacity (APHH-Beijing) campaign, and $PM_{2.5}$ OP was analysed using four acellular methods; ascorbic acid (AA), dithiothreitol (DTT), 2-7-dichlorofluoroscin/hydrogen peroxidase (DCFH) and electron paramagnetic resonance spectroscopy (EPR). Positive correlations of OP normalised per volume of air of all four assays with overall $PM_{2.5}$ mass was observed, with stronger correlations in the winter compared to the summer. In contrast, when OP assay values were normalised for particle mass, days with higher $PM_{2.5}$ mass concentrations ($\mu g\ m^{-3}$) were found to have lower intrinsic mass-normalised OP values as measured

https://doi.org/10.5194/acp-2020-1024
Preprint. Discussion started: 13 October 2020

Atmospheric Chemistry and Physics Discussions

by AA and DTT. This indicates that total $PM_{2.5}$ mass concentrations alone might not always be the best indicator for particle toxicity. Univariate analysis of OP values and an extensive range of additional measurements, 107 in total, including $PM_{2.5}$ composition, gas phase composition and meteorological data, provides detailed insight into chemical components or atmospheric processes that determine $PM_{2.5}$ OP variability. Multivariate statistical analyses highlighted associations of OP assay responses with varying chemical components in $PM_{2.5}$ for both mass- and volume-normalised data. Variable selection was used to produce subsets of measurements indicative of $PM_{2.5}$ sources, and used to model OP response; AA and DTT assays were well predicted by small panels of measurements, and indicated fossil fuel combustion processes, vehicle emissions and biogenic SOA as most influential in the assay response. Through comparative analysis of both mass- and volume-normalised data we also demonstrate the importance of also considering mass-normalised OP when correlating with particle composition measurements, which provides a more nuanced picture of compositional drivers and sources of OP compared to volume-normalised analysis, and which may be more useful in temporal and site comparative contexts.

1 Introduction

Large-scale epidemiological studies have consistently linked the exposure of airborne particulate matter (PM) with a range of adverse human health effects (Hart et al., 2015; Laden et al., 2006; Lepeule et al., 2012). A recent study by the World Health Organisation estimated that 1 in 8 deaths globally in 2014 were linked to air pollution exposure (World Health Organisation, 2016) with urban areas in India and China particularly affected (Lelieveld et al., 2020). However, large uncertainty remains regarding the physical and chemical characteristics of PM that result in adverse health outcomes upon exposure (Bates et al., 2019).

Studies have suggested that oxidative stress promoted by PM components *in vivo* could be a key mechanism that results in adverse health outcomes (Donaldson and Tran, 2002; Knaapen et al., 2004; Øvrevik et al., 2015). Oxidative stress occurs when excess concentrations of reactive oxygen species (ROS) overwhelm cellular anti-oxidant defences, resulting in an imbalance of the oxidant-antioxidant ratio in favour of the former, which can subsequently lead to inflammation and disease (Knaapen et al., 2004; Li et al., 2003, 2008). The term ROS typically refers to H_2O_2, in some cases including organic peroxides, the hydroxyl radical (OH), superoxide (O_2^-) and organic oxygen-centred radicals. Particle-bound ROS is exogenously delivered into the lung through PM inhalation, and ROS can be produced *in vivo via* redox-chemistry initiated by certain particle components, in addition to baseline tissue ROS produced by metabolic processes (Dellinger et al., 2001). The capability of PM to produce ROS with subsequent depletion of anti-oxidants upon inhalation is defined as oxidative potential (OP) (Bates et al., 2019).

OP is a fairly simple measure of PM redox activity, but reflects a complex interplay of particle size, composition and chemistries which induce oxidative stress by free radical generation which triggers cellular signal transduction and damage. These effects can be both localised (to lung epithelial surfaces and alveoli, reviewed by (Tao et al., 2003)) and systemic (through immune system activation and cytokine release (Miyata and van Eeden, 2011), translocation of ultrafine particles into the circulatory system (Oberdorster et al., 1992), increased circulating monocytes (Tan et al., 2000), and propagation to

https://doi.org/10.5194/acp-2020-1024
Preprint. Discussion started: 13 October 2020


Atmospheric Chemistry and Physics Discussions

other cells and organs (Laing et al., 2010; Meng and Zhang, 2006). Oxidative stress is implicated in the majority of toxicological effects related to air pollution (Ghio et al., 2012; Kelly, 2003; Pope and Dockery, 2006; Risom et al., 2005). A rapid and simple metric to capture the oxidative exposure burden which can be easily implemented for epidemiological studies will enable greater insight into the mechanisms of PM toxicity beyond total PM mass exposure and the most commonly measured (generally non-redox-active) toxic components of PM, such as measures of elemental or organic carbon and PAH concentrations.

There are now a wide range of acellular chemical methods that attempt to quantify the entire OP of PM and particle-bound ROS, as typically acellular assays allow faster measurement and are less labour intensive compared to cell cultures or *in vivo* methods (Bates et al., 2019). These include, but are not limited to, the dithiothreitol assay (DTT), ascorbic acid assay (AA), 2-7-dichlorofluoroscein/hydrogen peroxidase assay (DCFH), electron paramagnetic spectroscopy (EPR), glutathione assay (GSH) and 9-(1,1,3,3,tetramethylisoindolin-2-yloxyl-5-ethynyl)-10-(phenylethynyl)anthracene (BPEAnit). These acellular assays all have differing sensitivities to specific particle components that may contribute to aerosol OP. For instance, DTT has been shown to be sensitive to soluble metals (Shinyashiki et al., 2009), including copper and manganese (Charrier et al., 2015; Charrier and Anastasio, 2012), as well as a range of organic particle components including water soluble organic carbon (WSOC, a mixture of 100's to 1000's of compounds), oxidised polycyclic aromatic hydrocarbons (PAHs) e.g. quinones (Chung et al., 2006; McWhinney et al., 2013a), and humic-like substances (HULIS) (Dou et al., 2015; Verma et al., 2015a). AA is particularly sensitive to redox-active transition metals, most notably Fe (Godri et al., 2011) and Cu (Janssen et al., 2014; Pant et al., 2015), and has demonstrated sensitivity to organic carbon (Calas et al., 2018) including secondary organic aerosol (Campbell et al., 2019b). EPR is applied to speciate and quantify radical species either bound to aerosol particles (Arangio et al., 2016; Campbell et al., 2019a; Gehling and Dellinger, 2013), so-called environmentally persistent free radicals (EPFR), or radicals formed upon suspension of particles into aqueous solution (Gehling et al., 2014; Tong et al., 2016, 2017) or in some cases into synthetic lung lining fluid (Tong et al., 2018) consisting of a mixture of AA, glutathione and uric acid. EPR has the advantage of not being influenced by the dark colour of particulate suspensions (detection is *via* magnetic excitation rather than magnetic absorbance), does not require extraction of the PM from the filter, and that speciation of the free radical generated can be explored using spin-trap reagents that are selective for specific radicals (Miller et al., 2009). The DCFH assay has been shown to be particularly sensitive to hydrogen peroxide (H_2O_2) and organic peroxides (Venkatachari and Hopke, 2008; Wragg et al., 2016), also present in secondary organic aerosol (SOA) particles (Gallimore et al., 2017), and is a particularly useful assay for measuring particle-bound ROS (Wragg et al., 2016).

Despite several studies utilising the aforementioned assays, further exploratory work is required to determine specifically what sources, physical properties and chemical components influence aerosol OP variability. A limited amount of studies have explored the role of chemical composition on aerosol OP, and it is often unclear which specific chemical components are responsible for driving aerosol OP; for example, studies show transition metals such as Cu and Mn dominate DTT activity (Charrier et al., 2015; Charrier and Anastasio, 2012), whereas others highlight the enhanced role of organics, in particular water soluble organic carbon (WSOC) such as HULIS, and quinones (Cho et al., 2005; Fang et al., 2016). Furthermore, several

https://doi.org/10.5194/acp-2020-1024
Preprint. Discussion started: 13 October 2020


Atmospheric Chemistry and Physics Discussions

studies correlate volume-normalised OP measurements with compositional variability, but given the potential collinearity of many aerosol components with overall mass, mass-normalised intrinsic OP values may provide additional insight into the effect of chemical composition on aerosol OP (Bates et al., 2019; Puthussery et al., 2020). Thus, a comprehensive characterisation of gaseous and particle phase pollution conditions combined measurements utilising multiple OP assays simultaneously, providing a wide range of information on particle-bound ROS and aerosol OP, would enable the identification of the most important components that drive aerosol OP. Ultimately, a greater understanding of the specific aerosol characteristics that influence OP, as well as specific sources that contribute more to aerosol OP, could allow the development of more targeted and efficient air pollution mitigation strategies.

In this work, $PM_{2.5}$ filter samples collected in winter 2016 and summer 2017 during the APHH campaign were analysed using four acellular methods; AA, DCFH, DTT and EPR, providing a wealth of information on the health-relevant properties of $PM_{2.5}$ including particle-bound ROS, redox-active components contributing to aerosol OP, and the formation of superoxide radicals upon sample extraction. As the APHH campaign simultaneously captured a broad range of PM compositional data, we aimed to establish what individual PM components, meteorological and atmospheric conditions contributed to increased OP assay response, whether these influences and compositions differed between assays, and if the compositions reflected particular PM sources. We included 107 different measurements, comprising transition metals, AMS measurements, total elemental and organic carbon, and a broad panel of organic species relating to biomass and fossil fuel burning, cooking emissions, vehicular markers, secondary organic aerosol compounds, plus gaseous species and general atmospheric conditions. We also sought to investigate the differences between volume-based and mass-based responses, as mass-based analysis may facilitate site and temporal comparisons more readily than volume measurements and provide details on intrinsic particle properties that influence OP.

2 Materials and methods

2.1 Air Pollution and Human Health in a Chinese Megacity Campaign (APHH)

2.1.1 Site description

High-volume 24 hr aerosol filter samples were collected at the Institute of Atmospheric Physics (IAP) in Beijing, China (39°58'28" N, 116°22'15" E) (**Figure S1**). Winter PM was collected during the months of Nov-Dec 2016 and summer PM was collected during the months of May-June 2017. $n = 31$ filters for winter 2016 and $n = 34$ filters for summer 2017 were collected. A $PM_{2.5}$ high-volume sampler (RE-6070VFC, TICSH, USA) was used at a flow rate of ~1.06 m^3/min. $PM_{2.5}$ for subsequent OP analysis was collected onto quartz microfiber filters (Whatman, 20.3 × 25.4 cm) with a collection area of 405 cm^2.

https://doi.org/10.5194/acp-2020-1024
Preprint. Discussion started: 13 October 2020

Atmospheric Chemistry and Physics Discussions

2.1.2 $PM_{2.5}$ composition, gas phase composition and meteorological data

Oxidative potential measurements were correlated with a range of additional particle phase composition, gas phase composition and meteorological measurements conducted concurrently during the APHH-Beijing campaign (Shi et al., 2019). Briefly, the following composition data was collated: total organic and elemental carbon (OC, EC), soluble inorganic ions (K^+, Na^+, Ca^{2+}, NH_4^+, NO_3^-, SO_4^{2-} and Cl^-) measured using ion chromatography (IC), low-oxidised organic aerosol and more-oxidised organic aerosol (LOOOA/MOOOA) fractions using aerosol mass spectrometry (AMS), biomass burning markers (galactosan, mannosan and levoglucosan), 16 polycyclic aromatic hydrocarbons (PAHs) (see Elzein et al., 2019, 2020), C_{24}-C_{34} *n*-alkanes, aerosol cooking markers (palmitic acid, stearic acid, cholesterol), vehicle exhaust markers (17a(H)-22, 29,30-trisnorhopane (C27a) and 17b(H)-21a-norhopane (C30ba)), isoprene SOA markers (2-methylglyceric acid, 2-methylerythritol, 2-methylthreitol, 3-hydroxyglutaric acid), C_5-alkene triols (cis-2-methyl-1,3,4-trihydroxy-1-butene, 3-methyl-2,3,4-trihydroxy-1-butene, trans-2-methyl-1,3,4-trihydroxy-1-butene), α-pinene SOA tracers (cis-pinonic acid, pinic acid, 3-methyl-1,2,3-butanetricarboxylic acid (MBTCA), 2,3-dihydroxy-4-oxopentanoic acid, aged α-pinene SOA marker), β-caryophyllene SOA tracer (β-caryophyllinic acid) and an aromatic volatile organic compound (VOC) SOA tracer (3-isopropylpentanedioic acid) (Liu et al., 2020). The following additional data was obtained from the Centre for Environmental Data Analysis (CEDA) archive : concentrations of inorganic elements Al, Ti, V, Cr, Mn, Fe, Co, Ni, Cu, Zn, Cd, Sb, Ba and Pb in $PM_{2.5}$ using X-ray fluorescence (XRF) (Xu et al., 2020a), gas phase concentrations of methanol, acetonitrile, acetaldehyde, acrolein, acetone, isoprene, methacrolein, methyl ethyl ketone, benzene, toluene, C_2-benzenes and C_3-benzenes measured using proton transfer reaction time-of-flight mass spectrometry (PTR-ToF-MS) (Acton et al., 2018), gas phase concentrations of O_3, CO, NO, NO_2, NO_y and SO_2 as well as relative humidity (RH) and air temperature measurements (Shi et al., 2019), photolysis rates for singlet oxygen and nitrogen dioxide (J O^1D and J NO_2) (Whalley et al., 2020) and gas phase concentrations of hydroxyl radicals (OH), peroxy radicals (HO_2) and organic peroxy radicals (RO_2) measured using fluorescence assay gas expansion (FAGE) (Whalley et al., 2020).

2.2 Oxidative potential measurements

2.2.1 Reagents

Chemicals and gases were obtained from Sigma-Aldrich unless otherwise indicated and were used without further purification: ascorbic acid (≥99.0 %,), Chelex™ 100 sodium form, 0.1 M HCl solution, 0.1 M NaOH solution, dichlorofluorescein-diacetate (DCFH-DA), 1 M potassium phosphate buffer solution, horseradish peroxidase (HRP), methanol (HPLC grade), and *o*-phenylenediamine (≥99.5 %). H_2O used for the DCFH, HRP and AA solution were obtained from a Milli-Q high purity water unit (resistivity ≥ 18.2 M Ω cm^{-1}, Merck Millipore, USA). For DTT analysis, 9,10-phenanthrenequinone (PQN) (≥99 %), 5,5'-dithiobis(2-nitrobenzoic acid) (DTNB) (99 %), DL-dithiothreitol (DTT) (≥98 %), potassium phosphate dibasic (≥98 %, Krebs

https://doi.org/10.5194/acp-2020-1024
Preprint. Discussion started: 13 October 2020


Atmospheric Chemistry and Physics Discussions

buffer), potassium phosphate monobasic (≥98 %, Krebs buffer), and methanol (≥99.9 %) were all obtained from Fisher Chemical. Nitrogen (oxygen free) was obtained from BOC (Cambridge, UK).

2.2.2 Acellular oxidative potential assays

Four offline acellular methods for measuring $PM_{2.5}$ oxidative potential were utilised in this work; The DCFH/HRP assay (Fuller et al., 2014), which quantifies the fluorescent product 2,7-dichlorofluoroscein, the ascorbic acid (AA) assay (Campbell et al. (2019)) which quantifies the dominant product of AA oxidation, dehydroascorbic acid (DHA) *via* condensation with a dye and fluorescence spectroscopy, Electron Paramagnetic Resonance spectroscopy (EPR) (Miller et al., 2009) specifically for the measurement of superoxide (O_2^-) and the dithiothreitol (DTT) assay (e.g. Cho et al., 2005), which quantifies the rate of loss of DTT during absorbance measurements. These acellular methods have been widely applied in the literature to study particle OP (Bates et al., 2019). For detailed descriptions of the assay protocols, see Section S2 in the supplementary information.

2.3 Statistical analysis

We aimed to analyse the data as thoroughly as possible with respect to characterising the OP measured by each assay, and to attempt to robustly connect assays to both individual measurements and potential PM sources. As data were collated from several different experimental projects, and as analytical uncertainty values were not available for the majority of the data, the use of positive matrix factorization (PMF) was not undertaken for source apportionment, and will be published subsequently for selected analyses (Xu et al., 2020a). Multiple analytical platforms were used for the acquisition of compositional data, uncertainty estimates for each measurement were not easily estimable, a factor-based chemical mass balance approach was not required specifically, and temperature, relative humidity, actinic flux and other non-mass measurements could also be influential on the OP response, and are factors mainly independent of PM sources. On this basis we considered that PMF would not ultimately give useful models in the OP context. However, these issues are managed adequately by principal components analysis (PCA), which is a useful general unsupervised method for examining underlying variance and latent effects in data, and handles multicollinearity well, although it is not optimal for source apportionment (Paatero and Tapper, 1994).

PCA and partial least squares regression (PLSR) models were produced in SIMCA+ 16.0 (Umetrics, Umeå, Sweden). Missing values were not altered prior to model construction, although measurements with more than 56% missing values per season were discarded from models. R^2 and Q^2 values were used to assess the goodness-of-fit of the model and the goodness-of-prediction of the data through 7-fold cross-validation respectively. Data were unit-variance scaled and mean-centred to remove effects related to absolute data magnitude. Models were allowed to optimise to the maximum number of latent variables (LV) at which the cumulative Q^2 value stabilised, which for most PLSR models was a single LV. PLSR model robustness was assessed through permutation testing, where the classifier (i.e. OP assay response) for all samples was randomly permuted 999 times and the PLSR model constructed for each permutation; the model was considered robust if the real model R^2 and Q^2

https://doi.org/10.5194/acp-2020-1024
Preprint. Discussion started: 13 October 2020


Atmospheric Chemistry and Physics Discussions

values outperformed those from all random permutation models. Negative Q^2 values indicate no predictive power of the data in the model, and LVs with Q^2 significantly lower than the R^2 value (arbitrarily defined for this study as Q^2 at more than 10% below the R^2) can be considered at least partially overfitted.

Spearman rank correlations (R_s) between OP measurements and $PM_{2.5}$ were calculated using OriginPro (2020), and were used to assess the relationships between assay responses and individual measurements, with Mann-Whitney-U tests (in R) used for pairwise testing of the differences in seasonal response for both assays and individual measurements. All other multivariate analyses, multiple linear regression models and selected univariate analyses were produced in R 4.0.2 (R Core Team, Vienna, Austria), implemented in RStudio 1.3.959 (Boston, Massachusetts, USA).

For multiple linear regression models, outlier values were arbitrarily deemed to be those greater than 5 times the standard deviation and replaced with the season median where appropriate for analysis. Measurement subsets manually selected as relevant to source composition were then subjected to a variable selection process, whereby pairwise Spearman correlations for all measurements were calculated, and measurements removed from subsets if they were highly correlated with other measurements but predicted OP more poorly than the other co-correlated measurements, to reduce the number of variables contributing identical information in the final models. Multiple linear regression models were then further optimised from this initial subset using the *regsubsets* function in the *leaps* R package, to allow for between 4-8 variables which best predicted the OP response (models could be constructed with fewer or even more measurements, but the aim was to examine a small panel of contributors to potential source compositions). The variable selection process precludes the use of linear regression mode performance indicators such as the Aikake or Bayesian information criteria, as the model component sets are not identical. The stability of model predictions and features were assessed using bootstrap resampling of data, by randomly splitting one fifth of the data as a test set and using the remaining samples to construct the model and predict the left-out samples, for 500 random iterations. Stability was also assessed though overall variance in OP predictions, measurement feature coefficients and model residuals plots, and run order/date bias (not differentiable as samples were analysed in date order) was assessed in residuals plots. Although not all data distributions were strictly normal when examined in the univariate kernel density plots, data were not log-transformed for multiple linear regression models, as this creates non-linearity in the model component response, which can complicate interpretation. Model residuals were plotted for manual examination and were all generally normally distributed despite the relatively small number of samples, and biases were related to periods of missing measurements or samples with values below the limit of quantification. Code developed for analysis is publicly available at https://github.com/katewolfer/Beijing.

3 Results and discussion

Both volume-normalised (OP_v, per m^3 air) and particle mass normalised (OP_m, per μg $PM_{2.5}$) values are considered in this work, where the OP value of the specific assay and sample is normalised by the volume of air collected or by the total $PM_{2.5}$ mass on the filter, respectively. OP_v is useful when considering exposure or epidemiological outcomes, but OP_m is likely a

https://doi.org/10.5194/acp-2020-1024
Preprint. Discussion started: 13 October 2020

Atmospheric Chemistry and Physics Discussions

more informative metric when exploring how chemical composition influences $PM_{2.5}$ OP, and potentially enabling better OP response, site and composition intercomparisons (Bates et al., 2019). Henceforth, assay OP values will be referred to as AA_v, DTT_v, $DCFH_v$ and EPR_v for volume-normalised OP_v values, and AA_m, DTT_m, $DCFH_m$ and EPR_m for mass-normalised OP_m values. For comparison of mass normalised OP values, PM2.5 composition measurements were also normalised for total PM mass (e.g. ng/µg per µg $PM_{2.5}$)

3.1 Seasonal variation of OP_m and OP_v

24-hour $PM_{2.5}$ mass concentrations in winter 2016 (08/11/2016-09/12/2016) ranged from 8.1 – 328.7 µg m^{-3}, with an average $PM_{2.5}$ mass of 98.7 ± 75 µg m^{-3}, whereas in summer 2017 (21/05/2017-24/06/2017) $PM_{2.5}$ concentrations ranged of 13.6 – 85 µg m^{-3} with an average of 36.7 ± 16 µg m^{-3} (**Figure S7**) (Shi et al., 2019; Xu et al., 2020a). Average seasonal values for each assay are summarised in Table S1. A data set showing 24-hr average data, for AA_v and $PM_{2.5}$ mass in both the winter and summer campaign, is shown in **Figure 1** (for $DCFH_v$, DTT_v and EPR_v, see **Section S5** "Summary statistics for all measurements" in the Supplementary Information).

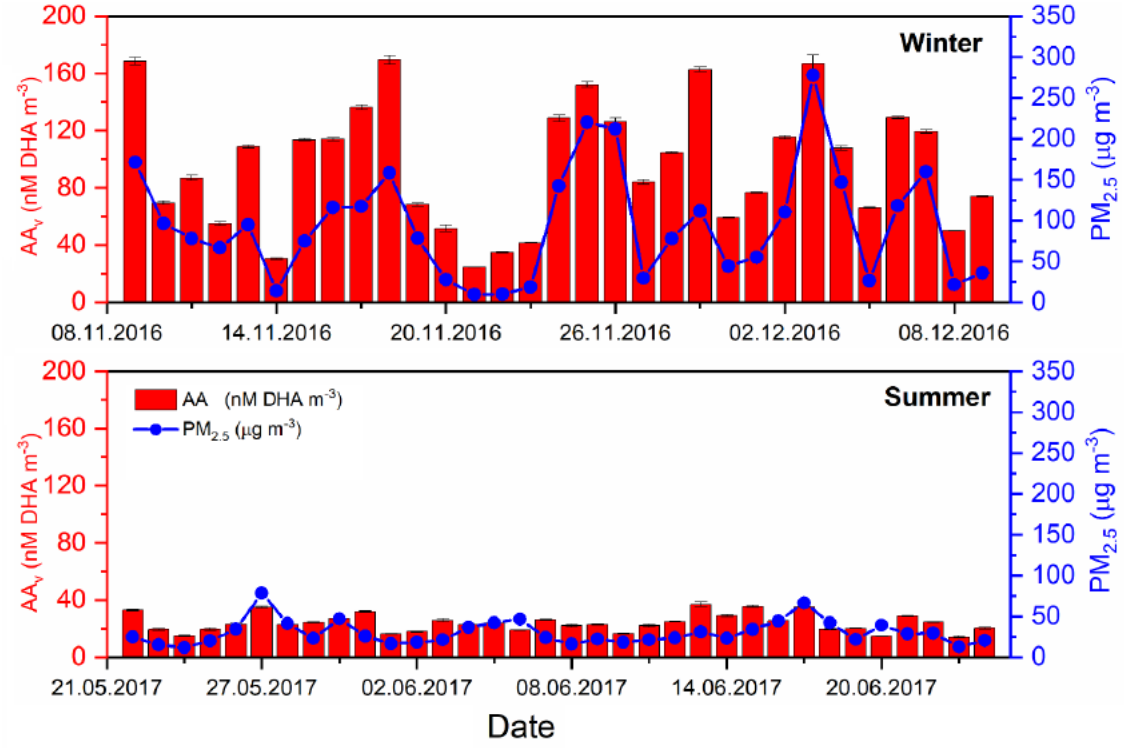

Figure 1. 24-hour averaged volume-normalised AA_v (red bars) and $PM_{2.5}$ mass (blue dots), analysed from 24-hour high volume filters, for both winter 2016 (08/11/2016 – 08/12/2016) and summer 2017 (21/05/2017-24/06/2017) (Shi et al., 2019; Xu et al., 2020a). Substantially higher average $PM_{2.5}$ mass concentrations (µg m^{-3}) and AA_v were observed in the winter season compared to the summer (see Table S1 for summary).

https://doi.org/10.5194/acp-2020-1024
Preprint. Discussion started: 13 October 2020

Atmospheric Chemistry and Physics Discussions

For all assays, a higher average $PM_{2.5}$ OP_v was observed in the winter compared to the summer in Beijing (**Table S1**). The average AA_v was 96.7 ± 42.7 nM [DHA] m^{-3} in the winter, whereas a mean value of 24.1 ± 6.1 nM [DHA] m^{-3} was observed in the summer. Given the recent introduction of this AA-based assay, which measures the formation of the AA oxidation product DHA rather than measuring the decay of AA *via* UV absorbance, limited literature values are available for direct comparison (Campbell et al., 2019b). Average $DCFH_v$ in the winter was 0.71 ± 0.52 nmol H_2O_2 m^{-3} compared to 0.17 ± 0.11 nmol H_2O_2 m^{-3} in the summer, which is within the range of $DCFH_v$ values observed in previous studies in Taiwan, the USA and Singapore (OP_{DCFH} 0.02 - 5.7 nmol H_2O_2 m^{-3}) (Hasson and Paulson, 2003; Hewitt and Kok, 1991; Hung and Wang, 2001; See et al., 2007; Venkatachari et al., 2005). Mean observed values for DTT_v in the winter and summer were 2.9 ± 0.11 nmol min^{-1} m^{-3} and 0.9 ± 0.40 nmol min^{-1} m^{-3}, respectively. The mean values of DTT_v observed in this study are greater than those measured in similar studies in Beijing (Liu et al., 2014) (0.11-0.49, mean = 0.19 nmol min^{-1} m^{-3}) with similar mass concentrations of $PM_{2.5}$ (mean = 140 μg m^{-3}), although they are within the range of DTT_v values observed in a number of previous studies in several locations, including Europe (Jedynska et al., 2017; Yang et al., 2015), the US (Fang et al., 2015; Verma et al., 2014) and Northern China (Liu et al., 2018) (0.1-14.7 nmol min^{-1} m^{-3}). The mean EPR_v values, relating to the specific detection of O_2^-, were 2.4×10^6 ± 1.6×10^6 and 5.8×10^5 ± 4.1×10^6 counts m^{-3} in the winter and summer campaign, respectively.

Spearman rank correlation coefficients of aerosol OP_v with $PM_{2.5}$ vary between the winter and summer seasons, and also between OP assays, as illustrated in **Figure 2**. All four assays, when normalised per volume (OP_v), show a stronger correlation with $PM_{2.5}$ mass concentration in the winter compared to the summer, consistent with results observed in Chamonix, France by Calas *et al*. (2018) For example, $DCFH_v$ correlates well with 24-hr average total $PM_{2.5}$ mass concentration (μg m^{-3}) in both winter (R_s = 0.96) and summer (R_s = 0.76) **(Figure 2B)**, whereas AA_v correlates well in the winter (R_s = 0.89) and poorly in summer (R_s = 0.21). Similar correlations of $DCFH_v$ with $PM_{2.5}$ mass concentrations in both winter and summer suggest that species influencing $DCFH_v$ variability (e.g. H_2O_2 and organic peroxides, likely particle-bound ROS) present in the particles are relatively consistent between both seasons. Similar to AA_v, differences between the seasons are also observed for DTT_v and EPR_v, where correlations of aerosol OP_v vs. $PM_{2.5}$ are stronger in winter compared to summer (**Figure 2C and 2D**), also generally consistent with previous studies, although in contrast to Calas et al. (2018), who observed no difference in EPR_v between seasons in Chamonix, although in that study the spin trap DMPO was used to study hydroxyl radicals, whereas in this study we focus on the formation of superoxide upon particle suspension in aqueous solution. The differences in the correlation shown in **Figure 2** suggest that the four assays are sensitive to different PM components and that in winter and summer different PM sources or components are important for the assay's responses (Calas et al., 2018; Saffari et al., 2013; Verma et al., 2014). **Figure 2** demonstrates that $PM_{2.5}$ mass could be a reasonable predictor of total OP_v in winter, but the poorer correlations between all OP_v assays and $PM_{2.5}$ in the summer indicate that a more detailed understanding is necessary to elucidate and ultimately predict aerosol OP. However, the variability in the strength of correlation between OP_v and $PM_{2.5}$ mass as well as the seasonal difference indicates that compositional differences in $PM_{2.5}$ or additional atmospheric processes influence $PM_{2.5}$ OP.

https://doi.org/10.5194/acp-2020-1024
Preprint. Discussion started: 13 October 2020

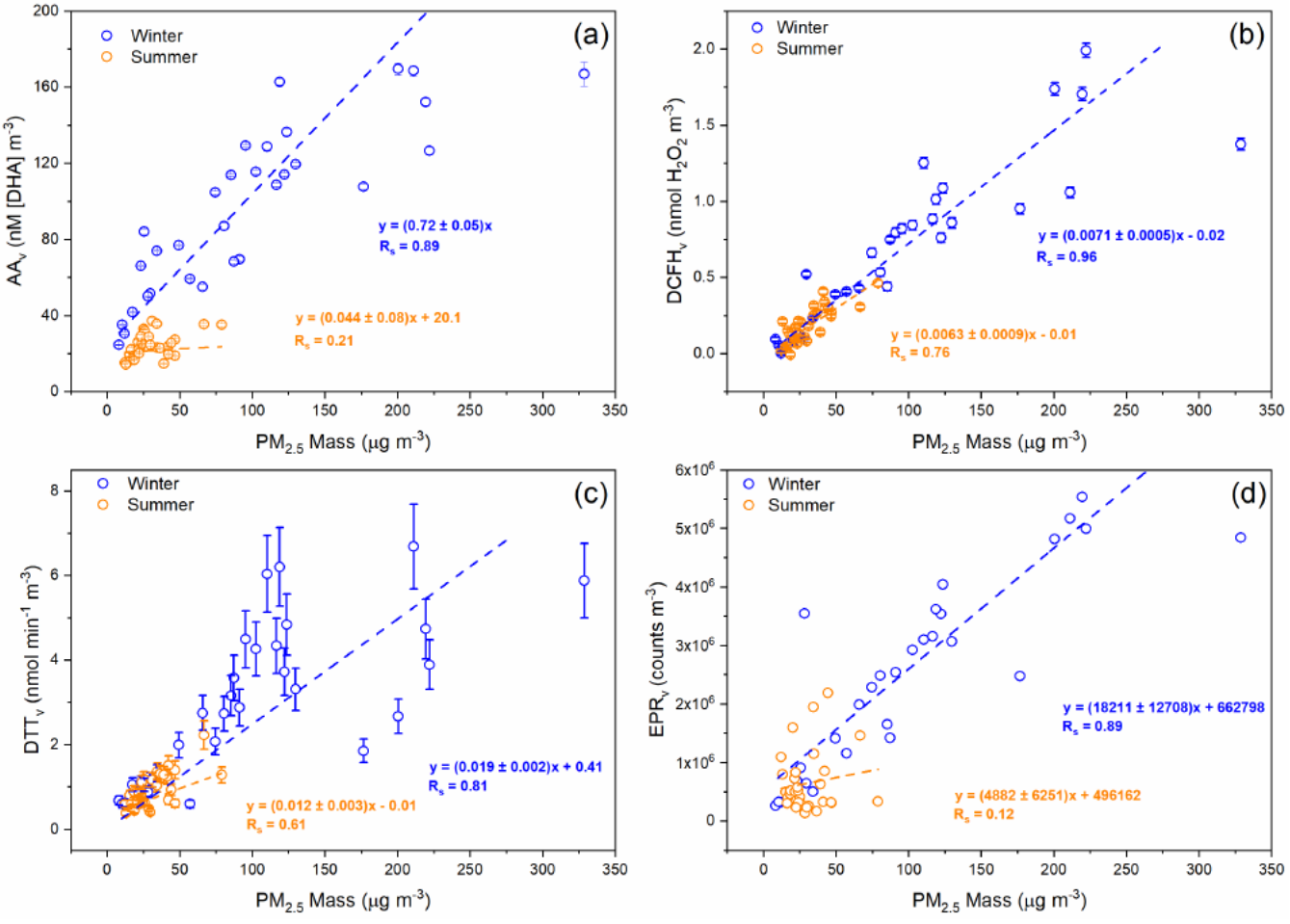

Figure 2. Comparison of $PM_{2.5}$ OP_v during winter 2016 (blue) and summer 2017 (orange) vs. $PM_{2.5}$ mass (μg m^{-3}). (a) AA_v, (b) $DCFH_v$, (c) DTT_v and (d) EPR_v. Each datapoint represents a 24-hour average for OP measurements and $PM_{2.5}$ mass. Corresponding R_s and linear fit equations are included. For AA_v, $DCFH_v$ and DTT_v, error bars represent the standard deviation observed over three repeat measurements for each filter sample, and in some cases the error is smaller than the data point. Uncertainty values are unavailable for EPR_v measurements.

To gain further insights into the potential particle-level compositional differences underlying assay OP response, the OP data for the four assays was normalised to the $PM_{2.5}$ mass in each sample. As shown in **Figure 3**, mass-normalised OP_m values vary up to ten-fold within a single season. AA_m, $DCFH_m$, DTT_m and EPR_m for both winter and summer are displayed in **Figure 3**, with colour bars indicating the 24-hr average total $PM_{2.5}$ mass (μg m^{-3}) for the corresponding OP_m measurement. The average OP_m response observed in this study shows a similar trend to OP_v (**Table S2**), where higher OP_m values are observed for winter compared to summer (**Figure 3**), as observed previously (Liu et al., 2018; Saffari et al., 2014). This demonstrates that there are specific properties of $PM_{2.5}$ in the winter that result in overall higher intrinsic OP_m compared to the summer.

For AA_m, an inverse relationship between total $PM_{2.5}$ mass concentration and AA_m is observed in both seasons, where days with high $PM_{2.5}$ mass loadings have correspondingly low AA_m values in both the winter and summer, with almost a 6-fold

https://doi.org/10.5194/acp-2020-1024
Preprint. Discussion started: 13 October 2020

Atmospheric Chemistry and Physics Discussions

difference between the AA_m on the highest $PM_{2.5}$ mass day ($PM_{2.5}$ = 328 μg m^{-3}, AA_m = 0.6 nM [DHA] μg^{-1}) and lowest $PM_{2.5}$ mass day observed during the winter campaign ($PM_{2.5}$ = 8 μg m^{-3}, AA_m = 3.53 nM [DHA] μg^{-1}). A similar trend is observed for DTT_m, where in general days with higher overall $PM_{2.5}$ mass concentrations have correspondingly low DTT_m values, which has also been observed previously (Wang et al., 2020b). The DTT_m response is also not correlated with Cu and Mn concentrations, despite the monotonic relationship between these components being demonstrated in other studies (Charrier et al., 2016). These results indicate that on high-pollution days a large fraction of the PM mass might be OP-inactive, resulting in low intrinsic OP_m values. In general, smaller particles have been observed to have higher DTT_m values compared to larger particles (Bates et al., 2019; Janssen et al., 2014), an effect which may also play a role here. Another possibility is that on higher $PM_{2.5}$ mass days, selected chemical species interact with or deactivate redox-active components present in $PM_{2.5}$ (e.g. the interaction of organics with metals (Tapparo et al., 2020)), therefore reducing the observed OP_m signal. It is also possible that components present in $PM_{2.5}$ on higher $PM_{2.5}$ mass concentration days interfere with the assay response. It is currently unclear which chemical components are responsible for the observed inverse relationship between $PM_{2.5}$ mass with AA_m and DTT_m. However, statistically significant inverse correlations are observed between AA_m and DTT_m in both the winter and summer with the chemically undetermined "unknown" fraction of $PM_{2.5}$ for DTT_m (R_s = -0.81) and AA_m (R_s = -0.75), implying that $PM_{2.5}$ chemical components unaccounted for in this study are likely responsible for the lower intrinsic AA_m and DTT_m values on high $PM_{2.5}$ mass days (See **Section 3.2** "Univariate analysis of PM OP and additional measurements", **Figure S11** and **Figure S12**).

In contrast, higher $DCFH_m$ responses are observed on days with greater $PM_{2.5}$ mass concentrations in both winter and summer. Increased $DCFH_m$ responses on more polluted days could indicate that the mass fraction of particle-bound ROS (e.g. organic peroxides from SOA) increases with increasing $PM_{2.5}$ mass concentration, or that the capacity of PM components to produce H_2O_2 upon extraction, as measured by DCFH, is enhanced. Previous studies have shown that on a mass-normalised basis, larger particles (PM_{10}) have greater potential for H_2O_2 generation in synthetic lung fluid, possibly *via* Fenton-type chemistry, as compared to smaller particles ($PM_{2.5}$) (Shen et al., 2011; Shen and Anastasio, 2011), likely related to components in smaller particles that relate to their specific sources. Despite the significant seasonal difference in EPR_m, no obvious relationship between EPR_m and $PM_{2.5}$ mass was observed in our study.

https://doi.org/10.5194/acp-2020-1024
Preprint. Discussion started: 13 October 2020

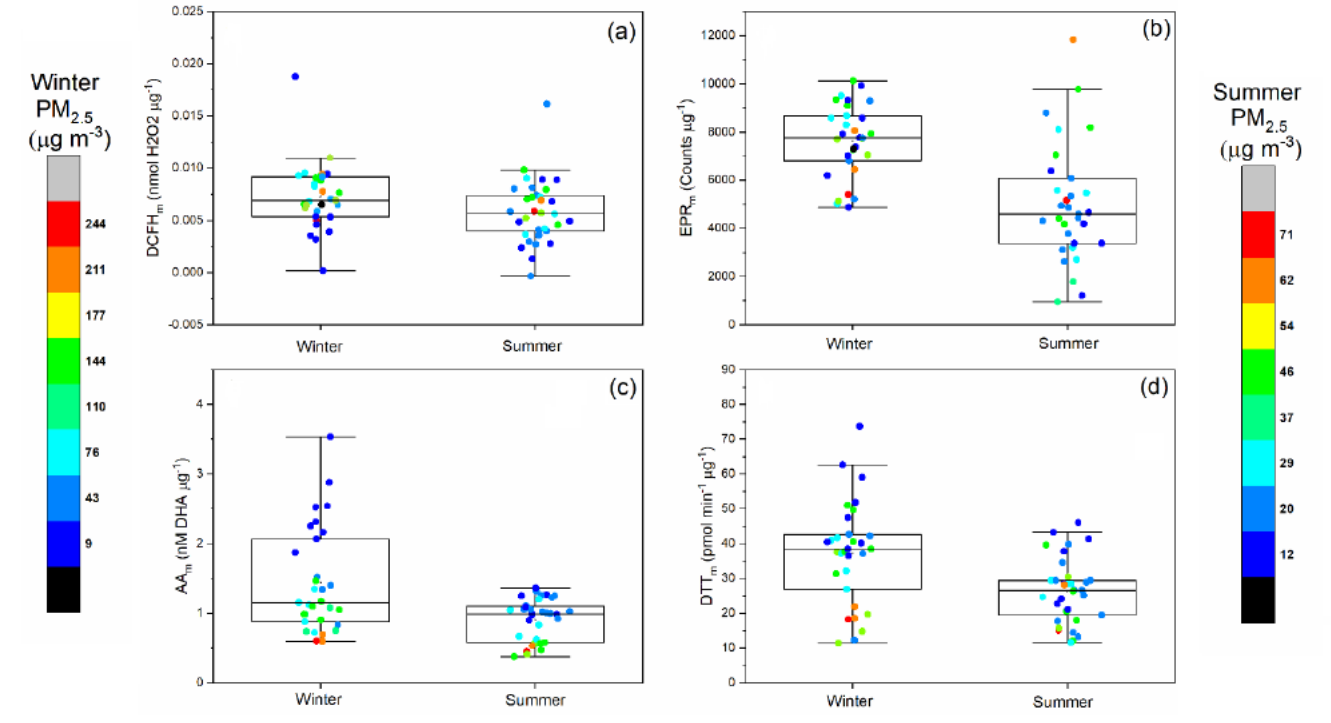

Figure 3. Summer and winter 24-hour averaged mass-normalised OP_m (A) AA_m (μM DHA μg^{-1}), (B) $DCFH_m$ (nmol H_2O_2 μg^{-1}), (C) EPR_m (counts μg^{-1}) and (D) DTT_m. Box plots indicate the median, 25% and 75% percentiles, and the data range. Data points are colour coded with respect to the 24-hour average $PM_{2.5}$ mass (μg m^{-3}), with a separate colour scale for winter and summer $PM_{2.5}$ masses given the difference in total $PM_{2.5}$ masses observed between the seasons. Grey in the colour scale indicates missing values.

Spearman rank correlations (R_s) between the four assays, for mass-normalised OP_m and volume-normalised OP_v are presented in **Table 1**. In terms of OP_v, all four assays show significantly strong correlations with each other in the winter season (R_s 0.72 – 0.89), but weaker correlations are observed between assays in the summer (R_s 0.01-0.58), a seasonal difference observed previously by Calas et al. (2018). In contrast, the only statistically significant correlation observed for OP_m is between AA_m and DTT_m in the winter season only ($R_s = 0.58$).

Seasonality of both OP_v and OP_m observed in the assays could be driven by changes in PM sources influencing overall OP, or a number of physical and chemical factors directly affecting particle composition. For instance, lower ambient temperatures in the winter may increase the partitioning of semi-volatile organic compounds, such as quinones and nitro-PAHs, which have been shown to influence DTT activity (Ntziachristos et al., 2007; Verma et al., 2011), observations which are supported by lab-based studies showing decreasing aerosol OP at higher temperatures (Biswas et al., 2009; Verma et al., 2011). Changing boundary layer height between the seasons may also contribute to higher concentrations of species responsible for increasing aerosol OP during the winter, compared to summer, especially affecting OP_v seasonality (Wang et al., 2020a). Furthermore, air mass history may play an important role in the observed seasonality of OP. For instance, it was observed that winter days with high $PM_{2.5}$ mass concentrations typically originate from regional sources south of Beijing, which is widely industrialised,

https://doi.org/10.5194/acp-2020-1024
Preprint. Discussion started: 13 October 2020

Atmospheric Chemistry and Physics Discussions

whereas high mass days in the summer typically have more varied air mass histories (Panagi et al., 2020; Steimer et al., 2020). There are likely varying contributions between different sources in different seasons, e.g. more photochemistry in the summer driving oxidation and biogenic sources, and more contributions from residential heating combustion in the winter (Xu et al., 2020a). In order to gain further insight into what causes the observed variability of OP, relationships between particle chemical composition and aerosol OP will be explored in detail below.

Table 1. Correlation of volume-normalised (OP_v, top panel) and mass-normalised (OP_m, bottom panel) assay responses in the winter (blue) and summer (orange) campaign. It should be noted that assay responses expressed as mass-normalised (OP per µg) are correlated with mass-normalised additional particle phase composition measurements (i.e. µg or ng per µg $PM_{2.5}$).

OP_v R_s	AA_v	$DCFH_v$	EPR_v	DTT_v
AA_v		**0.89*****	**0.86*****	**0.83*****
$DCFH_v$	0.35*		**0.86*****	**0.72*****
EPR_v	0.19	0.01		**0.88*****
DTT_v	0.41*	**0.58*****	0.07	

OP_m R_s	AA_m	$DCFH_m$	EPR_m	DTT_m
AA_m		-0.29	0.22	**0.60****
$DCFH_m$	-0.20		-0.08	-0.15
EPR_m	-0.26	0.15		0.27
DTT_m	0.2	-0.28	0.14	

Bold indicates $R_s \geq 0.5$, *$p < 0.05$, **$p < 0.01$, *** $p < 0.001$.

3.2 Univariate analysis of PM OP_m and additional measurements

Spearman rank correlations between OP_m of the four assays and 107 additional measurements conducted during the APHH campaign (see **Section 2.1.2** "$PM_{2.5}$ composition, gas phase composition and meteorological data"), were calculated for both the winter (n = 31) and summer (n = 33). We focus on OP_m in the forthcoming discussion; as mentioned previously, as we consider it a particularly informative metric when determining the role of chemical composition on OP (Bates et al., 2019; Puthussery et al., 2020) (all results are presented in **Section S7** "Assay correlations with individual component measurements").

The majority of additional particle phase composition, gas phase composition and meteorological measurements differed significantly by season. Exceptions included Al, V, Zn, Pb, Ca^{2+}, Na^+, NH_4^+, acetaldehyde, acetonitrile, methanol, methyl ethyl ketone, methyl vinyl ketone/methacrolein, trans-2-methyl-1,3,4-trihydroxy-1-butene, β-caryophyllinic acid, 3-hydroxyglutaric

https://doi.org/10.5194/acp-2020-1024
Preprint. Discussion started: 13 October 2020


Atmospheric Chemistry and Physics Discussions

acid, C5-alkene triols, cholesterol, LOOOA and MOOOA. Stacked bar plots illustrating the total daily concentrations for both mass-normalized and volume-normalized data are shown in **Figure 4** and **Figure S13**. Total concentrations of individual PM components (excluding all composite measures) account for approximately 0.3-0.8 μg/μg, i.e. 30 – 80% of the total PM mass (data not shown). Interestingly there were no marked or characteristic changes in mass composition associated with haze days; however, haze events were generally correlated with increased biomass burning marker concentration and total organic carbon in winter for the mass-normalised data (also observed during recent later winter haze events in Beijing (Li et al., 2019)), and small inorganic ion concentrations in both seasons in the volume-normalised data (**Figure S13**).

IC measurements (K^+, Na^+, Ca^{2+}, NH_4^+ NO_3^- and SO_4^{2-}) account for the greatest proportion of total particle mass in both seasons, all of which are major components of secondary inorganic PM mass (NH_4^+, NO_3^-, SO_4^{2-}), mineral dust (Ca^{2+}, K^+,), and marine aerosols (Na^+, Cl^-). These species were present at higher daily concentrations in summer than in winter. Summer compositions for each category were generally consistent for the whole sampling period, with a larger total proportion of SOA markers, whereas winter compositions were more variable, with greater contributions from elemental carbon, PAHs, *n*-alkanes and cooking-related compounds than for summer samples. Although PAHs are not redox-active (Charrier and Anastasio, 2012), they are precursors to redox-active oxy-PAHs (quinones) and nitro-PAHs (Atkinson and Arey, 2007), and have well-established intrinsic cellular toxicity (reviewed in Moorthy et al., 2015), mediated by their conversion to hydroxy-PAHs, which exert mutagenic and teratogenic effects, and also inducing transcriptional modifications and oxidative stress. EC and *n*-alkanes are also non-redox-active and the exact mechanism of their toxicities is unclear (Levy et al., 2012); however, SOA derived from the interaction of *n*-alkanes with NO_x with photo-oxidation (Lim and Ziemann, 2005; Presto et al., 2010) is likely both to contribute to the redox activity of samples (Tuet et al., 2017), and to have more toxic properties than its precursors (Xu et al., 2020b). The sample from 22 November 2016 has a particularly high concentration of cooking markers (palmitic acid, stearic acid and cholesterol). This could reflect the fact that the traditional Chinese winter solar term Xiao Xue (小雪,"Light Snow"), begins on this date (Li, 2006), a period associated with the preparation of warm foods as the ambient temperatures in northern China drop; a similar elevation of palmitic acid and stearic acid has been observed around the same week in a more recent study in Shanghai (Wang et al., 2020c).

https://doi.org/10.5194/acp-2020-1024
Preprint. Discussion started: 13 October 2020

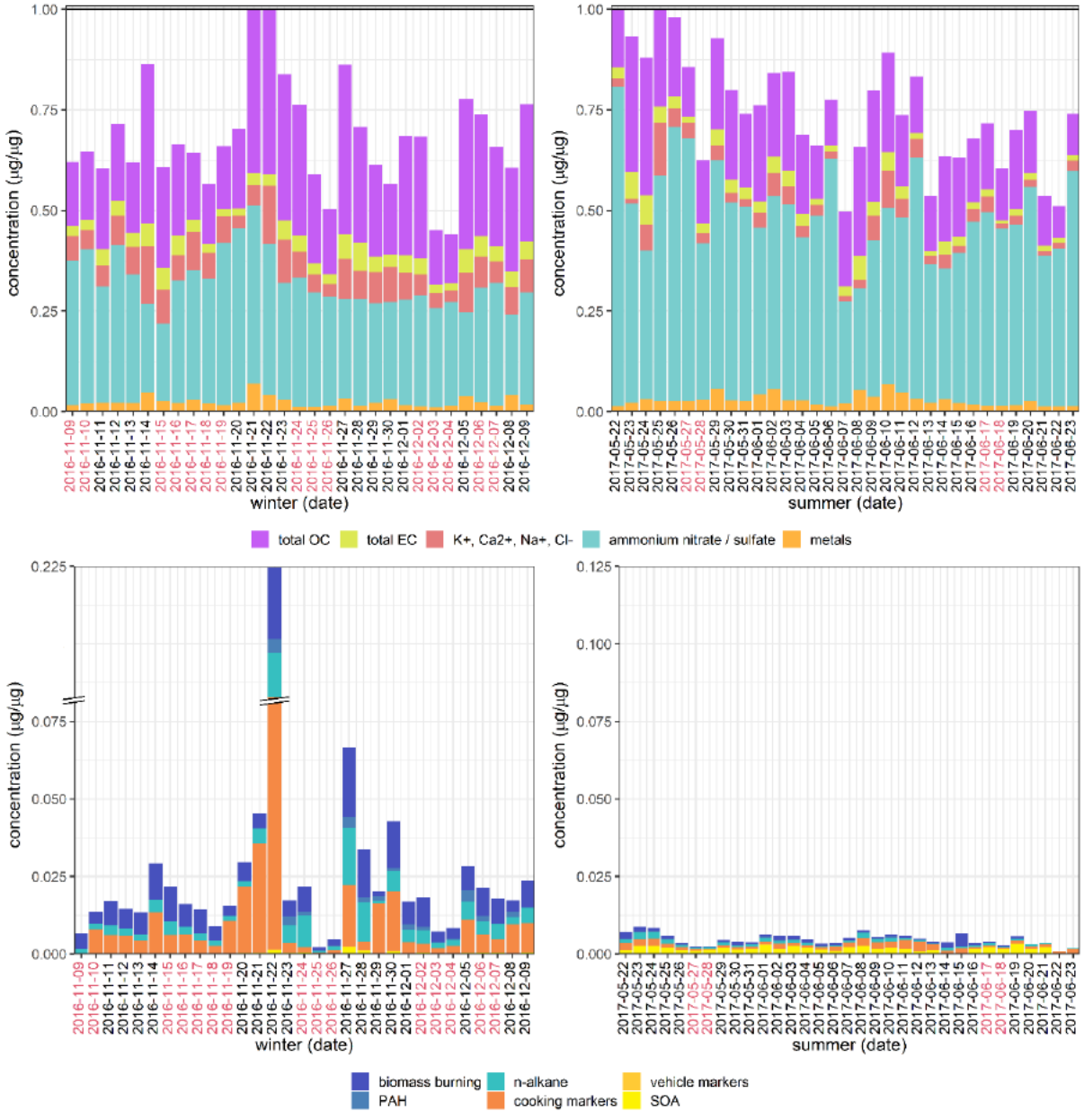

Figure 4. Stacked bar plots of total concentrations for mass-normalised data. **Abbreviations:** OC: organic carbon; EC: elemental carbon; PAH: polycyclic aromatic hydrocarbon; SOA: secondary organic aerosol "Metals" is the summed concentrations of Al, Ti, V, Cr, Mn, Fe, Co, Ni, Cu, Zn, Cd, Sb, Ba, Pb; "biomass burning" is the summed concentrations of palmitic acid, stearic acid and cholesterol; "PAH" is the summed concentrations of naphthalene, acenaphthylne, acenaphthene, fluorene, phenanthrene, fluoranthene, pyrene, benzo(a)anthracene, chrysene, benzo(b)fluoranthene, benzo(k)fluoranthene, benzo(a)pyrene, indeno(1,2,3-cd)pyrene, dibenzo(a,h)anthracene and benzo(ghi)perylene; "*n*-alkane" is the summed concentrations of C24, C25, C26, C27, C28, C29, C30, C31, C32, C33, C34; "cooking markers" is the summed concentrations of palmitic acid, stearic acid, cholesterol; "vehicle markers" is the summed concentrations of 17a(H)-22,29,30-trisnorhopane (C27a) and 17b(H),21a(H)-norhopane (C30ba); "SOA" is the summed concentrations of 2-methylthreitol, 2-methylerythritol, 2-methylglyceric acid, cis-2-methyl-1,3,4-trihydroxy-1-butene, -methyl-2,3,4-trihydroxy-1-butene, trans-2-methyl-1,3,4-trihydroxy-1-butene, C5-alkene triols, 2-methyltetrols, 3-hydroxyglutaric acid, cis-pinonic acid, acid, MBTCA, beta-caryophyllinic acid,

https://doi.org/10.5194/acp-2020-1024
Preprint. Discussion started: 13 October 2020

Atmospheric Chemistry and Physics Discussions

glutaric acid derivative, 3-acetylpentanedioic acid, 3-acetylhexanedioic acid, 3-isopropylpentanedioic acid and 2,3-dihydroxy-4-oxopentanoic acid. Dates marked in red indicate partial or total day haze events as described in Shi et al. (2019). Measurement uncertainty values were unavailable for most data types, and for selected dates in the upper plots, the sum of the total mass measurements is slightly more than 1 (i.e. more than 1μg per μg); for these dates, the data has been proportionately scaled. It should be noted that the OC measurement in the upper plots incorporates the variety of organic carbon species represented in the lower plots.

R_s calculated for OP_v and OP_m with the individual compositional measurements have strikingly different univariate correlations, as illustrated in correlation heatmaps (**Figure 5**). Cumulative scores, referring to the number of R_s correlations $\geq$ 0.5 for OP_m and OP_v (Table S3), demonstrate that for all assays, considerably more significant correlations are observed for OP_v in the winter compared to OP_m. For both OP_v and OP_m, all assays show more statistically significant correlations in winter compared to summer, particularly for the AA response (AA_m: 54 correlated features in winter, 15 in summer; AA_v: 67 correlated features in winter, 4 in summer).

Volume-based correlation analysis (**Figure 6A**) indicates that a very large number of the 107 atmospheric components measured in this study correlate statistically significantly with all four assays. The large number of correlations in the volume-normalised data indicate strong collinearity between concentrations of chemical components in $PM_{2.5}$ and overall $PM_{2.5}$ mass concentrations likely due to meteorological processes, complicating analysis of the sources and processes contributing to OP variability in particles. However, the mass-based analysis (**Figure 6B**) reveals that the mass fractions of chemical components and sources to which the four assays are sensitive to differ significantly (further illustrated by the weaker inter-assay correlations shown in Table 1), which demonstrates that mass-based analysis of OP data is also important to elucidate atmospheric processes and particle sources responsible for the different OP metrics.

A range of transition metals were all positively correlated with AA_m and DTT_m, including V, Cr, Mn, Fe, Co, Ni, Zn, Cd and Pb (all $R_s \geq 0.5$, $p < 0.05$). This reinforces the importance of their contribution to urban $PM_{2.5}$ and potential to exert oxidative stress in tissues, particularly Fe, Cr, V and Co which are commonly major components of vehicle emissions, which can undergo redox-cycling reactions producing ROS (Charrier et al., 2014; Shen and Anastasio, 2012; Valko et al., 2005) contributing to higher AA_m and DTT_m in the winter compared to the summer. Stronger correlations between Fe and AA_m are observed in the winter (R_s 0.73) compared to summer (R_s 0.48) despite Fe concentrations (μg/μg) being lower in winter samples than summer samples, again highlight the enhanced role of redox-active transition metals in winter. It is not established whether this seasonal difference is related to the chemical availability (i.e. redox state, solubility, speciation) of Fe, to the variability of emission sources of Fe between the seasons, or to some other important additional contribution to ROS in the summer; complexation of the Fe may differ between seasons, and the ligands can directly influence the redox state and bioavailability of the metal (Ghio et al., 1999). Interestingly, a mild inverse correlation of Fe with $DCFH_m$ is observed (**Table S8**, not statistically significant), which may be linked to the destruction of particle-bound organic peroxides by Fe *via* Fenton-type chemistry (Charrier et al., 2014), a process which the DCFH assay is specifically sensitive to (Gallimore et al., 2017; Wragg et al., 2016), and which has been observed in other recent studies (Paulson et al., 2019). No significant positive correlation between any metals measured in this study and $DCFH_m$ and EPR_m was observed. Few EPR studies have looked specifically at superoxide formation, as is

https://doi.org/10.5194/acp-2020-1024
Preprint. Discussion started: 13 October 2020

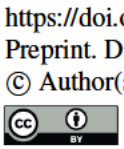

Atmospheric Chemistry and Physics Discussions

the case here, but those conducted so far show that EPR is less sensitive to transition metal chemistry compared to traditional EPR methods focussing on OH formation.

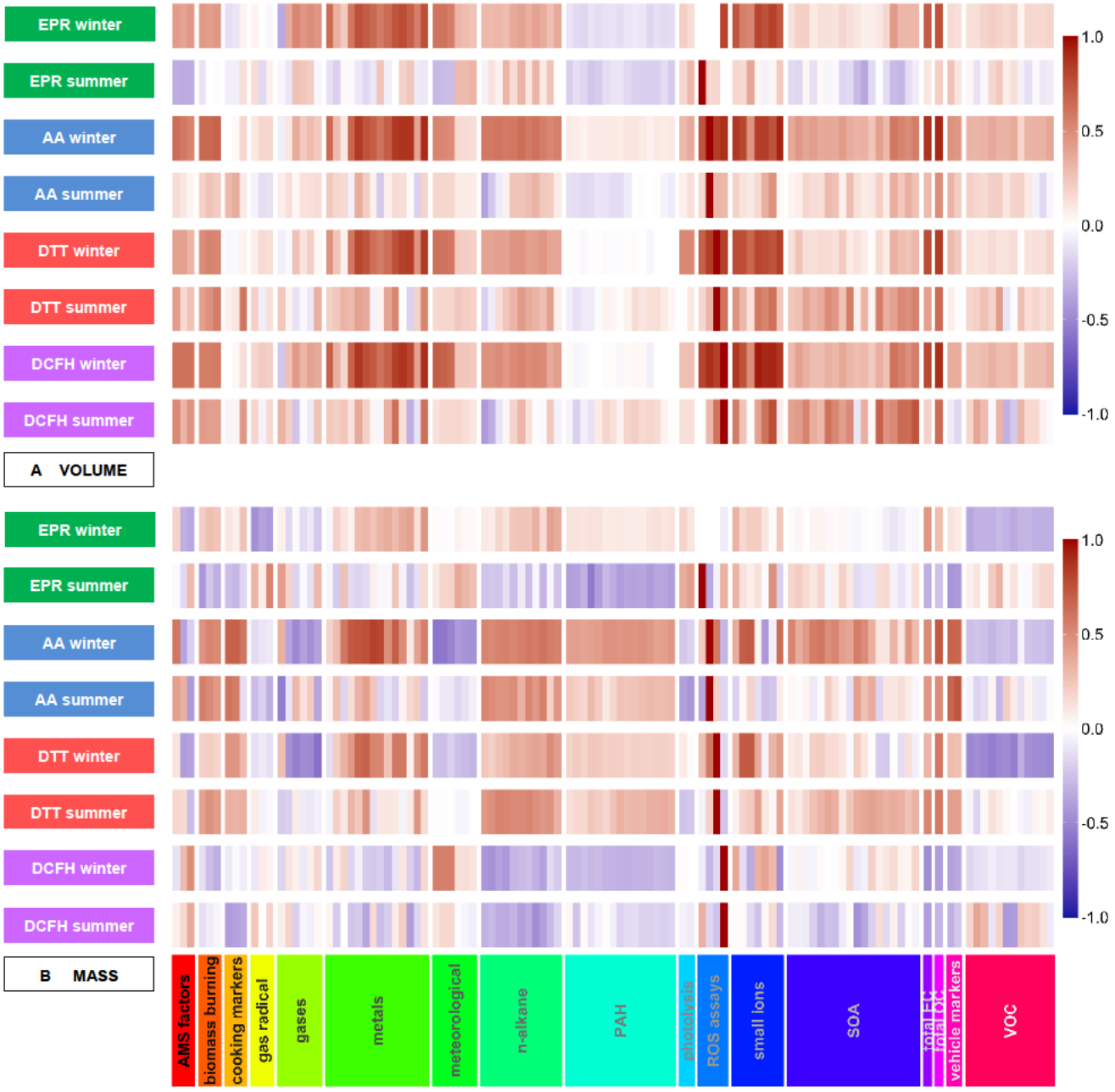

Figure 5. Heatmaps demonstrating the correlation of OP, expressed as volume-normalised OP_m (A) and mass-normalised OP_v (B) vs a range of additional measurements conducted during the APHH campaign. Red indicates positive correlation; blue indicates inverse correlation. For OP_m, particle-phase components are also mass normalised (µg per µg $PM_{2.5}$ and for OP_v, volume-normalised (µg or ng per m^3).

https://doi.org/10.5194/acp-2020-1024
Preprint. Discussion started: 13 October 2020


Atmospheric Chemistry and Physics Discussions

In the summer, from the measured transition metals, only Fe correlated significantly positively (Spearman correlation p-value < 0.05) with DTT_m and AA_m response (R_s = 0.48, 0.51 respectively), whereas in the winter, DTT_m and AA_m correlated with a number of transition metals including V, Cr, Mn, Fe, Co, Ni, Zn, Cd. Of particular note, AA_m is mildly correlated with Cu in winter samples (R_s 0.48), whereas no correlation is observed between DTT_m and Cu in either winter or summer, in agreement with a recent online DTT study also (Puthussery et al., 2020). In contrast, previous reports from other locations have implicated Cu as a dominant contributor to DTT oxidation, considering volume normalised and mass normalised data (Calas et al., 2018; Charrier et al., 2015). Interestingly, in contrast with OP_m, good correlations ($R_s > 0.6$) are observed in this study between AA_v, EPR_v, $DCFH_v$ and DTT_v and Cu in the winter, but poorer correlations are observed in the summer for all assays ($Rs < 0.39$). Higher average Cu concentrations in winter compared to summer (winter = 17.7 ng m^{-3}, summer = 4.9 ng m^{-3}) may explain the higher R_s observed for Cu vs. OP_v in winter compared to summer, whereas mass normalized concentrations of Cu are more similar between the seasons. Poor correlation of Cu concentrations with AA_m and DTT_m response in winter may hint at more insoluble Cu complex formation observed at this site in Beijing, as predominantly water-soluble Cu participates in redox reactions, therefore the sensitivity of AA and DTT towards Cu probably depends on the soluble fraction of Cu (Bates et al., 2019; Charrier and Anastasio, 2012; Fang et al., 2016). Furthermore, the presence of organic chelating ligands in PM may reduce the redox-activity of Cu and Fe (Charrier et al., 2014; Charrier and Anastasio, 2011; Shen and Anastasio, 2012).

Correlations between AA_m and DTT_m with total OC are observed in both summer and winter (**Tables S6** and **S7**), and with total EC in the winter season, whereas $DCFH_m$ is negatively correlated with total OC (**Table S8**). In contrast, $DCFH_m$ is positively correlated with MOOOA and LOOOA, whereas DTT_m and AA_m show no correlation and even exhibit slight negative correlations with MOOOA and LOOOA in both summer and winter. This potentially indicates that the MOOOA and LOOOA AMS fractions, typically associated with water-soluble organic carbon content (Verma et al., 2015b), may contain higher concentrations of particle-bound ROS (i.e. organic peroxides) as measured by $DCFH_m$, but on a per-mass basis these species may contribute less significantly to AA_m and DTT_m compared to redox-active transition metals and other organic components. Total OC and EC correlations with AA_m and DTT_m may relate to concentrations of redox-active organic components such as oxidized PAHs and quinones, which may not be represented by MOOOA and LOOOA factors and which have been shown to significantly contribute to DTT_m (Chung et al., 2006; McWhinney et al., 2013b).

Significant correlations are also observed between AA_m and a range of *n*-alkanes and hopanes (17a(H)-22, 29,30-trisnorhopane (C27a) and 17b(H)-21a-norhopane (C30ba), **Table S6**), markers of primary organic aerosol emitted from vehicles (Schauer et al., 1999; Subramanian et al., 2006). Although these species are not redox-active, they are co-emitted with redox-active transition metals such as Fe, V and Cu from vehicle activity, either directly (Bates et al., 2019) or *via* dust resuspension, and other organics contributing to SOA (Platt et al., 2014) and highlight the potential importance of vehicular emissions on AA_m. Vehicular emissions and dust-resuspension have been previously shown to be the dominant sources of Cu and Fe in Beijing (Gao et al., 2014). EPR_m, DTT_m and $DCFH_m$ responses do not show any significant correlations with these organic traffic markers.

https://doi.org/10.5194/acp-2020-1024
Preprint. Discussion started: 13 October 2020


Atmospheric Chemistry and Physics Discussions

Notably, AA_m correlates well with cis-pinonic acid, pinic acid and 3-methyl-2,3,4-butanetricarboxylic acid (MBTCA) in both seasons, all of which are biogenic SOA markers and products of α-pinene oxidation, with MBTCA a marker for OH-initiated ageing of first generation α-pinene oxidation products (Müller et al., 2012). AA sensitivity towards α-pinene SOA has been demonstrated previously (Campbell et al., 2019b). Although these three carboxylic acids are also not redox-active, they may correlate with the formation of particle-bound ROS such as peroxides or peroxy acids in SOA (Steimer et al., 2018), or with species that decompose liberate ROS upon extraction (e.g. (Tong et al., 2017)); these processes are highly likely to contribute to AA_m, highlighting the assay's sensitivity to redox-active particle phase organic components and particle-bound ROS. Generally, DTT_m has been previously shown to be relatively insensitive to SOA as observed here (Bates et al., 2015; Verma et al., 2015b), and both DTT_m and $DCFH_m$ correlate poorly with the SOA markers analysed in the present study (**Tables S7** and **S8**).

Compared to the three other assays, few significant correlations are observed between EPR_m and additional measurements, despite the much better correlations with the EPR_v data, particularly for the summer samples. However, seasonality in the EPR_m response is still observed, with substantial variability in the mass-normalised EPR_m response (≈ factor of 10 in the summer, factor of 2 in the winter, **Figure 3**). Therefore, we observe differences in aerosol composition influencing EPR_m, but with the current comprehensive measurements (i.e., 107 parameters) are unable to determine the specific $PM_{2.5}$ components responsible for the observed EPR_m variation.

The univariate analysis presented here clearly shows that OP_m enables a more nuanced identification of aerosol components linked to OP as compared to OP_v. Many more correlations are observed when considering volume-normalised OP_v, likely related to collinearity of species with overall $PM_{2.5}$ mass concentration due to meteorological effects. Metal and organic tracers of traffic emissions (exhaust and non-exhaust) such as Fe, Cu and hopanes and SOA markers show especially strong correlations with AA_m, whereas the other three OP_m metrics (DTT_m, $DCFH_m$ and EPR_m) provide a less clear picture.

3.3 Multivariate modelling of OP from measured components

To assess potential latent influences from the individual components on assay response and hence on OP, a systematic multivariate analysis was undertaken. Initially principal components analysis was applied to the whole set of independent measurements excluding the OP responses (i.e. the values to be predicted by the models), to investigate which contributed most to the variation in the data, whether there were relationships between measurements which characterised OP, and if the OP_m response could be predicted from the individual component measurements.

In the PCA model, the seasonal variation within the samples was clearly apparent (**Figure 6**). The first four principal components (PC) accounted for 68.2% of the observed variation in the dataset (R^2 or goodness-of-fit), of which 50.5% was stable through 7-fold cross-validation (Q^2, or model variation accounted for through cross-validation), indicating about half of the variation in the model was robust with respect to sample score prediction. The loadings plot for this model (**Figure 7**) indicated the primary drivers of seasonality in the first principal component were increased PAHs (Feng et al., 2019), *n*-alkanes (He et al., 2006) and biomass burning markers (He et al., 2006) in winter, and increased ozone (Zhao et al., 2018), ambient

https://doi.org/10.5194/acp-2020-1024
Preprint. Discussion started: 13 October 2020


Atmospheric Chemistry and Physics Discussions

505 temperature and selected SOA markers (including 2-methylerythritol (Liang et al., 2012) and 2-methylglyceric acid (Ding et al., 2016; Shen et al., 2018)) in summer, findings which are consistent with existing volume-based studies. When scores were coloured by OP, the AA_m (**Figure 6B**), DTT_m and $DCFH_m$, assay responses could be observed in the second and sometimes also the first principal components (although the EPR_m response demonstrated no specific trend, **Figure S14**). When loadings plots were examined by general measurement category (**Figure 7**), it was observed some categories of measurements cluster
510 together (e.g. PAH, *n*-alkanes, NO_x, temperature, relative humidity), but this was related to strong correlation of these species with the OP_m measurement and known compound behaviour rather than to intrinsic measurement bias, as other categories showed broader variation (e.g. inorganic and small organic ions, gases, metals and SOA markers).

https://doi.org/10.5194/acp-2020-1024
Preprint. Discussion started: 13 October 2020

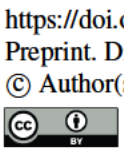

Atmospheric Chemistry and Physics Discussions

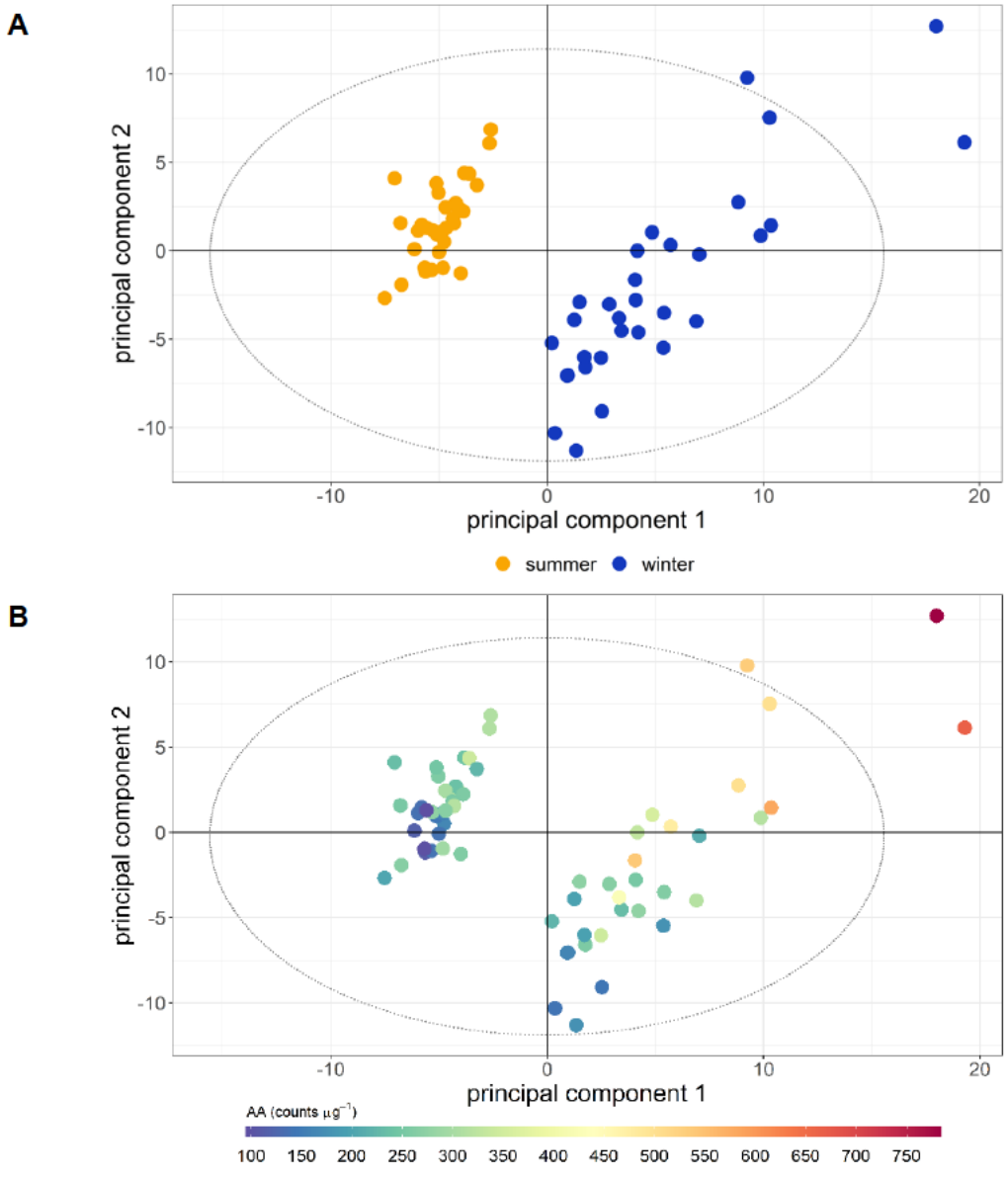

Figure 6. Principal components analysis scores plot of all data. A: coloured by season (winter/summer). B: coloured by AA_m response. Both principal component 1 and principal component 2 demonstrate variance associated with AA response, and there is greater variation associated with the winter response than the summer response. PC 1 R^2X 35.90%, Q^2 29.28%; PC 2 R^2X 19.34%, Q^2 23.73%; the model included four principal components, with a cumulative R^2X of 68.2% and Q^2 of 50.5%. Analogous colour-coded PCA plots for DTT_m, $DCFH_m$ and EPR_m are shown in **Figures S14-S16**.

https://doi.org/10.5194/acp-2020-1024
Preprint. Discussion started: 13 October 2020

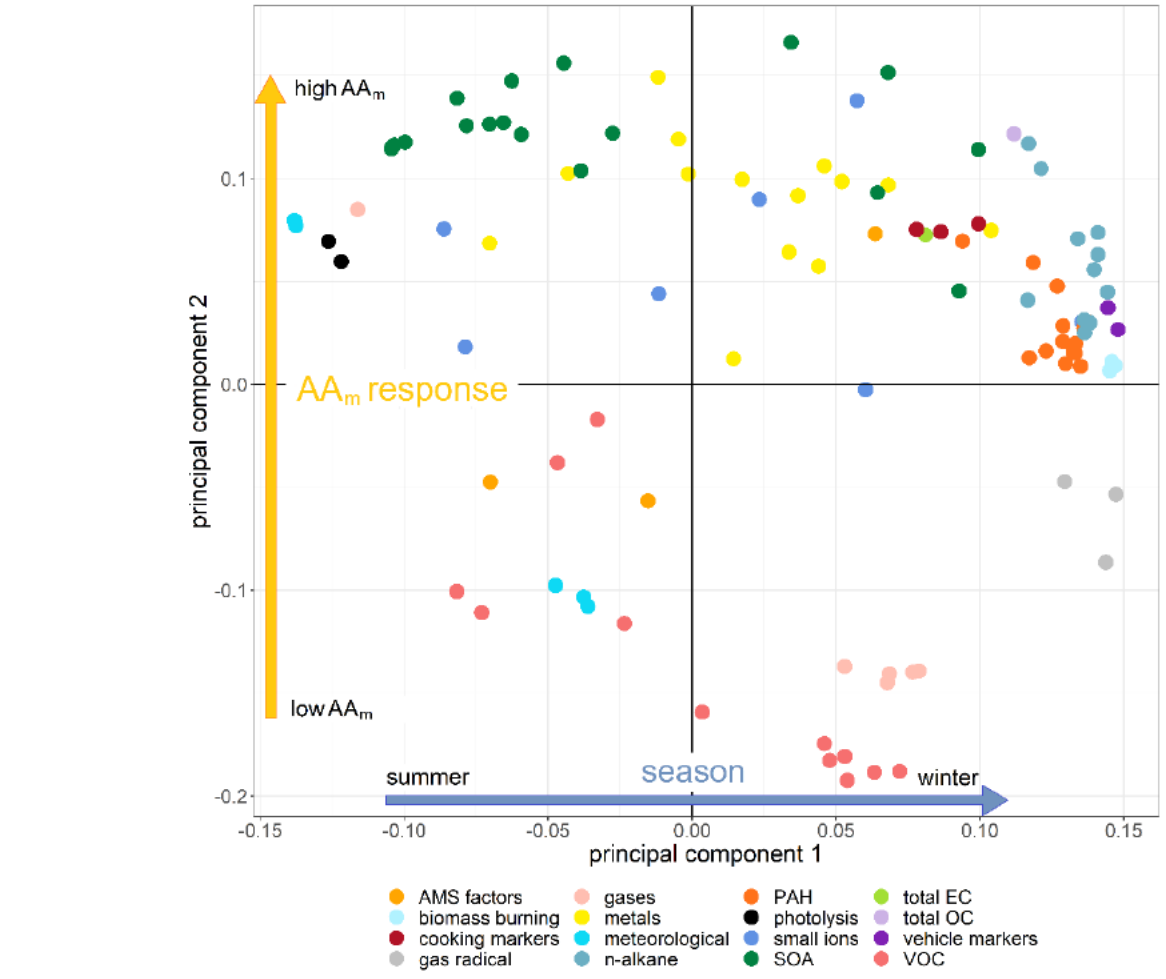

Figure 7. Principal components analysis loading plot for all data points. Points are coloured by measurement category; a fully labelled plot is provided in **Figure S17**. The plot is annotated with the same orientation as the scores plot, to indicate the direction of visualised trends in **Figure 6**. In PC 1, the winter classification is driven by increased gas radicals, *n*-alkanes, PAH, vehicle markers, biomass burning markers, total OC and selected metals and SOA markers; the summer classification is driven by increased temperature and photolysis, ozone (the single gas species in this section of the plot), selected SOA markers and metals, and selected VOCs. In PC 2, high AA_m response is associated with increased SOA, transition metals, cooking markers, *n*-alkanes and PAH concentrations in samples; low AA_m response associated with low VOCs, gases and selected meteorological parameters (relative humidity).

Partial least squares regression (PLSR) is a supervised regression extension of PCA, which models the variation in the data associated with a defined sample classification (Eriksson et al., 2013). PLSR models were constructed for each individual OP assay and season, to examine the most specific markers associated with assay response. **Table 2** gives the model performances for all PLSR assay models, and example PLSR scores plots for AA_m and DTT_m models (both seasons) are illustrated in **Figures 8** and **9** (analogous plots for other assays provided in **Figures S18** and **S19**). The performance indicators show that while the mass-normalised measurement data can be used to explain and predict a large majority of the variation associated with AA_m summer/winter and DTT_m winter assay response, the other assay responses were less consistent; R^2 and Q^2 values for these

https://doi.org/10.5194/acp-2020-1024
Preprint. Discussion started: 13 October 2020

Atmospheric Chemistry and Physics Discussions

models indicated that less than 70% of the variance in response can be predicted from the individual component measurements, and the predictions much less stable through cross-validation. These results could suggest either that assay responses are not as adequately sensitive at the µg/µg concentrations as for the total volume of PM per sample, or that a proportion of the OP_m response is contributed to by species not measured directly in this campaign, and which cannot also be inferred from total organic carbon measurements. As total OC is estimated from combustion properties of the sample rather than from a sum of individually validated component measurements, and as multiple organic and transition metal-organic complexed species contribute to the total OC measurements with unknown redox properties, these observations highlight the need for more comprehensive chemical characterisation of PM composition. Similarly to the univariate correlations, the summer samples were less well modelled in both mass-normalised and volume-normalised data, indicating either reduced assay sensitivity (which may also be compounded by the reduced collected filter PM mass in summer) or the influence of unmeasured components.

Table 2. Performance assessment of PLSR models for all assays, for both mass-normalised (left) and volume-normalised (right) data. Models are considered to perform well when both cumulative (i.e. across all latent variables included in the model) R^2 and Q^2 values are high, or at a minimum where Q^2 values are within 10% of the R^2 value, indicating that the variance is well accounted for in model cross-validation. Permutation tests were rejected for robustness if any single random permutation model performance surpassed the performance of the real cross-validated model; on this basis, the winter $DCFH_m$ and summer DTT_v models were rejected (highlighted with *), although fewer than three random models outperformed the real model, and none of the permuted model Q^2 values outperformed those of the real model.

		mass (µg/µg)				volume (µg/m³)			
assay	**season**	**optimal LVs**	**cumul. R^2**	**cumul. Q^2**	**permutation test pass**	**optimal LVs**	**cumul. R^2**	**cumul. Q^2**	**permutation test pass**
EPR	winter	1	43.2	19.3	no	2	83.9	75.2	**yes**
	summer	1	11.3	-10.0	no	1	52.0	3.7	no
AA	winter	1	81.4	78.2	**yes**	**2**	94.1	87.9	**yes**
	summer	2	79.3	49.7	**yes**	**1**	41.8	22.6	no
DTT	winter	2	76.0	62.0	**yes**	**2**	86.8	67.0	**yes**
	summer	1	47.4	31.6	no	1	66.2	50.9	no*
DCFH	winter	2	71.9	50.4	no*	2	67.0	55.2	**yes**
	summer	1	28.2	-6.6	no	1	86.0	66.7	**yes**

https://doi.org/10.5194/acp-2020-1024
Preprint. Discussion started: 13 October 2020

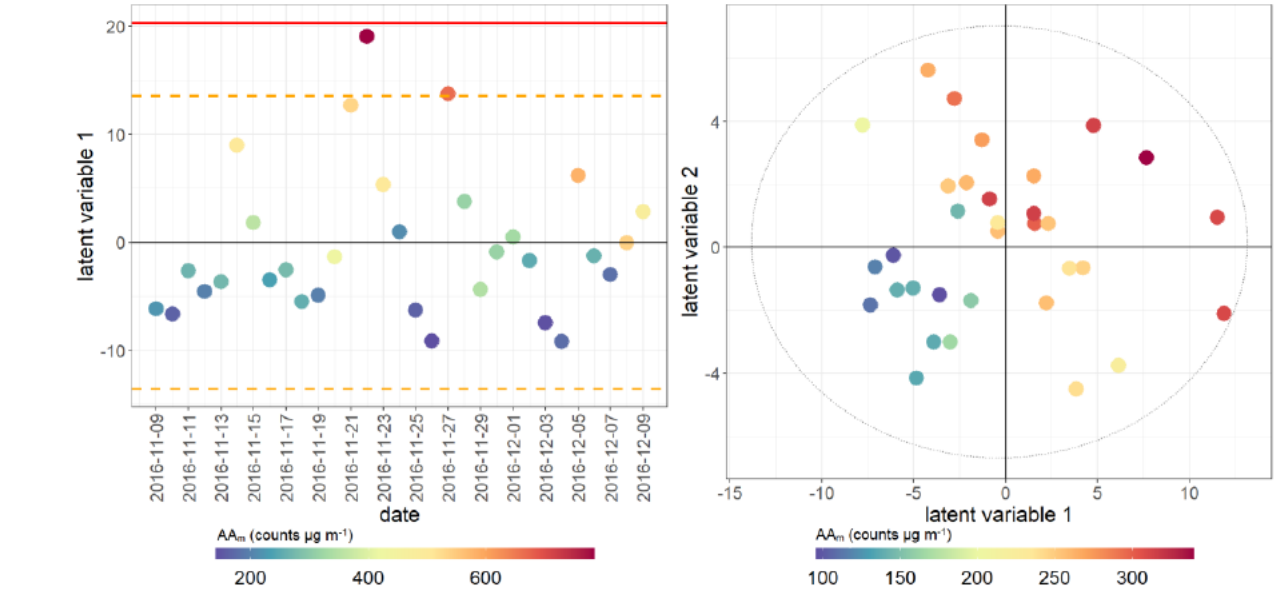

555

Figure 8. PLSR scores plot for AA_m assay. Model performance parameters given in Table 2. Left: winter samples; right: summer samples. Points coloured by overall AA assay response for both seasons. Red bar indicates 2 × SD for all scores, orange dotted line indicates 1 × SD for all scores. Models which have only one latent variable have the X-axis replaced by date for easier visualisation. The grey ellipse represents the Hotelling's T^2 statistic, a multivariate 95% confidence interval, and samples which are outside the ellipse may potentially be outliers.

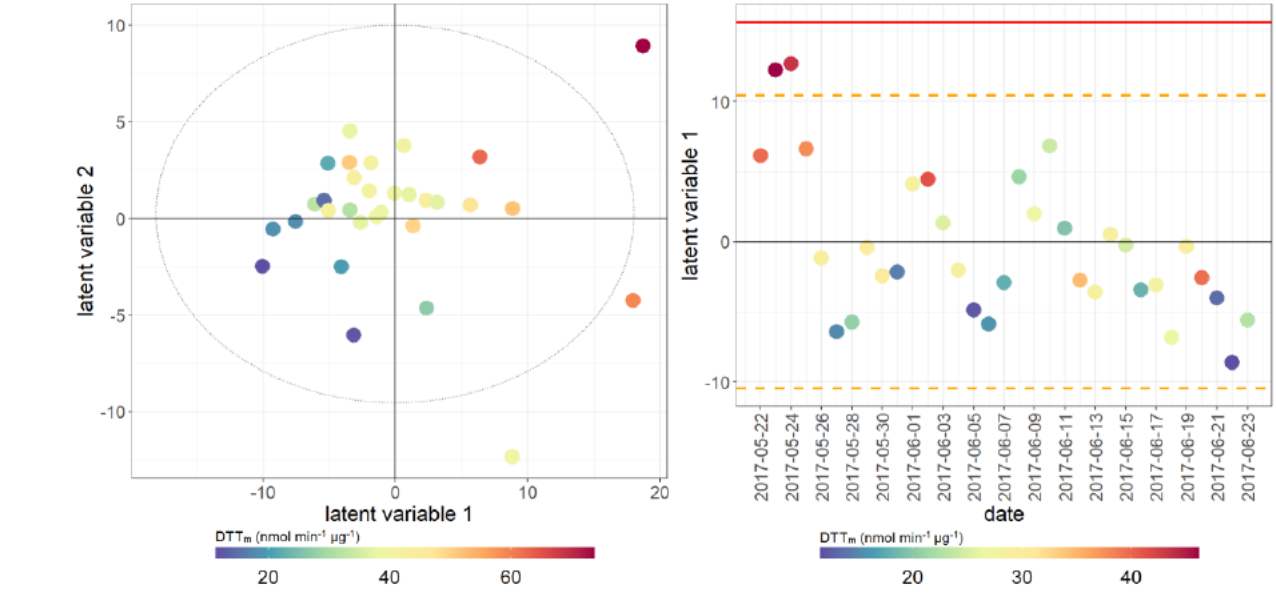

560

Figure 9. PLSR scores plot for DTT_m assay. Model performance parameters given in Table 2. Left: winter samples; right: summer samples. Points coloured by overall DTT assay response for both seasons.

Table 3 shows the top ten features in the variable importance in projection (VIP) for the PLSR loadings, which enable a ranking of the features which contribute most to the model (Naes and Martens, 1988). It is evident from these data that the

https://doi.org/10.5194/acp-2020-1024
Preprint. Discussion started: 13 October 2020

Atmospheric Chemistry and Physics Discussions

features which best model the OP_m seasonal response are derived from multiple particle sources and atmospheric aging processes. For example, the AA_m and DTT_m responses show similar trends in the multivariate models, but the main contributors to their responses have little overlap, with AA_m responses being more strongly associated with SOA tracers, PAHs and general measures of organic carbon, and the DTT_m more characterised by combustion and vehicle emissions markers (**Figure 10**). Notably, compounds which are not generally recognised as being redox-active were frequently observed to be important in PLSR classification, and though they do not directly contribute to the OP_m response, they are likely co-emitted with or are secondary products of redox-active particle components.

Table 3. Characteristic loadings most influential in PLSR models of OP_m as defined by ordered variable importance in projection for each model. Blue upward arrows indicate positive correlation with the assay measurement, red downward arrows for inverse correlation, and * for $p < 0.05$ in Spearman correlation of the feature with the assay in the univariate analysis.

EPR_m winter		AA_m winter		DTT_m winter		$DCFH_m$ winter	
feature	**VIP**	**feature**	**VIP**	**feature**	**VIP**	**feature**	**VIP**
indeno(1,2,3-cd)-pyrene *	2.12 ↑	cis-pinonic acid *	1.44 ↑	SO_2 *	1.46 ↓	NH_4^+	2.16 ↑
acenaphthylne	2.02 ↑	Cl^- *	1.42 ↑	Ca^{2+} *	1.40 ↑	chrysene *	1.61 ↓
benzo(ghi)-perylene *	2.01 ↑	total OC *	1.33 ↑	Fe *	1.37 ↑	benzo(b)-fluoranthene *	1.59 ↓
benzo(a)pyrene *	2.01 ↑	MOOOA *	1.30 ↑	fluorene	1.34 ↑	RH8 *	1.59 ↑
fluorene	1.82 ↑	pyrene *	1.30 ↑	acetaldehyde *	1.33 ↓	benzo(a)-anthracene*	1.58 ↓
benzo(a)-anthracene *	1.81 ↑	2-methylthreitol	1.29 ↑	phenanthrene *	1.33 ↑	pyrene *	1.58 ↓
dibenzo(a,h)-anthracene *	1.80 ↑	ORG *	1.29 ↑	acetone *	1.33 ↓	LOOOA *	1.57 ↑
phenanthrene *	1.77 ↑	benzo(k)-fluoranthene *	1.29 ↑	Cl^- *	1.31 ↑	fluoranthene *	1.56 ↓
chrysene *	1.66 ↑	3-methyl-2,3,4-trihydroxy-1-butene *	1.28 ↑	benzene *	1.31 ↓	RH120 * / RH240 *	1.55 ↑ 1.55 ↑
naphthalene *	1.62↑	fluoranthene *	1.27 ↑	toluene *	1.30 ↓	K^+ *	1.51 ↑

EPR_m summer		AA_m summer		DTT_m summer		$DCFH_m$ summer	
feature	**VIP**	**feature**	**VIP**	**feature**	**VIP**	**feature**	**VIP**
LOOOA	2.59 ↑	ORG *	1.80 ↑	OH	1.58 ↑	cis-pinonic acid *	2.38 ↓
T8 / T120 / T240	2.28/2.15/2.08 ↑	cis-pinonic acid *	1.62 ↑	dibenzo(a,h)-anthracene *	1.51 ↑	C31 *	1.76 ↓
O_3	2.00 ↑	MOOOA *	1.58 ↑	C26 *	1.48 ↑	pinic acid *	1.74 ↓
RO_2 *	1.76 ↑	cholesterol	1.58 ↓	benzo(a)-pyrene *	1.48 ↑	acetonitrile *	1.69 ↑
galactosan *	1.74 ↓	naphthalene *	1.57 ↑	total OC *	1.46 ↑	3-methyl-2,3,4-trihydroxy-1-butene	1.65 ↓
K^+	1.70 ↑	palmitic acid *	1.49 ↑	C30 *	1.46 ↑	benzo(ghi)-perylene	1.62 ↓
17a(H)-22,29,30-trisnorhopane (C27a)	1.55 ↓	RH8	1.39 ↓	C28 *	1.43 ↑	C32	1.61 ↓
cis-2-methyl-1,3,4-trihydroxy-1-butene	1.55 ↑	stearic acid *	1.39 ↑	benzo(ghi)-perylene *	1.41 ↑	dibenzo(a,h)-anthracene *	1.61 ↓
Ba	1.47 ↓	benzo(ghi)-perylene *	1.36 ↑	C33 *	1.40 ↑	acetaldehyde *	1.61 ↑
RH8	1.46 ↓	benzo(a)-pyrene *	1.34 ↑	C29 *	1.39 ↑	isoprene *	1.61 ↓

https://doi.org/10.5194/acp-2020-1024
Preprint. Discussion started: 13 October 2020

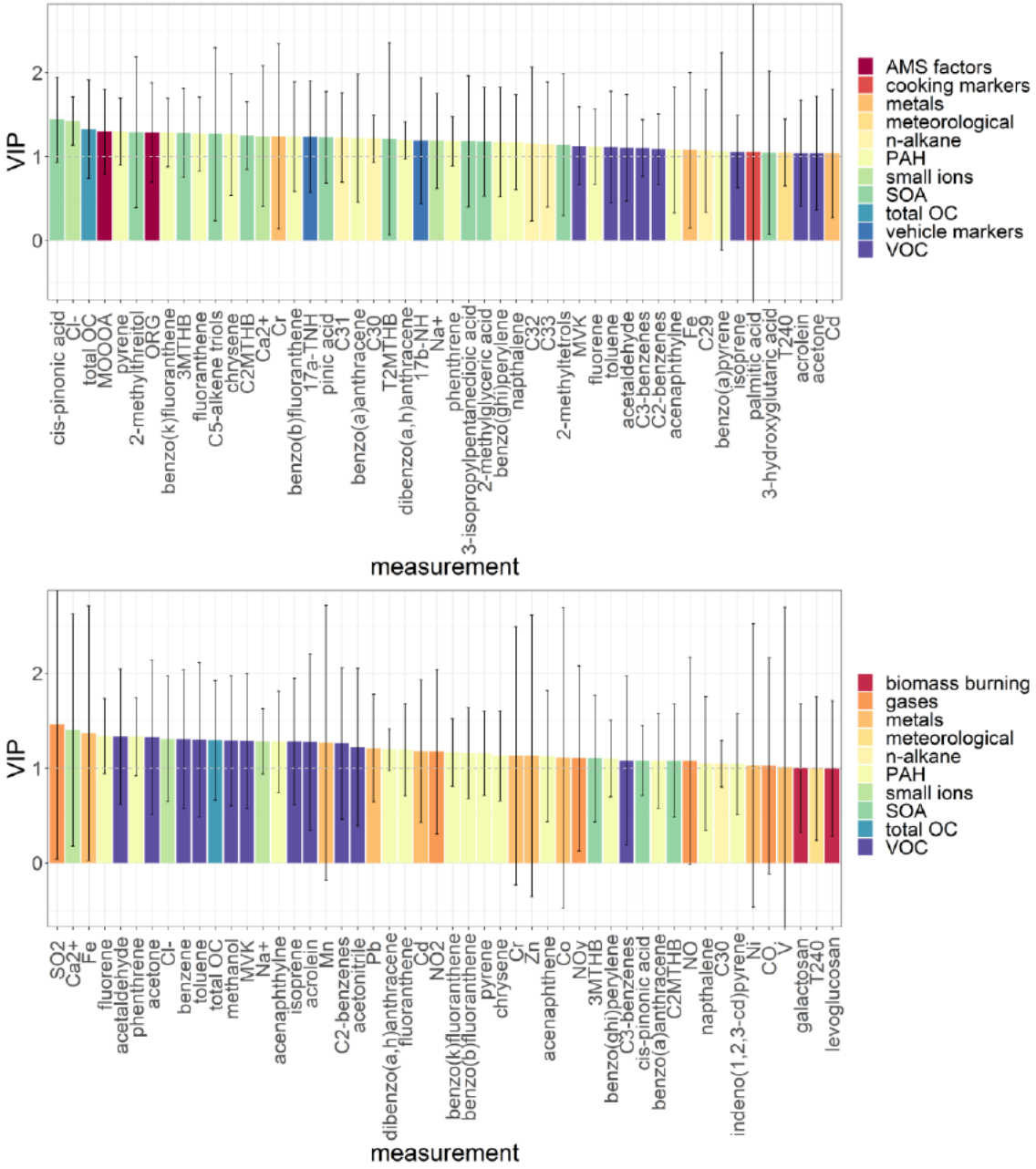

Figure 10. Variable importance in projection (VIP) plots. Above: winter AA_m PLSR model; below: winter DTT_m PLSR model (top 50 features only). Error bars represent the standard error or the mean for each feature and are often large due to the intrinsic noisiness and instability of the individual measurements. Terms with VIP > 1 contribute most significantly to the model. **Abbreviations:** 3MTHB: 3-methyl-2,3,4-trihydroxy-1-butene; C2MTHB: cis-2-methyl-1,3,4-trihydroxy-1-butene; T2MTHB: trans-2-methyl-1,3,4-trihydroxy-1-butene; 17a-TNH:17a(H)-22,29,30-trisnorhopane (C27a); 17b-NH: 17b(H),21a(H)-norhopane (C30ba); MVK: methyl vinyl ketone or methacrolein. Analogous plots for all other assays are given in **Figures S20-S27**.

https://doi.org/10.5194/acp-2020-1024
Preprint. Discussion started: 13 October 2020

Atmospheric Chemistry and Physics Discussions

3.4 Multiple Linear Regression (MLR) modelling to predict OP_m associated with specific sources

While multivariate model loadings highlighted the measurements most associated with assay response, they do not enable straightforward variable selection, which is important to characterise the specific compounds contributing to each assay OP response. Multiple linear regression modelling has been used in previous studies (Calas et al., 2018) to establish important contributors to total OP response, rather than looking at source apportionment, and only simple forward variable selection was used for model refinement. Here, relevant measurements were grouped into six categories (biogenic SOA, biomass burning, coal and fossil power generation, cooking, dust and vehicle emissions). The full method description, references, model formulae and performance parameters for the mass-normalised data models are presented in the Methods (**Section 2.3** "Statistical analysis") and in **Section S10**. Briefly, literature sources and the SPECIEUROPE database (Pernigotti et al., 2016) were used to establish which individual measurements were likely to be characteristic of each source, with several measurements appearing in multiple categories (e.g. total EC). All proxy and composite measurements (except total EC, as numerous organic carbon species are represented, but elemental carbon should be independent of most of these), AMS measurements, temperature, relative humidity and actinic flux measurements were excluded from models entirely, as the composite measures duplicate individual measurements and the atmospheric measurements complicate model interpretation. Multiple linear regression models were then constructed for each assay and season for each category, using both mass-normalised and volume-normalised data. MLR models further reinforced that not all putative sources and components of $PM_{2.5}$ contribute equally to OP_m response (**Table 4**).

Table 4. R^2 values for optimised subset multiple linear regression models of relevant source contributions. R^2 values greater than 0.7 are highlighted in bold. Full model performance indicators for mass-normalised models are provided in **Section S8** of the SI, including all model terms, residuals information, coefficients and p-values.

		EPR R^2		AA R^2		DTT R^2		DCFH R^2	
data type	**model**	**winter**	**summer**	**winter**	**summer**	**winter**	**summer**	**winter**	**summer**
µg/µg	vehicle emissions	**0.88**	**0.72**	**0.95**	**0.73**	**0.91**	**0.80**	**0.89**	0.62
µg/µg	biomass burning	0.41	0.29	0.49	0.47	0.45	0.41	0.58	0.31
µg/µg	coal/fossil fuel combustion	**0.84**	0.56	**0.88**	0.61	**0.86**	0.68	**0.75**	**0.71**
µg/µg	cooking markers	0.19	0.11	0.66	0.20	0.39	0.36	0.08	0.24
µg/µg	dust	0.23	0.23	**0.88**	0.47	**0.72**	0.46	0.50	0.26
µg/µg	biogenic SOA	0.55	0.35	**0.95**	**0.74**	**0.79**	0.61	0.55	**0.70**
µg/m³	vehicle emissions	**0.94**	**0.79**	**0.97**	**0.74**	**0.96**	**0.87**	**0.94**	**0.86**
µg/m³	biomass burning	**0.85**	0.23	**0.89**	0.24	**0.72**	0.62	**0.78**	0.53
µg/m³	coal/fossil fuel combustion	**0.91**	0.69	**0.95**	0.62	**0.88**	**0.77**	**0.93**	**0.91**
µg/m³	cooking markers	0.10	0.08	0.09	0.22	0.10	0.44	0.11	0.49
µg/m³	dust	**0.79**	0.21	**0.92**	0.30	**0.78**	0.54	**0.73**	0.63
µg/m³	biogenic SOA	**0.87**	0.36	**0.84**	0.59	**0.80**	0.63	**0.94**	**0.90**

OP_m response models based on measurements characteristic of vehicle emissions, coal/fossil fuel combustion and biomass burning gave accurate and robust predictions of particle-level OP_m, which are important contributors to PM (mass per volume) in Beijing urban background sites (Yu et al., 2013; Zheng et al., 2005). As expected, OP_v models gave very good predictions

https://doi.org/10.5194/acp-2020-1024
Preprint. Discussion started: 13 October 2020


Atmospheric Chemistry and Physics Discussions

for these source profiles, but also gave improved models of OP_v for biogenic SOA and dust compared with the mass-normalised data. Although the same base sets of predictor measurements for each source were used for each type of model (season, OP and PM normalisation), there was only partial overlap of predictors between models from the same source and season, again illustrating the complex dynamic between OP and overall mass/volume composition. As with the PLSR models, the most important contributors to regression models were often not redox-active species, indicating that they could be influencing or contributing to the oxidation state of the redox-active PM components, either through co-emission, propagation reactions or by direct oxidation of the species themselves. As with the univariate and multivariate analyses, the summer samples gave less robust linear regression models (and thus OP predictions) from both mass- and volume-normalised data. However, AA and DTT measurements produced the best subset modelling for all source panels, indicating that these assays might be most optimal for measuring OP in an urban environment, as they appear to reflect the variety of PM sources well.

Vehicle emissions, biogenic SOA and winter biomass burning contributions to AA and DTT response (as measured by the model R^2 value) were generally comparable across all assays, contrasting with the findings of Fang et al. (2016), who observed greater OP response in positive matrix factorization-chemical mass balance (PMF-CMB) models associated with traffic emissions for AA_v over DTT_v, and biomass burning for DTT_v over AA_v in multiple locations in the southeastern US. However, a more recent study conducted in the coastal areas adjacent to Beijing (Liu et al., 2018) observed similar seasonality to the present study in the DTT_m OP response. Vehicle emissions (Wang et al., 2016; Yu et al., 2019), coal combustion (Ma et al., 2018; Yu et al., 2019), biomass burning (Ma et al., 2018) and dust (Yu et al., 2019) sources have been shown in other studies using PMF models to contribute to OP_v in Beijing, all using the DTT assay. Cooking markers (palmitic acid, stearic acid and cholesterol) contributed a substantial proportion of the known organic fraction of the PM mass and volume concentrations (see **Figure 4**), but did not contribute robustly to the modelled OP response for either normalisation type, suggesting they are either not strongly contributing to or affected by oxidative conditions in PM, or that their variation over the sampling period cannot be linearly modelled. Similarly, biomass burning markers contribute a comparable number of variables in the model base sets, but appear to contribute much more significantly to the OP_v than to the OP_m response. Biogenic SOA and dust models (which incorporate K^+, Na^+, Ca^{2+}, Cl^-, Al, Ti, Mn, Fe and Zn) explain a significant proportion of winter OP_v responses, but are only strongly correlated with winter AA and DTT for mass-normalised models. This suggests these sources contribute to PM OP_v by total quantity rather than through their particularly high intrinsic OP_m, i.e. their mass as a proportion of the PM mass is smaller, but the number of particles per volume is greater, and the AA and DTT assays have a higher sensitivity for these species over the EPR and DCFH assays.

It should be noted that the MLR models represent a sub-optimal prediction of the OP response from measured components, as numerous species which are known source components (e.g. PAH in combustion processes and distinguishing gasoline from diesel vehicles, VOCs in biomass burning) could not be included in models. Not all measurements which were associated in the literature with a particular assay response passed the stages of variable selection for mass-normalised models, which could reflect a lower limit of detection in either the OP_m assay responses, or in the individual component measurements. Moreover, MLR models do not fully account for the proportion of each measurement which may originate from multiple sources, and

https://doi.org/10.5194/acp-2020-1024
Preprint. Discussion started: 13 October 2020


Atmospheric Chemistry and Physics Discussions

PMF-CMB or mixed effects models would address more adequately. Validation of the multivariate and MLR models using secondary datasets (both from Beijing and other locales) is also needed prior to their future implementation.

4 Conclusions

This study presents a detailed and comprehensive analysis of $PM_{2.5}$ oxidative potential measured in winter 2016 and summer 2017 during the APHH-Beijing campaign at a central site in Beijing, China. Four acellular methods for measuring OP were applied, and correlated with 107 additional atmospheric measurements (particle components, trace gases, meteorological parameters) to delineate chemical particle components and atmospheric processes and sources responsible for driving $PM_{2.5}$ OP. Higher volume-normalised and mass-normalised OP values across all assays were observed in the winter compared to the summer. An inverse correlation was observed between AA_m and DTT_m with overall $PM_{2.5}$ mass concentrations, i.e. days with higher $PM_{2.5}$ mass concentrations have lower intrinsic OP values. This is likely due to an increase in OP-inactive material in high $PM_{2.5}$ mass days, and/or a mass fraction that is at present undetermined and highlights that a focus on total PM exposure only does not necessarily capture accurately the toxicological effects of PM.

Univariate analysis with the additional 107 measurement parameters acquired during the APHH-Beijing campaign highlight significant assay-specific responses to chemical components of $PM_{2.5}$, as well as a seasonal difference between the components which drive aerosol OP. It also highlights the importance of considering both volume-normalised and mass-normalised OP metrics when drawing conclusions on the role of chemical composition on OP, as assay correlations vary significantly between the two metrics. The data presented in this study illustrates that mass-normalised OP_m values provide a more nuanced picture of specific chemical components and sources that influence intrinsic OP, whereas many more correlations with OP_v values are observed, likely due to collinearity of many chemical components with overall $PM_{2.5}$ mass concentrations driven by changes in meteorological conditions. Both metrics, mass-normalised OP as well as volume-normalised OP, are important to consider, with OP_v a more relevant metric with respect to exposure and epidemiological studies, whereas OP_m provides more insight into what sources and what composition drives OP concentrations in particles. Furthermore, OP_m may allow easier study and site inter-comparisons, and reduces the impact on analyses of collinearity between $PM_{2.5}$ mass and concentrations of PM components due to meteorological factors.

The multivariate statistical analyses encapsulated the observations from the univariate analyses into comprehensive single models of OP relating to PM composition, and the inference from the univariate analyses that OP_m measured by each assay is related to different compounds present in the particle was confirmed. Variable selection of measurements and evaluation through multiple linear regression models indicated that OP_m is well predicted by measurement panels characteristic of combustion sources, particularly (exhaust and non-exhaust) vehicle emissions, and biogenic SOA. At present no single assay is completely representative of the totality of OP effects present in atmospheric PM. The comprehensive statistical analysis performed here shows that all four OP assays are sensitive to a range of different aerosol components, sources and atmospheric

https://doi.org/10.5194/acp-2020-1024
Preprint. Discussion started: 13 October 2020

conditions and illustrate that with the current state of knowledge none of these four assays can be disregarded with respect to their relevance for particle toxicity.

Author Contributions. SJC collated data, analysed filters for AA and DCFH, performed data analysis and interpretation and wrote the manuscript. KW performed univariate and multivariate statistical analysis, data interpretation and wrote the manuscript. BU, JW, ST and NS analysed filters for AA, DCFH, DTT and EPR respectively. TV provided XRF and additional data. AMS data were provided by YS. PAH data was provided by AE and AL. SOA tracer data was provided by DL, LL and PF. All other authors contributed to data analysis, interpretation and writing of the manuscript.

Competing Interests. The authors declare that they have no conflict of interest

Special Issue Statement. This article is part of the special issue "In-depth study of air pollution sources and processes within Beijing and its surrounding region (APHH-Beijing) (ACP/AMT inter-journal SI)

Acknowledgements. This work was funded by the European Research Council (ERC grant 279405), by the Natural Environment Research Council (NERC) (NE/K008218/1) and the Swiss National Science Foundation (200021_192192 / 1). This work has also received funding from the European Union's Horizon 2020 research and innovation programme through the EUROCHAMP-2020 Infrastructure Activity under grant agreement No. 730997. SSS additionally acknowledges support from the Swiss National Science Foundation (fellowship P2EZP2_162258) and a 2017 LIFE PostDoc fellowship by the AXA Research Fund. We acknowledge the support from Pingqing Fu, Zifa Wang, Jie Li and Yele Sun from IAP for hosting the APHH-Beijing campaign at IAP. We thank Di Liu from the University of Birmingham, Siyao Yue, Liangfang Wei, Hong Ren, Qiaorong Xie, Wanyu Zhao, Linjie Li, Ping Li, Shengjie Hou, Qingqing Wang from IAP, Rachel Dunmore and James Lee from the University of York, Kebin He and Xiaoting Cheng from Tsinghua University, and James Allan and Hugh Coe from the University of Manchester for providing logistic and scientific support for the field campaigns.

References

Acton, J., Hewitt, N., Huang, Z. and Wang, X.: APHH: Volatile organic compound (VOC) mixing ratios made at the IAP-Beijing site during the summer and winter campaigns. Centre for Environmental Data Analysis, 18.06.2020 https://catalogue.ceda.ac.uk/uuid/de37c54e59a548ccb9f168ee724f3769, 2018.

Arangio, A. M., Tong, H., Socorro, J., Pöschl, U. and Shiraiwa, M.: Quantification of environmentally persistent free radicals and reactive oxygen species in atmospheric aerosol particles, Atmos. Chem. Phys., 16(20), 13105–13119, doi:10.5194/acp-16-13105-2016, 2016.

Atkinson, R. and Arey, J.: Mechanisms of the gas-phase reactions of aromatic hydrocarbons and pahs with oh and NO3

https://doi.org/10.5194/acp-2020-1024
Preprint. Discussion started: 13 October 2020

radicals, Polycycl. Aromat. Compd., 27(1), 15–40, doi:10.1080/10406630601134243, 2007.

Bates, J. T., Weber, R. J., Abrams, J., Verma, V., Fang, T., Klein, M., Strickland, M. J., Sarnat, S. E., Chang, H. H., Mulholland, J. A., Tolbert, P. E. and Russell, A. G.: Reactive Oxygen Species Generation Linked to Sources of Atmospheric Particulate Matter and Cardiorespiratory Effects, Environ. Sci. Technol., 49(22), 13605–13612, doi:10.1021/acs.est.5b02967, 2015.

Bates, J. T., Fang, T., Verma, V., Zeng, L., Weber, R. J., Tolbert, P. E., Abrams, J. Y., Sarnat, S. E., Klein, M., Mulholland, J. A. and Russell, A. G.: Review of Acellular Assays of Ambient Particulate Matter Oxidative Potential: Methods and Relationships with Composition, Sources, and Health Effects, Environ. Sci. Technol., 53(8), 4003–4019, doi:10.1021/acs.est.8b03430, 2019.

Biswas, S., Verma, V., Schauer, J. J., Cassee, F. R., Cho, A. K. and Sioutas, C.: Oxidative potential of semi-volatile and non volatile particulate matter (PM) from heavy-duty vehicles retrofitted with emission control technologies, Environ. Sci. Technol., 43(10), 3905–3912, doi:10.1021/es9000592, 2009.

Calas, A., Uzu, G., Kelly, F. J., Houdier, S., Martins, J. M. F., Thomas, F., Molton, F., Charron, A., Dunster, C., Oliete, A., Jacob, V., Besombes, J. L., Chevrier, F. and Jaffrezo, J. L.: Comparison between five acellular oxidative potential measurement assays performed with detailed chemistry on PM10 samples from the city of Chamonix (France), Atmos. Chem. Phys., 18(11), 7863–7875, doi:10.5194/acp-18-7863-2018, 2018.

Campbell, S., Stevanovic, S., Miljevic, B., Bottle, S. E., Ristovski, Z. D. and Kalberer, M.: Quantification of Particle-bound Organic Radicals in Secondary Organic Aerosol, Environ. Sci. Technol., 53, 6729–6737, doi:10.1021/acs.est.9b00825, 2019a.

Campbell, S. J., Utinger, B., Lienhard, D. M., Paulson, S. E., Shen, J., Griffiths, P. T., Stell, A. C. and Kalberer, M.: Development of a physiologically relevant online chemical assay to quantify aerosol oxidative potential, Anal. Chem., 91, 13088–13095, doi:10.1021/acs.analchem.9b03282, 2019b.

Charrier, J. G. and Anastasio, C.: Impacts of antioxidants on hydroxyl radical production from individual and mixed transition metals in a surrogate lung fluid, Atmos. Environ., 45(40), 7555–7562, doi:10.1016/j.atmosenv.2010.12.021, 2011.

Charrier, J. G. and Anastasio, C.: On dithiothreitol (DTT) as a measure of oxidative potential for ambient particles: evidence for the importance of soluble transition metals, Atmos. Chem. Phys., 12(19), 9321–9333, doi:10.5194/acp-12-9321-2012, 2012.

Charrier, J. G., McFall, A. S., Richards-Henderson, N. K. and Anastasio, C.: Hydrogen peroxide formation in a surrogate lung fluid by transition metals and quinones present in particulate matter, Environ. Sci. Technol., 48(12), 7010–7017, doi:10.1021/es501011w, 2014.

Charrier, J. G., Richards-Henderson, N. K., Bein, K. J., McFall, A. S., Wexler, A. S. and Anastasio, C.: Oxidant production from source-oriented particulate matter - Part 1: Oxidative potential using the dithiothreitol (DTT) assay, Atmos. Chem. Phys., 15(5), 2327–2340, doi:10.5194/acp-15-2327-2015, 2015.

Charrier, J. G., McFall, A. S., Vu, K. K. T., Baroi, J., Olea, C., Hasson, A. and Anastasio, C.: A bias in the "mass-normalized" DTT response – An effect of non-linear concentration-response curves for copper and manganese, Atmos. Environ., 144, 325–334, doi:10.1016/j.atmosenv.2016.08.071, 2016.

https://doi.org/10.5194/acp-2020-1024
Preprint. Discussion started: 13 October 2020

740 Cho, A. K., Sioutas, C., Miguel, A. H., Kumagai, Y., Schmitz, D. A., Singh, M., Eiguren-Fernandez, A. and Froines, J. R.: Redox activity of airborne particulate matter at different sites in the Los Angeles Basin, Environ. Res., 99(1), 40–47, doi:10.1016/j.envres.2005.01.003, 2005.

Chung, M. Y., Lazaro, R. A., Lim, D., Jackson, J., Lyon, J., Rendulic, D. and Hasson, A. S.: Aerosol-borne quinones and reactive oxygen species generation by particulate matter extracts, Environ. Sci. Technol., 40(16), 4880–4886,
745 doi:10.1021/es0515957, 2006.

Dellinger, B., Pryor, W. A., Cueto, R., Squadrito, G. L., Hegde, V. and Deutsch, W. A.: Role of free radicals in the toxicity of airborne fine particulate matter, Chem. Res. Toxicol., 14(10), 1371–1377, doi:10.1021/tx010050x, 2001.

Ding, X., He, Q. F., Shen, R. Q., Yu, Q. Q., Zhang, Y. Q., Xin, J. Y., Wen, T. X. and Wang, X. M.: Spatial and seasonal variations of isoprene secondary organic aerosol in China: Significant impact of biomass burning during winter, Sci. Rep.,
750 6(20411), 1–10, doi:10.1038/srep20411, 2016.

Donaldson, K. and Tran, C. L.: Inflammation Caused By Particles and Fibers, Inhal. Toxicol., 14(1), 5–27, doi:10.1080/089583701753338613, 2002.

Dou, J., Lin, P., Kuang, B. Y. and Yu, J. Z.: Reactive oxygen species production mediated by humic-like substances in atmospheric aerosols: Enhancement effects by pyridine, imidazole, and their derivatives, Environ. Sci. Technol., 49(11), 6457–
755 6465, doi:10.1021/es5059378, 2015.

Elzein, A., Dunmore, R. E., Ward, M. W., Hamilton, J. F. and Lewis, A. C.: Variability of polycyclic aromatic hydrocarbons and their oxidative derivatives in wintertime Beijing, China, Atmos. Chem. Phys. Discuss., 1–28, doi:10.5194/acp-2019-120, 2019.

Elzein, A., Stewart, G. J., Swift, S. J., Nelson, B. S., Crilley, L. R., Alam, M. S., Reyes-villegas, E., Gadi, R., Harrison, R. M.,
760 Hamilton, J. F. and Lewis, A. C.: A comparison of PM 2 . 5 -bound polycyclic aromatic hydrocarbons in summer Beijing (China) and Delhi (India), Atmos. Chem. Phys. Discuss., (August), 1–25, doi:https://doi.org/10.5194/acp-2020-770, 2020.

Eriksson, L., Byrne, T., Johansson, E., Trygg, J. and Vikstrom, C.: Multi-and megavariate data analysis basic principles and applications., 2013.

Fang, T., Verma, V., Guo, H., King, L. E., Edgerton, E. S. and Weber, R. J.: A semi-automated system for quantifying the
765 oxidative potential of ambient particles in aqueous extracts using the dithiothreitol (DTT) assay: Results from the Southeastern Center for Air Pollution and Epidemiology (SCAPE), Atmos. Meas. Tech., 8(1), 471–482, doi:10.5194/amt-8-471-2015, 2015.

Fang, T., Verma, V., Bates, J. T., Abrams, J., Klein, M., Strickland, M. J., Sarnat, S. E., Chang, H. H., Mulholland, J. A., Tolbert, P. E., Russell, A. G. and Weber, R. J.: Oxidative potential of ambient water-soluble PM 2 . 5 in the southeastern United States : contrasts in sources and health associations between ascorbic acid (AA) and dithiothreitol (DTT) assays, ,
770 3865–3879, doi:10.5194/acp-16-3865-2016, 2016.

Feng, B., Li, L., Xu, H., Wang, T., Wu, R., Chen, J., Zhang, Y., Liu, S., Ho, S. S. H., Cao, J. and Huang, W.: PM2.5-bound polycyclic aromatic hydrocarbons (PAHs) in Beijing: Seasonal variations, sources, and risk assessment, J. Environ. Sci. (China), 77, 11–19, doi:10.1016/j.jes.2017.12.025, 2019.

https://doi.org/10.5194/acp-2020-1024
Preprint. Discussion started: 13 October 2020

Fuller, S. J., Wragg, F. P. H., Nutter, J. and Kalberer, M.: Comparison of on-line and off-line methods to quantify reactive oxygen species (ROS) in atmospheric aerosols, Atmos. Environ., 92, 97–103, doi:10.1016/j.atmosenv.2014.04.006, 2014.

Gallimore, P. J., Mahon, B. M., Wragg, F. P. H., Fuller, S. J., Giorio, C., Kourtchev, I. and Kalberer, M.: Multiphase composition changes and reactive oxygen species formation during limonene oxidation in the new Cambridge Atmospheric Simulation Chamber (CASC), Atmos. Chem. Phys., 17, 9853–9868, doi:10.5194/acp-2017-186, 2017.

Gao, J., Tian, H., Cheng, K., Lu, L., Wang, Y., Wu, Y., Zhu, C., Liu, K., Zhou, J., Liu, X., Chen, J. and Hao, J.: Seasonal and spatial variation of trace elements in multi-size airborne particulate matters of Beijing, China: Mass concentration, enrichment characteristics, source apportionment, chemical speciation and bioavailability, Atmos. Environ., 99, 257–265, doi:10.1016/j.atmosenv.2014.08.081, 2014.

Gehling, W. and Dellinger, B.: Environmentally persistent free radicals and their lifetimes in PM2.5, Environ. Sci. Technol., 47(15), 8172–8178, doi:10.1021/es401767m, 2013.

Gehling, W., Khachatryan, L. and Dellinger, B.: Hydroxyl radical generation from environmentally persistent free radicals (EPFRs) in PM2.5, Environ. Sci. Technol., 48(8), 4266–4272, doi:10.1021/es401770y, 2014.

Ghio, A. J., Stonehuerner, J., Dailey, L. A. and Carter, J. D.: Metals associated with both the water-soluble and insoluble fractions of an ambient air pollution particle catalyze an oxidative stress, Inhal. Toxicol., 11(1), 37–49, doi:10.1080/089583799197258, 1999.

Ghio, A. J., Carraway, M. S. and Madden, M. C.: Composition of air pollution particles and oxidative stress in cells, tissues, and living systems, J. Toxicol. Environ. Heal. - Part B Crit. Rev., 15(1), 1–21, doi:10.1080/10937404.2012.632359, 2012.

Godri, K. J., Harrison, R. M., Evans, T., Baker, T., Dunster, C., Mudway, I. S. and Kelly, F. J.: Increased oxidative burden associated with traffic component of ambient particulate matter at roadside and Urban background schools sites in London, PLoS One, 6(7), doi:10.1371/journal.pone.0021961, 2011.

Hart, J. E., Liao, X., Hong, B., Puett, R. C., Yanosky, J. D., Suh, H., Kioumourtzoglou, M. A., Spiegelman, D. and Laden, F.: The association of long-term exposure to PM2.5 on all-cause mortality in the Nurses' Health Study and the impact of measurement-error correction, Environ. Heal., 14(1), 38, doi:10.1186/s12940-015-0027-6, 2015.

Hasson, A. S. and Paulson, S. E.: An investigation of the relationship between gas-phase and aerosol-borne hydroperoxides in urban air, J. Aerosol Sci., 34(4), 459–468, doi:10.1016/S0021-8502(03)00002-8, 2003.

He, L. Y., Hu, M., Huang, X. F., Zhang, Y. H. and Tang, X. Y.: Seasonal pollution characteristics of organic compounds in atmospheric fine particles in Beijing, Sci. Total Environ., 359(1–3), 167–176, doi:10.1016/j.scitotenv.2005.05.044, 2006.

Hewitt, C. N. and Kok, G. L.: Formation and occurrence of organic hydroperoxides in the troposphere: Laboratory and field observations, J. Atmos. Chem., 12(2), 181–194, doi:10.1007/BF00115779, 1991.

Hung, H. F. and Wang, C.-S.: Experimental determination of reactive oxygen species in Taipei aerosols, J. Aerosol Sci., 32(10), 1201–1211, doi:10.1016/S0021-8502(01)00051-9, 2001.

Janssen, N. A. H., Yang, A., Strak, M., Steenhof, M., Hellack, B., Gerlofs-Nijland, M. E., Kuhlbusch, T., Kelly, F., Harrison, R., Brunekreef, B., Hoek, G. and Cassee, F.: Oxidative potential of particulate matter collected at sites with different source

https://doi.org/10.5194/acp-2020-1024
Preprint. Discussion started: 13 October 2020


Atmospheric Chemistry and Physics Discussions

characteristics, Sci. Total Environ., 472, 572–581, doi:10.1016/j.scitotenv.2013.11.099, 2014.

Jedynska, A., Hoek, G., Wang, M., Yang, A., Eeftens, M., Cyrys, J., Keuken, M., Ampe, C., Beelen, R., Cesaroni, G., Forastiere, F., Cirach, M., de Hoogh, K., De Nazelle, A., Nystad, W., Akhlaghi, H. M., Declercq, C., Stempfelet, M., Eriksen, K. T., Dimakopoulou, K., Lanki, T., Meliefste, K., Nieuwenhuijsen, M., Yli-Tuomi, T., Raaschou-Nielsen, O., Janssen, N. A. H., Brunekreef, B. and Kooter, I. M.: Spatial variations and development of land use regression models of oxidative potential in ten European study areas, Atmos. Environ., 150, 24–32, doi:10.1016/j.atmosenv.2016.11.029, 2017.

Kelly, F. J.: Oxidative stress: its role in air pollution and adverse health effects, Occup. Environ. Med., 60(8), 612–616, doi:10.1136/oem.60.8.612, 2003.

Knaapen, A. M., Borm, P. J. A., Albrecht, C. and Schins, R. P. F.: Inhaled particles and lung cancer. Part A: Mechanisms, Int. J. Cancer, 109(6), 799–809, doi:10.1002/ijc.11708, 2004.

Laden, F., Schwartz, J., Speizer, F. E. and Dockery, D. W.: Reduction in fine particulate air pollution and mortality: Extended follow-up of the Harvard Six Cities Study, Am. J. Respir. Crit. Care Med., 173(6), 667–672, doi:10.1164/rccm.200503-443OC, 2006.

Laing, S., Wang, G., Briazova, T., Zhang, C., Wang, A., Zheng, Z., Gow, A., Chen, A. F., Rajagopalan, S., Chen, L. C., Sun, Q. and Zhang, K.: Airborne particulate matter selectively activates endoplasmic reticulum stress response in the lung and liver tissues, Am. J. Physiol. - Cell Physiol., 299(4), 736–749, doi:10.1152/ajpcell.00529.2009, 2010.

Lelieveld, J., Pozzer, A., Pöschl, U., Fnais, M., Haines, A. and Münzel, T.: Loss of life expectancy from air pollution compared to other risk factors: a worldwide perspective, Cardiovasc. Res., 116(11), 1910–1917, doi:10.1093/cvr/cvaa025, 2020.

Lepeule, J., Laden, F., Dockery, D. and Schwartz, J.: Chronic exposure to fine particles and mortality: An extended follow-up of the Harvard six cities study from 1974 to 2009, Environ. Health Perspect., 120(7), 965–970, doi:10.1289/ehp.1104660, 2012.

Levy, J. I., Diez, D., Dou, Y., Barr, C. D. and Dominici, F.: A meta-analysis and multisite time-series analysis of the differential toxicity of major fine particulate matter constituents, Am. J. Epidemiol., 175(11), 1091–1099, doi:10.1093/aje/kwr457, 2012.

Li, N., Hao, M., Phalen, R. F., Hinds, W. C. and Nel, A. E.: Particulate air pollutants and asthma: A paradigm for the role of oxidative stress in PM-induced adverse health effects, Clin. Immunol., 109(3), 250–265, doi:10.1016/j.clim.2003.08.006, 2003.

Li, N., Xia, T. and Nel, A. E.: The Role of Oxidative Stess in Ambient Particulate Matter Induced Lung Diseases and its Implications in the Toxicity of Engineered Nanoparticles, Free Radic. Bio. Med., 9(44), 1689–1699, doi:10.1038/mp.2011.182.doi, 2008.

Li, X., Jiang, L., Bai, Y., Yang, Y., Liu, S., Chen, X., Xu, J., Liu, Y., Wang, Y., Guo, X., Wang, Y. and Wang, G.: Wintertime aerosol chemistry in Beijing during haze period: Significant contribution from secondary formation and biomass burning emission, Atmos. Res., 218(October 2018), 25–33, doi:10.1016/j.atmosres.2018.10.010, 2019.

Li, Y.: Observational accuracy of sunrise and sunset times in the sixth century China, Chinese J. Astron. Astrophys., 6(5), doi:10.1088/1009-9271/6/5/16, 2006.

https://doi.org/10.5194/acp-2020-1024
Preprint. Discussion started: 13 October 2020

Liang, L., Engling, G., Duan, F., Cheng, Y. and He, K.: Characteristics of 2-methyltetrols in ambient aerosol in Beijing, China, Atmos. Environ., 59, 376–381, doi:10.1016/j.atmosenv.2012.05.052, 2012.

Lim, Y. Bin and Ziemann, P. J.: Products and mechanism of secondary organic aerosol formation from reactions of n-alkanes with OH radicals in the presence of NO x, Environ. Sci. Technol., 39(23), 9229–9236, doi:10.1021/es051447g, 2005.

Liu, D., Harrison, R. M., Vu, T., Xu, J., Shi, Z., Li, L., Sun, Y. and Fu, P.: Estimation of biogenic and anthropogenic precursor contributions to secondary organic aerosol in Beijing using molecular tracers, Prep., 2020.

Liu, Q., Baumgartner, J., Zhang, Y., Liu, Y., Sun, Y. and Zhang, M.: Oxidative potential and inflammatory impacts of source apportioned ambient air pollution in Beijing, Environ. Sci. Technol., 48(21), 12920–12929, doi:10.1021/es5029876, 2014.

Liu, W. J., Xu, Y. S., Liu, W. X., Liu, Q. Y., Yu, S. Y., Liu, Y., Wang, X. and Tao, S.: Oxidative potential of ambient PM2.5 in the coastal cities of the Bohai Sea, northern China: Seasonal variation and source apportionment, Environ. Pollut., 236, 514–528, doi:10.1016/j.envpol.2018.01.116, 2018.

Ma, Y., Cheng, Y., Qiu, X., Cao, G., Fang, Y., Wang, J., Zhu, T., Yu, J. and Hu, D.: Sources and oxidative potential of water-soluble humic-like substances (HULISWS) in fine particulate matter (PM2.5) in Beijing, Atmos. Chem. Phys., 18(8), 5607–5617, doi:10.5194/acp-18-5607-2018, 2018.

McWhinney, R. D., Badali, K., Liggio, J., Li, S. M. and Abbatt, J. P. D.: Filterable redox cycling activity: A comparison between diesel exhaust particles and secondary organic aerosol constituents, Environ. Sci. Technol., 47(7), 3362–3369, doi:10.1021/es304676x, 2013a.

McWhinney, R. D., Zhou, S. and Abbatt, J. P. D.: Naphthalene SOA: Redox activity and naphthoquinone gas-particle partitioning, Atmos. Chem. Phys., 13(19), 9731–9744, doi:10.5194/acp-13-9731-2013, 2013b.

Meng, Z. and Zhang, Q.: Oxidative damage of dust storm fine particles instillation on lungs, hearts and livers of rats, Environ. Toxicol. Pharmacol., 22(3), 277–282, doi:10.1016/j.etap.2006.04.005, 2006.

Miller, M. R., Borthwick, S. J., Shaw, C. A., McLean, S. G., McClure, D., Mills, N. L., Duffin, R., Donaldson, K., Megson, I. L., Hadoke, P. W. F. and Newby, D. E.: Direct impairment of vascular function by diesel exhaust particulate through reduced bioavailability of endothelium-derived nitric oxide induced by superoxide free radicals, Environ. Health Perspect., 117(4), 611–616, doi:10.1289/ehp.0800235, 2009.

Miyata, R. and van Eeden, S. F.: The innate and adaptive immune response induced by alveolar macrophages exposed to ambient particulate matter, Toxicol. Appl. Pharmacol., 257(2), 209–226, doi:10.1016/j.taap.2011.09.007, 2011.

Moorthy, B., Chu, C. and Carlin, D. J.: Polycyclic aromatic hydrocarbons: From metabolism to lung cancer, Toxicol. Sci., 145(1), 5–15, doi:10.1093/toxsci/kfv040, 2015.

Müller, L., Reinnig, M. C., Naumann, K. H., Saathoff, H., Mentel, T. F., Donahue, N. M. and Hoffmann, T.: Formation of 3-methyl-1,2,3-butanetricarboxylic acid via gas phase oxidation of pinonic acid - A mass spectrometric study of SOA aging, Atmos. Chem. Phys., 12(3), 1483–1496, doi:10.5194/acp-12-1483-2012, 2012.

Naes, T. and Martens, H.: Principal component regression in NIR analysis: viewpoints, background details and selection of components, J. Chemom., 2(2), 155–167, 1988.

https://doi.org/10.5194/acp-2020-1024
Preprint. Discussion started: 13 October 2020

Ntziachristos, L., Froines, J. R., Cho, A. K. and Sioutas, C.: Relationship between redox activity and chemical speciation of size-fractionated particulate matter, Part. Fibre Toxicol., 4, 1–12, doi:10.1186/1743-8977-4-5, 2007.

Oberdorster, G., Ferin, J., Gelein, R., Soderholm, S. C. and Finkelstein, J.: Role of the alveolar macrophage in lung injury: Studies with ultrafine particles, Environ. Health Perspect., 97, 193–199, doi:10.1289/ehp.97-1519541, 1992.

Øvrevik, J., Refsnes, M., Låg, M., Holme, J. A. and Schwarze, P. E.: Activation of proinflammatory responses in cells of the airway mucosa by particulate matter: Oxidant- and non-oxidant-mediated triggering mechanisms, Biomolecules, 5(3), 1399–1440, doi:10.3390/biom5031399, 2015.

Paatero, P. and Tapper, U.: Postivie Matrix Factorisation: A non-negative factor model with optimal utilization of error estimates of data values, Environmetrics, 5(2), 111–126, 1994.

Panagi, M., Fleming, Z. L., Monks, P. S., Ashfold, M. J., Wild, O., Hollaway, M., Zhang, Q., Squires, F. A. and Vande Hey, J. D.: Investigating the regional contributions to air pollution in Beijing: A dispersion modelling study using CO as a tracer, Atmos. Chem. Phys., 20(5), 2825–2838, doi:10.5194/acp-20-2825-2020, 2020.

Pant, P., Baker, S. J., Shukla, A., Maikawa, C., Godri Pollitt, K. J. and Harrison, R. M.: The PM10 fraction of road dust in the UK and India: Characterization, source profiles and oxidative potential, Sci. Total Environ., 530–531, 445–452, doi:10.1016/j.scitotenv.2015.05.084, 2015.

Paulson, S. E., Gallimore, P. J., Kuang, X. M., Chen, J. R., Kalberer, M. and Gonzalez, D. H.: A light-driven burst of hydroxyl radicals dominates oxidation chemistry in newly activated cloud droplets, Sci. Adv., 5(5), 1–8, doi:10.1126/sciadv.aav7689, 2019.

Pernigotti, D., Belis, C. A. and Spano, L.: SPECIEUROPE: The European data base for PM source profiles., Atmos. Pollut. Res., 7(2), 307–314, 2016.

Platt, S. M., Haddad, I. El, Pieber, S. M., Huang, R. J., Zardini, A. A., Clairotte, M., Suarez-Bertoa, R., Barmet, P., Pfaffenberger, L., Wolf, R., Slowik, J. G., Fuller, S. J., Kalberer, M., Chirico, R., Dommen, J., Astorga, C., Zimmermann, R., Marchand, N., Hellebust, S., Temime-Roussel, B., Baltensperger, U. and Prévôt, A. S. H.: Two-stroke scooters are a dominant source of air pollution in many cities, Nat. Commun., 5(May), 1–7, doi:10.1038/ncomms4749, 2014.

Pope, C. A. and Dockery, D. W.: Health effects of fine particulate air pollution: Lines that connect, J. Air Waste Manag. Assoc., 56(6), 709–742, doi:10.1080/10473289.2006.10464485, 2006.

Presto, A. A., Miracolo, M. A., Donahue, N. M. and Robinson, A. L.: Secondary organic aerosol formation from high-NOx Photo-oxidation of low volatility precursors: N-alkanes, Environ. Sci. Technol., 44(6), 2029–2034, doi:10.1021/es903712r, 2010.

Puthussery, J. V., Singh, A., Rai, P., Bhattu, D., Kumar, V., Vats, P., Furger, M., Rastogi, N., Slowik, J. G., Ganguly, D., Prevot, A. S. H., Tripathi, S. N. and Verma, V.: Real-Time Measurements of PM 2.5 Oxidative Potential Using a Dithiothreitol Assay in Delhi, India , Environ. Sci. Technol. Lett., doi:10.1021/acs.estlett.0c00342, 2020.

Risom, L., Møller, P. and Loft, S.: Oxidative stress-induced DNA damage by particulate air pollution, Mutat Res, 592(1–2), 119–137, doi:10.1016/j mrfmmm.2005.06.012, 2005.

https://doi.org/10.5194/acp-2020-1024
Preprint. Discussion started: 13 October 2020

910 Saffari, A., Daher, N., Shafer, M. M., Schauer, J. J. and Sioutas, C.: Seasonal and spatial variation in reactive oxygen species activity of quasi-ultrafine particles (PM0.25) in the Los Angeles metropolitan area and its association with chemical composition, Atmos. Environ., 79, 566–575, doi:10.1016/j.atmosenv.2013.07.058, 2013.

Saffari, A., Daher, N., Shafer, M. M., Schauer, J. J. and Sioutas, C.: Seasonal and spatial variation in dithiothreitol (DTT) activity of quasi-ultrafine particles in the Los Angeles Basin and its association with chemical species, J. Environ. Sci. Heal. -
915 Part A Toxic/Hazardous Subst. Environ. Eng., 49(4), 441–451, doi:10.1080/10934529.2014.854677, 2014.

Schauer, J. J., Kleeman, M. J., Cass, G. R. and Simoneit, B. R. T.: Measurement of emissions from air pollution sources. 2. C1 through C30 organic compounds from medium duty diesel trucks, Environ. Sci. Technol., 33(10), 1578–1587, doi:10.1021/es980081n, 1999.

See, S. W., Wang, Y. H. and Balasubramanian, R.: Contrasting reactive oxygen species and transition metal concentrations in
920 combustion aerosols, Environ. Res., 103(3), 317–324, doi:10.1016/j.envres.2006.08.012, 2007.

Shen, H. and Anastasio, C.: Formation of hydroxyl radical from San Joaquin Valley particles extracted in a cell-free surrogate lung fluid, Atmos. Chem. Phys., 11(18), 9671–9682, doi:10.5194/acp-11-9671-2011, 2011.

Shen, H. and Anastasio, C.: A comparison of hydroxyl radical and hydrogen peroxide generation in ambient particle extracts and laboratory metal solutions, Atmos. Environ., 46(530), 665–668, doi:10.1016/j.atmosenv.2011.10.006, 2012.

925 Shen, H., Barakat, A. I. and Anastasio, C.: Generation of hydrogen peroxide from San Joaquin Valley particles in a cell-free solution, Atmos. Chem. Phys., 11(2), 753–765, doi:10.5194/acp-11-753-2011, 2011.

Shen, R., Liu, Z., Liu, Y., Wang, L., Li, D., Wang, Y., Wang, G., Bai, Y. and Li, X.: Typical polar organic aerosol tracers in PM2.5 over the North China Plain: Spatial distribution, seasonal variations, contribution and sources, Chemosphere, 209, 758–766, doi:10.1016/j.chemosphere.2018.06.133, 2018.

930 Shi, Z., Vu, T., Kotthaus, S., Harrison, R. M., Grimmond, S., Yue, S., Zhu, T., Lee, J., Han, Y., Demuzere, M., Dunmore, R. E., Ren, L., Liu, D., Wang, Y., Wild, O., Allan, J., Acton, W. J., Barlow, J., Barratt, B., Beddows, D., Bloss, W. J., Calzolai, G., Carruthers, D., Carslaw, D. C., Chan, Q., Chatzidiakou, L., Chen, Y., Crilley, L., Coe, H., Dai, T., Doherty, R., Duan, F., Fu, P., Ge, B., Ge, M., Guan, D., Hamilton, J. F., He, K., Heal, M., Heard, D., Hewitt, C. N., Hollaway, M., Hu, M., Ji, D., Jiang, X., Jones, R., Kalberer, M., Kelly, F. J., Kramer, L., Langford, B., Lin, C., Lewis, A. C., Li, J., Li, W., Liu, H., Liu, J.,
935 Loh, M., Lu, K., Lucarelli, F., Mann, G., Mcfiggans, G., Miller, M. R., Mills, G., Monk, P., Nemitz, E., Ouyang, B., Palmer, P. I., Percival, C., Popoola, O., Reeves, C., Rickard, A. R., Shao, L., Shi, G., Spracklen, D., Stevenson, D., Sun, Y., Sun, Z., Tao, S., Tong, S., Wang, Q., Wang, W., Wang, X., Wang, X., Wang, Z., Wei, L., Whalley, L., Wu, X., Wu, Z., Xie, P., Yang, F., Zhang, Q., Zhang, Y., Zhang, Y. and Zheng, M.: Introduction to the special issue " In-depth study of air pollution sources and processes within Beijing and its surrounding region, , 7519–7546, 2019.

940 Shinyashiki, M., Eiguren-Fernandez, A., Schmitz, D. A., Di Stefano, E., Li, N., Linak, W. P., Cho, S. H., Froines, J. R. and Cho, A. K.: Electrophilic and redox properties of diesel exhaust particles, Environ. Res., 109(3), 239–244, doi:10.1016/j.envres.2008.12.008, 2009.

Steimer, S., Patton, D., Vu, T., Panagi, M., Monks, P., Harrison, R., Fleming, Z., Shi, Z. and Kalberer, M.: Seasonal Differences

https://doi.org/10.5194/acp-2020-1024
Preprint. Discussion started: 13 October 2020

in the Composition of Organic Aerosols in Beijing: a Study by Direct Infusion Ultrahigh Resolution Mass Spectrometry, Atmos. Chem. Phys. Discuss., (January), 1–26, doi:10.5194/acp-2019-1009, 2020.

Steimer, S. S., Delvaux, A., Campbell, S. J., Gallimore, P. J., Grice, P., Howe, D. J., Pitton, D., Claeys, M., Hoffmann, T. and Kalberer, M.: Synthesis and characterisation of peroxypinic acids as proxies for highly oxygenated molecules (HOMs) in secondary organic aerosol, Atmos. Chem. Phys., 18(15), 10973–10983, doi:10.5194/acp-18-10973-2018, 2018.

Subramanian, R., Donahue, N. M., Bernardo-Bricker, A., Rogge, W. F. and Robinson, A. L.: Contribution of motor vehicle emissions to organic carbon and fine particle mass in Pittsburgh, Pennsylvania: Effects of varying source profiles and seasonal trends in ambient marker concentrations, Atmos. Environ., 40(40), 8002–8019, doi:10.1016/j.atmosenv.2006.06.055, 2006.

Tan, W. C., Qiu, D., Liam, B. L., Ng, T. P., Lee, S. H., Van Eeden, S. F., D'Yachkova, Y. and Hogg, J. C.: The human bone marrow response to acute air pollution caused by forest fires, Am. J. Respir. Crit. Care Med., 161(4 I), 1213–1217, doi:10.1164/ajrccm.161.4.9904084, 2000.

Tao, F., Gonzalez-Flecha, B. and Kobzik, L.: Reactive oxygen species in pulmonary inflammation by ambient particulates, Free Radic. Biol. Med., 35(4), 327–340, doi:10.1016/S0891-5849(03)00280-6, 2003.

Tapparo, A., Di Marco, V., Badocco, D., D'Aronco, S., Soldà, L., Pastore, P., Mahon, B. M., Kalberer, M. and Giorio, C.: Formation of metal-organic ligand complexes affects solubility of metals in airborne particles at an urban site in the Po valley, Chemosphere, 241, 1–13, doi:10.1016/j.chemosphere.2019.125025, 2020.

Tong, H., Arangio, A. M., Lakey, P. S. J., Berkemeier, T., Liu, F., Kampf, C. J., Brune, W. H., Poschl, U. and Shiraiwa, M.: Hydroxyl radicals from secondary organic aerosol decomposition in water, Atmos. Chem. Phys., 16(3), 1761–1771, doi:10.5194/acp-16-1761-2016, 2016.

Tong, H., Lakey, P. S. J., Arangio, A. M., Socorro, J., Kampf, C. J., Berkemeier, T., Brune, W. H., Pöschl, U. and Shiraiwa, M.: Reactive oxygen species formed in aqueous mixtures of secondary organic aerosols and mineral dust influencing cloud chemistry and public health in the Anthropocene, Faraday Discuss., 200, 251–270, doi:10.1039/c7fd00023e, 2017.

Tong, H., Lakey, P. S. J., Arangio, A. M., Socorro, J., Shen, F., Lucas, K., Brune, W. H., Pöschl, U. and Shiraiwa, M.: Reactive Oxygen Species Formed by Secondary Organic Aerosols in Water and Surrogate Lung Fluid, Environ. Sci. Technol., 52, 11642–11651, doi:10.1021/acs.est.8b03695, 2018.

Tuet, W. Y., Chen, Y., Xu, L., Fok, S., Gao, D., Weber, R. J. and Ng, N. L.: Chemical oxidative potential of secondary organic aerosol (SOA) generated from the photooxidation of biogenic and anthropogenic volatile organic compounds, , 839–853, doi:10.5194/acp-17-839-2017, 2017.

Valko, M., Morris, H. and Cronin, M. T. D.: Metals, Toxicity and Oxidative Stress, Curr. Med. Chem., 12(10), 1161–1208, 2005.

Venkatachari, P. and Hopke, P. K.: Development and laboratory testing of an automated monitor for the measurement of atmospheric particle-bound reactive oxygen species (ROS)., Aerosol Sci. Technol., 42(8), 629–635, 2008.

Venkatachari, P., Hopke, P. K., Grover, B. D. and Eatough, D. J.: Measurement of particle-bound reactive oxygen species in rubidoux aerosols, J. Atmos. Chem., 50(1), 49–58, doi:10.1007/s10874-005-1662-z, 2005.

https://doi.org/10.5194/acp-2020-1024
Preprint. Discussion started: 13 October 2020


Atmospheric Chemistry and Physics Discussions

Verma, V., Pakbin, P., Cheung, K. L., Cho, A. K., Schauer, J. J., Shafer, M. M., Kleinman, M. T. and Sioutas, C.: Physicochemical and oxidative characteristics of semi-volatile components of quasi-ultrafine particles in an urban atmosphere, Atmos. Environ., 45(4), 1025–1033, doi:10.1016/j.atmosenv.2010.10.044, 2011.

Verma, V., Fang, T., Guo, H., King, L., Bates, J. T., Peltier, R. E., Edgerton, E., Russell, A. G. and Weber, R. J.: Reactive oxygen species associated with water-soluble PM2.5 in the southeastern United States: Spatiotemporal trends and source apportionment, Atmos. Chem. Phys., 14(23), 12915–12930, doi:10.5194/acp-14-12915-2014, 2014.

Verma, V., Wang, Y., El-Afifi, R., Fang, T., Rowland, J., Russell, A. G. and Weber, R. J.: Fractionating ambient humic-like substances (HULIS) for their reactive oxygen species activity - Assessing the importance of quinones and atmospheric aging, Atmos. Environ., 120, 351–359, doi:10.1016/j.atmosenv.2015.09.010, 2015a.

Verma, V., Fang, T., Xu, L., Peltier, R. E., Russell, A. G., Ng, N. L. and Weber, R. J.: Organic aerosols associated with the generation of reactive oxygen species (ROS) by water-soluble PM2.5, Environ. Sci. Technol., 49(7), 4646–4656, doi:10.1021/es505577w, 2015b.

Wang, G., Cheng, S., Wei, W., Zhou, Y., Yao, S. and Zhang, H.: Characteristics and source apportionment of VOCs in the suburban area of Beijing, China, Atmos. Pollut. Res., 7(4), 711–724, doi:10.1016/j.apr.2016.03.006, 2016.

Wang, H., Li, Z., Lv, Y., Zhang, Y., Xu, H., Guo, J. and Goloub, P.: Determination and climatology of diurnal cycle of atmospheric mixing layer height over Beijing 2013–2018: Lidar measurements and implication for airpollution, Atmos. Chem. Phys., 1–25, doi:10.5194/acp-2020-175, 2020a.

Wang, J., Jiang, H., Jiang, H., Mo, Y., Geng, X., Li, J., Mao, S., Bualert, S., Ma, S., Li, J. and Zhang, G.: Source apportionment of water-soluble oxidative potential in ambient total suspended particulate from Bangkok: Biomass burning versus fossil fuel combustion, Atmos. Environ., 235(May), 117624, doi:10.1016/j.atmosenv.2020.117624, 2020b.

Wang, Q., He, X., Zhou, M., Huang, D., Qiao, L., Zhu, S., Ma, Y., Wang, H., Li, L., Huang, C., Huang, X. H. H., Xu, W., Worsnop, D. R., Goldstein, A. H., Guo, H. and Yu, J. Z.: Hourly Measurements of Organic Molecular Markers in Urban Shanghai, China: Primary Organic Aerosol Source Identification and Observation of Cooking Aerosol Aging, ACS Earth Sp. Chem., doi:10.1021/acsearthspacechem.0c00205, 2020c.

Whalley, L. K., Slater, E. J., Woodward-Massey, R., Ye, C., Lee, J. D., Squires, F., Hopkins, J. R., Dunmore, R. E., Shaw, M., Hamilton, J. F., Lewis, A. C., Mehra, A., Worrall, S. D., Bacak, A., Bannan, T. J., Coe, H., Ouyang, B., Jones, R. L., Crilley, L. R., Kramer, L. J., Bloss, W. J., Vu, T., Kotthaus, S., Grimmond, S., Sun, Y., Xu, W., Yue, S., Ren, L., Joe, W., Acton, F., Hewitt, C. N., Wang, X., Fu, P., Heard, D. E. and Whalley, L.: Evaluating the sensitivity of radical chemistry and ozone formation to ambient VOCs and NO x in Beijing, , (x), 1–41, doi:10.5194/acp-2020-785, 2020.

World Health Organisation: Ambient Air Pollution: A Global Assessment of Exposure and Burden of Disease., 2016.

Wragg, F. P. H., Fuller, S. J., Freshwater, R., Green, D. C., Kelly, F. J. and Kalberer, M.: An automated online instrument to quantify aerosol-bound reactive oxygen species (ROS) for ambient measurement and health-relevant aerosol studies, Atmos. Meas. Tech., 9(10), 4891–4900, doi:10.5194/amt-9-4891-2016, 2016.

Xu, J., Liu, D., Wu, X., Vu, T. V., Zhang, Y. Z., Fu, P., Sun, Y., Xu, W., Ji, D., Harrison, R. M. and Shi, Z.: Source

https://doi.org/10.5194/acp-2020-1024
Preprint. Discussion started: 13 October 2020

Apportionment of Fine Aerosol at an Urban Site of Beijing Using a Chemical Mass Balance Model, Prep., 2020a.

Xu, J., Hu, W., Liang, D. and Gao, P.: Technology Photochemical impacts on the toxicity of PM 2 . 5, Crit. Rev. Environ. Sci. Technol., 0(0), 1–27, doi:10.1080/10643389.2020.1816126, 2020b.

Yang, A., Wang, M., Eeftens, M., Beelen, R., Dons, E., Leseman, D. L. A. C., Brunekreef, B., Cassee, F. R., Janssen, N. A. H. and Hoek, G.: Spatial variation and land use regression modeling of the oxidative potential of fine particles, Environ. Health Perspect., 123(11), 1187–1192, doi:10.1289/ehp.1408916, 2015.

Yu, L., Wang, G., Zhang, R., Zhang, L., Song, Y., Wu, B., Li, X., An, K. and Chu, J.: Characterization and source apportionment of PM2.5 in an urban environment in Beijing, Aerosol Air Qual. Res., 13(2), 574–583, doi:10.4209/aaqr.2012.07.0192, 2013.

Yu, S. Y., Liu, W. J., Xu, Y. S., Yi, K., Zhou, M., Tao, S. and Liu, W. X.: Characteristics and oxidative potential of atmospheric PM2.5 in Beijing: Source apportionment and seasonal variation, Sci. Total Environ., 650, 277–287, doi:10.1016/j.scitotenv.2018.09.021, 2019.

Zhao, H., Zheng, Y. and Li, C.: Spatiotemporal distribution of PM2.5 and O3 and their interaction during the summer and winter seasons in Beijing, China, Sustain., 10(12), doi:10.3390/su10124519, 2018.

Zheng, M., Salmon, L. G., Schauer, J. J., Zeng, L., Kiang, C. S., Zhang, Y. and Cass, G. R.: Seasonal trends in PM2.5 source contributions in Beijing, China, Atmos. Environ., 39(22), 3967–3976, doi:10.1016/j.atmosenv.2005.03.036, 2005.